

Université de Montréal

**Novel surface-tethered estrogen polymeric platforms in  
cardiovascular regenerative medicine**

par

Baowen Qi

Faculté de Pharmacie

Thèse présentée à la Faculté des études supérieures  
en vue de l'obtention du grade de Philosophiae Doctor (Ph.D.)  
en Sciences Pharmaceutiques  
option Chimie Médicinale

July, 2015

© Baowen Qi, 2015

Université de Montréal  
Faculté des études supérieures et postdoctorales  
Cette thèse intitulée:

**Novel surface-tethered estrogen polymeric platforms in  
cardiovascular regenerative medicine**

présentée par :  
Baowen Qi

a été évaluée par un jury composé des personnes suivantes :

Dr. Gaëlle Roullin, Président-rapporteur  
Dr. Françoise M. Winnik, Directeur  
Dr. Jean-François Tanguay, Co-directeur  
Dr. Anna Ritcey, Examineur externe  
Dr. Jean-François Masson, Membre du jury

## Résumé

L'estradiol (E2) est une hormone femelle qui joue un rôle essentiel, à la fois dans la régulation et dans la détermination de certaines conditions physiologiques *in vivo*, telle que la différenciation et la prolifération cellulaire. Lorsque l'E2 est donné en supplément, par exemple dans le cas de thérapie hormonale, deux effets sont observés, un effet génomique et un effet non-génomique, de par son interaction avec les récepteurs à œstrogène du noyau ou de la membrane cellulaire, respectivement. L'effet non-génomique est plus difficile à étudier biologiquement parce que l'effet se produit sur une échelle de temps extrêmement courte et à cause de la nature hydrophobe de l'E2 qui réduit sa biodisponibilité et donc son accessibilité aux cellules cibles. C'est pourquoi il est nécessaire de développer des systèmes d'administration de l'E2 qui permettent de n'étudier que l'effet non-génomique de l'œstrogène. Une des stratégies employée consiste à greffer l'E2 à des macromolécules hydrophiles, comme de l'albumine de sérum bovin (BSA) ou des dendrimères de type poly(amido)amine, permettant de maintenir l'interaction de l'E2 avec les récepteurs d'œstrogène de la membrane cellulaire et d'éviter la pénétration de l'E2 dans le noyau des cellules. Toutefois, ces systèmes macromolécules-E2 sont critiquables car ils sont peu stables et l'E2 peut se retrouver sous forme libre, ce qui affecte sa localisation cellulaire. L'objectif de cette thèse est donc de développer de nouvelles plateformes fonctionnalisées avec de l'E2 en utilisant les approches de synthèses ascendantes et descendantes. Le but de ces plateformes est de permettre d'étudier le mécanisme de l'effet non-génomique de l'E2, ainsi que d'explorer des applications potentielles dans le domaine biomédical.

L'approche ascendante est basée sur un ligand d'E2 activé, l'acide 17, $\alpha$ -éthynylestradiol-benzoïque, attaché de façon covalente à un polymère de chitosan avec des substitutions de phosphorylcholine (CH-PC-E2). L'estradiol est sous forme de pro-drogue attachée au polymère qui s'auto-assemble pour former un film. L'effet biologique de la composition chimique du film de chitosan-phosphorylcholine a été étudié sur des cellules endothéliales. Les films de compositions chimiques différentes ont préalablement été caractérisés de façon physicochimique. La topographie de la surface, la charge de surface, ainsi que la rhéologie des différents films contenant 15, 25, ou 40% molaires de

phosphorylcholine, ont été étudiés par microscopie à force atomique (AFM), potentiel zêta, résonance plasmonique de surface et par microbalance à cristal de quartz avec dissipation (QCM-D). Les résultats de QCM-D ont montré que plus la part molaire en phosphorylcholine est grande moins il y a de fibrinogène qui s'adsorbe sur le film de CH-PC. Des cellules humaines de veine ombilicale (HUVECs) cultivées sur des films de CH-PC25 et de CH-PC40 forment des amas cellulaire appelés sphéroïdes au bout de 4 jours, alors que ce n'est pas le cas lorsque ces cellules sont cultivées sur des films de CH-PC15. L'attachement de l'estradiol au polymère a été caractérisé par plusieurs techniques, telles que la résonance magnétique nucléaire de proton ( $^1\text{H}$  NMR), la spectroscopie infrarouge avec transformée de Fourier à réflexion totale atténuée (FTIR-ATR) et la spectroscopie UV-visible. La nature hydrogel des films (sa capacité à retenir l'eau) ainsi que l'interaction des films avec des récepteurs à E2, ont été étudiés par la QCM-D. Des études d'imagerie cellulaires utilisant du diacétate de diaminofluoresceine-FM ont révélé que les films hydrogels de CH-PC-E2 stimulent la production d'oxyde nitrique par les cellules endothéliales, qui joue un rôle protecteur pour le système cardiovasculaire. L'ensemble de ces études met en valeur les rôles différents et les applications potentielles qu'ont les films de type CH-PC-E2 et CH-PC dans le cadre de la médecine cardiovasculaire régénérative. L'approche descendante est basée sur l'attachement de façon covalente d'E2 sur des îlots d'or de 2  $\mu\text{m}$  disposés en rangées et espacés par 12  $\mu\text{m}$  sur un substrat en verre. Les îlots ont été préparés par photolithographie. La surface du verre a quant à elle été modifiée à l'aide d'un tripeptide cyclique, le cRGD, favorisant l'adhésion cellulaire. L'attachement d'E2 sur les surfaces d'or a été suivi et confirmé par les techniques de SPR et de QCM-D. Des études d'ELISA ont montré une augmentation significative du niveau de phosphorylation de la kinase ERK (marqueur important de l'effet non-génomique) après 1 heure d'exposition des cellules endothéliales aux motifs alternant l'E2 et le cRGD. Par contre lorsque des cellules cancéreuses sont déposées sur les surfaces présentant des motifs d'E2, ces cellules ne croissent pas, ce qui suggère que l'E2 n'exerce pas d'effet génomique. Les résultats de l'approche descendante montrent le potentiel des surfaces présentant des motifs d'E2 pour l'étude des effets non-génomiques de l'E2 dans un modèle *in vitro*.

**Mots-clés** : estradiol, effet non-génomique, approches ascendantes et descendantes, substrats en micromotifs, chitosan, phosphorylcholine, oxyde nitrique, médecine cardiovasculaire régénérative, kinase régulée par signal extracellulaire

## Abstract

Estradiol (E2) is an essential female hormone in the regulation and determination of various physiological conditions *in vivo*, such as cell proliferation and differentiation. When supplementing exogenous E2 as a clinical strategy for hormone therapy, it generates genomic and non-genomic effect simultaneously *via* binding to the estrogen receptors in the cell nucleus or membrane site. Compared to the genomic effect, it is quite difficult to monitor the E2-induced non-genomic biological behavior because this effect occurs in extremely transient time scale and the bioavailability and accessibility of E2 to target cells is very low due to the hydrophobic nature of E2. As a result, it is indispensable to develop E2 delivery systems to specifically understand estrogenic non-genomic nature. One of strategies is to graft E2 to the hydrophilic macromolecules, e.g. bovine serum albumin (BSA) or poly(amido)amine dendrimer, to maintain E2 interacting with membrane estrogen receptors instead of penetrating into the cell nucleus. However, the instability of those E2-macromolecules systems, either containing free E2 leaching or discrepancies of cellular localizations, led to controversies. Herein, the objective of present thesis is to develop novel E2-functionized platforms by the principle of bottom-up and top-down approaches for understanding the mechanism of estrogenic non-genomic effect, and further, to explore their potential applications in the biomedicine.

As a bottom-up approach, an activated E2 ligand, 17 $\alpha$ -ethinylestradiol-benzoic acid was covalently conjugated onto a phosphorylcholine substituted chitosan polymer (CH-PC-E2) as a prodrug strategy for the fabrication of self-assembled films. Through a series of combined physicochemical and cellular investigations, the relationship between various chemical compositions of chitosan-phosphorylcholine (CH-PC) films and cellular responses was also evaluated. Based on atomic force microscopy (AFM) examination, zeta-potential measurements, surface plasmon resonance (SPR), and quartz crystal microbalance with dissipation (QCM-D) measurements, surface topography, charge, and rheology of CH-PC films with 15, 25, and 40 mol% PC contents were characterized. Moreover, QCM-D measurements indicated that the amount of fibrinogen adsorbed on CH-PC films decreased significantly with increasing PC content. Finally, it was also showed that human umbilical vein endothelial cells (HUVECs) form spheroids on CH-PC25 and CH-PC40 films, but not on

CH-PC15 films cultured over 4 days. In addition, the CH-PC-E2 polymer conjugates were prepared and characterized by several techniques, such as  $^1\text{H}$  nuclear magnetic resonance ( $^1\text{H}$  NMR), Fourier transformed infrared-attenuated total reflection (FTIR-ATR) and UV/Vis spectra measurements. The hydrogel nature of CH-PC-E2 film as well as its interactions to estrogen receptors was further extensively investigated by QCM-D study. In the cellular study, CH-PC-E2 hydrogel films can significantly stimulate the production of nitric oxide, a protective molecule in the cardiovascular system, in the endothelial cells by a diaminofluorescein-FM diacetate imaging study. The studies above demonstrated the different roles and potential applications of CH-PC-E2 and CH-PC surfaces in the cardiovascular regenerative medicine. As a top-down approach, micropatterned substrates were used for E2 functionalization, which were prepared by photolithography *via* aligning  $\sim 2\ \mu\text{m}$  in diameter gold arrays onto a glass substrate. After that, a cell adhesive peptide, cyclic RGD was introduced to the glass surface in order to induce the attachment of cells. Meanwhile, estradiol was covalently immobilized on the gold surface and the process was monitored and validated by combining SPR and QCM-D studies. In the micropatterned substrate-coupled cell ELISA study, a phosphorylation level of extracellular signal-regulated kinase (ERK), which is an important non-genomic marker, was significantly elevated by this E2-functionalized micropatterned surface after 1 hour incubation. Furthermore, E2-functionalized micropatterned substrate didn't proliferate cancer cells indicating the absence of genomic effect stimulation. Based on these results, our E2-functionalized micropatterned substrates can function as an *in vitro* model for the elucidation of estrogenic non-genomic behaviors.

**Keywords** : estradiol, non-genomic effect, top-down and bottom-up approaches, micropatterned substrates, chitosan, phosphocholine, nitric oxide, cardiovascular regenerative medicine, extracellular signal-regulated kinase

# Table of Contents

<b>Résumé.....</b>	<b>i</b>
<b>Abstract.....</b>	<b>i</b>
<b>Table of Contents .....</b>	<b>v</b>
<b>List of figures.....</b>	<b>x</b>
<b>List of tables .....</b>	<b>xiv</b>
<b>List of abbreviations .....</b>	<b>i</b>
<b>Authors' contributions .....</b>	<b>iii</b>
<b>Acknowledgments .....</b>	<b>iv</b>
<b>CHAPTER ONE .....</b>	<b>1</b>
<b>Introduction and Literature Review .....</b>	<b>1</b>
1.1 Estrogen in cardiovascular medicine .....	1
1.1.1 Introduction to coronary artery heart disease.....	1
1.1.2 The anatomy and physiology of blood vessels .....	2
1.1.3 Estrogen effects on the cardiovascular system .....	3
1.1.4 Estrogen receptors and classical genomic effect .....	3
1.1.5 Estrogen non-genomic effect .....	4
1.1.6 Tools for estrogen non-genomic effect study .....	6
1.2 Polymeric biomaterials in cardiovascular medicine .....	7
1.2.1 Fundamental properties of polymeric biomaterials .....	7
1.2.2 Mechanical properties.....	7
1.2.3 Biodegradability.....	9
1.2.4 Cellular interactions .....	9
1.3 Non-fouling polymeric biomaterials in cardiovascular regenerative medicine .....	11
1.3.1 Overview of non-fouling polymeric biomaterials.....	11
1.3.2 Non-fouling polymeric biomaterials in cardiovascular regenerative medicine.....	16
1.4 Methods and Techniques .....	18
1.4.1 Surface plasmon resonance technology (SPR) .....	19
1.4.2 Quartz crystal microbalance with dissipation (QCM-D).....	20

1.4.3 Photolithography.....	20
1.5 Project hypothesis, thesis rationale and research objectives.....	21
1.5.1 Project hypothesis .....	21
1.5.2 Thesis rationale .....	24
1.5.3 Research objectives.....	25
1.6 References.....	26
<b>CHAPTER TWO .....</b>	<b>50</b>
<b>Phosphorylcholine-modified chitosan films as effective promoters of cell aggregation: correlation between the films properties and cellular response .....</b>	<b>50</b>
2.1 Abstract.....	51
2.2 Author Keywords.....	51
2.3 Introduction.....	52
2.4 Experimental Section .....	55
2.4.1 Materials .....	55
2.4.2 Synthesis and characterization of phosphorylcholine-chitosans (CH-PC).....	55
2.4.3 Preparation of CH-PC solutions .....	56
2.4.4 Dynamic light scattering (DLS) and zeta potential measurements of CH-PC solutions.....	56
2.4.5 Dynamic AFM measurements.....	56
2.4.6 Zeta potential measurements of CH-PC films.....	57
2.4.7 Surface plasmon resonance (SPR) measurements.....	57
2.4.8 Quartz crystal microbalance with dissipation (QCM-D) measurements.....	58
2.4.9 Ellipsometry measurements.....	59
2.4.10 Cell culture.....	59
2.4.11 Cell observation by optical microscopy.....	60
2.5 Results and discussion.....	60
2.5.1 Morphology and charge of the CH-PC Films.....	60
2.5.2 Hydration and mechanical properties of CH-PC films.....	63
2.5.3 Fibrinogen adsorption on CH-PC films.....	66
2.5.4 Aggregation of human umbilical vein endothelial cells (HUVECs) and MCF-7 cells on CH-PC films.....	68



2.6 Conclusions .....	70
2.7 Acknowledgements .....	72
2.8 References .....	72
2.9 Appendix A. Supporting information .....	77
<b>CHAPTER THREE .....</b>	<b>86</b>
<b>Synthesis, characterization and biological study of estrogen grafted chitosan phosphorylcholine polymer conjugates .....</b>	<b>86</b>
3.1 Abstract .....	87
3.2 Author Keywords .....	87
3.3 Introduction .....	88
3.4 Experimental section .....	89
3.4.1 Materials .....	89
3.4.2 Preparation of PC-substituted chitosan (CH-PC) .....	90
3.4.3 Conjugation 17 $\alpha$ -ethinylestradiol to 4-iodobenzoic acid .....	90
3.4.4 Preparation and characterization of CH-PC-E2 conjugates .....	91
3.4.5 Dynamic light scattering (DLS) measurements .....	91
3.4.6 Spectroscopic ellipsometry analysis .....	92
3.4.7 Quartz crystal microbalance with dissipation (QCM-D) studies .....	92
3.4.8 Cell culture .....	94
3.4.9 DAF-FM fluorescence imaging study .....	94
3.4.10 Statistics .....	95
3.5 Results and discussion .....	96
3.5.1 Characterization of CH-PC-E2 conjugates .....	96
3.5.2 Viscoelastic properties of CH-PC-E2 and CH-PC formulated thin films .....	98
3.5.3 The binding experiment of ER- $\alpha$ to CH-PC-E2 hydrogel film .....	100
3.5.4 CH-PC-E2 hydrogel film promotes intracellular nitric oxide (NO) production ..	102
3.6 Conclusions .....	104
3.7 Acknowledgements .....	104
3.8 References .....	105
3.9 Appendix B. Supporting information .....	111

<b>CHAPTER FOUR.....</b>	<b>115</b>
<b>Estradiol-tethered micropatterned surfaces for the study of estrogenic non-genomic pathways .....</b>	<b>115</b>
4.1 Abstract .....	116
4.2 Authors keywords .....	116
4.3 Introduction.....	117
4.4 Materials and methods .....	119
4.4.1 Materials .....	119
4.4.2 Cell culture.....	119
4.4.3 Glass surface modification and characterization .....	120
4.4.4 Gold surface modification monitored by XPS, SPR and QCM.....	120
4.4.5 Fabrication and modification of micropatterned surfaces .....	122
4.4.6 Detection of ERK phosphorylation by cell ELISA.....	123
4.4.7 MCF-7 cell proliferation assay .....	124
4.5 Results and discussions.....	124
4.5.1 Design of micropatterned substrates .....	124
4.5.2 Immobilization of cRGD onto glass substrates .....	126
4.5.3 XPS characterization of E2-PEG2k modified gold surfaces. ....	127
4.5.4 SPR evaluation of the interaction of ER- $\alpha$ with E2-modified gold substrates ....	128
4.5.5 QCM-D studies of the adsorption of ER- $\alpha$ on gold substrates modified with E2-PEG2k.....	130
4.5.6 Biological activity of E2-modified micropatterned substrates .....	132
4.6 Conclusions.....	134
4.7 Acknowledgements.....	134
4.8 References.....	135
4.9 Appendix C. Supporting information .....	140
<b>CHAPTER FIVE .....</b>	<b>144</b>
<b>GENERAL DISCUSSION .....</b>	<b>144</b>
5.1 Physical and biological properties of CH-PC polymer thin films .....	145
5.2 Synthesis, characterization and biological studies of CH-PC-E2 self-assembled films in the cardiovascular regenerative medicine .....	147

5.3 E2-tethered micropatterned substrates selectively activate non-genomic signal pathways .....	149
5.4 References .....	150
<b>CHAPTER SIX .....</b>	<b>154</b>
<b>CONCLUSIONS AND FUTURE WORKS.....</b>	<b>154</b>
6.1 Conclusions.....	155
6.2 Future perspectives .....	155
6.3 References.....	157

## List of figures

- Figure 1.1 Schematic representation of the genomic and nongenomic estrogen pathways. For the genomic pathway, E2 (red triangle) crosses the cell membrane and binds to the estrogen receptor (ER) in the cell nucleus, inducing gene transcription. For the non-genomic pathway, E2 interacts with ER or ER/GPR30 on the cell membrane, which activates several transduction pathways. .... 4
- Figure 1.2 Chemical structures of zwitterionic-based materials. (A) phosphorylcholine (PC), (B) sulfobetaine (SB), and (C) carboxybetaine (CB)..... 12
- Figure 1.3 Chemical structures of natural polysaccharides. (A) heparin, (B) chitosan, and (C) hyaluronic acid..... 14
- Figure 1.4 Tethering E2 to CH-PC polymers for the formulation of self-assembled thin films by bottom-up approach. .... 22
- Figure 1.5 Tethering E2 to photolithography-fabricated micropatterned substrates by top-down approach in order to specifically understand E2 non-genomic action. .... 23
- Figure 2.1 Chemical structure of phosphorylcholine-chitosans ..... 53
- Figure 2.2 (a) AFM topography images of CH-PC films ( $2\ \mu\text{m} \times 2\ \mu\text{m}$ ) acquired in a phosphate buffer pH 6.8; maximum height (Z-range): 12 nm (CH-PC15 and CH-PC25) and 25 nm (CH-PC40) and cross-sectional profiles along the X axis corresponding to the yellow lines drawn through the AFM images; (b) Height and width of the surface features determined by AFM..... 61
- Figure 2.3 SPR and QCM responses of MPS-modified gold substrates when exposed to solutions of CH-PC ( $1.0\ \text{g L}^{-1}$ ) in phosphate buffer, pH 6.8: a) changes in the SPR resonance angle ( $\Delta\theta_m$ ) and b) changes in resonance frequency ( $\Delta f_5/5$ , top) and dissipation ( $\Delta D_5$ , bottom) observed in the QCM-D experiments for the 5<sup>th</sup> overtone..... 63
- Figure 2.4 (A) Adsorption of fibrinogen on CH-PC films. Changes in resonance frequency and dissipation observed for the 5<sup>th</sup> overtone (upper and lower panels, respectively) for MPS-modified gold substrates coated with CH-PC upon exposure to a fibrinogen solution ( $0.1\ \text{g L}^{-1}$ , pH 6.8). The arrows indicate the time corresponding to the onset of the films rinse with PBS buffer. (B) Amount of fibrinogen adsorbed on the CH-PC coated substrates.. 67

Figure 2.5 Optical micrographs of HUVECs on CH-PC coated surfaces 1 day and 4 days after seeding (micrographs A to C and E to G, respectively), and on polystyrene tissue culture plates (micrographs E and H); Scale bar: 200  $\mu\text{m}$ . ..... 69

Figure 3.1 Synthetic route of CH-PC-E2 polymer conjugate ..... 95

Figure 3.2  $^1\text{H}$  NMR spectrum of CH-PC-E2 conjugate in  $\text{D}_2\text{O}$  at  $70^\circ\text{C}$ ..... 97

Figure 3.3 QCM-D study of *in situ* formed CH-PC-E2 and CH-PC hydrogel films on the silicon dioxide for overnight reaction at  $25^\circ\text{C}$ . (A) The shift of QCM-D frequency ( $\Delta f_5/5$ ) and dissipation ( $\Delta D_5/5$ ) showed the thin film formulations of CH-PC (black trace) and CH-PC-E2 (red trace) onto the silicon dioxide surfaces as a function of time. (B) The storage modulus (squares) and loss modulus (circles) of CH-PC and CH-PC-E2 hydrogel films are shown in a frequency dependent manner..... 99

Figure 3.4 ER- $\alpha$  adsorption experiment onto the CH-PC-E2 and CH-PC functionalized silicon dioxide sensor by QCM-D at  $25^\circ\text{C}$ . The time of ER- $\alpha$  (concentration:  $50 \text{ nmol L}^{-1}$ ) addition and PBS wash are indicated by the arrows. (A) The QCM-D frequency ( $\Delta f_5/5$ ) and dissipation ( $\Delta D_5/5$ ) shift showed the adsorption of ER- $\alpha$  onto the CH-PC film (black trace) and CH-PC-E2 film (red trace) and as a function of time. (B)  $\Delta D$ - $\Delta f$  plots for ER- $\alpha$  adsorption corresponds to the ER- $\alpha$  non-specific adsorption of the CH-PC film (black trace) to the specific adsorption of the CH-PC-E2 film (red trace). ..... 101

Figure 3.5 DAF-FM fluorescence imaging study of EA.hy926 cells incubated on the CH-PC and CH-PC-E2 films for 1 hour. Nitric oxide production levels were determined by using DAF-FM for the CH-PC functionalized substrates (A&D), CH-PC-E2 functionalized substrates (B&E), and CH-PC-E2 functionalized substrates pretreated with ICI 182,780 (C&F) for 1 hour. The top panels correspond to phase contrast micrographs and the bottom panels correspond to DAF-FM fluorescence images from the identical sites. (Scale bar:  $100\mu\text{m}$ ). The quantitative NO production levels were also shown by analyzing the emission peak intensity (G). Data were calculated by three independent samples. Probability values were considered significant which are represented as  $*p < 0.05$ ..... 103

Figure 4.1 (A and B) Schematic representations of the micropatterned substrate employed. cRGD (for the interaction with integrin) and E2 (for the interaction with mER) are co-immobilized onto a PEGylated micropatterned surface to ensure cell adhesion and E2 presentation to the cell membrane. (C) SEM image of the micropatterned surface

consisting of gold circular regions (diameter: 2  $\mu\text{m}$ ) arrayed with a 12- $\mu\text{m}$  pitch (scale bar: 5  $\mu\text{m}$ ); and chemical sequences performed on glass surfaces (D) and on gold surfaces (E). ..... 125

Figure 4.2 Cyclic RGD (cRGD) functionalized glass substrate enhanced MCF-7 cell adhesion.

(A) Optical images of MCF-7 cell onto the PEGylated glass substrate after 1 hour incubation at 37 °C, 5% CO<sub>2</sub>. (B) Optical images of MCF-7 cell onto the linear RGD functionalized glass substrate after 1 hour incubation at 37 °C, 5% CO<sub>2</sub>. (C) Optical images of MCF-7 cell onto the cRGD functionalized glass substrate after 1 hour incubation at 37 °C, 5% CO<sub>2</sub>. (D) Quantification analysis of cell numbers. All the data are expressed as mean  $\pm$ S.E. of triplicate determinations. P<0.05 is considered as the significantly statistical difference. .... 127

Figure 4.3 (A) SPR traces corresponding to the addition of ER- $\alpha$  solutions onto the E2-

modified PEGylated gold substrate (red) and a control PEGylated gold substrate (black); temperature: 25°C. (B) ER- $\alpha$  coverage (ng/cm<sup>2</sup>) as a function of ER- $\alpha$  concentration of the solution injected on the E2-modified PEGylated gold substrate (red symbols) and on the control PEGylated gold substrate (black symbols); the circles are the surface coverage values after rinsing the substrates with buffer. .... 129

Figure 4.4 (A) Frequency ( $\Delta f$ ) and dissipation ( $\Delta D$ ) shifts as a function of the concentration of

the ER- $\alpha$  solution injected in the QCM-D cell compartment fitted an E2-modified substrate (red trace) and the control substrate (black trace); (B) ER- $\alpha$  coverage (ng/cm<sup>2</sup>) as a function of ER- $\alpha$  concentration of the solution injected on the E2-modified PEGylated gold substrate (red symbols) and on the control PEGylated gold substrate (black symbols); the circles are the surface coverage values after rinsing the substrates with buffer. (C)  $\Delta D$ - $\Delta f$  plots for the ER- $\alpha$  adsorption onto the E2-modified surface (red trace) and the control surface (black trace). Different concentrations are also indicated by different colors for amino-PEG substrate and E2-PEG substrate. Amino-PEG substrate: 1 nM (black), 5 nM (green), 10 nM (cyan), 50 nM (yellow), and 100 nM (blue); E2-PEG substrate: 1 nM (red), 5 nM (navy), 10 nM (pink), 50 nM (brown), and 100 nM (purple). ..... 131

Figure 4.5 Cellular response to E2-functionalized micropatterned substrates. Optical

micrographs of starved MCF-7 cells seeded on micropatterned substrates which glass

areas functionalized with cRGD and gold dots modified with NH<sub>2</sub> (A) or E2 (B) incubated for 1 hr at 37 °C, 5% CO<sub>2</sub>; scale bars: 100 μm; the micrograph (C) is a magnified view of (B); scale bar: 25 μm; the arrows point to gold dots. (D) ERK phosphorylation of MCF-7 cells on each substrate; bars: mean ± S.E. of triplicate determinations. (E) MCF-7 cell proliferation on amino- or E2-immobilized micropatterned substrates after a 2-day incubation. .... 133

## List of tables

Table 1.1 Summary of the E2 non-genomic effects .....	5
Table 1.2 Summary of non-fouling materials .....	15
Table 2.1 Physico-chemical properties of films formed by CH-PC15, CH-PC25, CH-PC40, and CH thin films formed on MPS-modified gold surfaces at pH 5.5. ....	65
Table 2.2 Overview of the properties of CH-PC films. ....	71
Table 3.1 Viscoelastic properties of CH-PC and CH-PC-E2 hydrogel films formed <i>in situ</i> ....	99



## List of abbreviations

A	Surface area
Å	Angstrom
AFM	Air force microscope
BMS	Bare metal stents
BSA	Bovine serum albumin
°C	Degree celsius
CABG	Coronary artery bypass graft
CAHD	Coronary artery heart disease
CB	Carboxylbetaine
CH	Chitosan
CVDs	Cardiovascular diseases
D <sub>2</sub> O	Deuterium oxide
DLS	Dynamic light scattering
DMSO	Dimethyl sulfoxide
DS	Substitution degree
E <sub>2</sub>	Estradiol
ECs	Endothelial cells
ECMs	Extra cellular matrices
EDC	Estrogen dendrimer conjugate
EE <sub>2</sub>	17 $\alpha$ -ethinylestradiol
ELISA	Enzyme-linked immunosorbent assay
eNOS	Endothelial nitric oxide synthases
ER	Estrogen receptor
ERK	Extracellular signal-regulated kinase
GPR	G protein-coupled transmembrane receptor
h	Hour
HPLC	High performance liquid chromatography
hMSCs	Human Mesenchymal Stem cells
<sup>1</sup> H NMR	Proton nuclear magnetic resonance
HRT	Hormonal replacement therapy
HUVEC	Human umbilical vein endothelial cells
iNOS	Inducible nitric oxide synthases
ISR	In-stent restenosis
kDa	Kilo Dalton
K	Binding constant

LBL	Layer-by-layer
MAPK	Mitogen-activated protein kinase
<i>N</i> <sub>agg</sub>	Aggregation number
NOs	Nitric oxide
NOS	Nitric oxide synthases
nNOS	Neuronal nitric oxide synthases
PAMAM	Polyamidoamine
PBMA	Poly (butyl methacrylate)
PC	Phosphorylcholine
PCI	Percutaneous coronary intervention
PDMS	Polydimethylsiloxane
PEG	Poly(ethylene glycol)
PET	Polyethylene terephthalate
PEVA	Poly(ethylene vinyl acetate)
PI3K	Phosphatidylinositol-4, 5-bisphosphate 3-kinase
PKC	Phospholipase C protein kinase C
PLA	Poly lactides
PLGA	Poly lactic-co-glycolic Acid
PMMA	Poly(methylmethacrylate)
PNIPAM	Poly(N-isopropylacrylamide)
PTCA,	Percutaneous transluminal coronary angioplasty
PTFE	polytetrafluoroethylene
QCM-D	Quartz-crystal microbalance
$R_H$	Hydrodynamic radius
SAT	Subacute stent thrombosis
SB	Sulfobetaine
SDS	Sodium dodecyl sulfate
SPR	Surface plasmon resonance
XPS	X-ray photoelectron spectroscopy

## Authors' contributions

The present thesis is based on three articles. The current status of articles and authors' contribution is described below:

**Chapter 2:** “Phosphorylcholine-modified chitosan films as effective promoters of cell aggregation” has been published in *Macromolecular Bioscience* 15 (2015), 490–500. DOI: 10.1002/mabi.201400439. In this manuscript, the physical and biological properties of chitosan phosphorylcholine (CH-PC) polymers were systematically investigated. It explained the principles of developing appropriate CH-PC polymer backbones for the subsequent E2 immobilization study from a polymer perspective. My contribution in this project included carrying out cellular studies, interpreting the results and assisted Dr. Sayaka Toita for the synthesis of CH-PC polymers. Dr. Piotr Kujawa contributed characterization of polymer films, including SPR and QCM-D data modeling. Dr. Gregory Beaune helped to data interpretation and refined figures. All this work was supervised by Dr. Françoise M. Winnik. All authors agreed that this manuscript had been published.

**Chapter 3:** “Synthesis, characterization and biological study of estrogen grafted chitosan phosphorylcholine polymer conjugates” is in preparation. In this manuscript, E2 was tethered onto a selected CH-PC polymer backbone as a functional film in the protection of cardiovascular system. My contribution in this project included synthesis and characterization of CH-PC-E2 polymers and cellular studies. Dr. Xingping Qiu helped to the E2-benzoic acid synthesis. All this work was supervised by Dr. Jun Nakanishi and Dr. Françoise M. Winnik. All authors agreed this manuscript to be published.

**Chapter 4:** “Estradiol-tethered micropatterned surfaces for the study of estrogenic non-genomic pathways” is to be submitted to *Chemical communication*. In this manuscript, E2 was immobilized to the micropatterned substrates prepared by top-down approach for the activation of non-genomic signaling pathway. My contribution in this project included preparation and characterization of E2-tethered micropatterned surfaces, as well as estrogen receptor binding studies by SPR and QCM-D. The cell ELISA study was performed by Dr. Yoshihisa Shimizu. All this work was supervised by Dr. Jun Nakanishi and Dr. Françoise M. Winnik. All authors agreed this manuscript to be published.

## Acknowledgments

It would not have been possible to complete my PhD project without many people's professional technical support, profound knowledge and warmly encouragement. To start with, I would like to express my greatest gratitude to my thesis supervisor, Professor Françoise Winnik, who directed me for the completion of all my research as well as trained me as an independent researcher for my future career. I appreciated a lot for her profound knowledge and valuable advices.

I would also like to thank Dr. Jun Nakanishi and Dr. Pitor Kujawa in International Center for Materials Nanoarchitectonics, National Institute for Material Science (MANA, NIMS) in Tsukuba, Japan. Their consistent experiences and efforts instructed my thesis in a well-ordered track. I also thank to my collaborator: Dr. Grégory Beaune, Dr. Sayaka Toita, Dr. Yoshihisa Shimizu, and Dr. Yiu-Ting Richard Lau in MANA. They gave me a huge amount of help in both technical and theoretical aspects. Moreover, I specially thank to staffs in MANA foundry: Ms. Tomoko Ohki, Mr. Akihiko Ohi, Mr. Hideki. Yoshikawa and Mr. Hidefumi Iga for the micropatterned surface preparation.

Meanwhile, I appreciated the great help and invaluable friendship from all my past and present colleagues in the University of Montreal. I will never forget their kindness and discussions during my PhD stage. My sincere thanks also go to Ms. Patricia Moraille and Dr. Cedric Malveau for the help of AFM and NMR measurement.

I am also thankful for my progress report committee members: Prof. Jean-Francois Tanguay and Prof. Grégoire Leclair for their availability and thoughtful discussions.

I also greatly appreciated all the financial support from following institutes and agencies: Faculty of Pharmacy, University of Montreal, China Scholarship Council (CSC), Natural Sciences and Engineering Research Council (NSERC), and World Premier International Research Center Initiative (WPI).

Finally, I would like to show my heartfelt thanks to my beloved family for their constant and unconditional love. Their sacrifice and dedication in the past few year would engrave on my memory forever.

# CHAPTER ONE

## Introduction and Literature Review

### 1.1 Estrogen in cardiovascular medicine

#### 1.1.1 Introduction to coronary artery heart disease

Cardiovascular diseases (CVDs), which cover a variety of dysfunctions in tissues ranging from the cardiac muscle to the vascular system, are associated with a high rate of mortality and morbidity worldwide.<sup>[1, 2]</sup> Coronary artery heart disease (CAHD), also known as atherosclerosis, is one of the most severe CVDs, and is characterized by the deposition of cholesterol and accumulation of plaque within the arterial wall.<sup>[3]</sup> Epidemiological studies indicate that the causes of CAHD are diverse, including environmental influences (e.g. hormonal changes due to long-term smoking) and chronic physiological disorders (e.g. hypertension and diabetes).<sup>[4]</sup> The long-term consequences of atherosclerosis may include thrombus formation, which can lead to an acute myocardial infarction.<sup>[5]</sup> Acute myocardial infarction can be fatal, as it leads to a reduction in the oxygen supply (perfusion) to the heart, as well as creating an abnormality in myocardial energy metabolism.<sup>[6]</sup> To reduce the risk of myocardial infarction death, anticoagulant drugs, such as heparin<sup>[7]</sup> and warfarin<sup>[8]</sup>, are widely prescribed in clinics. However, those drugs are associated with an increased risk of bleeding in some patients, which can lead to imbalanced hemostasis.<sup>[9]</sup> Thus, there is currently an incentive to develop novel medical intervention strategies that reduce the incidence of CAHD.<sup>[10]</sup>

Coronary artery bypass graft (CABG) surgery, percutaneous transluminal coronary angioplasty (PTCA), and endovascular stenting are current clinical strategies for the revascularization of atherosclerotic arteries and can significantly increase the life expectancy and quality of life for some patients.<sup>[11, 12]</sup> For example, patients treated by CABG surgery had a significantly lower mortality than a control group, when comparing mortality at 5 years (10.2% vs 15.8%), and 10 years (26.4% vs 30.5%) post-intervention.<sup>[13]</sup> At 12 months, the

rates of death and myocardial infarction were similar between the CABG and percutaneous coronary intervention (PCI), patients, but stroke was significantly more likely to occur with CABG (2.2% vs. 0.6% with PCI).<sup>[14]</sup> However, adverse cardiac complications were significantly higher in the PCI group (17.8%, vs. 12.4% for CABG), likely because of an increased rate of repeat revascularization. In conjunction with surgical treatment, novel medical devices (e.g. artificial heart valve or stent) are also being developed for the amelioration of these cardiovascular diseases, which will greatly enhance the quality of patients' lives.<sup>[15]</sup>

### **1.1.2 The anatomy and physiology of blood vessels**

One of the therapeutic targets of coronary artery heart disease is the blood vessel, which is the main part of the circulatory system for nutrients and oxygen transportation throughout the body. They are classified as arteries, capillaries, and veins.<sup>[16]</sup> The inner wall of the blood vessels is lined with endothelial cells. These endothelial cells comprise the endothelium, which provides a mechanical barrier against the circulating blood. They also act as an interface that can sense alterations in blood flow and plasma constituents, as well as secrete a variety of powerful chemical mediators that regulate vascular remodeling.<sup>[17]</sup> In contrast, smooth muscle cells are located principally along the outer layer of the endothelium. They are also involved in biochemical vaso-regulatory processes, but in a far less efficient manner than endothelial cells.<sup>[18]</sup> Interactions between endothelial cells and smooth muscle cells are crucial to determine various pathophysiology of cardiovascular systems, including arteriogenesis and atherosclerosis<sup>[19]</sup>

Nitric oxide (NO) is a gaseous free radical cellular messenger generated by three types of nitric oxide synthases (NOS): neuronal (nNOS), inducible (iNOS) and endothelial NOS (eNOS).<sup>[20]</sup> NO is an important signal molecule produced by endothelial cells, serving to inhibit platelet aggregation, leukocyte adhesion, and smooth muscle cell proliferation.<sup>[21]</sup> Moreover, NO is recognized for its protective role within the vasculature by preventing biochemical cascades leading to thrombus formation.<sup>[22]</sup> For example, it has been shown that NO exerts a protective effect on vasculature through inhibiting platelet aggregation in a

transgenic mouse model. Blood clotting time was markedly decreased in eNOS-deficient versus *wild-type* mice ( $77\pm 3$  versus  $133\pm 3$  seconds).<sup>[23]</sup>

### 1.1.3 Estrogen effects on the cardiovascular system

17 $\beta$ -estradiol (E2) is a female hormone produced by human ovaries that controls and regulates several physiological conditions. Synthetic estradiols are used in contraception and in hormonal replacement therapy (HRT) for menopausal women.<sup>[24]</sup> For example, ethinyl estradiol (EE2), which mimics the endocrine properties of E2, is used in oral contraceptive formulations such as Norlestrin, Brevicon, and Ortho–Novum.<sup>[25]</sup> As such, estradiol plays critical roles in female sexual maturation and reproduction by initiating epithelial proliferation of the vagina, uterus, and breast.<sup>[26]</sup> It has been observed that the incidence of cardiovascular disease differs significantly between men and women, or between premenopausal women and postmenopausal women. This fact hinted that E2 may confer cardio-protective effects in addition to its hormonal functions.<sup>[27, 28]</sup> In cardiological studies, E2 has been shown to decrease the development of atherosclerosis and to elicit protection against ischemia by directly exerting the effects within the blood vessels.<sup>[29]</sup> Moreover, it has been reported that the local delivery of E2, *via* either an infusion catheter<sup>[30-32]</sup> or phosphorylcholine-coated stent, inhibited neointimal proliferation in coronary arteries following stent implantation.<sup>[33]</sup>

### 1.1.4 Estrogen receptors and classical genomic effect

E2 acts as a mediator via binding estrogen receptors (ERs).<sup>[34]</sup> ERs exist in two main forms, ER $\alpha$  and ER $\beta$ , encoded by two genes, ESR1 and ESR2, respectively, that are discovered at different chromosomal locations.<sup>[35]</sup> E2 passively diffuses into the cells where it binds to ERs in the nucleus.<sup>[36]</sup> Once bound, the estrogen receptor dimerizes and converts to an activated form. The dimerized ERs bind estrogen response elements (EREs) in the enhancer regions of estrogen-responsive genes, thereby activating the transcription of estrogen-inducible genes.<sup>[37]</sup> This phenomenon is regarded as a genomic effect or nucleus effect.<sup>[38]</sup> It is also interesting to note that this effect has also been shown to promote the proliferation, angiogenesis, and metastasis of tumor cells, which causes non-negligible adverse effect.<sup>[39]</sup> There are multiple pathways to induce this genomic effect:<sup>[40]</sup> A) E2-nucleus ER complexes

bind to estrogen receptor elements (EREs) at the promoter regions of target gene, thereby inducing their expressions (ERE-dependent genomic pathway). B) E2-nucleus ERs complexes bind to transcription factor complexes (ERE-independent genomic pathway). C) Instead of E2, growth factors themselves are also able to activate multiple kinase cascades and induce phosphorylation of nuclear estrogen receptors (Growth factor-dependent genomic pathway).

### 1.1.5 Estrogen non-genomic effect

E2 can trigger several alternative pathways *via* direct or indirect signal transduction rather than through the genomic effect. These pathways are regarded as the non-genomic effects<sup>[41]</sup> that are initiated on either the membrane or the cytosolic sides of the cell (Figure 1.1).<sup>[38]</sup> E2-elicited non-genomic effects are very rapid (seconds to minutes) in comparison to the activation of genomic-mediated effects (hours to days).<sup>[42]</sup>

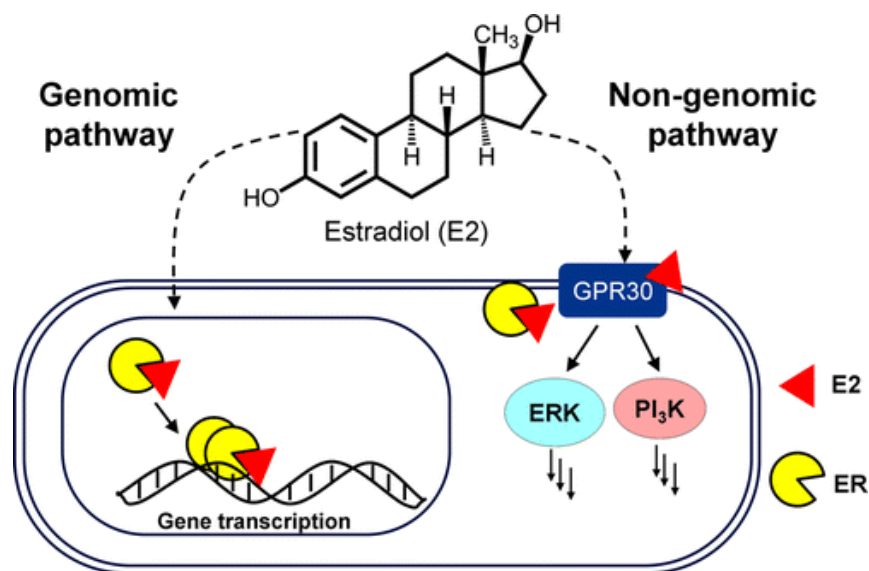


Figure 1.1 Schematic representation of the genomic and nongenomic estrogen pathways. For the genomic pathway, E2 (red triangle) crosses the cell membrane and binds to the estrogen receptor (ER) in the cell nucleus, inducing gene transcription. For the non-genomic pathway, E2 interacts with ER or ER/GPR30 on the cell membrane, which activates several transduction pathways (Figure taken from [43]).



Extracellular-signal-regulated kinase (ERK), a component of the mitogen-activated protein kinase (MAPK) family, and AKT kinase, a component of the phosphatidylinositol-4, 5-bisphosphate 3-kinase (PI3K) family, are involved in E2-mediated responses.<sup>[42, 44-47]</sup> In the ERK/MAPK pathway, the E2-induction is associated with several phosphorylation cascades.<sup>[48, 49]</sup> The majority of studies in MCF-7 cells reported the activation of ERK1/2 by E2 ranging from 2 to 15 min of its activity.<sup>[48, 50-53]</sup> But, some studies under similar conditions described E2 leading to elevations in ERK1/2 activity only after 2 h of induction, with persistent activation for up to 1 day.<sup>[54, 55]</sup> The difference in these results might originate from the differed cell culture methods. In the PI3K/AKT pathway, E2 leads to the release of nitric oxide (NO),<sup>[56]</sup> cyclic amines (cAMP, cGMP)<sup>[57, 58]</sup> and calcium<sup>[59]</sup> in a variety of cell types. Moreover, E2-induced non-genomic effects trigger the activation of phospholipase C (PLC)/protein kinase C (PKC) signal transduction pathways.<sup>[60]</sup> The cell signal pathways triggered by E2 non-genomic effects are summarized in the Table 1.1.

Table 1.1 Summary of the E2 non-genomic effects

Signal pathway	Time	E2 dose	Analyzed Protein	Cell line
PI3K/AKT <sup>[56]</sup>	5 to 30 mins	25 nM	PI3K/AKT and eNOS	HUVEC
PI3K/AKT <sup>[61]</sup>	15 mins to 2 hrs	1 $\mu$ M	PI3K/AKT	Endometrial cancer cells
PI3K/AKT <sup>[62]</sup>	0 to 60 mins	10 nM	PI3K/AKT	HepG2 cells
ERK/MAPK <sup>[50]</sup>	15 min to 1 day	1 $\mu$ M	pERK 1/2	HepG2 cells
ERK/MAPK <sup>[51]</sup>	2 min to 2 hrs	10 nM	pERK 1/2	MCF-7 cells
ERK/MAPK <sup>[52]</sup>	15 min	10 nM	pERK 1/2	MCF-7 cells

It has also been hypothesized that E2 exerts non-genomic actions by interacting directly with growth factor receptors.<sup>[63]</sup> This process is directed through E2-mediated tyrosine kinase's activation of growth factor receptors, such as the epidermal growth factor receptor (EGFR).<sup>[64, 65]</sup> The activation of growth factor receptors, in turn, triggers downstream cell signal transduction cascades such as MAPK.<sup>[49, 66]</sup>

Other studies reported that the E2-induced non-genomic effect was mediated through a G protein-coupled transmembrane receptor, GPR30.<sup>[67]</sup> Recent studies have also implicated GPR30 as a potential candidate for the activation of membrane-initiated estrogen signaling.<sup>[68]</sup> Supporting this claim, it has been demonstrated that GPR30 increased both ER- $\alpha$  and EGFR activities in patients undergoing clinical treatment for breast cancer.<sup>[69]</sup> However, the assumption, that GPR30 is responsible for an E2-mediated non-genomic effect is still under dispute.<sup>[63]</sup>

### **1.1. 6 Tools for estrogen non-genomic effect study**

Estrogen conjugated to membrane-impermeable proteins, e.g. E2-BSA, have been used to determine the non-nuclear ER actions in various cell types.<sup>[70-72]</sup> However, freshly prepared solutions of E2-BSA always contain free E2 which cannot be fully removed during the synthesis process. Moreover, E2-BSA binds to the ER only poorly because certain E2-BSA preparations are of very high molecular weight, suggesting extreme high steric hindrance.<sup>[73]</sup> Last, but maybe not least, E2-BSA is readily degraded by the cell, making long-term experiments problematic and *in vivo* studies impossible.<sup>[74]</sup>

Recently, an estrogen dendrimer conjugate (EDC) has been prepared for the stimulation of membrane-mediated non-genomic effects.<sup>[75]</sup> Such E2-dendrimer systems also activated vascular endothelial cell migration, which could regulate the processes of cardiovascular protection without enhancing growth of breast cancer cells.<sup>[76]</sup> Nonetheless, confocal microscopic studies showed that EDC can also penetrate into cytoplasmic sites at MCF-7 cells. As a result, a detailed profile of an estrogen-initiated short-term signaling pathway has not been elucidated yet as using the estrogen conjugate systems.

## 1.2 Polymeric biomaterials in cardiovascular medicine

### 1.2.1 Fundamental properties of polymeric biomaterials

Polymeric biomaterials are widely developed for *in vitro* and *in vivo* applications to study complex biological phenomena.<sup>[77]</sup> The essential design criteria for polymeric biomaterials are related to their high-quality performance, structural and functional stability, and physiological compatibility.<sup>[78]</sup> To date, various polymeric materials have been tested for the preparation of biomaterials, these include polystyrene,<sup>[79]</sup> poly(methyl methacrylate) (PMMA),<sup>[80]</sup> polydimethylsiloxane (PDMS),<sup>[81]</sup> and polyurethane.<sup>[82]</sup> For example, PMMA is a transparent polymer commonly known as Plexiglass.<sup>[83]</sup> Thin films of PMMA can be modified by aminolysis reaction to introduce amine groups,<sup>[84]</sup> which can confer resistance against non-specific protein adsorption.<sup>[80]</sup> PDMS is the most commonly used material for the preparation of microfluidic devices due to its elastomeric properties and ease in molding.<sup>[85]</sup> PDMS micro-fabricated surfaces were prepared as a synthetic cornea in an attempt to stimulate stromal restoration.<sup>[86]</sup> Once the polymeric biomaterials are placed into the biological environment, many factors should be considered: surface charge, surface topology, surface energy and chemistry, to name a few.<sup>[87]</sup> Therefore, it is critical to develop cost-effective and efficient approaches to understand the physical properties of polymeric biomaterials, and to widen the design parameters for suitable constructs.

### 1.2.2 Mechanical properties

In order to provide an appropriate microenvironment for supporting cells or entire tissues *in vitro* and *in vivo*, biomaterials should have reliable mechanical properties.<sup>[87, 88]</sup> Generally, once biomaterials enter in contact with living organisms, deformation of biomaterials or cells will occur due to forces exerted by external environment, e.g. blood stream. The elastic modulus (or modulus of elasticity) is a constant that define quantitatively the ability of a biomaterial to resist deformation under external force as well as to recover the initial state after removal of the force, including Young's modulus and shear modulus. Young's modulus is usually expressed as E, representing the elastic resistance of objects to

tensile strength e.g., elongation or compression. Young's modulus can be calculated by following equation (1):

$$E = \frac{\sigma}{\varepsilon} \quad (1)$$

where  $E$  is the Young's modulus,  $\sigma$  is the tensile strength,  $\varepsilon$  is the extensional strain.

Shear modulus is usually expressed as  $G$ , representing the resistance of objects to deformation in shear. The relation between shear modulus ( $G$ ) and Young's modulus can be expressed as following equation (2):

$$G = \frac{E}{2(1+\nu)} \quad (2)$$

where  $E$  is Young's modulus,  $\nu$  is Poisson's ratio.<sup>[89-92]</sup>

Moreover, some soft biomaterials, such as hydrogels, exhibit both viscous and elastic characteristics, which are recognized as viscoelasticity. Viscoelasticity is composed of the storage modulus  $G'$ , which defines the elastic property of materials and the loss modulus and  $G''$ , which governs the viscous property of materials.<sup>[93-96]</sup> Both  $G'$  and  $G''$  can be characterized by a power-law frequency dependence with critical exponents  $\alpha$  and  $\beta$ , respectively ( $G' \propto f^\alpha$  and  $G'' \propto f^\beta$ ). Knowing the viscosity of material  $\eta(f)$ , the loss modulus can be calculated based on the equation (3):

$$G''(f) = 2\pi f \eta(f). \quad (3)$$

Polymeric biomaterials have a wide range of elasticity values ( $E$  or  $G'$ ) from a few Pa to hundred MPa in a similar range of tissue or organs *in vivo*, which could offer various choices for the biomedical applications.<sup>[98]</sup> For example, the elastic modulus of synthetic PEG is in a range of a few kPa, and could be used to prepare extra cellular matrices (ECMs) to support cell and tissue growth in a three dimensional manner.<sup>[99, 100]</sup> By tuning the elastic modulus of polyacrylamide gel based substrate from 1 kPa to 100 kPa, adult human mesenchymal stem cells (hMSCs) differentiate into neuron, muscle, or osteogenic cells, respectively.<sup>[101]</sup> Thus, a substantial understanding of the intrinsic mechanical properties of

polymeric biomaterials will facilitate the design and development of functional biomaterials more efficiently.

### 1.2.3 Biodegradability

The term of biodegradation is generally defined as the breakdown of the polymer materials by the hydrolytic or enzymatic cleavage reactions.<sup>[102]</sup> For tissue engineering applications, it is desirable to develop biodegradable polymer materials with predictable erosion kinetics. Hydrolysis is a major degradation mechanism *in vivo* that degrades larger polymer chains to smaller chains or monomers.<sup>[103]</sup> The effect of pH is critical in this hydrolytic process.<sup>[104]</sup> For example, polylactide (PLA) polymers have the slowest hydrolysis rate at pH~4.<sup>[105]</sup> Enzymatic cleavage is another important mechanism for polymer degradation.<sup>[106]</sup> The rate of *in vivo* enzymatic degradation of polymers depends on the distribution and concentration of the cleavage enzymes.<sup>[107]</sup> In most of cases, hydrolytic and enzymatic cleavage reaction occurs simultaneously.<sup>[108]</sup>

Both natural and synthetic polymers have been extensively investigated as biodegradable biomaterials. Natural polymers are promising due to their susceptibility to *in vivo* degradation.<sup>[109]</sup> For example, cellulose is a main composition of plants and natural fibers, which is degradable by several microorganisms. Cellulose-based hydrogels can facilitate the scarless healing processes upon degradation.<sup>[110]</sup> Synthetic polymers also demonstrate biodegradability and easily undergo chemically-tailored reactions for specific biomedical applications.<sup>[111]</sup> For example, by grafting PEG to a synthetic biodegradable polycarbonate, the degradation takes place within one day. It may be useful in clinical applications ranging from cosmetic surgery to cancer treatment.<sup>[112]</sup> As a consequence, investigations into polymeric materials will help to develop safe and environment friendly products by taking advantage of their biodegradable properties.

### 1.2.4 Cellular interactions

The interactions between cells and implanted biomaterials, especially cell adhesion to surfaces, are determined by the nature of biomaterials.<sup>[113]</sup> When deposited on an adhesive substrate, cells are favorable to be spread out. As given a certain time, the cells proliferate and

form a two-dimensional monolayer. However, when the spreading of cells is unfavorable, e.g. in the case of non-adhesive surfaces, cells spontaneously move by active cell motility and eventually meet to form compact clusters and three-dimensional aggregates (spheroid).<sup>[114, 115]</sup> The forces influencing cell adhesion include:

(1) Surface energy interaction. The primary factor of cell adhesion to the surface relies on the balance of surface energy, e.g. surface hydrophobicity and hydrophilicity.<sup>[116]</sup> Generally, surfaces with high-energies are able to enhance cell adhesion compared with surfaces with low-energies.<sup>[117]</sup> As a result, surfaces with high-energies are usually used for the cellular adhesion.

(2) Electrostatic interaction. Because a major part of the cell membrane is negatively charged, the surface charges of the biomaterial surfaces are usually designed to be positive to ensure cell adhesion.<sup>[118]</sup>

(3) ECM protein interaction. ECM proteins, such as fibronectin, can easily adsorb onto the biomaterial surfaces due to their wide-spread existence *in vitro* and *in vivo* environments, suggesting that the influence of these proteins is also predominant in the process of cell adhesion.<sup>[119, 120]</sup>

Functionalized surfaces that are able to induce, in a predictable way, cell adhesion will be useful. For example, a thermosensitive polymer poly (N-isopropylacrylamide) (PNIPAM) is able to undergo phase transition from hydrophilic to hydrophobic by tuning the temperature from room temperature to physiological conditions (~37 °C).<sup>[121]</sup> PNIPAM was recently used to prepare thermosensitive functionalized surfaces for harvesting cells in a confluent monolayer. This novel cell culture platform allows formation of cell monolayers in an environment that is more relevant to the real-life situation and hence transplantation-favorable to host tissues.<sup>[122, 123]</sup> To sum up, controlling the cellular responses, e.g. cell adhesion or cell spread, to biomaterials is a fundamental step in biomaterial research.

## 1.3 Non-fouling polymeric biomaterials in cardiovascular regenerative medicine

### 1.3.1 Overview of non-fouling polymeric biomaterials

Non-specific protein (e.g. fibrinogen, fibronectin, and vitronectin) adsorption<sup>[124]</sup> and blood cell adhesion<sup>[116]</sup> onto a biomaterial surface triggers a foreign body reaction which can lead to detrimental consequences.<sup>[125]</sup> This process is known as biofouling or fouling.<sup>[116]</sup> Non-fouling is the term used to define the ability of a material to resist non-specific protein adsorption and blood cell adhesion *in vivo* and hence to not cause adverse effects when they are placed in contact with living organisms.<sup>[126]</sup> Several properties of polymeric materials, such as their composition, hydrophobicity/hydrophilicity, charge, and topology are responsible for biocompatibility.<sup>[127]</sup> The origin of the non-fouling characteristic of a polymeric biomaterial is due to the formation of a highly hydrated layer near the surface, which generates an energetic barrier to prohibit immune responses occurrence.<sup>[128, 129]</sup> The mechanism of non-fouling characteristic of polymeric materials can be explained as follows. Briefly, the polar groups of proteins can form hydrogen bonds with the surrounding water medium. However, if the surface of polymeric materials (e.g. PEG) is very hydrophilic, the water molecules can penetrate into the polymers to form a net-like structure, which is regarded as the “surface-bound” water. Meanwhile, both the protein and material surface tend to expulse water molecules to facilitate protein adsorption, which generate physical and energetic barriers (also known as dehydration entropic effects).<sup>[126, 130]</sup> The non-fouling characteristic of polymeric materials is fundamentally determined by numerous factors, i.e. film thickness and packing density or chain conformation and flexibility.<sup>[130]</sup> As a result, non-fouling characteristic is certainly one of the most significant characteristics of biomaterials, when considering their practical biomedical applications.

Poly (ethylene glycol) (PEG), zwitterionic-based materials, and some polysaccharides are among the most widely used non-fouling materials (summarized in the Table 1.2).<sup>[131, 132]</sup> PEGylated materials are the most commonly used biomaterials due to their highly hydrophilic and flexible nature. As introduced previously, a water barrier can be generated between PEG and proteins to entropically impede non-specific adsorption occurrence.<sup>[128]</sup> Moreover, the

high chain flexibility of PEG yields compression of chains and hence sterically repulses protein adsorption.<sup>[133]</sup> The end of PEG can be tailored by different functional moieties, such as thiol, amine, and carboxylic acid, for the different biological applications.<sup>[130]</sup> For example, thiol end functionalized PEG enables its immobilization onto gold surfaces and the thickness of the PEG layer is correlated with the response to the biological environment.<sup>[134]</sup> Zwitterionic-based materials, such as phosphorylcholine, sulfobetaine, and carboxybetaine derivatives (structures shown in Fig. 1.2), possessing covalently linked cationic and anionic groups,<sup>[135]</sup> are known to reduce non-specific protein adsorption and inhibit cell adhesion.<sup>[136, 137]</sup> Phosphorylcholine (PC) is present on phospholipids of the outer layer of the cell membrane. It has an excellent ability to reduce nonspecific protein adsorption.<sup>[138]</sup> The key factors, e.g. hydration and ionic solvation, leading to the non-fouling behavior of PC were determined by molecular simulation techniques.<sup>[139]</sup> Similar to phosphorylcholine, both sulfobetaine (SB) and carboxybetaine (CB) also showed strong anti-fouling capacities.<sup>[140, 141]</sup> When poly-(sulfobetaine) was grafted onto a poly-(ether urethane) surface by atom-transfer radical-polymerization(ATRP), the surface exhibited extremely low fibrinogen adsorption.<sup>[142]</sup>

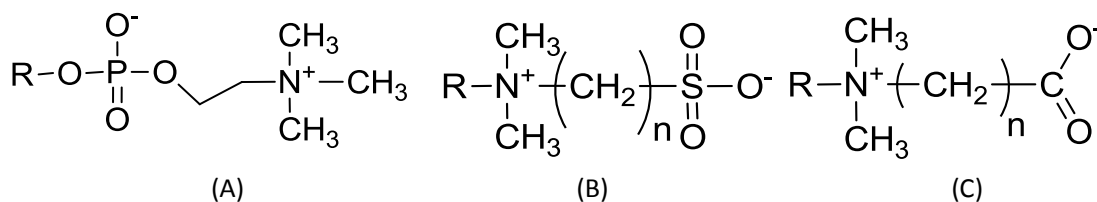


Figure 1.2 Chemical structures of zwitterionic-based materials. (A) phosphorylcholine (PC), (B) sulfobetaine (SB), and (C) carboxybetaine (CB).

The natural polysaccharide heparin, a potent anticoagulant, has shown promising biomedical applications due to its antimicrobial and anti-inflammatory capacities.<sup>[143-145]</sup> It is a glycosaminoglycan consisting of a sulfated disaccharide repeat unit (Fig.1.3A). The most common disaccharide unit is composed of a 2-O-sulfated iduronic acid and 6-O-sulfated, or N-sulfated, glucosamine.<sup>[146]</sup> The molecular weight of heparin ranges from 4 to 40 kDa.<sup>[147]</sup> Heparin, which is a polyanion, adopts an extended conformation *in vivo*.<sup>[148, 149]</sup> Heparin-coated surfaces showed a good biocompatibility, which decreases the incidence of restenosis



and reduces thrombogenesis and inflammatory reactions.<sup>[150]</sup> Hyaluronic acid (HA) is anionic polysaccharide, composed of *D*-glucuronic acid and *D*-N-acetylglucosamine, linked *via* alternating  $\beta$ -1,4 and  $\beta$ -1,3 glycosidic bonds (Fig. 1.3B).<sup>[151]</sup> The molecular weight of HA ranges between 100 kDa to 8000 kDa *in vivo*.<sup>[152]</sup> The glucuronic acid, carboxylic acid, the primary and secondary hydroxyl, and the *N*-acetyl groups of HA can be chemically modified for conjugating different moieties in order to prepare HA-based hydrogels.<sup>[153]</sup> HA hydrogels can promote the proliferation and migration of mesenchymal cells and enhance the endogenous tissue repair process.<sup>[154]</sup> The ultralow protein adsorption of HA is also demonstrated by surface plasmon resonance (SPR) (only 0.6–16.1 ng/cm<sup>2</sup>).<sup>[155]</sup> Chitosan is a cationic polysaccharide extracted from *N*-acetylation of chitin.<sup>[156]</sup> It has been studied for applications in several fields,<sup>[157]</sup> such as wound healing,<sup>[158]</sup> drug delivery,<sup>[159]</sup> gene therapy,<sup>[160]</sup> and tissue engineering.<sup>[161]</sup> It is a linear polycation composed of  $\beta$ -*D*-glucosamine and  $\beta$ -*D*-N-acetylglucosamine residues in 1→4 linkages (Fig. 1.3C).<sup>[162]</sup> It is soluble in acidic solutions, but it is poorly soluble in neutral pH conditions.<sup>[163]</sup> Moreover, the solubility of chitosan is highly associated with degradability, which is decided by its physical and chemical properties, such as deacetylation and molecule weight.<sup>[164]</sup> For instance, deacetylation can not only affects the degradation rate, but also enhance the solubility of chitosan at neutral pH.<sup>[164, 165]</sup> The molecular weight also affects chitosan solubility.<sup>[166]</sup> If chitosan was degraded into low molecular weight chitosan (LMWC) with the molecular weight below 10Da, the water solubility of chitosan largely increased.<sup>[167]</sup> The non-fouling nature of chitosan was also widely acknowledged. In a previous study, it was also demonstrated that chitosan nanocoating protects against adsorption of BSA, TGF- $\beta$ 1 and human plasma due to its surface hydrophilicity.<sup>[168]</sup> Chitosan has also been developed as scaffold for wound healing purposes because of its antibacterial activity.<sup>[169]</sup> By using heparin /chitosan blended films, such antibacterial activity was further enhanced.<sup>[170]</sup> Besides its biodegradability and non-fouling features, chitosan also has cell adhesive properties as a artificial component of the extracellular matrix.<sup>[171]</sup> Chitosan films are known to support cell adhesion, as has been observed in the cases of dorsal root ganglions,<sup>[172]</sup> keratinocytes, and fibroblasts.<sup>[173]</sup>

Take these facts together, non-fouling materials should be extensively used in the cardiovascular regenerative medicine in order to produce neither inflammatory nor immune responses, while retaining the capacity of cell adhesion.

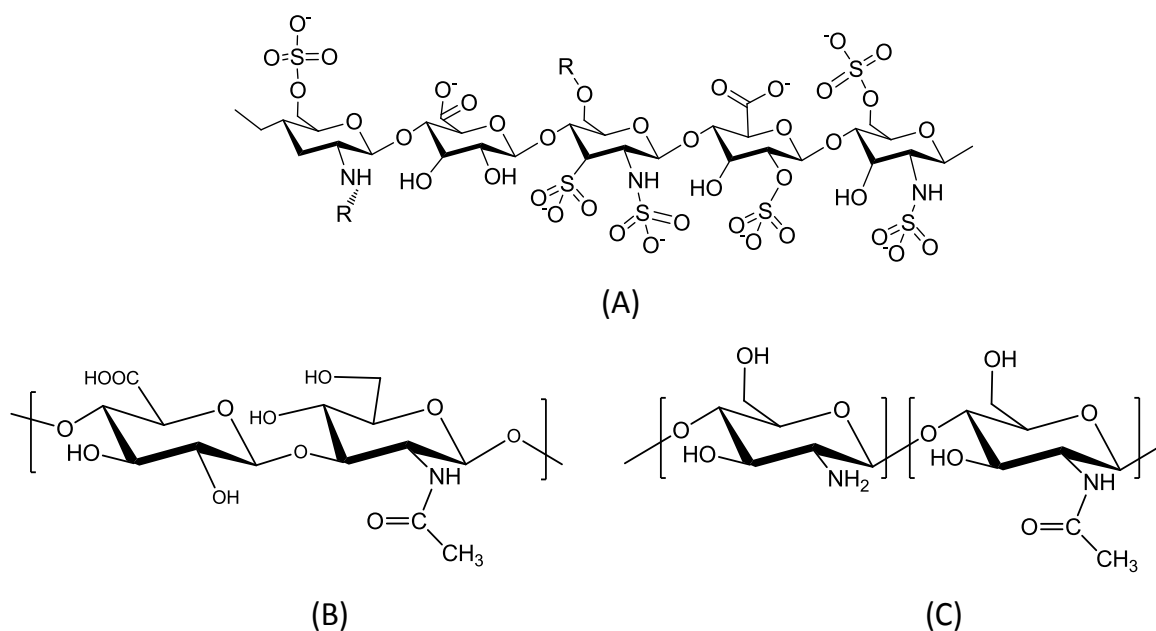


Figure 1.3 Chemical structures of natural polysaccharides. (A) heparin, (B) chitosan, and (C) hyaluronic acid.

Table 1.2 Summary of non-fouling materials

Polymer	Preparation method	Surface characterization method	Method to assess biocompatibility
PEG <sup>[134]</sup>	Self assembled monolayer	Ellipsometry, AFM	Endothelial cells adhesion kinetics study
PEG-block-polycarbonate <sup>[174]</sup>	Covalently immobilization	QCM-D, SEM	Bacterial viability assay, platelet adhesion study, static hemolysis assay
Catecholates anchored PEG <sup>[175]</sup>	Chemical deposition	Ellipsometry	Human blood assay, bone-derived stromal cells, bacterial adhesion
PC <sup>[135]</sup>	Self assembled monolayer	XPS, ellipsometry, SPR	Human Fg and BSA adsorption study
Poly(sulfobetaine methacrylate) <sup>[176]</sup>	Chemical deposition	ATR/FT-IR, XPS, SEM	BSA adsorption study
Carboxybetaine <sup>[177]</sup>	Self assembled monolayer	Contact angle measurement, XPS, QCM-D	BSA adsorption and blood cell adhesion study
Carboxybetaine graft polysiloxanes (PDMS- <i>g</i> -CB) <sup>[178]</sup>	Chemical deposition	ATR/FT-IR, XPS, SEM, contact angle measurement	BSA, Hgb and lysozyme adsorption study
HA <sup>[155]</sup>	Covalently immobilization	Contact angle measurement, AFM, SPR	BSA, lysozyme and soybean milk adsorption study
Chitosan <sup>[168]</sup>	Physical adsorption	SEM, AFM, MTT viability test.	BSA, human blood adsorption study

### 1.3.2 Non-fouling polymeric biomaterials in cardiovascular regenerative medicine

Implantable biomaterials or blood contact devices are widely used to cure cardiovascular diseases or alleviate symptoms.<sup>[179]</sup> One such example is the cardiovascular stent. Revascularization procedures, such as a coronary balloon angioplasty, are often accompanied by various complications (e.g. restenosis).<sup>[180]</sup> The introduction of a stent into an artery after angioplastic surgery can expand blood vessels and restore blood flow through narrowed arteries.<sup>[181]</sup> Silicone rubber or plastic was initially used to support the blood vessels in order to maintain the intravascular blood flow.<sup>[182]</sup> Stainless steel AISI 316L<sup>[183]</sup> or titanium (Ti)<sup>[184]</sup>, possessing exceptional corrosion resistance and mechanical properties, are the commonly used medical metals for cardiovascular stent nowadays. However, it is widely acknowledged that dominant side effect can be induced by these bare metal stents (BMS), e.g., late in-stent restenosis, a phenomenon that reoccurs of angina.<sup>[185, 186]</sup> Recently, synthetic or natural polymer coated drug-eluting stents have proven to be superior to BMS in many respects.<sup>[187, 188]</sup> They are able to reduce significantly the incidence of restenosis by locally-controlled release of drugs to the neointimal and inflammatory areas.<sup>[189]</sup> In order to be usable, the polymer coating material must support the vessel lumen to maintain its patency, and naturally degrade within a certain time. Nowadays, two types of commercially available DESs are available (Cypher® and Taxus®) which are the most widely used in the clinical setting. They have embedded anti-proliferative agents (Rapamycin in the case of Cypher®<sup>[190]</sup> and paclitaxel in the case of Taxus®<sup>[191]</sup>) with hydrophobic polymer surfaces. However, both Cypher® and Taxus® have some drawbacks. For example, they use durable thick polymers ((polyethylene vinyl acetate (PEVA)/ poly(butyl methacrylate (PBMA) for Cypher® and poly(styrene-*b*-isobutylene-*b*-styrene) for Taxus®).<sup>[192]</sup> As a result, new generation of polymer coated stents are still highly in demand. A PEG-coated titanium surface shows excellent blood compatibility by resisting platelets and leukocytes adhesions.<sup>[193]</sup> In a porcine coronary restenosis model, grafting PEG to the biodegradable polymer poly(D, *L*-lactide-*co*-glycolide) (PLGA), significantly inhibited neointimal hyperplasia 1 month after of implantation.<sup>[194]</sup> Phosphorylcholine (PC) and sulfobetaine (SB) are also attracting attention as new generation of stent coating materials. Recently, a PC and SB derivative materials coated magnesium alloy

surface demonstrated promising results in the reducing acute thrombotic responses.<sup>[195]</sup> Especially, PC-coated stent is extensively studied both in pre-clinical and clinical trials. In the mid-term (6 months) results, the symptoms of acute myocardial infarction of the patients were also significantly alleviated after implanting PC-coated stent.<sup>[196]</sup> The reliability of PC-coated stents was also validated in the long-term assessment.<sup>[197]</sup>

Another example of polymeric materials being used in cardiovascular medicine is vascular grafting. In arterial bypass procedures, synthetic polymers are widely used to redirect blood flow in the specific site of the body and have shown an excellent 5 year survival rate for the patients (exceeding 95 %).<sup>[198]</sup> The approach for reconstructing and remodeling tissues is to recruit autologous endothelial cells (EC) or endothelial progenitor cells (EPC) after implantation of the graft and to promote similar neovascularization to a native vessel by supporting local angiogenesis.<sup>[199, 200]</sup> This *in situ* endothelialization of a vascular graft following implantation is a promising solution for enhancing graft patency rates.<sup>[201]</sup> Commercially available synthetic vascular graft materials are either expanded polytetrafluoroethylene (ePTFE) or poly(ethylene terephthalate) (Dacron).<sup>[202]</sup> In some cases, the diameter of grafts should be as small as possible, in order to reach the target vessel site through narrow vasculature. However, these materials are not suitable for smaller-diameter (with internal <6 mm) tubes used in vascular bypass surgery, resulting in a high rate of graft failure.<sup>[203]</sup> The major reason is that they increase the risk of thrombus due to their low biocompatibility.<sup>[204]</sup> In this aspect, non-fouling polymer coating surfaces can be utilized as an alternative. For example, the PEG was grafted onto poly-(ethylene terephthalate) (PET) and greatly improved hemo-compatibility of the PET surfaces.<sup>[205]</sup> In addition, the PEG grafted PET was prepared to generate polymer brushes *via* a surface-initiated atom-transfer radical polymerization method and showed an excellent anti-fouling effect during the platelet adhesion assays.<sup>[206]</sup> In a porcine model, grafting PEG to poly (propylene sulphide) effectively reduced thrombogenicity and enhanced the graft patency of small diameter vascular grafts.<sup>[207]</sup> In the clinical trial, PEG-hirudin/iloprost coated PTFE based small diameter grafts inhibited the progress of pseudointima and intimal hyperplasia in the patient as well.<sup>[208]</sup> However, *in vitro* regular 2-dimensional vascular graft based endothelialization is usually initiated by using cellular monolayer.<sup>[209]</sup> Unfortunately, the efficacy of 2-dimensional vascular graft for the

tissue rebuilding shows distinctive low-efficiency features compared to *in vivo* conditions, as endothelial cells are prone to apoptosis with respect to lack of oxygen and nutrition supply after engraftment in tissues.<sup>[210]</sup> In an effort to narrow the gap between *in vitro* and *in vivo* conditions, polymeric substrates have been developed to culture endothelial cells as multi-cellular 3D spheroids, in which the cells grow into a small capsule-like shape.<sup>[211]</sup> The advantages of such 3D spheroids cell culture have been well-acknowledged due to they can better mimic the real *in vivo* physiological conditions and they are currently being explored with the goal of developing efficient 3D vasculature or micro-vessel formation *in vivo* as well.<sup>[212-214]</sup>

Polysaccharide-based materials also played vital roles in cardiovascular regenerative medicine in terms of cardiac cell injection delivery system or implantable scaffold strategy.<sup>[215]</sup> Among them, hydrogels composed of hyaluronic acid (HA) were shown to induce neovascularization and enhance cardiac function in an animal model of myocardial infarction.<sup>[216]</sup> However, the poor performance of HA in terms of mechanical properties limits its direct clinical application.<sup>[217]</sup> In order to resolve this issue, varying amounts of methacrylate substitution of HA hydrogels were carried out conferring varied mechanical properties were injected into the heart.<sup>[218]</sup> Moreover, anionic polymer HA and cationic polymer chitosan were deposited by a layer-by-layer assembly approach for the preparation of polyelectrolyte multi-layers and used in the regeneration of blood vessels.<sup>[219]</sup> The excellent biocompatibility of these polyelectrolyte multi-layers enables the inhibition of blood clots on damaged arterial walls.<sup>[220]</sup> Further, the excellent mechanical performance of HA/chitosan multi-layers along with their high water content exhibited strong resistance against platelet adhesion.<sup>[183]</sup> In future, developing new-generation intelligent interfaces for cardiovascular regenerative medicine, e.g. a micro-fabricated polymeric scaffold that dynamically controls the cell's microenvironment in three dimensions and hence mimicks physiological conditions in a more real life manner, would be the next aim.<sup>[221, 222]</sup>

## 1.4 Methods and Techniques

In order to study physical chemistry properties of surface functional biomaterials, surface analytical tools with high sensitivities, such as SPR or QCM-D, are widely used to

detect the polymer/protein adsorption kinetics in real time. Those techniques are flexible to provide additional mechanical and biologically relevant information of biomaterials, which can mimic their interactions to bio-organisms under real physiological conditions. Moreover, some micro/nanotechnologies based techniques, such as photolithography, contributed to fabricate surface functional biomaterials in desired shapes or geometries, leading us to a better understanding of surface functional biomaterials' fundamental mechanisms. Herein, SPR, QCM-D and photolithography will be introduced as following sections.

### 1.4.1 Surface plasmon resonance technology (SPR)

Surface plasmon resonance technology (SPR) is a label-free analytical technique with high sensitivity to monitor biomolecular interactions in real-time.<sup>[223]</sup> It is widely used for the study of dynamic binding characteristics between receptor/ligand or antibody/antigen in the clinical diagnosis, gene sequencing, proteomics, cell signaling, drug screening, and environmental science.<sup>[224]</sup>

When a polarized incident light hits a metal interface at a certain critical angle, the total internal reflection occurs to the excitation of surface plasmon within the metal interface.<sup>[225]</sup> At the moment of surface plasmon resonance occurs, most of the incident light photons are absorbed, while the energy is transferred to the electrons. In the reflected light intensity response curve, a small peak could be observed corresponding to SPR minimum resonance angle,  $\Theta_m$ .<sup>[226]</sup> When specific molecule adsorption occurs on the metal surface, changes of SPR minimum resonance angle is accordance with the changes of refractive index of the metal surface, which are proportional to the molecular mass bound to the substrate.<sup>[227]</sup>

In 1983, Liedberg et al., firstly applied SPR technology to analyze antigen-antibody interaction.<sup>[228]</sup> In 1990, SPR was commercially available and used as a standard analytical tool in life sciences and pharmaceutical research.<sup>[229]</sup> Nowadays, SPR technology has been extended to the study of binding kinetics of biological molecules interactions, such as protein-protein/DNA,<sup>[230]</sup> drug molecule-target proteins<sup>[231]</sup> and other biological molecules. SPR also plays a vital role in monitoring estrogen biology. For instance, Rich et.al systematically investigated the binding affinity between ER- $\alpha$  and E2 with its derivatives by SPR.<sup>[232]</sup> SPR also was used to detect the presence of E2 in the water environment by immobilization of ER- $\alpha$  to a gold substrate as a biosensor.<sup>[233]</sup>

## 1.4.2 Quartz crystal microbalance with dissipation (QCM-D)

Quartz crystal microbalance with dissipation (QCM-D) is a cost-effective and high-resolution analytical technique to measure the surface mass changes caused by the specific adsorption of target molecules by the principle of piezoelectric effect of quartz crystal.<sup>[234]</sup> When an external voltage is applied on the quartz crystal sensor, the quartz crystal will oscillate at its fundamental resonance frequency.<sup>[235]</sup> The alternation of two parameters measured by QCM-D, resonance frequency ( $\Delta f$ ) and dissipation ( $\Delta D$ ), reflected the adsorbed mass and the viscoelastic properties of surface-bound materials.<sup>[236]</sup> The amount of adsorbed material for a thin, nondissipative layer can be calculated using the Sauerbrey equation.<sup>[237]</sup> However, the linear relationship between the adsorbed mass and  $\Delta f$  is invalid for hydrated layers characterized by high dissipation shifts. For such films, in order to calculate the adsorbed mass and viscoelastic properties, theoretical viscoelasticity modeling is necessary.<sup>[238]</sup> In the viscoelasticity model, the dissipation factor reveals the viscous losses induced by the deposited mass and carries information on the viscoelasticity of the adsorbed layer, reflecting the conformation and binding strength of the adsorbed layer.<sup>[239, 240]</sup>

Nowadays, QCM-D is widely applied into the measurement of physical and biological responses of proteins, nucleic acids, enzymes or cells, including signal transduction, antibody characterization and protein conformational changes.<sup>[241]</sup> In the estrogen biology, Su et al provided additional evidences of ER- $\alpha$  conformational changes after binding to an estrogen receptor element (ERE)-immobilized QCM-D crystal sensor.<sup>[242]</sup> In their subsequent study, they plotted of ER- $\alpha$  adsorption using  $\Delta D$  as a function of  $\Delta f$ , that reflected the dissipation changes depending on surface mass. It suggested that changes of formation occurred from a water-rich and a less structured protein layer in the case of non ERE-immobilized surface to a dehydrated and tightly-bound protein layer in the case of ERE-immobilized sensor surface.<sup>[243]</sup>

## 1.4.3 Photolithography

Micro/nanotechnologies engaged in the fabrication of biomaterials are classified as bottom-up or top-down approaches.<sup>[244, 245]</sup> A bottom-up approach consists in synthesizing the material from small species *via* physical interactions or chemical reactions. A top-down approach consists in starting with a bulk material and breaking it into smaller pieces using



mechanical, chemical, or other form of energy.<sup>[246]</sup> Photolithography is a highly accurate and reproducible top-down fabrication method to design micropatterning biosensors with wide ranges of sizes (from 10nm to 100µm).<sup>[247]</sup> In recent studies, photolithography is capable of coupling with molecular self-assembly bottom-up approach and fabricating unique functional micropatterning substrates for biological applications.<sup>[248]</sup> The patterning process by photolithography generally contains five stages: spin coating, baking, irradiation, developing, and lift-off. Briefly, a selective substrate is firstly coated with a thin layer (metal or biologically active molecules, such as aluminum, titanium, peptides, proteins, polymers, and etc.). After baking and spin-coating a photo-resist material layers, the substrate undergoes photo-irradiation. Then, a metal patterned thin layer is formed in an organic solvent (e.g., acetone) and finally processed post-modification with biologically active molecules.<sup>[249]</sup>

The applications of micropatterning technology range from drug screening to diagnosis of diseases.<sup>[250, 251]</sup> In the realm of drug screening, development of micropatterning technique can provide cost- and time-saving alternatives for *in vivo* animal experiments, and further to understand drug mechanisms on the single cell or gene hierarchy by fixing the cells in a sensitive site.<sup>[252]</sup> It greatly enhances the efficiency of high-throughput drug screening and reduces the drug development cycle. As a rapid and sensitive method, micropatterning based biosensors can be used to simplify the process of diseases diagnosis in early phase by integrating a variety of biological receptors.<sup>[253]</sup> In terms of tissue engineering applications, the morphology and elasticity of the micro-patterning surfaces is controllable, and hence to determine the fate of stem cells, such as attachment, growth, differentiation, and migration.<sup>[254]</sup> Furthermore, use of micro-patterning technique can construct biochips that sizes are in identical of single cells, which stimulates tissue regeneration and repair through mimicking a unique physiological environment.<sup>[255]</sup>

## **1.5 Project hypothesis, thesis rationale and research objectives**

### **1.5.1 Project hypothesis**

The research described in this thesis involves the preparation of surface-tethered E2 biomaterials by bottom-up and top-down approaches in order to systematically investigate the

potential applications of E2 in cardiovascular regenerative medicine and to understand the detailed biological mechanisms.

For the bottom-up approach, a hypothesis that CH-PC is an available polymer for the E2 tethering will be validated as shown in the Figure 1.4. We also set a premise that CH-PC-E2 conjugates can be self-assembled to functional films undergoing air-drying and rehydration process. Finally, CH-PC-E2 functional films recognize estrogen receptors in the cell membrane and stimulate cardiovascular protective molecule NO production that are beneficial to the cardiovascular system.

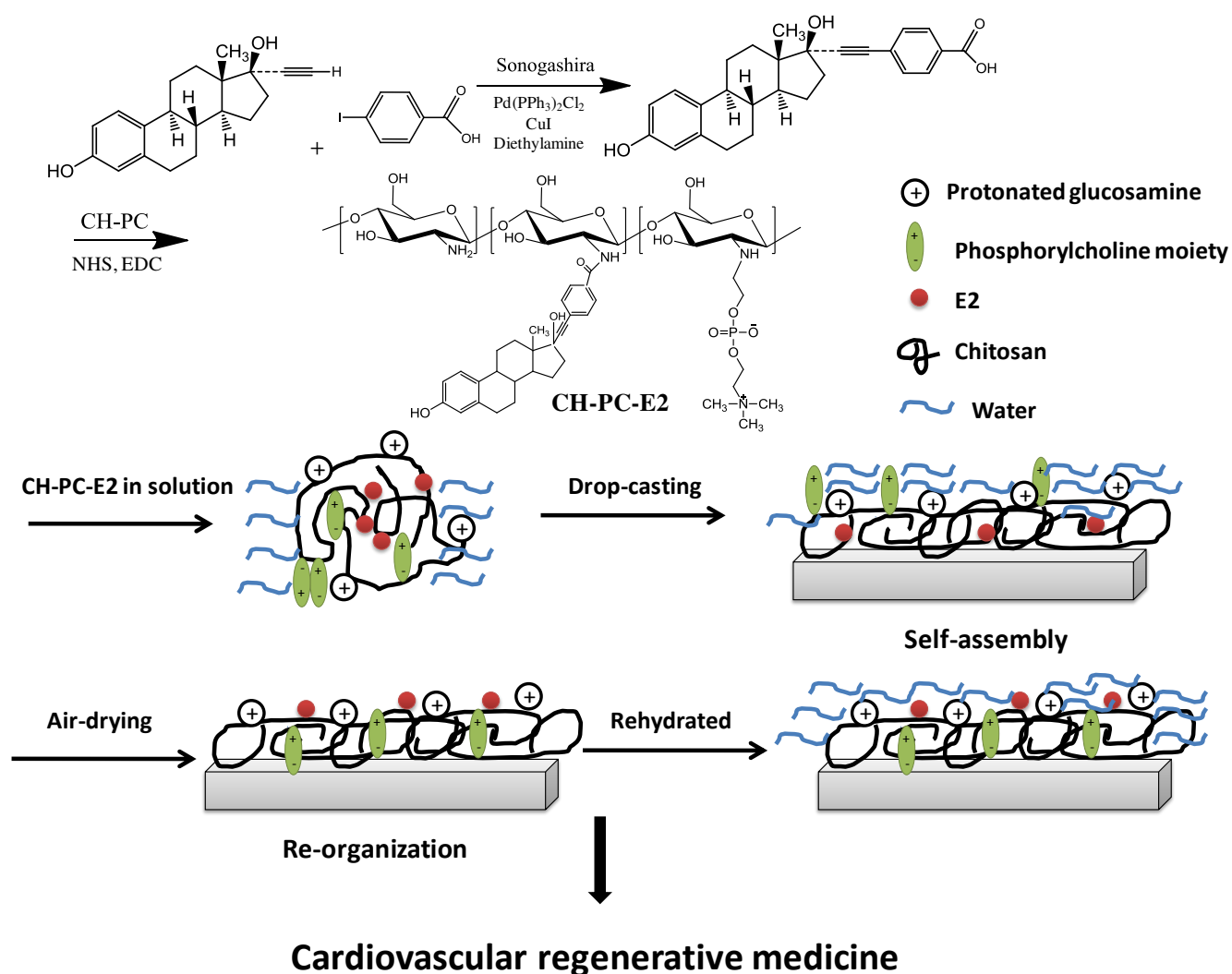


Figure 1.4 Tethering E2 to CH-PC polymers for the formulation of self-assembled thin films by bottom-up approach.

In order to further elucidate the biological mechanisms of surface-tethered E2, we assume that surface-tethered E2 could exert biological responses through its non-genomic action. This hypothesis will be confirmed through an investigation of tethering E2 to micropatterned substrates prepared by photolithography as shown in the Figure 1.5. Then, the influence to the phosphorylation level of ERK, which is a significant marker of non-genomic signal pathways, will be determined by E2-tethered micropatterned substrates. Finally, the genomic action of micropatterned surface-tethered E2 will also be assessed by cancer cell proliferation studies.

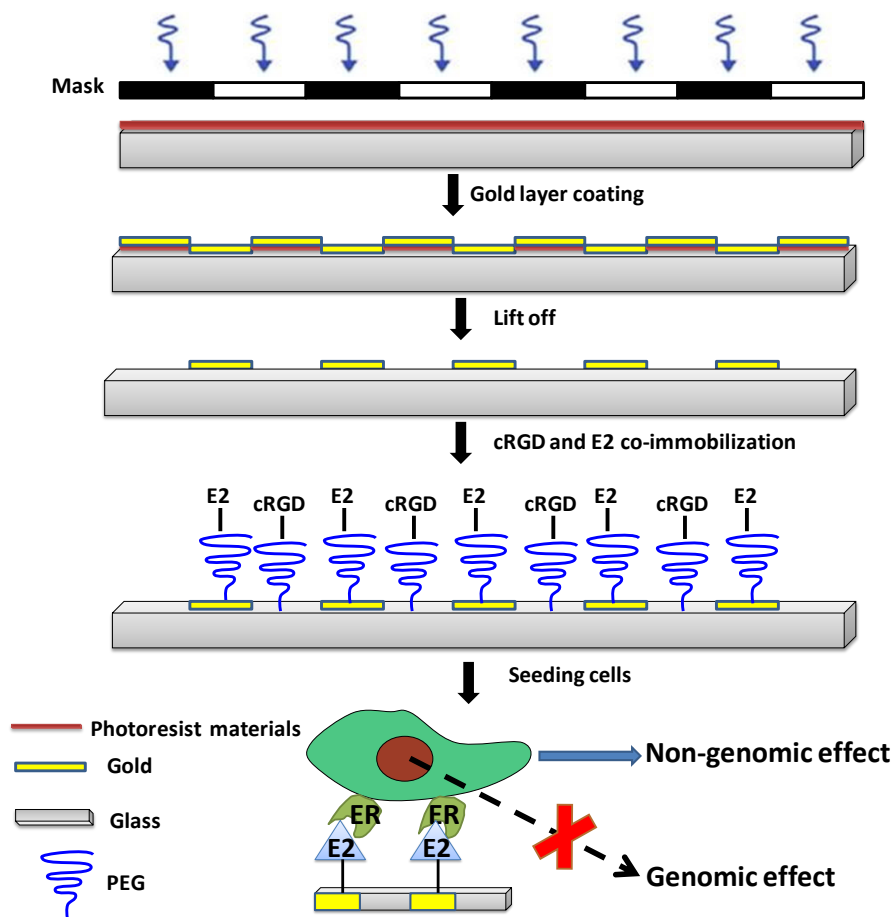


Figure 1.5 Tethering E2 to photolithography-fabricated micropatterned substrates by top-down approach in order to specifically understand E2 non-genomic action.

## 1.5.2 Thesis rationale

In the first part of the thesis, E2 will be covalently grafted onto chitosan phosphorylcholine (CH-PC) polymer backbone as a prodrug strategy. This CH-PC-E2 conjugate will be used for the fabrication of functional self-assembled film *via* a bottom-up approach. There are several advantages for grafting PC and E2 moiety to chitosan: 1) The solubility of chitosan is remarkably increased after PC conjugation; 2) The biocompatibility of chitosan is greatly enhanced due to the anti-fouling properties of the PC group. The relevant physical characteristics and cellular studies in CH-PC films will be presented in a separated chapter; 3) The conjugation of E2 to a CH-PC backbone might increase the stability of E2 and preferentially interact with cell or tissue more efficiently in comparison with using the E2 alone.<sup>[256]</sup> Due to the co-existence of PC and E2 groups, the properties of CH-PC-E2 conjugate in solutions will be investigated by dynamic light scattering (DLS) and zeta-potential measurement in order to understand the inter- or intra-molecule interactions. Moreover, the physical and mechanical properties of CH-PC-E2 films will be characterized by different techniques, e.g. AFM and QCM-D. Finally, the cardiovascular beneficial effect of CH-PC-E2 film will be explored by determining its effect on nitric oxide (NO) stimulation, which is a widely accepted protective signal molecule in the cardiovascular system. These studies above will provide a new perspective on the potential biomedical applications of CH-PC-E2 conjugates, such as novel coating materials in the cardiovascular devices. In the second part of the thesis, the purpose is to establish an *in vitro* model for non-genomic effect studies *via* construction of E2-functionalized micropatterned substrates. To start with, a PEGylated surface will be used for the activated E2 ligand immobilization since PEG can preclude non-specific interactions of irrelevant molecules and enhance the flexibility of E2 specific interactions to the cell surface. Moreover, a cell adhesive ligand will be co-immobilized with the activated E2 ligand for ensuring the cell attachment. In attempting to achieve these goals, micropatterned substrates will be used and fabricated by aligning gold circular regions onto the glass substrate *via* a photolithograph, while exposing them to UV radiations in the presence of a photomask.<sup>[257, 258]</sup> The micropatterned substrates developed by this top-down approach, which are identical in size to the site of cells, can be used for controlling the cell microenvironment. Moreover, the relationship between the amounts of surface-immobilized

E2 and its corresponding biological activity should be evaluated due to the small molecule weight of E2 (M.W. ~400). By combining SPR and QCM-D techniques, the quantitative information concerning the results of E2 modification on the gold region will be obtained. Further, the biological activity of surface-immobilized E2 will be determined *via* interactions to estrogen receptors *in situ*. After investigating the relevant physical and chemical properties of the E2-functionalized micropatterned substrate, a selected non-genomic effect signaling pathway will be validated. A challenge here is that the presence of ER in the cell membrane has not been confirmed with certainty, although numerous *in vitro* measurements argue in favor of this assumption. In the present study, ERK activity activated by E2-functionalized micropatterned substrate will be evaluated by a cell ELISA method, which is an exclusive technique that allows measuring the ERK activity quantitatively *in situ*. Furthermore, the cell proliferation study will be performed to determine the influence of E2-functionalized micropatterned substrate to E2 genomic effect. Taken these results together, E2-functionalized micropatterned substrates may act as biosensors to study the E2 non-genomic properties and possibly contribute to clarifying several issues in steroid biology.

### **1.5.3 Research objectives**

- 1) To prepare and characterize CH-PC-based films with different PC substituted ratios as well as to study their biological properties *in vitro*;
- 2) To prepare and characterize CH-PC-E2 conjugates as well as to further investigate the potential roles of CH-PC-E2 conjugates in the cardiovascular regenerative medicine;
- 3) To understand the E2 non-genomic or genomic behavior and study relevant cell signal pathways by E2-functionalized micropatterned substrates.

## 1.6 References

- [1] Reddy KS; Yusuf, S, Emerging epidemic of cardiovascular disease in developing countries. *Circulation* **1998**, *97*: 596-601.
- [2] Lawes CMM; Vander Hoorn, S; Rodgers, A; Int Soc, H, Global burden of blood-pressure-related disease, 2001. *Lancet* **2008**, *371*: 1513-1518.
- [3] Soehnlein O, Multiple roles for neutrophils in atherosclerosis. *Circulation Research* **2012**, *110*: 875-888.
- [4] Perk J; De Backer, G; Gohlke, H; Graham, I; Reiner, Z; Verschuren, WMM; Albus, C; Benlian, P; Boysen, G; Cifkova, R; Deaton, C; Ebrahim, S; Fisher, M; Germano, G; Hobbs, R; Hoes, A; Karadeniz, S; Mezzani, A; Prescott, E; Ryden, L; Scherer, M; Syvanne, M; Reimer, W; Vrints, C; Wood, D; Zamorano, JL; Zannad, F, European guidelines on cardiovascular disease prevention in clinical practice. *European Journal of Preventive Cardiology* **2012**, *19*: 585-667.
- [5] Kunicki TJ; Ruggeri, ZM, Platelet collagen receptors and risk prediction in stroke and coronary artery disease. *Circulation* **2001**, *104*: 1451-1453.
- [6] Libby P; Ridker, PM; Maseri, A, Inflammation and atherosclerosis. *Circulation* **2002**, *105*: 1135-1143.
- [7] Hirsh J; Anand, SS; Halperin, JL; Fuster, V, Guide to anticoagulant therapy: Heparin a statement for healthcare professionals from the american heart association. *Circulation* **2001**, *103*: 2994-3018.
- [8] Hirsh J; Fuster, V; Ansell, J; Halperin, JL, American heart association/american college of cardiology foundation guide to warfarin therapy. *Circulation* **2003**, *107*: 1692-1711.
- [9] Desai J; Kolb, JM; Weitz, JJ; Aisenberg, J, Gastrointestinal bleeding with the new oral anticoagulants - defining the issues and the management strategies. *Thrombosis and Haemostasis* **2013**, *110*: 205-212.
- [10] Parikh SA; Edelman, ER, Endothelial cell delivery for cardiovascular therapy. *Advanced Drug Delivery Reviews* **2000**, *42*: 139-161.
- [11] Fajadet J; Chieffo, A, Current management of left main coronary artery disease. *European Heart Journal* **2012**, *33*: 36-169.

- [12] van Domburg RT; Kappetein, AP; Bogers, A, The clinical outcome after coronary bypass surgery: A 30-year follow-up study. *European Heart Journal* **2009**, *30*: 453-458.
- [13] Yusuf S; Zucker, D; Peduzzi, P; Fisher, LD; Takaro, T; Kennedy, JW; Davis, K; Killip, T; Passamani, E; Norris, R; Morris, C; Mathur, V; Varnauskas, E; Chalmers, TC, Effect of coronary-artery bypass graft-surgery on survival - overview of 10-year results from randomized trials by the coronary-artery bypass graft-surgery trialists collaboration. *Lancet* **1994**, *344*: 563-570.
- [14] Serruys PW; Morice, MC; Kappetein, AP; Colombo, A; Holmes, DR; Mack, MJ; Stahle, E; Feldman, TE; van den Brand, M; Bass, EJ; Van Dyck, N; Leadley, K; Dawkins, KD; Mohr, FW; Investigators, S, Percutaneous coronary intervention versus coronary-artery bypass grafting for severe coronary artery disease. *New England Journal of Medicine* **2009**, *360*: 961-972.
- [15] Pober BR; Johnson, M; Urban, Z, Mechanisms and treatment of cardiovascular disease in williams-beuren syndrome. *Journal of Clinical Investigation* **2008**, *118*: 1606-1615.
- [16] Bryant M, The heart and circulatory system--a review. *Journal of nephrology nursing* **1984**, *1*: 130, 159-178.
- [17] Sumpio BE; Riley, JT; Dardik, A, Cells in focus: Endothelial cell. *International Journal of Biochemistry & Cell Biology* **2002**, *34*: 1508-1512.
- [18] Rensen SSM; Doevendans, P; van Eys, G, Regulation and characteristics of vascular smooth muscle cell phenotypic diversity. *Netherlands Heart Journal* **2007**, *15*: 100-108.
- [19] Brown DJ; Rzucidlo, EM; Merenick, BL; Wagner, RJ; Martin, KA; Powell, RJ, Endothelial cell activation of the smooth muscle cell phosphoinositide 3-kinase/akt pathway promotes differentiation. *Journal of Vascular Surgery* **2005**, *41*: 509-516.
- [20] Naseem KM, The role of nitric oxide in cardiovascular diseases. *Molecular aspects of medicine* **2005**, *26*: 33-65.
- [21] Radomski MW; Palmer, RM; Moncada, S, The anti-aggregating properties of vascular endothelium: Interactions between prostacyclin and nitric oxide. *British journal of pharmacology* **1987**, *92*: 639-46.
- [22] de Mel A; Murad, F; Seifalian, AM, Nitric oxide: A guardian for vascular grafts? *Chemical Reviews* **2011**, *111*: 5742-5767.

- [23] Freedman JE; Sauter, R; Battinelli, EM; Ault, K; Knowles, C; Huang, PL; Loscalzo, J, Deficient platelet-derived nitric oxide and enhanced hemostasis in mice lacking the nosiii gene. *Circulation Research* **1999**, *84*: 1416-1421.
- [24] Stevenson S; Thornton, J, Effect of estrogens on skin aging and the potential role of serms. *Clinical Interventions in Aging* **2007**, *2*: 283-297.
- [25] Maier WE; Herman, JR, Pharmacology and toxicology of ethinyl estradiol and norethindrone acetate in experimental animals. *Regulatory Toxicology and Pharmacology* **2001**, *34*: 53-61.
- [26] Katz E; Ricciarelli, E; Adashi, EY, The potential relevance of growth-hormone to female reproductive physiology and pathophysiology. *Fertility and Sterility* **1993**, *59*: 8-34.
- [27] Collins P; Rosano, GMC; Sarrel, PM; Ulrich, L; Adamopoulos, S; Beale, CM; McNeill, JG; Poolewilson, PA, 17-beta-estradiol attenuates acetylcholine-induced coronary arterial constriction in women but not men with coronary heart-disease. *Circulation* **1995**, *92*: 24-30.
- [28] Mendelsohn ME, Protective effects of estrogen on the cardiovascular system. *American Journal of Cardiology* **2002**, *89*: 12-17.
- [29] Moolman JA, Unravelling the cardioprotective mechanism of action of estrogens. *Cardiovascular Research* **2006**, *69*: 777-780.
- [30] Chandrasekar B; Sirois, MG; Geoffroy, P; Lauzier, D; Nattel, S; Tanguay, JF, Local delivery of 17 beta-estradiol improves reendothelialization and decreases inflammation after coronary stenting in a porcine model. *Thrombosis and Haemostasis* **2005**, *94*: 1042-1047.
- [31] Chandrasekar B; Tanguay, JF, Local delivery of 17-beta-estradiol decreases neointimal hyperplasia after coronary angioplasty in a porcine model. *Journal of the American College of Cardiology* **2000**, *36*: 1972-1978.
- [32] Abizaid A; Albertal, M; Costa, MA; Abizaid, AS; Staico, R; Feres, F; Mattos, LA; Sousa, A; Moses, J; Kipshidize, N; Roubin, GS; Mehran, R; New, G; Leon, MB; Sousa, JE, First human experience with the 17-beta-estradiol-eluting stent - the estrogen and stents to eliminate restenosis (easter) trial. *Journal of the American College of Cardiology* **2004**, *43*: 1118-1121.
- [33] New G; Moses, JW; Roubin, GS; Leon, MB; Colombo, A; Iyer, SS; Tio, FO; Mehran, R; Kipshidze, N, Estrogen-eluting, phosphorylcholine-coated stent implantation is associated



with reduced neointimal formation but no delay in vascular repair in a porcine coronary model. *Catheterization and Cardiovascular Interventions* **2002**, *57*: 266-271.

[34] Cadenas C; Bolt, HM, Estrogen receptors in human disease. *Archives of Toxicology* **2012**, *86*: 1489-1490.

[35] Herynk MH; Fuqua, SAW, Estrogen receptor mutations in human disease. *Endocrine Reviews* **2004**, *25*: 869-898.

[36] Kapoor R; Nimmagadda, D; Sheng, JJ, Cellular localization studies on human estrogen sulfotransferase sult1e1 in human embryonic kidney 293 cells. *Drug metabolism and disposition: the biological fate of chemicals* **2007**, *35*: 17-20.

[37] Mani SK; Mermelstein, PG; Tetel, MJ; Anesetti, G, Convergence of multiple mechanisms of steroid hormone action. *Hormone and Metabolic Research* **2012**, *44*: 569-576.

[38] Nadal A; Diaz, M; Valverde, MA, The estrogen trinity: Membrane, cytosolic, and nuclear effects. *News in Physiological Sciences* **2001**, *16*: 251-255.

[39] Al Saleh S; Al Mulla, F; Luqmani, YA, Estrogen receptor silencing induces epithelial to mesenchymal transition in human breast cancer cells. *Plos One* **2011**, *6*: 10.

[40] Bjornstrom L; Sjoberg, M, Mechanisms of estrogen receptor signaling: Convergence of genomic and nongenomic actions on target genes. *Molecular Endocrinology* **2005**, *19*: 833-842.

[41] Falkenstein E; Tillmann, HC; Christ, M; Feuring, M; Wehling, M, Multiple actions of steroid hormones - a focus on rapid, nongenomic effects. *Pharmacological Reviews* **2000**, *52*: 513-555.

[42] Losel RM; Falkenstein, E; Feuring, M; Schultz, A; Tillmann, HC; Rossol-Haseroth, K; Wehling, M, Nongenomic steroid action: Controversies, questions, and answers. *Physiological Reviews* **2003**, *83*: 965-1016.

[43] Miao ZM; Kujawa, P; Lau, YTR; Toita, S; Qi, BW; Nakanishi, J; Cloutier, I; Tanguay, JF; Winnik, FM, Tuning the properties and functions of 17 beta-estradiol-polysaccharide conjugates in thin films: Impact of sample history. *Biomacromolecules* **2012**, *13*: 4098-4108.

[44] Mendelsohn ME; Karas, RH, Rapid progress for non-nuclear estrogen receptor signaling. *Journal of Clinical Investigation* **2010**, *120*: 2277-2279.

[45] Bratton MR; Duong, BN; Elliott, S; Weldon, CB; Beckman, BS; McLachlan, JA; Burow, ME, Regulation of er alpha-mediated transcription of bcl-2 by pi3k-akt crosstalk:

Implications for breast cancer cell survival. *International Journal of Oncology* **2010**, *37*: 541-550.

[46] Zielniok K; Gajewska, M; Motyl, T, Molecular actions of 17 beta-estradiol and progesterone and their relationship with cellular signaling pathways. *Postepy Higieny I Medycyny Doswiadczalnej* **2014**, *68*: 777-792.

[47] Li M; Zhang, H; Zhao, X; Yan, L; Wang, C; Li, C; Li, C, Spry4-mediated erk1/2 signaling inhibition abolishes 17beta-estradiol-induced cell growth in endometrial adenocarcinoma cell. *Gynecological endocrinology : the official journal of the International Society of Gynecological Endocrinology* **2014**, *30*: 600-604.

[48] Improta-Brears T; Whorton, AR; Codazzi, F; York, JD; Meyer, T; McDonnell, DP, Estrogen-induced activation of mitogen-activated protein kinase requires mobilization of intracellular calcium. *Proceedings of the National Academy of Sciences of the United States of America* **1999**, *96*: 4686-4691.

[49] Creighton CJ; Hilger, AM; Murthy, S; Rae, JM; Chinnaiyan, AM; El-Ashry, D, Activation of mitogen-activated protein kinase in estrogen receptor alpha-positive breast cancer cells in vitro induces an in vivo molecular phenotype of estrogen receptor alpha-negative human breast tumors. *Cancer Research* **2006**, *66*: 3903-3911.

[50] Hammes SR; Levin, ER, Extranuclear steroid receptors: Nature and actions. *Endocr. Rev.* **2007**, *28*: 726-741.

[51] Migliaccio A; DiDomenico, M; Castoria, G; deFalco, A; Bontempo, P; Nola, E; Auricchio, F, Tyrosine kinase/p21(ras)/map-kinase pathway activation by estradiol-receptor complex in mcf-7 cells. *Embo Journal* **1996**, *15*: 1292-1300.

[52] Duan RQ; Xie, W; Burghardt, RC; Safe, S, Estrogen receptor-mediated activation of the serum response element in mcf-7 cells through mapk-dependent phosphorylation of elk-1. *Journal of Biological Chemistry* **2001**, *276*: 11590-11598.

[53] Pratt MAC; Satkunarathnam, A; Novosad, DM, Estrogen activates raf-1 kinase and induces expression of egr-1 in mcf-7 breast cancer cells. *Molecular and Cellular Biochemistry* **1998**, *189*: 119-125.

[54] Keshamouni VG; Mattingly, RR; Reddy, KB, Mechanism of 17-beta-estradiol-induced erk1/2 activation in breast cancer cells. *Journal of Biological Chemistry* **2002**, *277*: 22558-22565.

- [55] Wang G-S; Huang, Y-G; Li, H; Bi, S-J; Zhao, J-L, Erk/camp rapid signaling mediates 17 beta-estradiol-induced proliferation of human breast cancer cell line mcf-7 cells. *International Journal of Clinical and Experimental Medicine* **2014**, *7*: 156-162.
- [56] Haynes MP; Sinha, D; Russell, KS; Fulton, D; Morales-Ruiz, M; Sessa, WM; Bender, JR, Membrane estrogen receptor engagement activates endothelial nitric oxide synthase via the pi3-kinase-akt pathway in human endothelial cells. *Circulation* **2000**, *102*: 225-226.
- [57] Aronica SM; Kraus, WL; Katzenellenbogen, BS, Estrogen action via the camp signaling pathway - stimulation of adenylate-cyclase and camp-regulated gene-transcription. *Proceedings of the National Academy of Sciences of the United States of America* **1994**, *91*: 8517-8521.
- [58] Zivadinovic D; Gametchu, B; Watson, CS, Membrane estrogen receptor-alpha levels in mcf-7 breast cancer cells predict camp and proliferation responses. *Breast Cancer Research* **2005**, *7*: R101-R112.
- [59] Guo ZY; Krucken, J; Benten, WPM; Wunderlich, F, Estradiol-induced nongenomic calcium signaling regulates genotropic signaling in macrophages. *Journal of Biological Chemistry* **2002**, *277*: 7044-7050.
- [60] Marino M; Acconcia, F; Bresciani, F; Weisz, A; Trentalance, A, Distinct nongenomic signal transduction pathways controlled by 17 beta-estradiol regulate DNA synthesis and cyclin d-1 gene transcription in hepg2 cells. *Molecular Biology of the Cell* **2002**, *13*: 3720-3729.
- [61] Guo RX; Wei, LH; Tu, Z; Sun, PM; Wang, JL; Zhao, D; Li, XP; Tang, JM, 17 beta-estradiol activates pi3k/akt signaling pathway by estrogen receptor (er)-dependent and er-independent mechanisms in endometrial cancer cells. *Journal of Steroid Biochemistry and Molecular Biology* **2006**, *99*: 9-18.
- [62] Marino M; Acconcia, F; Trentalance, A, Biphasic estradiol-induced akt phosphorylation is modulated by pten via map kinase in hepg2 cells. *Mol. Biol. Cell* **2003**, *14*: 2583-2591.
- [63] Razandi M; Pedram, A; Merchenthaler, I; Greene, GL; Levin, ER, Plasma membrane estrogen receptors exist and functions as dimers. *Molecular Endocrinology* **2004**, *18*: 2854-2865.

- [64] Zabransky DJ; Park, BH, Estrogen receptor and receptor tyrosine kinase signaling: Use of combinatorial hormone and epidermal growth factor receptor/human epidermal growth factor receptor 2-targeted therapies for breast cancer. *Journal of Clinical Oncology* **2014**, *32*: 1084-1086.
- [65] Schiff R; Massarweh, SA; Shou, J; Bharwani, L; Mohsin, SK; Osborne, CK, Cross-talk between estrogen receptor and growth factor pathways as a molecular target for overcoming endocrine resistance. *Clinical Cancer Research* **2004**, *10*: 331-336.
- [66] Schaeffer HJ; Weber, MJ, Mitogen-activated protein kinases: Specific messages from ubiquitous messengers. *Molecular and Cellular Biology* **1999**, *19*: 2435-2444.
- [67] Filardo EJ; Quinn, JA; Bland, KI; Frackelton, AR, Estrogen-induced activation of erk-1 and erk-2 requires the g protein-coupled receptor homolog, gpr30, and occurs via trans-activation of the epidermal growth factor receptor through release of hb-egf. *Molecular Endocrinology* **2000**, *14*: 1649-1660.
- [68] Thomas P; Pang, Y; Filardo, EJ; Dong, J, Identity of an estrogen membrane receptor coupled to a g protein in human breast cancer cells. *Endocrinology* **2005**, *146*: 624-632.
- [69] Chen Y; Li, Z; He, Y; Shang, DD; Pan, JG; Wang, HM; Chen, HM; Zhu, ZX; Wan, L; Wang, XD, Estrogen and pure antiestrogen fulvestrant (ici 182 780) augment cell-matrigel adhesion of mcf-7 breast cancer cells through a novel g protein coupled estrogen receptor (gpr30)-to-calpain signaling axis. *Toxicology and Applied Pharmacology* **2014**, *275*: 176-181.
- [70] Sylvia VL; Walton, J; Lopez, D; Dean, DD; Boyan, BD; Schwartz, Z, 17-beta estradiol-bsa conjugates and 17 beta-estradiol regulate growth plate chondrocytes by common membrane associated mechanisms involving pkc dependent and independent signal transduction. *Journal of Cellular Biochemistry* **2001**, *81*: 413-429.
- [71] Aguilar R; Bellido, C; Garrido-Gracia, JC; Alonso, R; Sanchez-Criado, JE, Estradiol and its membrane-impermeable conjugate estradiol-bsa inhibit tamoxifen-stimulated prolactin secretion in incubated rat pituitaries. *Reproduction* **2006**, *131*: 763-769.
- [72] Razandi M; Pedram, A; Levin, ER, Estrogen signals to the preservation of endothelial cell form and function. *Journal of Biological Chemistry* **2000**, *275*: 38540-38546.
- [73] Stevis PE; Deecher, DC; Suhadolnik, L; Mallis, LM; Frail, DE, Differential effects of estradiol and estradiol-bsa conjugates. *Endocrinology* **1999**, *140*: 5455-5458.

- [74] Temple JL; Wray, S, Bovine serum albumin-estrogen compounds differentially alter gonadotropin-releasing hormone-1 neuronal activity. *Endocrinology* **2005**, *146*: 558-563.
- [75] Harrington WR; Kim, SH; Funk, CC; Madak-Erdogan, Z; Schiff, R; Katzenellenbogen, JA; Katzenellenbogen, BS, Estrogen dendrimer conjugates that preferentially activate extranuclear, nongenomic versus genomic pathways of estrogen action. *Molecular Endocrinology* **2006**, *20*: 491-502.
- [76] Chambliss KL; Wu, QA; Oltmann, S; Konaniah, ES; Umetani, M; Korach, KS; Thomas, GD; Mineo, C; Yuhanna, IS; Kim, SH; Madak-Erdogan, Z; Maggi, A; Dineen, SP; Roland, CL; Hui, DY; Brekken, RA; Katzenellenbogen, JA; Katzenellenbogen, BS; Shaul, PW, Non-nuclear estrogen receptor alpha signaling promotes cardiovascular protection but not uterine or breast cancer growth in mice. *Journal of Clinical Investigation* **2010**, *120*: 2319-2330.
- [77] Gunatillake PA; Adhikari, R, Biodegradable synthetic polymers for tissue engineering. *European cells & materials* **2003**, *5*: 1-16; discussion 16.
- [78] van Marion MH; Bax, NAM; van Spreeuwel, ACC; van der Schaft, DWJ; Bouten, CVC, Material-based engineering strategies for cardiac regeneration. *Current Pharmaceutical Design* **2014**, *20*: 2057-2068.
- [79] Baker SC; Atkin, N; Gunning, PA; Granville, N; Wilson, K; Wilson, D; Southgate, J, Characterisation of electrospun polystyrene scaffolds for three-dimensional in vitro biological studies. *Biomaterials* **2006**, *27*: 3136-3146.
- [80] Ito Y; Zheng, J; Imanishi, Y; Yonezawa, K; Kasuga, M, Protein-free cell culture on an artificial substrate with covalently immobilized insulin. *Proceedings of the National Academy of Sciences of the United States of America* **1996**, *93*: 3598-3601.
- [81] Klenkler BJ; Griffith, M; Becerril, C; West-Mays, JA; Sheardown, H, Egf-grafted pdms surfaces in artificial cornea applications. *Biomaterials* **2005**, *26*: 7286-7296.
- [82] Zdrahala RJ; Zdrahala, IJ, Biomedical applications of polyurethanes: A review of past promises, present realities, and a vibrant future. *Journal of Biomaterials Applications* **1999**, *14*: 67-90.
- [83] Ni M; Tong, WH; Choudhury, D; Rahim, NAA; Iliescu, C; Yu, H, Cell culture on mems platforms: A review. *International Journal of Molecular Sciences* **2009**, *10*: 5411-5441.

- [84] Soper SA; Henry, AC; Vaidya, B; Galloway, M; Wabuyele, M; McCarley, RL, Surface modification of polymer-based microfluidic devices. *Analytica Chimica Acta* **2002**, *470*: 87-99.
- [85] Zhou JW; Khodakov, DA; Ellis, AV; Voelcker, NH, Surface modification for pdms-based microfluidic devices. *Electrophoresis* **2012**, *33*: 89-104.
- [86] Merrett K; Griffith, CM; Deslandes, Y; Pleizier, G; Dube, MA; Sheardown, H, Interactions of corneal cells with transforming growth factor beta 2-modified poly dimethyl siloxane surfaces. *Journal of Biomedical Materials Research Part A* **2003**, *67A*: 981-993.
- [87] Mitragotri S; Lahann, J, Physical approaches to biomaterial design. *Nature Materials* **2009**, *8*: 15-23.
- [88] Grainger DW, All charged up about implanted biomaterials. *Nature Biotechnology* **2013**, *31*: 507-509.
- [89] Janmey PA; Miller, RT, Mechanisms of mechanical signaling in development and disease. *Journal of Cell Science* **2011**, *124*: 9-18.
- [90] Meyers MA; Mishra, A; Benson, DJ, Mechanical properties of nanocrystalline materials. *Progress in Materials Science* **2006**, *51*: 427-556.
- [91] Salvetat JP; Briggs, GAD; Bonard, JM; Bacsá, RR; Kulik, AJ; Stockli, T; Burnham, NA; Forro, L, Elastic and shear moduli of single-walled carbon nanotube ropes. *Physical Review Letters* **1999**, *82*: 944-947.
- [92] Pal R, Novel shear modulus equations for concentrated emulsions of two immiscible elastic liquids with interfacial tension. *Journal of Non-Newtonian Fluid Mechanics* **2002**, *105*: 21-33.
- [93] Voinova MV; Rodahl, M; Jonson, M; Kasemo, B, Viscoelastic acoustic response of layered polymer films at fluid-solid interfaces: Continuum mechanics approach. *Physica Scripta* **1999**, *59*: 391-396.
- [94] Cortes F; Jesus Elejabarrieta, M, Modelling viscoelastic materials whose storage modulus is constant with frequency. *International Journal of Solids and Structures* **2006**, *43*: 7721-7726.
- [95] Meyers MA; Chen, PY; Lin, AYM; Seki, Y, Biological materials: Structure and mechanical properties. *Progress in Materials Science* **2008**, *53*: 1-206.
- [96] Bao G; Suresh, S, Cell and molecular mechanics of biological materials. *Nature Materials* **2003**, *2*: 715-725.

- [97] Eisele NB; Andersson, FI; Frey, S; Richter, RP, Viscoelasticity of thin biomolecular films: A case study on nucleoporin phenylalanine-glycine repeats grafted to a histidine-tag capturing qcm-d sensor. *Biomacromolecules* **2012**, *13*: 2322-2332.
- [98] Gribova V; Crouzier, T; Picart, C, A material's point of view on recent developments of polymeric biomaterials: Control of mechanical and biochemical properties. *J. Mater. Chem.* **2011**, *21*: 14354-14366.
- [99] Rizzi SC; Ehrbar, M; Halstenberg, S; Raeber, GP; Schmoekel, HG; Hagenmuller, H; Muller, R; Weber, FE; Hubbell, JA, Recombinant protein-co-peg networks as cell-adhesive and proteolytically degradable hydrogel matrixes. Part ii: Biofunctional characteristics. *Biomacromolecules* **2006**, *7*: 3019-3029.
- [100] Geckil H; Xu, F; Zhang, X; Moon, S; Demirci, U, Engineering hydrogels as extracellular matrix mimics. *Nanomedicine* **2010**, *5*: 469-484.
- [101] Engler AJ; Sen, S; Sweeney, HL; Discher, DE, Matrix elasticity directs stem cell lineage specification. *Cell* **2006**, *126*: 677-689.
- [102] Makadia HK; Siegel, SJ, Poly lactic-co-glycolic acid (plga) as biodegradable controlled drug delivery carrier. *Polymers* **2011**, *3*: 1377-1397.
- [103] Ikada Y; Tsuji, H, Biodegradable polyesters for medical and ecological applications. *Macromolecular Rapid Communications* **2000**, *21*: 117-132.
- [104] Lyu SP; Untereker, D, Degradability of polymers for implantable biomedical devices. *International Journal of Molecular Sciences* **2009**, *10*: 4033-4065.
- [105] Eyal AM; Canari, R, Ph-dependence of carboxylic and mineral acid-extraction by amine-based extractants - effects of pk(a), amine basicity, and diluent properties. *Industrial & Engineering Chemistry Research* **1995**, *34*: 1789-1798.
- [106] Smith R; Oliver, C; Williams, DF, The enzymatic degradation of polymers in vitro. *Journal of biomedical materials research* **1987**, *21*: 991-1003.
- [107] Kijchavengkul T; Auras, R, Perspective compostability of polymers. *Polymer International* **2008**, *57*: 793-804.
- [108] Gopferich A, Mechanisms of polymer degradation and erosion. *Biomaterials* **1996**, *17*: 103-114.

- [109] Sell SA; Wolfe, PS; Garg, K; McCool, JM; Rodriguez, IA; Bowlin, GL, The use of natural polymers in tissue engineering: A focus on electrospun extracellular matrix analogues. *Polymers* **2010**, *2*: 522-553.
- [110] Sannino A; Demitri, C; Madaghiele, M, Biodegradable cellulose-based hydrogels: Design and applications. *Materials* **2009**, *2*: 353-373.
- [111] Nair LS; Laurencin, CT, Biodegradable polymers as biomaterials. *Prog. Polym. Sci.* **2007**, *32*: 762-798.
- [112] Zawaneh PN; Singh, SP; Padera, RF; Henderson, PW; Spector, JA; Putnam, D, Design of an injectable synthetic and biodegradable surgical biomaterial. *Proceedings of the National Academy of Sciences of the United States of America* **2010**, *107*: 11014-11019.
- [113] Langer R; Tirrell, DA, Designing materials for biology and medicine. *Nature* **2004**, *428*: 487-492.
- [114] Douezan S; Brochard-Wyart, F, Active diffusion-limited aggregation of cells. *Soft Matter* **2012**, *8*: 784-788.
- [115] Napolitano AP; Dean, DM; Man, AJ; Youssef, J; Ho, DN; Rago, AP; Lech, MP; Morgan, JR, Scaffold-free three-dimensional cell culture utilizing micromolded nonadhesive hydrogels. *Biotechniques* **2007**, *43*: 494-501.
- [116] Vladkova TG, Surface engineered polymeric biomaterials with improved biocontact properties. *International Journal of Polymer Science* **2010**, *72*: 74-85.
- [117] Dewez JL; Doren, A; Schneider, YJ; Rouxhet, PG, Competitive adsorption of proteins: Key of the relationship between substratum surface properties and adhesion of epithelial cells. *Biomaterials* **1999**, *20*: 547-559.
- [118] Michel R; Gradzielski, M, Experimental aspects of colloidal interactions in mixed systems of liposome and inorganic nanoparticle and their applications. *International Journal of Molecular Sciences* **2012**, *13*: 11610-11642.
- [119] Shmulewitz A; Langer, R; Patton, J, Convergence in biomedical technology. *Nature Biotechnology* **2006**, *24*: 277-280.
- [120] Ruoslahti E, Fibronectin in cell adhesion and invasion. *Cancer metastasis reviews* **1984**, *3*: 43-51.
- [121] Osa M, Aqueous solution properties of poly(n-isopropylacrylamide). *Kobunshi Ronbunshu* **2009**, *66*: 273-288.



- [122] Ebara M; Yamato, M; Aoyagi, T; Kikuchi, A; Sakai, K; Okano, T, Temperature-responsive cell culture surfaces enable "on-off" affinity control between cell integrins and rgds ligands. *Biomacromolecules* **2004**, *5*: 505-510.
- [123] Akiyama Y; Kikuchi, A; Yamato, M; Okano, T, Ultrathin poly(n-isopropylacrylamide) grafted layer on polystyrene surfaces for cell adhesion/detachment control. *Langmuir* **2004**, *20*: 5506-5511.
- [124] Horbett TA, The role of adsorbed proteins in animal-cell adhesion. *Colloids and Surfaces B-Biointerfaces* **1994**, *2*: 225-240.
- [125] Bridges AW; Garcia, AJ, Anti-inflammatory polymeric coatings for implantable biomaterials and devices. *Journal of diabetes science and technology* **2008**, *2*: 984-94.
- [126] Tanaka M; Hayashi, T; Morita, S, The roles of water molecules at the biointerface of medical polymers. *Polymer Journal* **2013**, *45*: 701-710.
- [127] Wang K; Zhou, C; Hong, Y; Zhang, X, A review of protein adsorption on bioceramics. *Interface Focus* **2012**, *2*: 259-277.
- [128] Sheth SR; Leckband, D, Measurements of attractive forces between proteins and end-grafted poly(ethylene glycol) chains. *Proceedings of the National Academy of Sciences of the United States of America* **1997**, *94*: 8399-8404.
- [129] McPherson T; Kidane, A; Szleifer, I; Park, K, Prevention of protein adsorption by tethered poly(ethylene oxide) layers: Experiments and single-chain mean-field analysis. *Langmuir* **1998**, *14*: 176-186.
- [130] Chen S; Li, L; Zhao, C; Zheng, J, Surface hydration: Principles and applications toward low-fouling/nonfouling biomaterials. *Polymer* **2010**, *51*: 5283-5293.
- [131] Binazadeh M; Kabiri, M; Unsworth, LD, Poly(ethylene glycol) and poly(carboxy betaine) based nonfouling architectures: Review and current efforts. In *Proteins at interfaces iii: State of the art*, Horbett, T.; Brash, J. L.; Norde, W., Eds. Amer Chemical Soc: Washington, **2012**, *1120*: 621-643.
- [132] Morra M; Cassineli, C, Non-fouling properties of polysaccharide-coated surfaces. *Journal of Biomaterials Science-Polymer Edition* **1999**, *10*: 1107-1124.
- [133] Alcantar NA; Aydil, ES; Israelachvili, JN, Polyethylene glycol-coated biocompatible surfaces. *Journal of Biomedical Materials Research* **2000**, *51*: 343-351.

- [134] Mougín K; Ham, AS; Lawrence, MB; Fernandez, EJ; Hillier, AC, Construction of a tethered poly(ethylene glycol) surface gradient for studies of cell adhesion kinetics. *Langmuir* **2005**, *21*: 4809-4812.
- [135] Chen SF; Zheng, J; Li, LY; Jiang, SY, Strong resistance of phosphorylcholine self-assembled monolayers to protein adsorption: Insights into nonfouling properties of zwitterionic materials. *Journal of the American Chemical Society* **2005**, *127*: 14473-14478.
- [136] Iwasaki Y; Ishihara, K, Cell membrane-inspired phospholipid polymers for developing medical devices with excellent biointerfaces. *Science and Technology of Advanced Materials* **2012**, *13*: 14.
- [137] Schlenoff JB, Zwitteration: Coating surfaces with zwitterionic functionality to reduce nonspecific adsorption. *Langmuir* **2014**, *30*: 9625-9636.
- [138] Ostuni E; Chapman, RG; Liang, MN; Meluleni, G; Pier, G; Ingber, DE; Whitesides, GM, Self-assembled monolayers that resist the adsorption of proteins and the adhesion of bacterial and mammalian cells. *Langmuir* **2001**, *17*: 6336-6343.
- [139] He Y; Hower, J; Chen, SF; Bernards, MT; Chang, Y; Jiang, SY, Molecular simulation studies of protein interactions with zwitterionic phosphorylcholine self-assembled monolayers in the presence of water. *Langmuir* **2008**, *24*: 10358-10364.
- [140] Lowe AB; McCormick, CL, Synthesis and solution properties of zwitterionic polymers. *Chemical Reviews* **2002**, *102*: 4177-4189.
- [141] Zhang Z; Chao, T; Chen, SF; Jiang, SY, Superlow fouling sulfobetaine and carboxybetaine polymers on glass slides. *Langmuir* **2006**, *22*: 10072-10077.
- [142] Zhang Z; Chen, SF; Chang, Y; Jiang, SY, Surface grafted sulfobetaine polymers via atom transfer radical polymerization as superlow fouling coatings. *J. Phys. Chem. B* **2006**, *110*: 10799-10804.
- [143] Kuorwel KK; Cran, MJ; Sonneveld, K; Miltz, J; Bigger, SW, Antimicrobial activity of biodegradable polysaccharide and protein-based films containing active agents. *Journal of Food Science* **2011**, *76*: R90-R102.
- [144] Doh K-O; Yeo, Y, Application of polysaccharides for surface modification of nanomedicines. *Therapeutic delivery* **2012**, *3*: 1447-56.
- [145] Page C, Heparin and related drugs: Beyond anticoagulant activity. *ISRN pharmacology* **2013**, *2013*: 710-743.

- [146] Sasisekharan R; Venkataraman, G, Heparin and heparan sulfate: Biosynthesis, structure and function. *Current Opinion in Chemical Biology* **2000**, *4*: 626-631.
- [147] Gray E; Mulloy, B; Barrowcliffel, TW, Heparin and low-molecular-weight heparin. *Thrombosis and Haemostasis* **2008**, *99*: 807-818.
- [148] Zhu H-L; Fernandez, C; Fan, J-B; Shewmaker, F; Chen, J; Minton, AP; Liang, Y, Quantitative characterization of heparin binding to tau protein implication for inducer-mediated tau filament formation. *Journal of Biological Chemistry* **2010**, *285*: 3592-3599.
- [149] Marszalek PE; Oberhauser, AF; Li, HB; Fernandez, JM, The force-driven conformations of heparin studied with single molecule force microscopy. *Biophys. J.* **2003**, *85*: 2696-2704.
- [150] Liu L; Guo, S; Chang, J; Ning, C; Dong, C; Yan, D, Surface modification of polycaprolactone membrane via layer-by-layer deposition for promoting blood compatibility. *Journal of Biomedical Materials Research Part B-Applied Biomaterials* **2008**, *87B*: 244-250.
- [151] Atkins ED; Sheehan, JK, The molecular structure of hyaluronic acid. *The Biochemical journal* **1971**, *125*: 92-98.
- [152] Necas J; Bartosikova, L; Brauner, P; Kolar, J, Hyaluronic acid (hyaluronan): A review. *Veterinarni Medicina* **2008**, *53*: 397-411.
- [153] Burdick JA; Prestwich, GD, Hyaluronic acid hydrogels for biomedical applications. *Advanced Materials* **2011**, *23*: 41-56.
- [154] Sundelacruz S; Kaplan, DL, Stem cell- and scaffold-based tissue engineering approaches to osteochondral regenerative medicine. *Seminars in Cell & Developmental Biology* **2009**, *20*: 646-655.
- [155] Liu X; Huang, R; Su, R; Qi, W; Wang, L; He, Z, Grafting hyaluronic acid onto gold surface to achieve low protein fouling in surface plasmon resonance biosensors. *Acs Applied Materials & Interfaces* **2014**, *6*: 13034-13042.
- [156] Dutta PK; Dutta, J; Tripathi, VS, Chitin and chitosan: Chemistry, properties and applications. *Journal of Scientific & Industrial Research* **2004**, *63*: 20-31.
- [157] Muzzarelli RAA; Muzzarelli, C, Chitosan chemistry: Relevance to the biomedical sciences. In *Polysaccharides 1: Structure, characterization and use*, Heinze, T., Ed. Springer-Verlag Berlin: Berlin, 2005, *186*: 151-209.

- [158] Dai TH; Tanaka, M; Huang, YY; Hamblin, MR, Chitosan preparations for wounds and burns: Antimicrobial and wound-healing effects. *Expert Review of Anti-Infective Therapy* **2011**, *9*: 857-879.
- [159] Prabakaran M; Mano, JF, Chitosan-based particles as controlled drug delivery systems. *Drug Delivery* **2005**, *12*: 41-57.
- [160] Mansouri S; Lavigne, P; Corsi, K; Benderdour, M; Beaumont, E; Fernandes, JC, Chitosan-DNA nanoparticles as non-viral vectors in gene therapy: Strategies to improve transfection efficacy. *European Journal of Pharmaceutics and Biopharmaceutics* **2004**, *57*: 1-8.
- [161] Dang JM; Leong, KW, Natural polymers for gene delivery and tissue engineering. *Advanced Drug Delivery Reviews* **2006**, *58*: 487-499.
- [162] Rinaudo M, Chitin and chitosan: Properties and applications. *Prog. Polym. Sci.* **2006**, *31*: 603-632.
- [163] Sogias IA; Khutoryanskiy, VV; Williams, AC, Exploring the factors affecting the solubility of chitosan in water. *Macromolecular Chemistry and Physics* **2010**, *211*: 426-433.
- [164] Croisier F; Jerome, C, Chitosan-based biomaterials for tissue engineering. *European Polymer Journal* **2013**, *49*: 780-792.
- [165] Tomihata K; Ikada, Y, In vitro and in vivo degradation of films of chitin and its deacetylated derivatives. *Biomaterials* **1997**, *18*: 567-575.
- [166] Li J; Du, YM; Liang, HB, Low molecular weight water-soluble chitosans: Preparation with the aid of cellulase, characterization, and solubility. *Journal of Applied Polymer Science* **2006**, *102*: 1098-1105.
- [167] Qinna NA; Karwi, QG; Al-Jbour, N; Al-Remawi, MA; Alhussainy, TM; Al-So'ud, KA; Al Omari, MMH; Badwan, AA, Influence of molecular weight and degree of deacetylation of low molecular weight chitosan on the bioactivity of oral insulin preparations. *Marine Drugs* **2015**, *13*: 1710-1725.
- [168] Bulwan M; Wojcik, K; Zapotoczny, S; Nowakowska, M, Chitosan-based ultrathin films as antifouling, anticoagulant and antibacterial protective coatings. *Journal of Biomaterials Science-Polymer Edition* **2012**, *23*: 1963-1980.

- [169] Kong M; Chen, XG; Xing, K; Park, HJ, Antimicrobial properties of chitosan and mode of action: A state of the art review. *International Journal of Food Microbiology* **2010**, *144*: 51-63.
- [170] Liu CX; Zhang, DR; He, Y; Zhao, XS; Bai, RB, Modification of membrane surface for anti-biofouling performance: Effect of anti-adhesion and anti-bacteria approaches. *J. Membr. Sci.* **2010**, *346*: 121-130.
- [171] Mengatto LN; Helbling, IM; Luna, JA, Recent advances in chitosan films for controlled release of drugs. *Recent patents on drug delivery & formulation* **2012**, *6*: 156-70.
- [172] Freier T; Koh, HS; Kazazian, K; Shoichet, MS, Controlling cell adhesion and degradation of chitosan films by n-acetylation. *Biomaterials* **2005**, *26*: 5872-5878.
- [173] Chatelet C; Damour, O; Domard, A, Influence of the degree of acetylation on some biological properties of chitosan films. *Biomaterials* **2001**, *22*: 261-268.
- [174] Ding X; Yang, C; Lim, TP; Hsu, LY; Engler, AC; Hedrick, JL; Yang, Y-Y, Antibacterial and antifouling catheter coatings using surface grafted peg-b-cationic polycarbonate diblock copolymers. *Biomaterials* **2012**, *33*: 6593-6603.
- [175] Khalil F; Franzmann, E; Ramcke, J; Dakischew, O; Lips, KS; Reinhardt, A; Heisig, P; Maison, W, Biomimetic peg-catecholates for stabile antifouling coatings on metal surfaces: Applications on tio2 and stainless steel. *Colloids and Surfaces B-Biointerfaces* **2014**, *117*: 185-192.
- [176] Zhou R; Ren, P-F; Yang, H-C; Xu, Z-K, Fabrication of antifouling membrane surface by poly(sulfobetaine methacrylate)/polydopamine co-deposition. *Journal of Membrane Science* **2014**, *466*: 18-25.
- [177] Huang C-J; Chang, Y-C, In situ surface tailoring with zwitterionic carboxybetaine moieties on self-assembled thin film for antifouling biointerfaces. *Materials* **2014**, *7*: 130-142.
- [178] Cheng L; Liu, Q; Lei, Y; Lin, Y; Zhang, A, The synthesis and characterization of carboxybetaine functionalized polysiloxanes for the preparation of anti-fouling surfaces. *Rsc Advances* **2014**, *4*: 54372-54381.
- [179] Lam MT; Wu, JC, Biomaterial applications in cardiovascular tissue repair and regeneration. *Expert review of cardiovascular therapy* **2012**, *10*: 1039-49.
- [180] Hansson GK, Mechanisms of disease - inflammation, atherosclerosis, and coronary artery disease. *New England Journal of Medicine* **2005**, *352*: 1685-1695.

- [181] Dejaegere PPT; Defeyter, PJ; Vandergiessen, WJ; Serruys, PW, Endovascular stents - preliminary clinical-results and future-developments. *Clinical Cardiology* **1993**, *16*: 369-378.
- [182] Dotter CT; Judkins, MP, Transluminal treatment of arteriosclerotic obstruction. Description of a new technic and a preliminary report of its application. *Circulation* **1964**, *30*: 654-70.
- [183] Kujawa P; Schmauch, G; Viitala, T; Badia, A; Winnik, FM, Construction of viscoelastic biocompatible films via the layer-by-layer assembly of hyaluronan and phosphorylcholine-modified chitosan. *Biomacromolecules* **2007**, *8*: 3169-3176.
- [184] Jaganathan SK; Supriyanto, E; Murugesan, S; Balaji, A; Asokan, MK, Biomaterials in cardiovascular research: Applications and clinical implications. *BioMed research international* **2014**, *2014*: 459465.
- [185] Tavakol M; Ashraf, S; Brener, SJ, Risks and complications of coronary angiography: A comprehensive review. *Global journal of health science* **2012**, *4*: 65-93.
- [186] Naylor AR; Bolia, A; Abbott, RJ; Pye, IF; Smith, J; Lennard, N; Lloyd, AJ; London, NJM; Bell, PRF, Randomized study of carotid angioplasty and stenting versus carotid endarterectomy: A stopped trial. *Journal of Vascular Surgery* **1998**, *28*: 326-334.
- [187] Iakovou I; Schmidt, T; Bonizzoni, E; Ge, L; Sangiorgi, GM; Stankovic, G; Airolidi, F; Chieffo, A; Montorfano, M; Carlino, M; Michev, I; Corvaja, N; Briguori, C; Gerckens, U; Grube, E; Colombo, A, Incidence, predictors, and outcome of thrombosis after successful implantation of drug-eluting stents. *JAMA-J. Am. Med. Assoc.* **2005**, *293*: 2126-2130.
- [188] Joner M; Finn, AV; Farb, A; Mont, EK; Kolodgie, FD; Ladich, E; Kutys, R; Skoriija, K; Gold, HK; Virmani, R, Pathology of drug-eluting stents in humans - delayed healing and late thrombotic risk. *Journal of the American College of Cardiology* **2006**, *48*: 193-202.
- [189] Takimura CK; Campos, C; Melo, P; Campos, JC; Gutierrez, PS; Borges, TFC; Curado, L; Morato, SP; Laurindo, FRM; Neto, PAL, Preclinical study of a biodegradable polymer-based stent with abluminal sirolimus release. *Arquivos Brasileiros De Cardiologia* **2014**, *102*: 432-439.
- [190] Kimura T; Morimoto, T; Nakagawa, Y; Kawai, K; Miyazaki, S; Muramatsu, T; Shiode, N; Namura, M; Sone, T; Oshima, S; Nishikawa, H; Hiasa, Y; Hayashi, Y; Nobuyoshi, M; Mitudo, K; Investigators, JCR, Very late stent thrombosis and late target lesion

revascularization after sirolimus-eluting stent implantation five-year outcome of the j-cypher registry. *Circulation* **2012**, *125*: 584-611.

[191] Grube E; Silber, S; Hauptmann, KE; Mueller, R; Buellfeld, L; Gerckens, U; Russell, ME, Six- and twelve-month results from a randomized, double-blind trial on a slow-release paclitaxel-eluting stent for de novo coronary lesions. *Circulation* **2003**, *107*: 38-42.

[192] Rodriguez-Granillo A; Rubilar, B; Rodriguez-Granillo, G; Rodriguez, AE, Advantages and disadvantages of biodegradable platforms in drug eluting stents. *World journal of cardiology* **2011**, *3*: 84-92.

[193] Hansson KM; Tosatti, S; Isaksson, J; Wettero, J; Textor, M; Lindahl, TL; Tengvall, P, Whole blood coagulation on protein adsorption-resistant peg and peptide functionalised peg-coated titanium surfaces. *Biomaterials* **2005**, *26*: 861-872.

[194] Lim KS; Park, J-K; Jeong, MH; Nah, J-W; Kim, D-G; Bae, IH; Park, DS; Kim, JM; Kim, JH; Cho, DL; Sim, DS; Park, K-H; Hong, YJ; Ahn, Y, Comparison of sirolimus loaded plga-peg co-polymer coronary stent and bare metal stent in a porcine coronary restenosis model. *Macromolecular Research* **2014**, *22*: 639-646.

[195] Ye S-H; Jang, Y-S; Yun, Y-H; Shankarraman, V; Woolley, JR; Hong, Y; Gamble, LJ; Ishihara, K; Wagner, WR, Surface modification of a biodegradable magnesium alloy with phosphorylcholine (pc) and sulfobetaine (sb) functional macromolecules for reduced thrombogenicity and acute corrosion resistance. *Langmuir* **2013**, *29*: 8320-8327.

[196] Galli M; Sommariva, L; Prati, F; Zerboni, S; Politi, A; Bonatti, R; Mameli, S; Butti, E; Pagano, A; Ferrari, G, Acute and mid-term results of phosphorylcholine-coated stents in primary coronary stenting for acute myocardial infarction. *Catheterization and Cardiovascular Interventions* **2001**, *53*: 182-187.

[197] Lewis AL; Tolhurst, LA; Stratford, PW, Analysis of a phosphorylcholine-based polymer coating on a coronary stent pre- and post-implantation. *Biomaterials* **2002**, *23*: 1697-1706.

[198] Abbott WM; Callow, A; Moore, W; Rutherford, R; Veith, F; Weinberg, S, Evaluation and performance standards for arterial prostheses. *Journal of Vascular Surgery* **1993**, *17*: 746-756.

- [199] Avci-Adali M; Ziemer, G; Wendel, HP, Induction of epc homing on biofunctionalized vascular grafts for rapid in vivo self-endothelialization - a review of current strategies. *Biotechnology Advances* **2010**, *28*: 119-129.
- [200] de Mel A; Jell, G; Stevens, MM; Seifalian, AM, Biofunctionalization of biomaterials for accelerated in situ endothelialization: A review. *Biomacromolecules* **2008**, *9*: 2969-2979.
- [201] Kapadia MR; Popowich, DA; Kibbe, MR, Modified prosthetic vascular conduits. *Circulation* **2008**, *117*: 1873-1882.
- [202] Ravi S; Chaikof, EL, Biomaterials for vascular tissue engineering. *Regenerative Medicine* **2010**, *5*: 107-120.
- [203] Seifu DG; Purnama, A; Mequanint, K; Mantovani, D, Small-diameter vascular tissue engineering. *Nature Reviews Cardiology* **2013**, *10*: 410-421.
- [204] Del Gaudio C; Ercolani, E; Galloni, P; Santilli, F; Baiguera, S; Polizzi, L; Bianco, A, Aspirin-loaded electrospun poly(epsilon-caprolactone) tubular scaffolds: Potential small-diameter vascular grafts for thrombosis prevention. *Journal of Materials Science-Materials in Medicine* **2013**, *24*: 523-532.
- [205] Fukai R; Dakwa, PHR; Chen, W, Strategies toward biocompatible artificial implants: Grafting of functionalized poly(ethylene glycol)s to poly(ethylene terephthalate) surfaces. *Journal of Polymer Science Part a-Polymer Chemistry* **2004**, *42*: 5389-5400.
- [206] Li JH; Tan, DS; Zhang, XQ; Tan, H; Ding, MM; Wan, CX; Fu, Q, Preparation and characterization of nonfouling polymer brushes on poly(ethylene terephthalate) film surfaces. *Colloids and Surfaces B-Biointerfaces* **2010**, *78*: 343-350.
- [207] Karrer L; Duwe, J; Zisch, AH; Khabiri, E; Cikirikcioglu, M; Napoli, A; Goessl, A; Schaffner, T; Hess, OM; Carrel, T; Kalangos, A; Hubbell, JA; Walpoth, BH, Pps-peg surface coating to reduce thrombogenicity of small diameter eptfe vascular grafts. *International Journal of Artificial Organs* **2005**, *28*: 993-1002.
- [208] Heise M; Schmidmaier, G; Husmann, I; Heidenhain, C; Schmidt, J; Neuhaus, P; Settmacher, U, Peg-hirudin/iloprost coating of small diameter eptfe grafts effectively prevents pseudointima and intimal hyperplasia development. *European Journal of Vascular and Endovascular Surgery* **2006**, *32*: 418-424.
- [209] Jimenez-Vergara AC; Guiza-Arguello, V; Becerra-Bayona, S; Munoz-Pinto, DJ; McMahan, RE; Morales, A; Cubero-Ponce, L; Hahn, MS, Approach for fabricating tissue



engineered vascular grafts with stable endothelialization. *Annals of Biomedical Engineering* **2010**, *38*: 2885-2895.

[210] Liu J-C, A novel strategy for engineering vascularized grafts in vitro. *World journal of stem cells* **2010**, *2*: 93-6.

[211] Fennema E; Rivron, N; Rouwkema, J; van Blitterswijk, C; de Boer, J, Spheroid culture as a tool for creating 3d complex tissues. *Trends in Biotechnology* **2013**, *31*: 108-115.

[212] Alajati A; Laib, AM; Weber, H; Boos, AM; Bartol, A; Ikenberg, K; Korff, T; Zentgraf, H; Obodozie, C; Graeser, R; Christian, S; Finkenzeller, G; Stark, GB; Heroult, M; Augustin, HG, Spheroid-based engineering of a human vasculature in mice. *Nature Methods* **2008**, *5*: 439-445.

[213] Bhang SH; Lee, S; Lee, T-J; La, W-G; Yang, H-S; Cho, S-W; Kim, B-S, Three-dimensional cell grafting enhances the angiogenic efficacy of human umbilical vein endothelial cells. *Tissue Engineering Part A* **2012**, *18*: 310-319.

[214] Laib AM; Bartol, A; Alajati, A; Korff, T; Weber, H; Augustin, HG, Spheroid-based human endothelial cell microvessel formation in vivo. *Nature Protocols* **2009**, *4*: 1202-1215.

[215] Silva AKA; Juenet, M; Meddahi-Pelle, A; Letourneur, D, Polysaccharide-based strategies for heart tissue engineering. *Carbohydrate Polymers* **2015**, *116*: 267-277.

[216] Abdalla S; Makhoul, G; Minh, D; Chiu, RCJ; Cecere, R, Hyaluronic acid-based hydrogel induces neovascularization and improves cardiac function in a rat model of myocardial infarction. *Interactive Cardiovascular and Thoracic Surgery* **2013**, *17*: 767-772.

[217] Ouasti S; Donno, R; Cellesi, F; Sherratt, MJ; Terenghi, G; Tirelli, N, Network connectivity, mechanical properties and cell adhesion for hyaluronic acid/peg hydrogels. *Biomaterials* **2011**, *32*: 6456-6470.

[218] Ifkovits JL; Tous, E; Minakawa, M; Morita, M; Robb, JD; Koomalsingh, KJ; Gorman, JH; Gorman, RC; Burdick, JA, Injectable hydrogel properties influence infarct expansion and extent of postinfarction left ventricular remodeling in an ovine model. *Proceedings of the National Academy of Sciences of the United States of America* **2010**, *107*: 11507-11512.

[219] Croll TI; O'Connor, AJ; Stevens, GW; Cooper-White, JJ, A blank slate? Layer-by-layer deposition of hyaluronic acid and chitosan onto various surfaces. *Biomacromolecules* **2006**, *7*: 1610-1622.

- [220] Thierry B; Winnik, FM; Merhi, Y; Silver, J; Tabrizian, M, Bioactive coatings of endovascular stents based on polyelectrolyte multilayers. *Biomacromolecules* **2003**, *4*: 1564-1571.
- [221] Bianchi F; Vassalle, C; Simonetti, M; Vozzi, G; Domenici, C; Ahluwalia, A, Endothelial cell function on 2d and 3d micro-fabricated polymer scaffolds: Applications in cardiovascular tissue engineering. *Journal of Biomaterials Science-Polymer Edition* **2006**, *17*: 37-51.
- [222] Seunarine K; Gadegaard, N; Tormen, M; O Meredith, D; O Riehle, M; Wilkinson, CDW, 3d polymer scaffolds for tissue engineering. *Nanomedicine* **2006**, *1*: 281-296.
- [223] Helmerhorst E; Chandler, DJ; Nussio, M; Mamotte, CD, Real-time and label-free biosensing of molecular interactions by surface plasmon resonance: A laboratory medicine perspective. *The Clinical biochemist. Reviews / Australian Association of Clinical Biochemists* **2012**, *33*: 161-73.
- [224] Hoang Hiep N; Park, J; Kang, S; Kim, M, Surface plasmon resonance: A versatile technique for biosensor applications. *Sensors* **2015**, *15*: 10481-10510.
- [225] Daghestani HN; Day, BW, Theory and applications of surface plasmon resonance, resonant mirror, resonant waveguide grating, and dual polarization interferometry biosensors. *Sensors* **2010**, *10*: 9630-9646.
- [226] Snopok BA, Theory and practical application of surface plasmon resonance for analytical purposes. *Theoretical and Experimental Chemistry* **2012**, *48*: 283-306.
- [227] Tang Y; Zeng, X; Liang, J, Surface plasmon resonance: An introduction to a surface spectroscopy technique. *Journal of Chemical Education* **2010**, *87*: 742-746.
- [228] Liedberg B; Nylander, C; Lunström, I, Surface plasmon resonance for gas detection and biosensing. *Sens. Actuator B-Chem.* **1983**, *4*: 299-304.
- [229] Jason-Moller L; Murphy, M; Bruno, J, Overview of biacore systems and their applications. *Current protocols in protein science / editorial board, John E. Coligan ... [et al.]* **2006**, *19*: 13-19.
- [230] Majka J; Speck, C, Analysis of protein-DNA interactions using surface plasmon resonance. In *Analytics of protein-DNA interactions*, Seitz, H., Ed. Springer-Verlag Berlin: Berlin, **2007**, *104*: 13-36.

- [231] Arkin MR; Wells, JA, Small-molecule inhibitors of protein-protein interactions: Progressing towards the dream. *Nature Reviews Drug Discovery* **2004**, *3*: 301-317.
- [232] Rich RL; Hoth, LR; Geoghegan, KF; Brown, TA; LeMotte, PK; Simons, SP; Hensley, P; Myszka, DG, Kinetic analysis of estrogen receptor/ligand interactions. *Proceedings of the National Academy of Sciences of the United States of America* **2002**, *99*: 8562-8567.
- [233] Habauzit D; Armengaud, J; Roig, B; Chopineau, J, Determination of estrogen presence in water by spr using estrogen receptor dimerization. *Analytical and Bioanalytical Chemistry* **2008**, *390*: 873-883.
- [234] Marx KA, Quartz crystal microbalance: A useful tool for studying thin polymer films and complex biomolecular systems at the solution-surface interface. *Biomacromolecules* **2003**, *4*: 1099-1120.
- [235] Benes E; Groschl, M; Burger, W; Schmid, M, Sensors based on piezoelectric resonators. *Sens. Actuator A-Phys.* **1995**, *48*: 1-21.
- [236] Rodahl M; Kasemo, B, A simple setup to simultaneously measure the resonant frequency and the absolute dissipation factor of a quartz crystal microbalance. *Rev. Sci. Instrum.* **1996**, *67*: 3238-3241.
- [237] Kankare J, Sauerbrey equation of quartz crystal microbalance in liquid medium. *Langmuir* **2002**, *18*: 7092-7094.
- [238] Hook F; Kasemo, B; Nylander, T; Fant, C; Sott, K; Elwing, H, Variations in coupled water, viscoelastic properties, and film thickness of a mefp-1 protein film during adsorption and cross-linking: A quartz crystal microbalance with dissipation monitoring, ellipsometry, and surface plasmon resonance study. *Analytical Chemistry* **2001**, *73*: 5796-5804.
- [239] Su XD; Robelek, R; Wu, YJ; Wang, GY; Knoll, W, Detection of point mutation and insertion mutations in DNA using a quartz crystal microbalance and muts, a mismatch binding protein. *Analytical Chemistry* **2004**, *76*: 489-494.
- [240] Zhou C; Friedt, JM; Angelova, A; Choi, KH; Laureyn, W; Frederix, F; Francis, LA; Campitelli, A; Engelborghs, Y; Borghs, G, Human immunoglobulin adsorption investigated by means of quartz crystal microbalance dissipation, atomic force microscopy, surface acoustic wave, and surface plasmon resonance techniques. *Langmuir* **2004**, *20*: 5870-5878.

- [241] Dixon MC, Quartz crystal microbalance with dissipation monitoring: Enabling real-time characterization of biological materials and their interactions. *Journal of biomolecular techniques* **2008**, *19*: 151-158.
- [242] Su X; Lin, C-Y; O'Shea, SJ; Teh, HF; Peh, WYX; Thomsen, JS, Combinational application of surface plasmon resonance spectroscopy and quartz crystal microbalance for studying nuclear hormone receptor-response element interactions. *Analytical Chemistry* **2006**, *78*: 5552-5558.
- [243] Peh WYX; Reimhult, E; Teh, HF; Thomsen, JS; Su, X, Understanding ligand binding effects on the conformation of estrogen receptor alpha-DNA complexes: A combinational quartz crystal microbalance with dissipation and surface plasmon resonance study. *Biophysical Journal* **2007**, *92*: 4415-4423.
- [244] Liu Y; Mai, S; Li, N; Yiu, CKY; Mao, J; Pashley, DH; Tay, FR, Differences between top-down and bottom-up approaches in mineralizing thick, partially demineralized collagen scaffolds. *Acta Biomaterialia* **2011**, *7*: 1742-1751.
- [245] Biswas A; Bayer, IS; Biris, AS; Wang, T; Dervishi, E; Faupel, F, Advances in top-down and bottom-up surface nanofabrication: Techniques, applications & future prospects. *Advances in Colloid and Interface Science* **2012**, *170*: 2-27.
- [246] Walt DR, Nanomaterials - top-to-bottom functional design. *Nature Materials* **2002**, *1*: 17-18.
- [247] Wu MH; Whitesides, GM, Fabrication of arrays of two-dimensional micropatterns using microspheres as lenses for projection photolithography. *Applied Physics Letters* **2001**, *78*: 2273-2275.
- [248] Falconnet D; Koenig, A; Assi, T; Textor, M, A combined photolithographic and molecular-assembly approach to produce functional micropatterns for applications in the biosciences. *Advanced Functional Materials* **2004**, *14*: 749-756.
- [249] Tourovskaia A; Barber, T; Wickes, BT; Hirdes, D; Grin, B; Castner, DG; Healy, KE; Folch, A, Micropatterns of chemisorbed cell adhesion-repellent films using oxygen plasma etching and elastomeric masks. *Langmuir* **2003**, *19*: 4754-4764.
- [250] Xu F; Wu, J; Wang, S; Durmus, NG; Gurkan, UA; Demirci, U, Microengineering methods for cell-based microarrays and high-throughput drug-screening applications. *Biofabrication* **2011**, *3*:4-10.

- [251] Esch EW; Bahinski, A; Huh, D, Organs-on-chips at the frontiers of drug discovery. *Nature Reviews Drug Discovery* **2015**, *14*: 248-260.
- [252] Nakanishi J; Takarada, T; Yamaguchi, K; Maeda, M, Recent advances in cell micropatterning techniques for bioanalytical and biomedical sciences. *Analytical Sciences* **2008**, *24*: 67-72.
- [253] Sin MLY; Mach, KE; Wong, PK; Liao, JC, Advances and challenges in biosensor-based diagnosis of infectious diseases. *Expert Review of Molecular Diagnostics* **2014**, *14*: 225-244.
- [254] Barthes J; Oezcelik, H; Hindie, M; Ndreu-Halili, A; Hasan, A; Vrana, NE, Cell microenvironment engineering and monitoring for tissue engineering and regenerative medicine: The recent advances. *Biomed Research International* **2014**, *9*: 56-98.
- [255] Cagnin S; Cimetta, E; Guiducci, C; Martini, P; Lanfranchi, G, Overview of micro- and nano-technology tools for stem cell applications: Micropatterned and microelectronic devices. *Sensors* **2012**, *12*: 15947-15982.
- [256] Fan VH; Au, A; Tamama, K; Littrell, R; Richardson, LB; Wright, JW; Wells, A; Griffith, LG, Tethered epidermal growth factor provides a survival advantage to mesenchymal stem cells. *Stem Cells* **2007**, *25*: 1241-1251.
- [257] Ito Y; Chen, GP; Imanishi, Y, Micropatterned immobilization of epidermal growth factor to regulate cell function. *Bioconjugate Chemistry* **1998**, *9*: 277-282.
- [258] Chen GP; Ito, YY, Gradient micropattern immobilization of egf to investigate the effect of artificial juxtacrine stimulation. *Biomaterials* **2001**, *22*: 2453-2457.

## CHAPTER TWO

---

### **Phosphorylcholine-modified chitosan films as effective promoters of cell aggregation: correlation between the films properties and cellular response**

Baowen Qi<sup>1</sup>, Piotr Kujawa<sup>2</sup>, Sayaka Toita<sup>1</sup>, Gregory Beaune<sup>2</sup>, Françoise M. Winnik<sup>1,2</sup>

<sup>1</sup>Faculté de Pharmacie and Département de Chimie, Université de Montreal, CP 6128 Succursale Centre Ville, Montreal, QC, H3C 3J7, Canada

<sup>2</sup>World Premier International (WPI) Research Center Initiative, International Center for Materials Nanoarchitectonics (MANA), National Institute for Materials Science (NIMS), 1-1 Namiki Tsukuba, Ibaraki 305-0044, Tsukuba, Japan

Article published in: *Macromolecular Bioscience*, **2015**, 15, 490–500.

#### **Summary of transition**

In order to develop a self-assembly bottom-up approach for the E2 surface immobilization, we selected a chitosan phosphorylcholine (CH-PC) biopolymer as a backbone due to its cationic nature and good biocompatibility. In this chapter, the physical and biological properties of CH-PC thin films were extensively investigated by the combination of SPR, QCM-D, and cellular studies. Combined with SPR and QCM-D measurements, it demonstrated that the non-fouling properties of CH-PC films were highly dependent on the incorporated PC contents. Moreover, the facts that endothelial cells (HUVEC) form 3D spheroid structures on the higher level of PC contents of CH-PC films indicated the potentials of CH-PC platforms in the cardiovascular regenerative medicine. However, the relevant *in vivo* studies were not performed. In future, 3D spheroid of HUVEC cultured on the CH-PC films should be developed and transplanted into myocardial ischaemia animal models to investigate their cardiovascular protective efficacy by survival rate or histological analysis. The present study provided detailed information for the next chapter of the preparation CH-PC-E2 conjugates from a polymer perspective.

## **2.1 Abstract**

This study describes the elaboration and characterization of chitosan-phosphorylcholine (CH-PC) films able to support the formation of cell aggregates (spheroids), which are important for tissue engineering and pharmacological studies. The surface topography, charge, thickness, and rheology of CH-PC thin films of different levels of PC incorporation were characterized by AFM, zeta-potential measurements, SPR spectroscopy, and QCM-D measurements. The combined studies indicate that CH-PC films are highly hydrated gels, independently of the level of PC incorporation (15 to 40 mol% PC/glucosamine units). However, QCM-D studies also established that the amount of fibrinogen adsorbed on CH-PC films decreased significantly with increasing PC content. On the macroscopic scale, the CH-PC surfaces underwent a transition from moderately cell-adhesive (CH-PC15) to non-adhesive (CH-PC40). Optical micrographs of HUVEC and MCF-7 cell lines cultured on CH-PC surfaces showed that they form spheroids on CH-PC25 and CH-PC40 films.

## **2.2 Author Keywords**

Chitosan; Biopolymers; Polyelectrolyte; Adsorption; Thin films

## 2.3 Introduction

The implementation of nanotechnology and nanoarchitectonics<sup>[1]</sup> in the design of biomaterials has had a major impact on contemporary medicine, particularly in the case of medical implants and drug delivery systems. Nanofunctionalized biomaterials play also a crucial role as *in vitro* models to study complex biological phenomena, including cell motion, proliferation, and adhesion.<sup>[2-6]</sup> Current research thrusts are directed towards the design of nanostructured surfaces able to reproduce *in vitro* the three dimensional environment experienced by cells. Such smart substrates could provide reliable and cost-effective assays in the study of the clinical outcome of new therapies, in addition to, or in lieu of, animal studies. A particularly promising approach consists in carrying *in vitro* assays on three-dimensional cell aggregates, or spheroids, rather than on flat cellular monolayers. Such methods are highly relevant to oncological conditions, such as tumor invasion and metastasis.<sup>[7, 8]</sup> There are also relevant in studies of the cardiovascular system, where spheroids of endothelial cells (ECs) are excellent tools to study the differentiation and functions of endothelial ECs, whereas ECs cultured on standard 2-dimensional surfaces lose many of their differentiated phenotypic properties.<sup>[9]</sup> Currently, cell biologists dispose of only a few substrates known to promote cell aggregation. Several methods have evolved that promote the formation of cell–cell junctions and the creation of cell aggregates. Current methods used to produce spheroids include the culture of cells in non-adhesive tissue culture plates placed on an orbital shaker,<sup>[10, 11]</sup> the hanging-drop method which induces the re-aggregation of islets into relatively uniform spherical clusters,<sup>[12, 13]</sup> and the hydrogel micro-well cell-culture method.<sup>[14, 15]</sup> For *in-vivo* implantations studies, it is preferable to assemble spheroids directly on the biomaterials to be implanted. This method allows one to modulate cell/substrate interactions via the adhesive properties of the substrate. Chitosan<sup>[16, 17]</sup> and hyaluronic acid membranes,<sup>[18]</sup> for instance, were used to prepare non-adhesive surfaces. However, in all cases reported so far, cell aggregation on a given material was cell line dependent. The availability of simple substrates able to induce spheroid formation in a predictable way would certainly stimulate research in this field, ultimately widening the range of spheroid-based assays. Cells spontaneously diffuse and meet to form compact clusters when they are placed on non-adhesive substrates where spreading is energetically unfavorable. In this situation, cells are considered to be in a partial



wetting regime in which the cell substrate adhesion energy is less than the cell-cell adhesion energy.<sup>[19]</sup> Therefore, one simple approach to build a library of substrates prone to induce cell aggregation consists in preparing thin films using biopolymers consisting of a cell-adherent backbone carrying various amounts of cell repelling functions exposed to the film/cell medium interface. This palette of substrates could then be used to select the optimal substrate for a given cell line.

Chitosan (CH), a polysaccharide derived from natural chitin, is a ubiquitous component of biomaterials in important medical fields, particularly as a substrate in tissue engineering and drug delivery.<sup>[20]</sup> Chitosan is biodegradable, biocompatible, and has antibacterial properties. It interacts with components of the extracellular matrix and has adhesive properties towards most cell types. Chemically, it is a linear polycation composed of  $\beta$ -D-glucosamine and  $\beta$ -D-N-acetylglucosamine residues linked through (1  $\rightarrow$  4) linkages. Chitosan dissolves readily in acidic aqueous solutions, but it is insoluble in neutral water.<sup>[21]</sup> We reported several years ago, the synthesis of chitosans bearing phosphorylcholine (PC) groups (CH-PC, Figure 2.1), designed to be soluble in water over a wide pH range by virtue of the hydrophilicity of the PC groups.

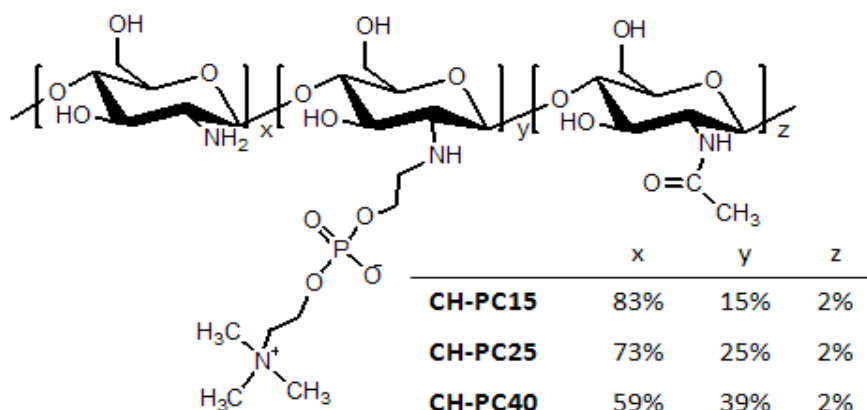


Figure 2.1 Chemical structure of phosphorylcholine-chitosans

We demonstrated that CH-PC samples are readily soluble under physiological conditions when the level of PC incorporation equals or exceeds ca. 15-20 mol% PC per glucosamine unit.<sup>[22]</sup> Similarly to chitosan, CH-PCs are nontoxic and biodegradable.<sup>[22, 23]</sup> In view of their high solubility in neutral water, CH-PCs were used to prepare estradiol-prodrugs.<sup>[24]</sup> However, CH-PCs were never tested as substrates for spheroid growth. Remembering that the zwitterionic PC functional group is known to reduce nonspecific adsorption to the solid/liquid interface,<sup>[25]</sup> it would appear that the CH-PC architecture is ideally suited to promote and modulate cell aggregation. The study reported here was carried out to test this hypothesis.

Precisely-designed CH-PC samples of identical molar mass and different levels of PC incorporation, synthesized under homogeneous conditions,<sup>[22]</sup> were cast on substrates to form thin films. The films were subjected to atomic force microscopy (AFM) examination, zeta-potential measurements, surface plasmon resonance (SPR) spectroscopy, and quartz crystal microbalance with dissipation (QCM-D) measurements in order to determine important mechanical cues, such as surface topography, roughness, charge, and rheology, known to influence the adhesion of cells on a substrate.<sup>[26-28]</sup> Human umbilical vein endothelial cells (HUVEC) selected as model endothelial cells and MCF-7 human breast cancer cells were cultured on CH-PC surfaces of varying PC content and monitored by optical microscopy over a period of 4 days. These preliminary *in vitro* studies indicate that both cell types form spheroids on CH-PC substrates and that, on a given substrate, the rate of aggregation depends markedly on cell type. The origin of this discrimination among the CH-PC surfaces is discussed in light of the physico-chemical properties of the films and their non-fouling properties assessed via QCM-D determination of the amount of fibrinogen adsorbed on their surface. The dynamics of HUVEC aggregation on CH-PC substrates were evaluated within the context of the Douezan and Brochard-Wyart model, based on the random diffusion of cells on non-adhesive substrates.

## 2.4 Experimental Section

### 2.4.1 Materials

Water (18.2 M $\Omega$ ·cm) was deionized using a Milli-Q water purification system (Millipore). Sodium cyanoborate, sodium 3-mercapto-1-propane sulfonate (MPS), and fibrinogen from human plasma were purchased from Sigma-Aldrich Co. All solvents were of reagent grade and used as received. Spectra/Pore membranes (Spectrum) were employed for dialysis. Chitosan (CH) (Mw 50~100 kDa, DDA: 88%) was purchased from Fisher Scientific Inc. It was deacetylated to a DDA of 98%, following a known procedure.<sup>[22]</sup> Phosphorylcholine glyceraldehyde was prepared as described previously.<sup>[29]</sup>

### 2.4.2 Synthesis and characterization of phosphorylcholine-chitosans (CH-PC)

The CH-PC samples were obtained by reaction of deacetylated CH with various amounts of phosphorylcholine-glyceraldehyde (PC-CHO) (Figure 2.1) following a modification of the procedure described in Tiera *et al.*,<sup>[22]</sup> which is described for the synthesis of CH-PC25. A solution of PC-CHO (0.38 g, 1.56 mmol) in water (10 mL) was added dropwise to a solution of deacetylated chitosan (0.52 g, 3.2 mmol of monosaccharide residue) in aqueous acetic acid (20 mL, 2 wt%) kept at 0 °C. At the end of the addition, the solution was stirred for 30 min at 0 °C. The pH of the reaction mixture was adjusted to 6.5 by adding aqueous NaOH (1.0 M). The reaction mixture was stirred for 1 h at room temperature. It was cooled to 0 °C, and a solution of sodium cyanoborohydride (0.48 g, 7.61 mmol) in water (10 mL) was added dropwise under stirring. Thereafter, the reaction mixture was warmed to room temperature and stirred for 20 h. It was dialyzed (membrane of MWCO 12,000-14,000 Da) first against water for 2 days, then against aqueous NaOH (0.05 M) for 1 day, and finally against water for 2 days. The polymer CH-PC25 was isolated by lyophilization (yield: 72%). The degree of PC substitution was calculated from the <sup>1</sup>H NMR spectrum of CH-PC solutions (10 mg mL<sup>-1</sup>) in D<sub>2</sub>O/DCl (100/1, v/v) recorded at 70 °C (see Figure SI.2.1) and by a colorimetric assay for phosphorus.<sup>[29, 30]</sup> The two methods yielded identical values, within experimental uncertainty.

### 2.4.3 Preparation of CH-PC solutions

Solutions of CH-PC in 0.08 N HCl (pH  $\sim$  3, 2.0 g L<sup>-1</sup>) were prepared and kept overnight at room temperature. Subsequently, they were filtered through a 0.45  $\mu$ m filter. Their pH was adjusted to 6.8 by addition of a few drops of aqueous NaOH (10%). The resulting solutions were diluted to a concentration of 1.0 g L<sup>-1</sup> with a 10 mM phosphate buffer (pH=7.4). The resulting solutions were kept overnight at ambient temperature and filtered through a 0.45  $\mu$ m filter prior to use.

### 2.4.4 Dynamic light scattering (DLS) and zeta potential measurements of CH-PC solutions.

DLS experiments were performed on a CGS-3 goniometer (ALV GmbH) equipped with an ALV/LSE-5003 digital correlator (ALV GmbH), a He-Ne laser ( $\lambda$  = 632 nm) and a C25P circulating water bath (Thermo Haake). The scattering angle was set at 90°. A cumulant analysis was applied to obtain the diffusion coefficient of the scattering objects in solution. The hydrodynamic radii ( $R_h$ ) of the nanoparticles were calculated from the diffusion coefficients using the Einstein-Smoluchowski equation. The zeta potential ( $\zeta$ -potential) of polymers in solution was determined with a Delsa Nano C instrument (Beckman Coulter, USA) equipped with a flow cell. Both DLS and  $\zeta$ -potential measurements were performed at 25°C with polymer solutions (1.0 g L<sup>-1</sup>) in a 10 mM phosphate buffer pH 6.8.

### 2.4.5 Dynamic AFM measurements

AFM imaging was performed in the tapping mode<sup>TM</sup> at ambient temperature with a MultiMode scanning probe microscope and NanoScope 5 controller (Bruker). Images were acquired with samples immersed in phosphate buffer (pH 6.8). Surfaces were analyzed using sharp silicon nitride levers (model SNL-10, Bruker) with a radius of curvature of 6 nm, a nominal spring constant of 0.24 N m<sup>-1</sup>, and a resonance frequency of 32 kHz in liquid. The scan rate and image resolution were 1 Hz and 512  $\times$  512 pixels, respectively. Images were corrected for bow/tilt by a third-order plane fit correction. Glass slides coated with 2 nm Ti and 20 nm Au were used as substrates. They were cleaned with a piranha solution containing concentrated sulfuric acid and 35 vol% hydrogen peroxide (v/v 7/3) (*WARNING: Piranha*

*solution is extremely reactive and should be handled with extreme caution.*) and rinsed with deionized water and ethanol before use. CH-PC films were prepared by immersing the slides in a CH-PC solution ( $1.0 \text{ g L}^{-1}$ ) for 4 h. The slides were rinsed with a phosphate buffer solution and transferred to an AFM liquid cell filled with the same buffer.

#### **2.4.6 Zeta potential measurements of CH-PC films**

The zeta potential of the CH-PC films was measured with a Delsa Nano C instrument (Beckman Coulter, USA) equipped with a flat surface cell. Rectangular glass supports (30 x 10 mm) cleaned with a piranha solution and rinsed with water and ethanol prior to use were kept in a CH-PC solution ( $1.0 \text{ g L}^{-1}$ ) for 4 h. Subsequently, they were placed in a sample cell filled with a suspension of particles (polystyrene) in 10 mM NaCl at a pH 6.8 kept at 25 °C. The electrophoretic movement of the particles under the applied electric field was detected along the vertical direction toward the center of the sample cell using the Doppler shift of scattered light

#### **2.4.7 Surface plasmon resonance (SPR) measurements**

SPR measurements were carried out with a SR7000 instrument (Reichert Inc.) equipped with a flow cell ( $1 \mu\text{L}$ , surface area:  $12 \text{ mm}^2$ ), an injector port, a six-way low-pressure solvent selection valve, and a syringe pump (model PHD 2000, Harvard Apparatus) described previously.<sup>[31]</sup> Surface plasmons were excited at the metal/solution interface in the Kretschmann configuration using the p-polarized output from a GaAlAs laser (15 mW, 780 nm) and a hemicylindrical sapphire prism. The prism stayed in optical contact (Cargille immersion oil Type A liquid,  $n = 1.515$ ) with the underside of a gold-coated glass slide. Light totally internally reflected from the gold/solution interface was detected with a 3696-pixel CCD linear array for which the optical pixel signals were digitized with a 14-bit analogue-to-digital converter. In the angle tracking mode the SPR minimum pixel, which corresponds to the minimum SPR angle ( $\theta_m$ ), was tracked with time by a centroid algorithm using the signal from a few pixels on either side of the pixel of lowest intensity. Reflected light intensity versus pixel number curves (referred to as array scans) were generated as well. The shifts in the minimum pixel were converted to resonance angle changes ( $\Delta\theta_m$ ) using the pixel-to-

incident angle relation, *i.e.*, 1 pixel = 0.00506°, established through calibration of the SR7000 instrument across the refractive index range of 1.33-1.38 with pure water and aqueous solutions of 4-50 wt% ethylene glycol, as described in details in Badia *et al.*<sup>[31]</sup> Shifts in  $\Delta\Theta_m$  calculated from angle tracking agreed well with those obtained from array scans. The Fresnel model was used to calculate the “dry” film surface coverage ( $\Gamma_d$ ) from the shift in  $\Delta\Theta_m$  (see ESI). D263 glass slides (12.5 mm × 12.5 mm × 0.9 mm) coated with 1 nm Cr and 45 nm Au (Reichert Inc.) were cleaned with a piranha solution and rinsed with deionized water and ethanol before use. They were submerged in a MPS solution in ethanol (1 mM) for at least 16 h. The substrates were rinsed copiously with ethanol to remove excess MPS and dried with nitrogen, and placed in the sample cell. Phosphate buffer was passed through the cell (50  $\mu\text{L min}^{-1}$ ) to establish the baseline. Next, a polymer solution was injected manually into the sample loop and carried into the measurement chamber by a constant flow of buffer until the shift in SPR minimum position was constant (ca. 30 min.). The cell was then rinsed with the buffer.

#### **2.4.8 Quartz crystal microbalance with dissipation (QCM-D) measurements**

QCM-D measurements were carried out with a QCM-D model E4 system (Biolin) that allows for simultaneous measurements of frequency changes ( $\Delta f$ ) and energy dissipation changes ( $\Delta D$ ).<sup>[32, 33]</sup> QCM-D signals were registered for the fundamental frequency (5 MHz) and  $m = 5$  overtones (15, 25, ..., 55 MHz). For clarity, the results are presented as the normalized frequency and dissipation shifts registered for the fifth overtone (25 MHz). The layer thickness and the film mechanical properties were calculated based on the Voigt viscoelastic model.<sup>[31]</sup> The surface coverage (or “wet” mass)  $\Gamma_w$  was calculated based on  $\Delta f$  and  $\Delta D$  for five overtones. The film density was obtained by combining QCM-D and SPR data (equation (SI 3)-(SI 4)). This density value was used in final modeling procedure to calculate the film thickness  $d$ , and storage and loss moduli ( $G'$  and  $G''$ , respectively). In the model it was assumed that  $G'$  and  $G''$  are characterized by a power-law frequency dependence with critical exponents  $\alpha$  and  $\beta$ , respectively ( $G' \propto f^\alpha$  and  $G'' \propto f^\beta$ ).

Cleaned gold-coated 5-MHz AT-cut quartz crystals (Quartz Pro) were submerged in a MPS solution in ethanol (1 mM) for at least 16 h. They were rinsed copiously with ethanol to remove excess MPS, dried with nitrogen and placed in the sample compartment. A solution of CH-PC in a phosphate buffer was introduced into the sample cell at a flow rate of  $20 \mu\text{L min}^{-1}$  until the frequency and dissipation reached constant values. Next, the cell was flushed with buffer to remove excess polymer. For studies of fibrinogen adsorption on CH-PC, a solution of fibrinogen ( $0.1 \text{ g L}^{-1}$ ) was introduced into the cell at a rate of  $20 \mu\text{L min}^{-1}$ . Free fibrinogen was removed subsequently by rinsing the chamber with phosphate buffer. All the experiments were performed at  $20.00 \pm 0.05 \text{ }^\circ\text{C}$ .

#### 2.4.9 Ellipsometry measurements

Ellipsometry measurements were carried out on an M-2000V multi-wavelength ellipsometer (J.A. Woollam Co.) at an incident angle of  $75^\circ$  with a wavelength range of 370 to 1000 nm. Data were analyzed with the WVASE32 software, supplied by the manufacturer. The film thickness was estimated using the relation of Cauchy (equation 1):

$$n(\lambda) = A_n + \frac{B_n}{\lambda^2} + \frac{C_n}{\lambda^4} \quad (1)$$

where  $\lambda$  is the wavelength and  $n$  is the refractive index. The refractive index value was taken as 1.59, based on previous publications.<sup>[34]</sup>

CH-PCx films were prepared on silicon wafers cleaned with a piranha solution (*Caution, see above*), washed with deionized water and dried. A few drops of a CH-PC solution ( $1.0 \text{ g L}^{-1}$ ) in a 10 mM phosphate buffer of pH 6.8 were placed on a cleaned wafer which was then air-dried in a hood for 17 hrs. The film was rinsed with water and dried prior to measurements.

#### 2.4.10 Cell culture

Polymer-coated substrates were prepared by drop-casting CH-PC solutions in phosphate buffer pH 6.8 ( $1.0 \text{ g L}^{-1}$ ) in 96-well plates ( $50 \mu\text{L}$  per well), followed by water evaporation at ambient conditions in a fume hood. Human umbilical vein endothelial cells (HUVECs) (purchased from Lonza) were grown within three passages in endothelial growth

medium-2 (EGM-2; Lonza) supplemented with 10% fetal bovine serum. The cultures were maintained in an atmosphere of humidified 95% air and 5% CO<sub>2</sub> at 37 °C. HUVECs were harvested using 0.25% trypsin-EDTA and seeded on CH-PC films at a density of 50,000 cells per well. MCF-7 human breast cancer cells (HTB-22<sup>TM</sup>), purchased from the American Type Culture Collection, were cultured in Eagle's Minimum Essential Medium (MEM, Sigma), supplemented with 10% (v/v) fetal bovine serum, 2 mM L-glutamine (Wako), 1 mM sodium pyruvate (Wako), 1% non-essential amino acids (Gibco) and 1% penicillin-streptomycin solution (Wako) in a humidified 5% CO<sub>2</sub> atmosphere at 37°C. Cells were harvested by using 10,000 cells per well. Immediately prior to cell seeding, the CH-PCx films coated well plates were sterilized with 75% ethanol, washed three times with phosphate buffer, and conditioned for 5 min in the EGM-2 culture medium (HUVEC) or MEM supplemented with 10% FBS (MCF-7).

#### **2.4.11 Cell observation by optical microscopy**

Observations of cells were conducted over a period of 4 days after seeding using a motorized inverted IX81 microscope (Olympus) equipped with a charge-coupled device camera (Retiga-EXi, Q-Imaging), a motorized stage (Molecular Devices), and controlled by the MetaMorph Imaging System (ver. 7.6.3.0, Molecular Devices).

## **2.5 Results and discussion**

### **2.5.1 Morphology and charge of the CH-PC Films**

The nanoscale topography of the substrates, known to affect cell adhesion, was assessed by atomic force microscopy (AFM), an effective tool for studying the morphology of nanostructured surfaces in real-space and under realistic conditions. CH-PC films cast on hydrophilic glass and immersed in a pH 6.8 phosphate buffer were observed by AFM. Selected images and cross-sectional profiles taken along the X-axis are presented in Figure 2.2 for films obtained with the three CH-PC samples. All films present surface features that increase in size from small islets to larger globular structures with increasing levels of PC groups on the polymer. Islets ~ 1.5 nm in height and ~ 13 to 22 nm in width form predominantly in the case of CH-PC15. More pronounced features can be seen on the surfaces



of CH-PC25 and CH-PC40 films. Globular protrusions  $\sim 3$  nm in height and  $\sim 40$  to  $56$  nm in width are observed on the surface of CH-PC25 films. In the case of CH-PC40 films, the protrusions are larger ( $\sim 4$  nm in height and  $\sim 53$  to  $71$  nm in width).

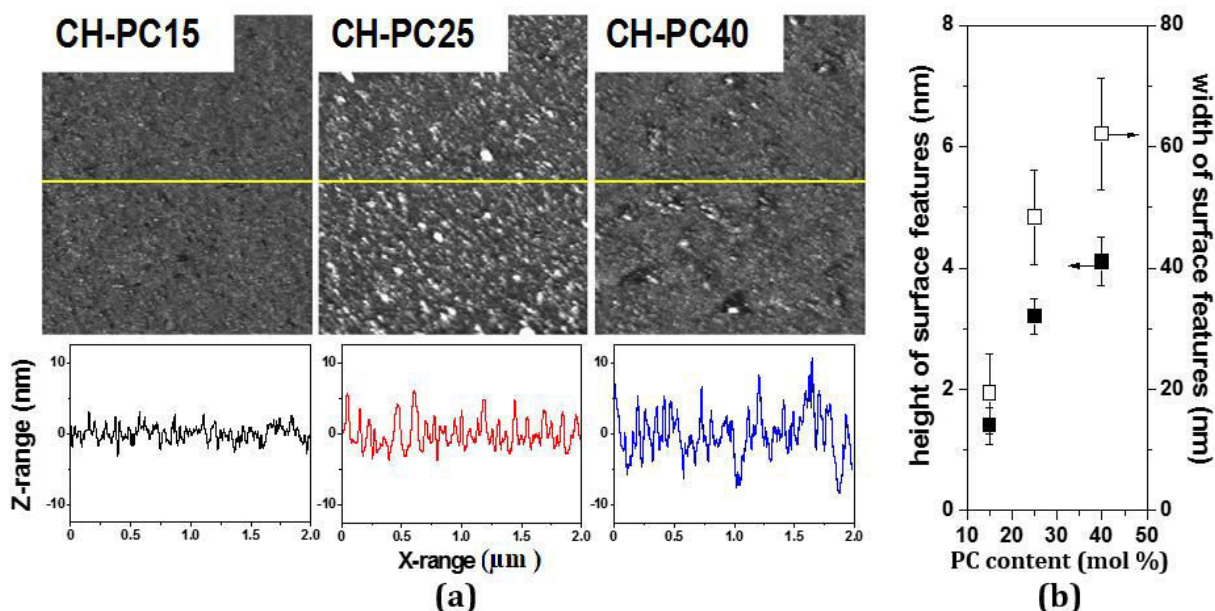


Figure 2.2 (a) AFM topography images of CH-PC films ( $2 \mu\text{m} \times 2 \mu\text{m}$ ) acquired in a phosphate buffer pH 6.8; maximum height (Z-range): 12 nm (CH-PC15 and CH-PC25) and 25 nm (CH-PC40) and cross-sectional profiles along the X axis corresponding to the yellow lines drawn through the AFM images; (b) Height and width of the surface features determined by AFM.

Intrigued by the distinctively different features of the film surfaces depending on the polymer structure, we examined CH-PC solutions by dynamic light scattering (DLS) measurements. Although the solutions were clear to the eye, DLS revealed the existence in solution of loosely self-assembled CH-PC assemblies of broad size distribution, with hydrodynamic radii ( $R_h$ ) on the order of  $\sim 100$  nm. The  $R_h$  values exhibited a slight dependence on the PC-incorporation level. The polymer with the fewest PC substituents (CH-PC15) forms significantly larger objects ( $R_h = 117 \pm 5$  nm), compared to the more substituted chitosans ( $R_h = 84 \pm 4$  nm and  $96 \pm 5$  nm, for CH-PC25 and CH-PC40, respectively), pointing to the prevalent role of ion-pairing among PC groups in controlling the solution properties of

CH-PC samples.<sup>[24]</sup> For all polymers, the particles exhibited a positive zeta-potential ( $22 \pm 3$  mV), independently of their PC-substitution levels. The islets observed by AFM are much smaller than the size of the nanoparticles detected by DLS in solutions of this polymer, particularly in the case of CH-PC15, which indicates that loosely bound nanoparticles formed in solution reorganize upon adsorption on the negatively charged MPS surface.

Surface topography has a direct influence on cell affinity towards the underlying substrate. Cell adhesion and spreading can be significantly inhibited by the nanoscale features (ca. 100 nm) that approximately match the length scale of integrin clustering in focal adhesion.<sup>[35, 36]</sup> Focal contact formation is disrupted to a lesser degree in the case of very large (*e.g.* a few micrometers) or very small (< 50 nm) surface features. For films of CH-PC15, the width of the surface features (ca. 18 nm) could inhibit cellular adhesion somewhat, but they may be too small to induce cellular aggregation. In the case of CH-PC25 and CH-PC40 films, the width of the surface features becomes significantly larger (ca. 40 to 70 nm). They are within the range of distances required for integrin clustering, which may favor the formation of spheroids.

Films of the three polymers coated on hydrophilic glass were positively charged. The  $\zeta$ -potential of CH-PC15 films ( $+ 21.0 \pm 2.0$  mV) was similar to the  $\zeta$ -potential of the nano-assemblies formed by this polymer in buffer ( $+ 23.7 \pm 2.1$  mV). The  $\zeta$ -potentials of CH-PC25 and CH-PC40 films ( $+ 16.3 \pm 1.7$  mV and  $+ 13.2 \pm 1.2$  mV, respectively) were lower than the values recorded for the respective nanostructures in solution, adding further evidence of partial disruption of the CH-PC25 and CH-PC40 particles upon adsorption on the glass substrate and concomitant migration of PC groups from the aggregate interior towards the water/film interface.<sup>[24]</sup> The amount of interfacial charges influences cellular behavior significantly, mainly by controlling protein adsorption at the surface.<sup>[37]</sup> Cell attachment to substrates is usually mediated by adhesion proteins contained in serum-supplemented culture medium *in vitro* or blood *in vivo*. The ability of the substrates to adsorb such proteins from serum determines their ability to support cell adhesion. As a general rule, cell affinity towards a surface increases with increasing charge density of the substrate. The more a surface is charged, the more it is coated with proteins from cell medium or blood, and it is through this adsorbed protein layer that cells sense the surface and adsorb as well. Therefore, the low zeta

potential values observed for the films of high PC content, *i.e.* CH-PC-25 and CH-PC40, are favorable factors for reducing cell-substrate affinity and hence enhancing cell aggregation.

### 2.5.2 Hydration and mechanical properties of CH-PC films

In addition to surface charge and topography, cellular aggregation can be significantly influenced by the mechanical properties of the underlying films and by their hydration level. The aim of combined surface plasmon resonance (SPR) and quartz crystal microbalance with dissipation (QCM-D) experiments presented below was to determine how these physicochemical parameters are affected by the amount of PC groups in the films. For these experiments the polymers were deposited on gold substrates coated with MPS used to form a negatively charged interface analogous to the substrates used for AFM imaging and  $\zeta$ -potential measurements. Changes of the SPR resonance angle,  $\Delta\theta$ , and the QCM-D frequency,  $F$ , were recorded as a function of time following injection of a CH-PC solution in the sample cell of the SPR and QCM-D systems fitted with MPS-coated gold. The corresponding SPR and QCM-D traces are presented in Figure 2.3.

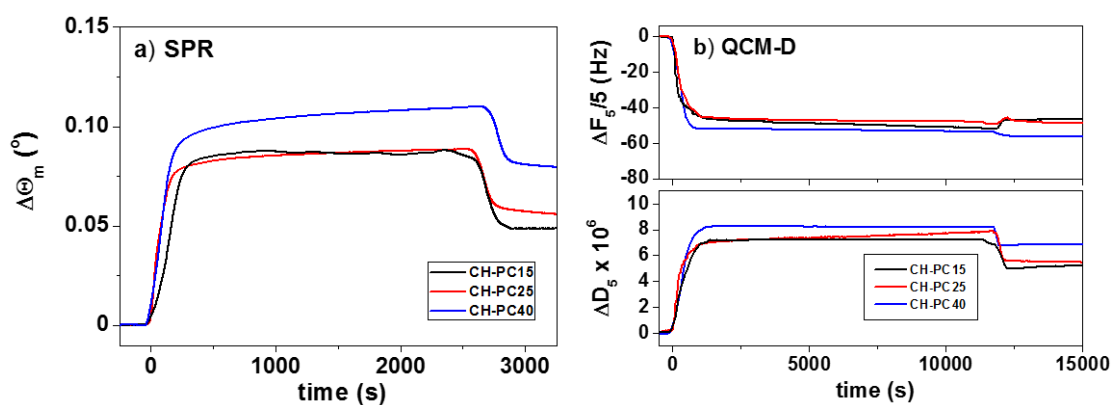


Figure 2.3 SPR and QCM responses of MPS-modified gold substrates when exposed to solutions of CH-PC ( $1.0 \text{ g L}^{-1}$ ) in phosphate buffer, pH 6.8: a) changes in the SPR resonance angle ( $\Delta\theta_m$ ) and b) changes in resonance frequency ( $\Delta f_5/5$ , top) and dissipation ( $\Delta D_5$ , bottom) observed in the QCM-D experiments for the 5<sup>th</sup> overtone.

Immediately upon injection of polymer solutions, the resonance angle  $\theta$  and the frequency  $F$  underwent rapid changes. The resonance angle increased, while the frequency decreased, implying that the polymers adsorb on the substrates. This process was accompanied

by an increase in the dissipation,  $D$ , measured in the QCM-D experiments (Figure 2.3b, lower panel). When  $\theta$ ,  $F$ , and  $D$  reached constant values, the flow of the polymer solution was discontinued. It was replaced by a flow of buffer, which caused a slight decrease of the SPR resonance angle and weak changes of the QCM frequency and dissipation signals. Hence, a small amount of excess polymer was removed by the flow of buffer. The SPR and QCM-D signal change due to polymer adsorption was calculated by comparing the signals in polymer free buffer. The values of the shifts  $\Delta\theta_m$ ,  $\Delta f_5/5$ , and  $\Delta D_5$  recorded by SPR and QCM-D at the end of the adsorption/rinse sequence for the three CH-PC samples are listed in Table 2.1 together with values recorded for chitosan used as a control sample (see SI for details on the chitosan adsorption protocol). From the changes of the SPR and QCM-D signals, it is possible to evaluate the amount of adsorbed polymer. The “dry” polymer mass,  $\Gamma_d$ , which corresponds to the weight of adsorbed polymer without solvent, was calculated from the film thickness determined from SPR data using a Fresnel model. The adsorbed “wet” mass,  $\Gamma_w$ , defined as the sum of the weight of adsorbed polymer and the mass of the water trapped in the film, was obtained from the QCM-D data, using the Voigt viscoelastic model. This data treatment, which assumes that the experimentally obtained frequency depends on the film storage and loss moduli, has proven to be useful to model protein films.<sup>[38]</sup> It was used also to describe the dynamics and composition of films formed by estradiol-conjugated CH-PC samples.<sup>[24]</sup> Details of the calculations and data modeling are provided in SI. The wet and dry mass of adsorbed CH-PC films increase with increasing level of PC incorporation. The wet mass of each film was one order of magnitude larger than its dry mass (Table 2.1).

Table 2.1 Physico-chemical properties of films formed by CH-PC15, CH-PC25, CH-PC40, and CH thin films formed on MPS-modified gold surfaces at pH 5.5.<sup>a</sup>

Polymer	SPR measurements		QCM-D measurements			Water content [wt%]	Density [g dm <sup>-3</sup> ]	Thickness [nm]	G' [MPa]	G'' [MPa]
	$\Delta\theta_m$	$\Gamma_d$	$\Delta f_5/5$	$\Delta D_5 \times 10^6$	$\Gamma_w$					
	[°]	[mg m <sup>-2</sup> ]	[Hz]		[mg m <sup>-2</sup> ]					
<b>CH-PC15</b>	0.04932	0.908	-46.3	5.2	10.1	91%	1038	9.72	0.75	0.34
<b>CH-PC25</b>	0.06128	1.132	-48.1	5.5	11.8	90%	1039	11.3	0.60	0.22
<b>CH-PC40</b>	0.07873	1.467	-55.6	6.9	15.9	92%	1036	15.3	0.62	0.27
<b>CH<sup>b</sup></b>	0.02479	0.420	-13.5	2.9	4.39	90%	1045	3.97	-	-

<sup>a</sup> $\Delta\theta_m$  – SPR resonance angle,  $\Gamma_d$  – “dry” mass,  $\Delta f_5/5$  – QCM-D frequency shift for the 5<sup>th</sup> overtone,  $\Delta D_5$  – QCM-D dissipation change for the 5<sup>th</sup> overtone,  $\Gamma_w$  – “wet” mass, G' -storage modulus at 25 MHz, and G'' - loss modulus at 25 MHz. The estimated error in reported values is 5%, except for G' and G'' where it equals ca. 10%. <sup>b</sup> Experiments were performed with solutions of CH in an acetate buffer at pH 5.5, since chitosan is insoluble in water at neutral pH. Due to the low amount of adsorbed polymer, it was not possible to estimate the values of the storage and loss moduli.

The water content of the CH-PC films determined from  $\Gamma_d$  and  $\Gamma_w$  (see details in SI) is  $91 \pm 1\text{wt}\%$ , a value similar to the water content of chitosan film (90%). PC groups are hygroscopic and surrounded by a hydration shell formed by ca. 23 - 24 water molecules per PC group<sup>[39]</sup> held together by weak electrostatic interactions (ionic hydration).<sup>[40]</sup> One would expect that the presence of PC groups linked to CH would increase the film hydration level proportionally to the amount of PC moieties. The QCM-SPR data indicate that this not the case. This observation may be an indication that the PC groups are preferentially located on the film/water interface, where they interact freely with surrounding water molecules, as suggested also by the zeta-potential measurements (see above). This result is important, as PC groups must be exposed on the film/water interface in order to act as nonfouling groups. The migration of PC groups towards the film/water interface has been reported previously.<sup>[41, 42]</sup> The thickness (d) of the films, estimated from QCM-D data using  $1037 \pm 2 \text{ g dm}^{-3}$  as the average film density (equation (SI 3)) increases from  $\sim 4 \text{ nm}$  for CH films to  $\sim 15 \text{ nm}$  for CH-PC40 films, comparing to data measured by SPR  $\sim 0.4 \text{ nm}$  for CH films and  $\sim 1.4 \text{ nm}$  for CH-

PC40 films. The difference in film thickness reflects a difference in the chain conformation adopted by the polymers in the hydrated films. CH-PC films result from the adsorption on the surface of preformed nanoparticles with numerous PC-PC crosslinking points (see DLS results above). These connecting points are preserved in the films, preventing the polymers chains from adopting an extended conformation.

The storage and loss moduli of the films ranged from 0.22 to 0.75 MHz, which are typical values of biopolymer-based hydrogels, multilayers, and thin films.<sup>[43]</sup> The frequency dependence of the storage and loss moduli of CH-PC films was approximated by power laws with exponents  $\alpha$  and  $\beta$ , respectively:  $G' \propto f^\alpha$  and  $G'' \propto f^\beta$ ,<sup>[43, 44]</sup> that led to  $\alpha$  and  $\beta$  values approximately equal to 1, which are characteristic of gels or solutions of entangled polymers probed on short time scales.<sup>[44, 45]</sup> They support the description of CH-PC films as highly hydrated, entangled polymer gels with temporary junctions formed through ion pairing between PC groups. Overall, the SPR and QCM-D experiments indicate that the thickness and the rheology of hydrated CH-PC films adsorbed on MPS-coated gold exhibit a weak dependence on the amount of PC groups bound to the chitosan chains.

### 2.5.3 Fibrinogen adsorption on CH-PC films.

The importance of the adsorption of plasma proteins in controlling cell/surface interactions is commonly acknowledged. A model protein, fibrinogen, was chosen in this study since it plays an important role in regulating cell adhesion and activation. Fibrinogen is a large plasma protein that is negatively charged in physiological conditions ( $340 \text{ kg mol}^{-1}$ ,  $\text{pI} = 5.5$ ) and readily adsorbs on most surfaces. CH-PC films were assembled on MPS surfaces in the QCM-D sample cell following the protocol described above. After rinsing with PBS buffer, a fibrinogen solution ( $0.1 \text{ g L}^{-1}$ ) in the same buffer was injected in the cell. Changes of the frequency and dissipation were monitored as a function of time following fibrinogen injection (Figure 2.4). The amount of fibrinogen adsorbed on each film (Figure 2.4, left panel) was estimated from the frequency shifts using the Sauerbrey equation (equation (SI 2)). Since the CH-PC films on which fibrinogen is adsorbed exhibit some dissipation, the adsorbed values obtained by the Sauerbrey equation are mere estimates of the real amount of adsorbed

fibrinogen. Nonetheless, the values obtained give useful information on the relative non-fouling characteristics of the three CH-PC surfaces.

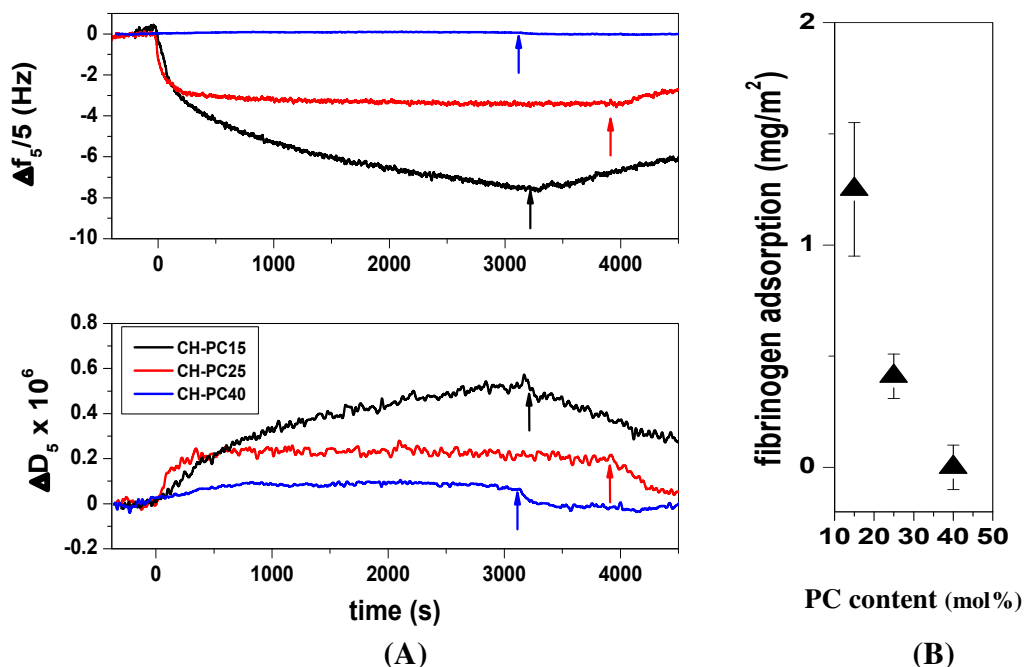


Figure 2.4 (A) Adsorption of fibrinogen on CH-PC films. Changes in resonance frequency and dissipation observed for the 5<sup>th</sup> overtone (upper and lower panels, respectively) for MPS-modified gold substrates coated with CH-PC upon exposure to a fibrinogen solution (0.1 g L<sup>-1</sup>, pH 6.8). The arrows indicate the time corresponding to the onset of the films rinse with PBS buffer. (B) Amount of fibrinogen adsorbed on the CH-PC coated substrates.

Films of CH-PC15 retained  $\sim 0.13 \mu\text{g cm}^{-2}$  fibrinogen, a value almost one order of magnitude lower than the amount of fibrinogen adsorbed on high affinity substrates.<sup>[46]</sup> For CH-PC40 films, the amount of adsorbed fibrinogen was less than  $0.01 \mu\text{g cm}^{-2}$ , the detection limit of the QCM-D employed. It was slightly above the detection limit in the case of CH-PC25 films. These results confirm that the PC groups retain their anti-fouling characteristics upon covalent attachment to chitosan and indicate that the film resistance against fibrinogen adsorption increases with increasing degree of PC substitution on the chitosan chains. The significant effect of PC incorporation level on the amount of fibrinogen adsorbed on CH-PC surfaces may be attributed to the increase in the surface concentration of PC as a result of the

migration of PC groups towards the water/film interface inferred from zeta potential measurements and QCM-D data (*vide supra*). Noting that the size of a fibrinogen molecule (length  $\times$  diameter = ca.  $45 \times 10$  nm  $\times$  nm) is of the same order as the size of the features observed on the surface of wet CH-PC films by AFM, it is likely that surface topography also affects the modality and extent of protein adsorption on CH-PC films.<sup>[47, 48]</sup>

#### **2.5.4 Aggregation of human umbilical vein endothelial cells (HUVECs) and MCF-7 cells on CH-PC films**

Substrates for cellular assays were prepared by drop casting a CH-PC solution onto cell culture dishes. Previous studies revealed that the drop-cast CH-PC films were positively charged.<sup>[24]</sup> Their thickness, determined by ellipsometry, was  $6.6 \pm 0.1$  nm,  $10.0 \pm 0.1$  nm, and  $11.4 \pm 0.1$  nm, respectively, for CH-PC15, CH-PC25, and CH-PC40. These values are on the same order as the thickness of the films prepared in-situ and analyzed by QCM and SPR (see above). The cell adhesion properties of CH-PC films were assessed by monitoring as a function of cultivation time the aggregation status of HUVECs and MCF-7 cells seeded on the various substrates. HUVECs adopted a spherical shape on CH-PC15 films. Within 4 days, they formed small clusters that became loosely connected with time (Figure 2.5A and Figure 2.5E). On CH-PC25 and CH-PC40 films, HUVECs started to form clusters after 2 hrs. The clusters grew with time and eventually formed 3D aggregates. The diameter of the aggregates ranged from 200 to 400  $\mu$ m after 1 day (Figure 2.5B and Figure 2.5C) and after 4 days they reached values exceeding 500  $\mu$ m and 800  $\mu$ m on CH-PC25 and CH-PC40, respectively. The size of the aggregates is commensurate with objects, also named spheroids, consisting of a large number of cells (Figure 2.5F and Figure 2.5G). Interestingly, tubular extensions formed on the rim of the spheroids (arrow in Figure 2.5G). These protrusions are known to contribute favorably to the vascularization of cellular grafts.<sup>[49]</sup> HUVECs cultivated on uncoated polystyrene plates used as control adhesive substrates, adopted an elongated shape and eventually reached confluence (Figure 2.5D and 2.5H). Identical *in vitro* assays were carried out with MCF-7 cells, commonly used to tumors. Representative micrographs recorded 1-day and 4-days of cultivation on the three CH-PC films are presented in Figure SI.2.4 in SI. As in the case of HUVECS, MCF-7 cells formed spheroids on CH-PC 40 and CH-PC 25 film. This



observation is a strong indication that the propensity of CH-PC films (25 to 40% PC) to promote cell aggregation is not cell line dependant, although the kinetics of cell aggregation may differ depending on cell type. Our observations differ from results obtained previously S. Meng *et al.* who reported that a CH-PC sample synthesized by an heterogeneous process formed substrates adhesive towards HUVECs even though the PC content of the polymer was high ( $\sim 0.60$  wt% Phosphorus).<sup>[50]</sup> The CH-PC samples described here were obtained under homogeneous conditions that favor random distribution of the PC groups along the CH chain, which may affect the adhesive characteristics of thin films formed by the polymers.

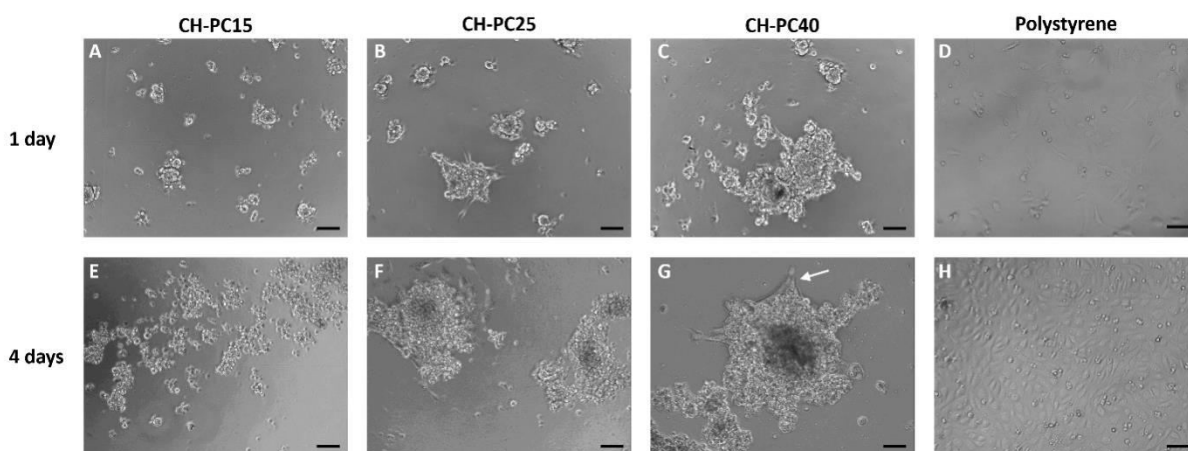


Figure 2.5 Optical micrographs of HUVECs on CH-PC coated surfaces 1 day and 4 days after seeding (micrographs A to C and E to G, respectively), and on polystyrene tissue culture plates (micrographs E and H); Scale bar: 200  $\mu\text{m}$ .

To describe the dynamics of HUVEC aggregation on CH-PC25 and CH-PC40 films, we measured the number of clusters per unit area,  $N(t)$ , at different times. A “cluster” is defined as any set of connected cells, including unique cells. S. Douezan and F. Brochard-Wyart have shown that the number of clusters per unit area in function of the time can be modeled by equation (2):

$$N(t) = \frac{N_0}{1 + KN_0 t} \quad (2)$$


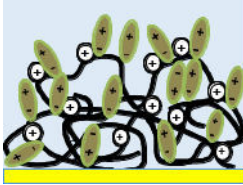
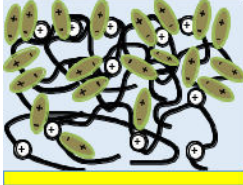
where  $N_0$  is the initial number of cells per unit area and  $V_{cell} \sim d_{cell} V_{cell}$  (respectively, the cell diameter and the average cell velocity) is the rate constant in the collision theory.<sup>[51]</sup> We fitted the experimental data with equation (2) for the different substrates (see Figure SI. 2.5 in ESI).




A good agreement with the theoretical model was obtained using  $K \approx 5.4 \times 10^{-13} \text{ m}^2 \text{ s}^{-1}$ . For CH-PC25 films and  $K \approx 9.6 \times 10^{-13} \text{ m}^2 \text{ s}^{-1}$  for CH-PC40 films. These values yield a cell velocity  $V_{cell} \sim K / d_{cell} \sim 0.1 \text{ } \mu\text{m s}^{-1}$ . The  $K$  and  $V_{cell}$  values obtained here are similar to the rate constant  $K \approx 1.5 \times 10^{-13} \text{ m}^2 \text{ s}^{-1}$  and cell velocity  $V_{cell} = 0.07 \text{ } \mu\text{m}^{-1}$  determined earlier in the case of cells deposited on poly(ethylene glycol)-poly-L-lysine coated substrates known for their non-adhesive characteristics.<sup>[19]</sup>

## 2.6 Conclusions

Table 2.2 presents an overview of the key features of the three CH-PC films. While the thickness of the films increases significantly with PC content, there are only slight differences among other physical attributes of the CH-PC substrates, such as water content, surface topography, and rheological properties. Nonetheless, differences among substrates are recognized by fibrinogen, an important protein involved in cell adhesion. Fibrinogen is adsorbed onto CH-PC15 substrates and to a much lesser extent to CH-PC25 substrate. It does not adsorb on CH-PC40 films. We attribute this discrimination to an increase of the concentration of the antifouling PC group on the film/water interface as the PC degree of substitution of chitosan passes from 10 to 40 mol%. Cells readily detect differences among the films and respond accordingly in terms of adhesion behavior, yet physico-chemical methods applicable in the case of wet films are not sufficiently sensitive to detect significant differences between the substrates. High sensitivity analyses performed on dry films, such as X-ray photoelectron spectroscopy (XPS), are not reliable herein view of the extensive surface reorganization that occurs upon drying CH-PC substrates.<sup>[24]</sup> This study demonstrates that CH-PC films form promising platforms for 3D-cellular grafts as well as oncological studies.

Table 2.2 Overview of the properties of CH-PC films.

CH-PC <sub>x</sub> films	Film properties			Fibrinogen adsorption <sup>b</sup> [μg cm <sup>-2</sup> ]	HUVEC 3D aggregates <sup>c</sup>
	Thickness <sup>a</sup>	Water content <sup>a</sup> [wt%]	Zeta potential [mV]		
 CH-PC15	9.5 nm	~90	+23.7	~0.13	No
 CH-PC25	11.3 nm	~90	+16.3	~0.04	Yes
 CH-PC40	15.4 nm	~90	+13.2	<0.01	Yes

 CH-PC backbone   
  Protonated glucosamine   
  Phosphorylcholine moiety

a) From QCM and SPR data ; <sup>b)</sup> from QCM data ; <sup>c)</sup> optical microscopy observation after 4 days.

## 2.7 Acknowledgements

The authors thank Dr. A. Badia (Université de Montréal) for helpful discussions on SPR data analysis and Dr. J. Nakanishi (WPI-MANA) for providing access to cell biology equipment. The technical assistance of Dr. K. Iiyama (WPI-MANA) in the use of the AFM equipment is also acknowledged.

This work was supported by the World Premier International Research Center Initiative (WPI) MEXT, Japan. Mr. B. Qi was supported by the NIMS Internship Program 2013 and a doctoral scholarship from the Chinese Scholarship Council (CSC).

## 2.8 References

- [1] Kujawa P; Winnik, FM, Innovation in nanomedicine through materials nanoarchitectonics. *Langmuir* **2013**, *29*: 7354-7361.
- [2] Lutolf MP; Hubbell, JA, Synthetic biomaterials as instructive extracellular microenvironments for morphogenesis in tissue engineering. *Nature Biotechnology* **2005**, *23*: 47-55.
- [3] Levental I; Georges, PC; Janmey, PA, Soft biological materials and their impact on cell function. *Soft Matter* **2007**, *3*: 299-306.
- [4] Alves NM; Pashkuleva, I; Reis, RL; Mano, JF, Controlling cell behavior through the design of polymer surfaces. *Small* **2010**, *6*: 2208-2220.
- [5] Cha C; Liechty, WB; Khademhosseini, A; Peppas, NA, Designing biomaterials to direct stem cell fate. *Acs Nano* **2012**, *6*: 9353-9358.
- [6] Higuchi A; Ling, Q-D; Chang, Y; Hsu, S-T; Umezawa, A, Physical cues of biomaterials guide stem cell differentiation fate. *Chemical Reviews* **2013**, *113*: 3297-3328.
- [7] Benien P; Swami, A, 3d tumor models: History, advances and future perspectives. *Future Oncology* **2014**, *10*: 1311-1327.
- [8] Levinger I; Ventura, Y; Vago, R, Life is three dimensional-as in vitro cancer cultures should be. In *Advances in cancer research, vol 121*, Tew, K. D.; Fisher, P. B., Eds. **2014**, *121*: 383-414.

- [9] Bhang SH; Lee, S; Lee, T-J; La, W-G; Yang, H-S; Cho, S-W; Kim, B-S, Three-dimensional cell grafting enhances the angiogenic efficacy of human umbilical vein endothelial cells. *Tissue Engineering Part A* **2012**, *18*: 310-319.
- [10] O'Sullivan ES; Johnson, AS; Omer, A; Hollister-Lock, J; Bonner-Weir, S; Colton, CK; Weir, GC, Rat islet cell aggregates are superior to islets for transplantation in microcapsules. *Diabetologia* **2010**, *53*: 937-945.
- [11] Beaune G; Stirbat, TV; Khalifat, N; Cochet-Escartin, O; Garcia, S; Gurchenkov, VV; Murrell, MP; Dufour, S; Cuvelier, D; Brochard-Wyart, F, How cells flow in the spreading of cellular aggregates. *Proceedings of the National Academy of Sciences of the United States of America* **2014**, *111*: 8055-8060.
- [12] Cavallari G; Zuellig, RA; Lehmann, R; Weber, M; Moritz, W, Rat pancreatic islet size standardization by the "hanging drop" technique. *Transplantation Proceedings* **2007**, *39*: 2018-2020.
- [13] Stirbat TV; Mgharbel, A; Bodennec, S; Ferri, K; Mertani, HC; Rieu, J-P; Delanoe-Ayari, H, Fine tuning of tissues' viscosity and surface tension through contractility suggests a new role for alpha-catenin. *Plos One* **2013**, *8*:55-68.
- [14] Bernard AB; Lin, C-C; Anseth, KS, A microwell cell culture platform for the aggregation of pancreatic beta-cells. *Tissue Engineering Part C-Methods* **2012**, *18*: 583-592.
- [15] Tu T-Y; Wang, Z; Bai, J; Sun, W; Peng, WK; Huang, RY-J; Thiery, J-P; Kamm, RD, Rapid prototyping of concave microwells for the formation of 3d multicellular cancer aggregates for drug screening. *Advanced Healthcare Materials* **2014**, *3*: 609-616.
- [16] Hsu S-h; Lin, Y; Lin, T-C; Tseng, T-C; Lee, H-T; Liao, Y-C; Chiu, I-M, Spheroid formation from neural stem cells on chitosan membranes. *Journal of Medical and Biological Engineering* **2012**, *32*: 85-90.
- [17] Chen Y-H; Wang, IJ; Young, T-H, Formation of keratocyte spheroids on chitosan-coated surface can maintain keratocyte phenotypes. *Tissue Engineering Part A* **2009**, *15*: 2001-2013.
- [18] Lai J-Y; Tu, IH, Adhesion, phenotypic expression, and biosynthetic capacity of corneal keratocytes on surfaces coated with hyaluronic acid of different molecular weights. *Acta Biomaterialia* **2012**, *8*: 1068-1079.

- [19] Douezan S; Guevorkian, K; Naouar, R; Dufour, S; Cuvelier, D; Brochard-Wyart, F, Spreading dynamics and wetting transition of cellular aggregates. *Proceedings of the National Academy of Sciences of the United States of America* **2011**, *108*: 7315-7320.
- [20] Muzzarelli RAA, Chitins and chitosans for the repair of wounded skin, nerve, cartilage and bone. *Carbohydrate Polymers* **2009**, *76*: 167-182.
- [21] Rinaudo M, Chitin and chitosan: Properties and applications. *Prog. Polym. Sci.* **2006**, *31*: 603-632.
- [22] Tiera MJ; Qiu, X-P; Bechaouch, S; Shi, Q; Fernandes, JC; Winnik, FM, Synthesis and characterization of phosphorylcholine-substituted chitosans soluble in physiological ph conditions. *Biomacromolecules* **2006**, *7*: 3151-3156.
- [23] Tardif K; Cloutier, I; Miao, Z; Lemieux, C; St-Denis, C; Winnik, FM; Tanguay, J-F, A phosphorylcholine-modified chitosan polymer as an endothelial progenitor cell supporting matrix. *Biomaterials* **2011**, *32*: 5046-5055.
- [24] Miao Z; Kujawa, P; Lau, Y-TR; Toita, S; Qi, B; Nakanishi, J; Cloutier, I; Tanguay, J-F; Winnik, FM, Tuning the properties and functions of 17 beta-estradiol-polysaccharide conjugates in thin films: Impact of sample history. *Biomacromolecules* **2012**, *13*: 4098-4108.
- [25] Schlenoff JB, Zwitteration: Coating surfaces with zwitterionic functionality to reduce nonspecific adsorption. *Langmuir* **2014**, *30*: 9625-9636.
- [26] Stevens MM; George, JH, Exploring and engineering the cell surface interface. *Science* **2005**, *310*: 1135-1138.
- [27] Martins GV; Merino, EG; Mano, JF; Alves, NM, Crosslink effect and albumin adsorption onto chitosan/alginate multilayered systems: An in situ qcm-d study. *Macromolecular Bioscience* **2010**, *10*: 1444-1455.
- [28] Aggarwal N; Altgarde, N; Svedhem, S; Michanetzis, G; Missirlis, Y; Groth, T, Tuning cell adhesion and growth on biomimetic polyelectrolyte multilayers by variation of ph during layer-by-layer assembly. *Macromolecular Bioscience* **2013**, *13*: 1327-1338.
- [29] Miyazawa K; Winnik, FM, Solution properties of hydrophobically-modified phosphorylcholine-based polymers in water and in the presence of surfactants. *J. Phys. Chem. B* **2003**, *107*: 10677-10682.

- [30] Kuijpers AJ; Engbers, GHM; Meyvis, TKL; de Smedt, SSC; Demeester, J; Krijgsveld, J; Zaat, SAJ; Dankert, J; Feijen, J, Combined gelatin-chondroitin sulfate hydrogels for controlled release of cationic antibacterial proteins. *Macromolecules* **2000**, *33*: 3705-3713.
- [31] Badia A; Chen, CI; Norman, LL, Calibration of a fan-shaped beam surface plasmon resonance instrument for quantitative adsorbed thin film studies-no metal film thickness or optical properties required. *Sens. Actuator B-Chem.* **2013**, *176*: 736-745.
- [32] Reviakine I; Johannsmann, D; Richter, RP, Hearing what you cannot see and visualizing what you hear: Interpreting quartz crystal microbalance data from solvated interfaces. *Analytical Chemistry* **2011**, *83*: 8838-8848.
- [33] Höök F; Kasemo, B, The qcm-d technique for probing biomacromolecular recognition reactions. *Springer Ser Chem Sens Biosens* **2007**: 425-447.
- [34] Ligler FS; Lingerfelt, BM; Price, RP; Schoen, PE, Development of uniform chitosan thin-film layers on silicon chips. *Langmuir* **2001**, *17*: 5082-5084.
- [35] Biggs MJ; Richards, RG; Gadegaard, N; McMurray, RJ; Affrossman, S; Wilkinson, CDW; Oreffo, ROC; Dalby, MJ, Interactions with nanoscale topography: Adhesion quantification and signal transduction in cells of osteogenic and multipotent lineage. *Journal of Biomedical Materials Research Part A* **2009**, *91A*: 195-208.
- [36] Selhuber-Unkel C; Erdmann, T; Lopez-Garcia, M; Kessler, H; Schwarz, US; Spatz, JP, Cell adhesion strength is controlled by intermolecular spacing of adhesion receptors. *Biophysical Journal* **2010**, *98*: 543-551.
- [37] Wilson CJ; Clegg, RE; Leavesley, DI; Percy, MJ, Mediation of biomaterial-cell interactions by adsorbed proteins: A review. *Tissue Engineering* **2005**, *11*: 1-18.
- [38] Eisele NB; Andersson, FI; Frey, S; Richter, RP, Viscoelasticity of thin biomolecular films: A case study on nucleoporin phenylalanine-glycine repeats grafted to a histidine-tag capturing qcm-d sensor. *Biomacromolecules* **2012**, *13*: 2322-2332.
- [39] Morisaku T; Watanabe, J; Konno, T; Takai, M; Ishihara, K, Hydration of phosphorylcholine groups attached to highly swollen polymer hydrogels studied by thermal analysis. *Polymer* **2008**, *49*: 4652-4657.
- [40] Kitano H; Mori, T; Takeuchi, Y; Tada, S; Gemmei-Ide, M; Yokoyama, Y; Tanaka, M, Structure of water incorporated in sulfobetaine polymer films as studied by atr-ftir. *Macromolecular Bioscience* **2005**, *5*: 314-321.

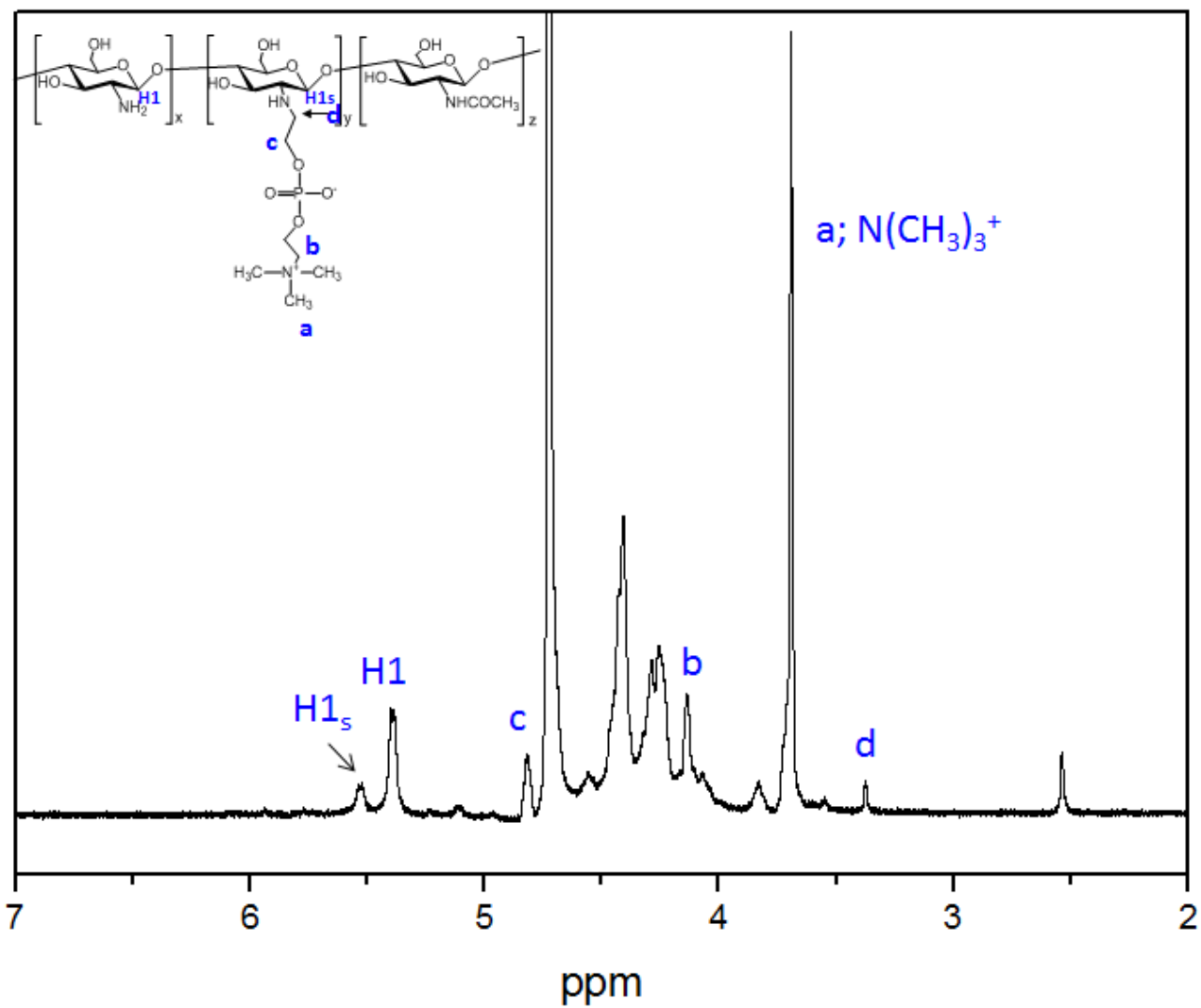
- [41] Yang S; Zhang, S-P; Winnik, FM; Mwale, F; Gong, Y-K, Group reorientation and migration of amphiphilic polymer bearing phosphorylcholine functionalities on surface of cellular membrane mimicking coating. *Journal of Biomedical Materials Research Part A* **2008**, 84A: 837-841.
- [42] Zhu AP; Wang, SQ; Yuan, YL; Shen, J, Cell adhesion behavior of chitosan surface modified by bonding 2-methacryloyloxyethyl phosphorylcholine. *Journal of Biomaterials Science-Polymer Edition* **2002**, 13: 501-510.
- [43] Ferry JD, 3rd ed., wiley, new york. *Viscoelastic Properties of Polymers* **1980**, 76: 1886-1902.
- [44] Rubinstein MC, R. H. , , Oxford, u.K.,. *J. Mech. Behav. Biomed. Mater.* **2003**, 32: 54-78.
- [45] Cai L-H; Panyukov, S; Rubinstein, M, Mobility of nonsticky nanoparticles in polymer liquids. *Macromolecules* **2011**, 44: 7853-7863.
- [46] Hulander M; Lundgren, A; Faxalv, L; Lindahl, TL; Palmquist, A; Berglin, M; Elwing, H, Gradients in surface nanotopography used to study platelet adhesion and activation. *Colloids and Surfaces B-Biointerfaces* **2013**, 110: 261-269.
- [47] Hall CE; Slayter, HS, The fibrinogen molecule: Its size, shape, and mode of polymerization. *The Journal of biophysical and biochemical cytology* **1959**, 5: 11-6.
- [48] Roach P; Farrar, D; Perry, CC, Surface tailoring for controlled protein adsorption: Effect of topography at the nanometer scale and chemistry. *Journal of the American Chemical Society* **2006**, 128: 3939-3945.
- [49] Nakatsu MN; Sainson, RCA; Aoto, JN; Taylor, KL; Aitkenhead, M; Perez-del-Pulgar, S; Carpenter, PM; Hughes, CCW, Angiogenic sprouting and capillary lumen formation modeled by human umbilical vein endothelial cells (huvec) in fibrin gels: The role of fibroblasts and angiopoietin-1. *Microvascular Research* **2003**, 66: 102-112.
- [50] Meng S; Liu, Z; Zhong, W; Wang, Q; Du, Q, Phosphorylcholine modified chitosan: Appetent and safe material for cells. *Carbohydrate Polymers* **2007**, 70: 82-88.
- [51] Douezan S; Brochard-Wyart, F, Active diffusion-limited aggregation of cells. *Soft Matter* **2012**, 8: 784-788.



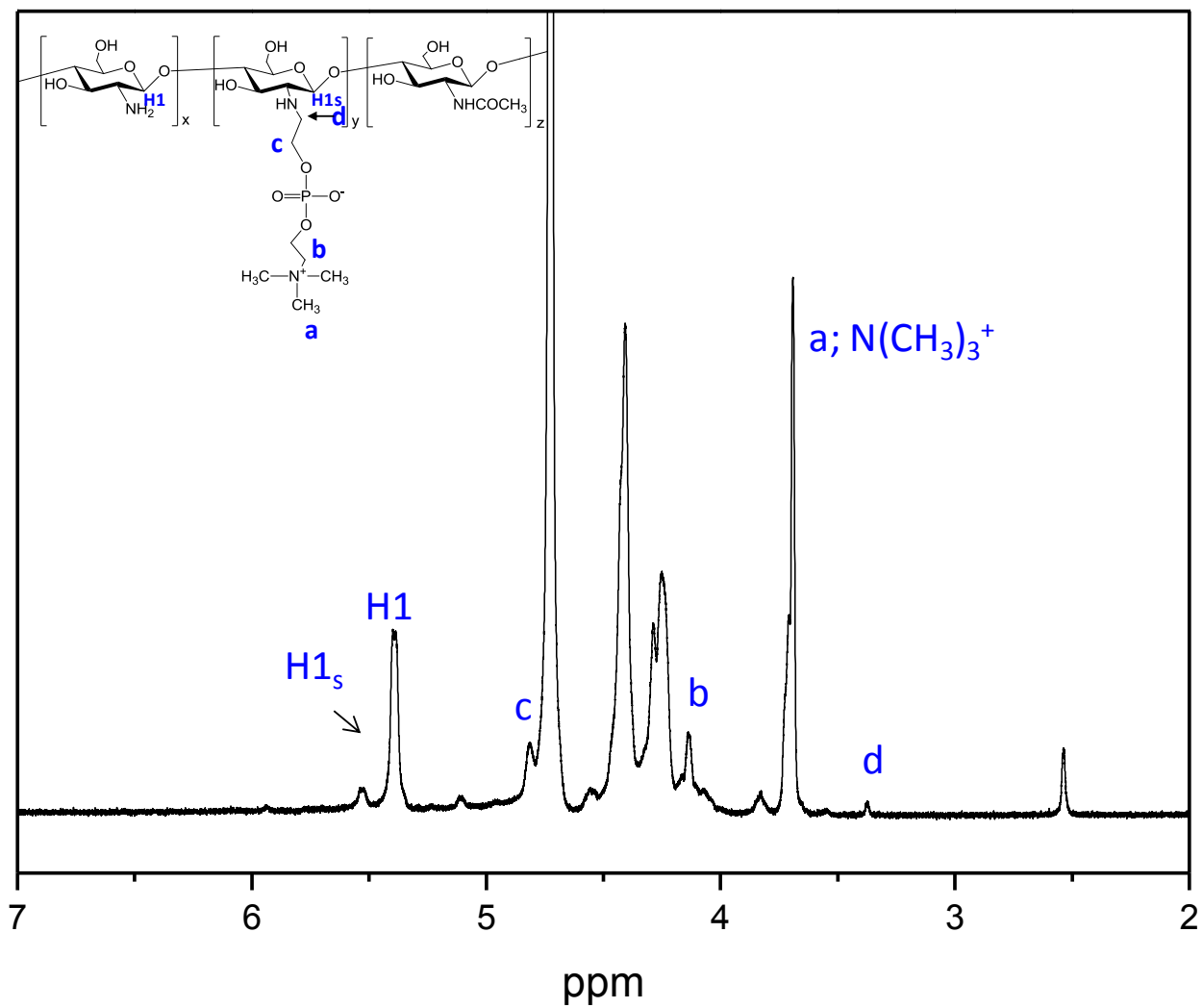
## 2.9 Appendix A. Supporting information

### Determination of the PC-substitution level of CH-PC by $^1\text{H}$ NMR spectroscopy

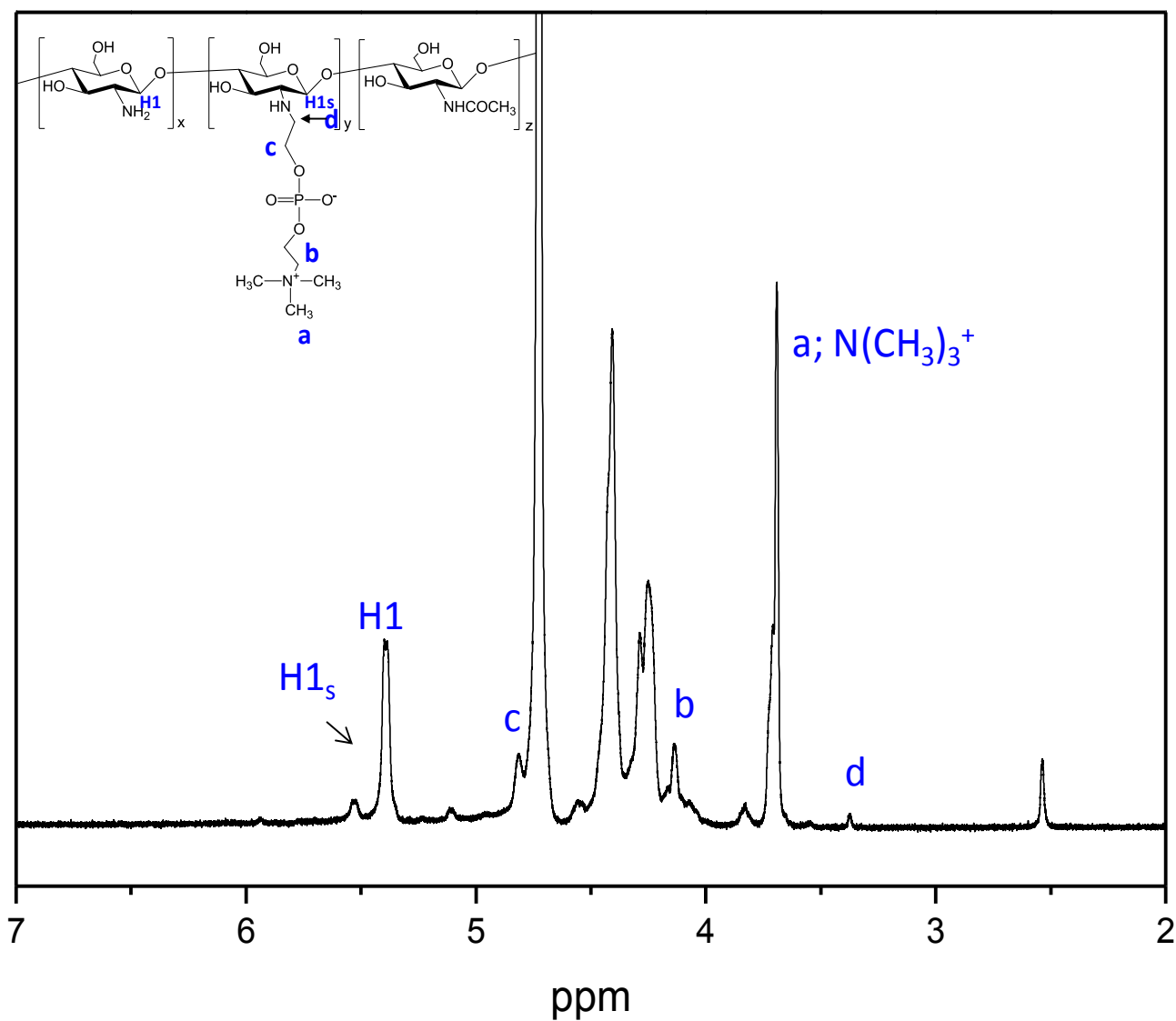
$^1\text{H}$  NMR spectra of CH-PC solutions (10 mg/mL) in  $\text{D}_2\text{O}/\text{DCl}$  (100/1, v/v) were recorded at 70 °C on a Bruker ARX-400 400-MHz spectrometer (**Figure SI.2.1**, **Figure SI.2.2** and **Figure SI.2.3**). The PC substitution level was determined by two methods: 1) Table from the areas ( $I_{\text{CH}_2}$ ) of the signal at  $\delta 4.9$  ppm attributed to the resonance of the methylene group of  $\text{NHCH}_2\text{CH}_2\text{OP}$  (signal c, Figure SI.2.1) and of the signals due to the anomeric protons of PC-substituted and unsubstituted glucosamine residues,  $\text{H}_{1\text{s}}$  and  $\text{H}_1$ , using  $\text{DS} = (1/2) I_{\text{CH}_2} / I_{\text{H}_1} + I_{\text{H}_{1\text{s}}}$  or from the areas of the signals due to the two types of anomeric protons,  $\text{H}_{1\text{s}}$  and  $\text{H}_1$  using  $\text{DS} = I_{\text{H}_{1\text{s}}} / I_{\text{H}_1} + I_{\text{H}_{1\text{s}}}$ .



**Figure SI.2.1**  $^1\text{H}$  NMR spectrum of CH-PC40, temperature 70 °C, solvent D<sub>2</sub>O/DCl.



**Figure SI.2.2** <sup>1</sup>H NMR spectrum of CH-PC25, temperature 70 °C, solvent D<sub>2</sub>O/DCI (1%).



**Figure SI.2.3** <sup>1</sup>H NMR spectrum of CH-PC15, temperature 70 °C, solvent D<sub>2</sub>O/DCl (1%).

### SPR data modeling

To apply Fresnel modeling, the real and imaginary components ( $\epsilon'$  and  $\epsilon''$ , respectively) of the dielectric functions of the surface plasmon-supporting metal layer at the wavelength of excitation (780 nm here) must be known. For optically transparent media,  $\epsilon'' = 0$  and the dielectric constant  $\epsilon'$  is equal to the square of the refractive index,  $\epsilon' = n^2$ . The changes in resonance angle position  $\Delta\theta_m$  were calculated using a six-layer model incorporating the sapphire prism ( $\epsilon' = 3.1002$ ),<sup>[1]</sup> the Cr adhesion layer ( $\epsilon' = -2.0185$ ,  $\epsilon'' =$

37.5755,  $d = 1$  nm),<sup>[2]</sup> the Au layer ( $\varepsilon' = -23.886$ ,  $\varepsilon'' = 1.7435$ ,  $d = 45$  nm),<sup>[3]</sup> the polymer film ( $\varepsilon'_f$  and  $d_f$  unknown), and the buffer solution ( $\varepsilon'_s = 1.7814$  for phosphate buffer pH 6.8). It is generally not possible to determine both  $\varepsilon'_f$  and  $d_{\text{SPR}}$  for an adsorbed, thin organic film from a single  $\Delta\Theta_m$  value. Any number of different combinations of  $\varepsilon'$  and  $d_d$  can produce the same shift in resonance angle. Thus, to obtain the film thickness from  $\Delta\Theta_m$ , the film index of refraction must be known. The value of  $\varepsilon'_f$  employed here was 2.1025 (corresponding to  $n_f = 1.45$ ) for CH-PC films.<sup>[4, 5]</sup> Modeling was performed by using Winspall software (version 3.02). Knowing the dry film thickness  $d_d$ , the surface coverage  $\Gamma_d$  (*i.e.* adsorbed “dry” mass per unit area) can be calculated using the relation:

$$\Gamma_d = d_d \frac{n_f - n_s}{dn/dc} \quad (\text{SI 1})$$

where  $n_s$  is the refractive index of buffer and  $dn/dc$  is the refractive index increment of polymer solution. The values of  $dn/dc$  were taken from previous study.<sup>[6]</sup> The thickness of the Au layer was determined using a multiwavelength ellipsometer equipped with a QTH lamp and rotating compensator (Model M-2000V, J.A. Woollam Co., Inc.).

### QCM-D data modeling.

The amount of adsorbed material for a thin, nondissipative layer can be calculated using the Sauerbrey relationship,<sup>[7]</sup> where  $\Delta f$  is linearly related to the adsorbed mass, including the mass of coupled water, expressed as surface coverage  $\Gamma_w$  (*i.e.* adsorbed “wet” mass per unit area):

$$\Gamma_w = -\frac{c\Delta f}{m} \quad (\text{SI 2})$$

where  $C$  is a constant based on the physical properties of the quartz crystal ( $C = 0.177 \text{ mg m}^{-2} \text{ Hz}^{-1}$ ) and  $m$  is the overtone number ( $m = 1, 3, \dots$ ). However, the linear relationship between the adsorbed mass and  $\Delta f$  is invalid for hydrated layers characterized by high dissipation shifts, as in the case studied here. For such films, in order to calculate the adsorbed mass and viscoelastic properties, theoretical modeling is necessary.

QCM-D data were modeled by the Voigt viscoelastic model<sup>[8, 9]</sup> using the QTools 3.0 software (Biolin).<sup>[10]</sup> The frequency and dissipation changes recorded for five overtones were used for the modeling. The buffer density and the viscosity were fixed at  $1000 \text{ g dm}^{-3}$  and  $1$

mPa s<sup>-1</sup>, respectively. The films were modeled as homogeneous viscoelastic layers characterized by the acoustic thickness  $d$ , density  $\rho$ , and the frequency-dependent storage and loss moduli  $G'(f)$  and  $G''(f)$ , respectively, as described earlier.<sup>[11, 12]</sup> The loss modulus can be calculated based on film viscosity  $\eta(f)$  from the equation  $G''(f) = 2\pi f\eta(f)$ . It was assumed both  $G'$  and  $G''$  are characterized by a power-law frequency dependence with critical exponents  $\alpha$  and  $\beta$ , respectively ( $G' \propto f^\alpha$  and  $G'' \propto f^\beta$ ). To extract the thickness and the viscoelastic properties of a film upon modelization, it is necessary to input the estimated film density. In contrast, the calculated surface coverage  $\Gamma_w$ , that is, the product density by thickness, remains largely unaffected for a broad range of density values. We confirmed that changing the film density between 1000 and 1700 g dm<sup>-3</sup> essentially does not influence the surface coverage of the adsorbed film estimated through modeling. Once the surface coverage of the film is known, its density can be calculated by combining QCM-D and SPR data, as described below. This density value was lastly used in final modeling procedure to determine storage modulus, film viscosity and thickness. The parameters fitted were (i) the layer shear storage modulus  $G'(f)$  between 10<sup>3</sup> and 10<sup>7</sup> Pa, (ii) the layer viscosity  $\eta(f)$  between 0.001 and 0.1 kg m<sup>-1</sup> s<sup>-1</sup>, and (iii) the layer density  $d$  between 10<sup>-10</sup> and 10<sup>-7</sup> m.

Calculations of water content and layer density. Combining the dry mass per unit area  $\Gamma_d$  obtained by SPR and the wet mass per unit area  $\Gamma_w$  obtained by QCM-D, the mass fraction of water  $x$  in the film can be calculated from relation:

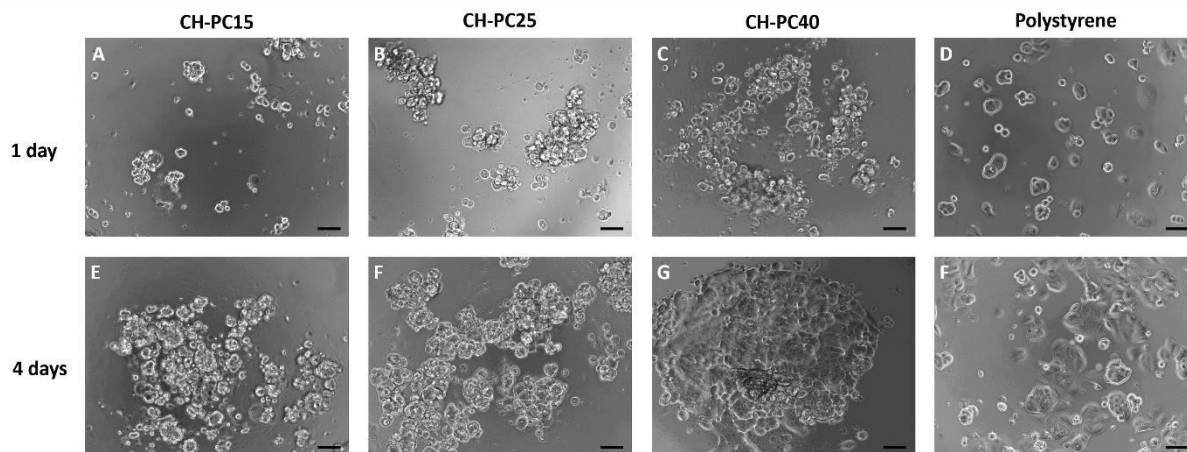
$$x = 1 - \frac{\Gamma_d}{\Gamma_w} \quad (\text{SI 3})$$

Knowing the water content, the density of the adsorbed layer  $\rho$  can be estimated from the ideal mixing relation:

$$\frac{1}{\rho} = \frac{1-x}{\rho_p} + \frac{x}{\rho_s} \quad (\text{SI 4})$$

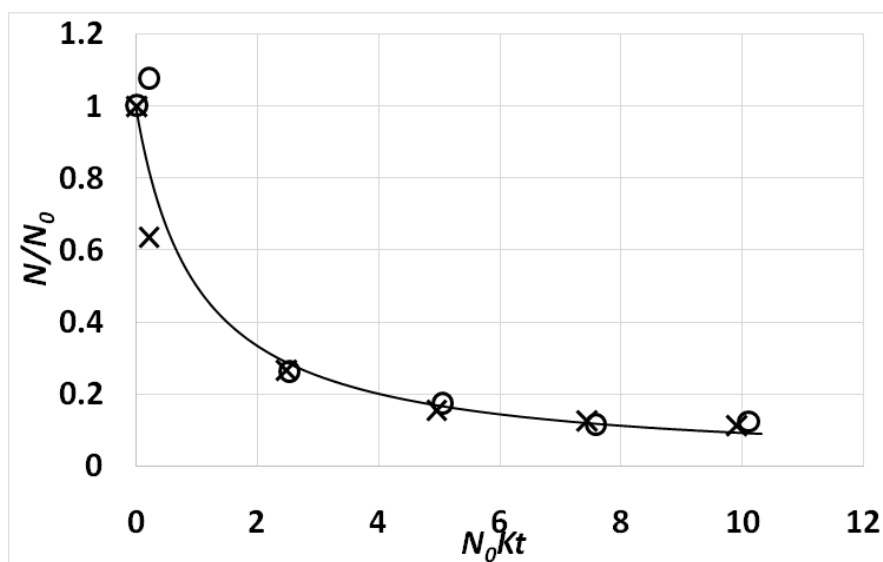
where  $\rho_s$  is the density of buffer, and  $\rho_p$  is the density of polymer.<sup>[13, 14]</sup> The densities of CH-PC polymers were estimated from their partial specific volume calculated based on group contribution method<sup>[15]</sup> as 1700, 1650, and 1600 g dm<sup>-3</sup> for CH derivatives bearing 15, 25, and 40 mol% of PC units, respectively. The value estimated by this method for unmodified chitosan (1770 g dm<sup>-3</sup>) agrees very well with the value determined experimentally by Errington *et al.* ( $\rho_p = 1770 \pm 120$  g dm<sup>-3</sup>).<sup>[16]</sup>

## MCF-7 cell line observation by optical microscopy



**Figure SI.2.4** Optical micrographs of MCF-7 cells on CH-PC coated surfaces 1 day and 4 days after seeding (micrographs A to C and E to G, respectively), and on polystyrene tissue culture plates (micrographs E and H); Scale bar: 200  $\mu\text{m}$ .

## Aggregation of HUVECs



**Figure SI.2.5.** Plot of the changes of  $N_0/N$  as a function of time, where  $N$  is the number of objects per unit area at  $t$ ,  $N_0$  is the initial number of objects per unit area,  $K$  is the rate constant of aggregation. (x) Stands for substrates coated with CH-PC25 films and (O) for substrates coated with CH-PC40 films. The solid line corresponds to the theoretical predictions (the two predictions cannot be distinguished at this scale) using equation (2).

## References

- [1] Gray DE, American institute of physics handbook,. *McGraw-Hill, New York, 1972*.
- [2] Palik ED, Handbook of optical constants of solids. *Academic Press Inc., Orlando 1985*.
- [3] Badia A; Chen, CI; Norman, LL, Calibration of a fan-shaped beam surface plasmon resonance instrument for quantitative adsorbed thin film studies-no metal film thickness or optical properties required. *Sens. Actuator B-Chem. 2013, 176: 736-745*.
- [4] Holmlin RE; Chen, XX; Chapman, RG; Takayama, S; Whitesides, GM, Zwitterionic sams that resist nonspecific adsorption of protein from aqueous buffer. *Langmuir 2001, 17: 2841-2850*.
- [5] Zhou H; Yi, R; Li, J; Su, Y; Liu, X, Microwave-assisted synthesis and characterization of hexagonal fe<sub>3</sub>o<sub>4</sub> nanoplates. *Solid State Sciences 2010, 12: 99-104*.
- [6] Tiera MJ; Qiu, XP; Bechaouch, S; Shi, Q; Fernandes, JC; Winnik, FM, Synthesis and characterization of phosphorylcholine-substituted chitosans soluble in physiological ph conditions. *Biomacromolecules 2006, 7: 3151-3156*.
- [7] Sauerbrey G., *Zeitschrift für Phys 1959, 155: 206-232*.
- [8] White CC; Schrag, JL, Theoretical predictions for the mechanical response of a model quartz crystal microbalance to two viscoelastic media: A thin sample layer and surrounding bath medium. *Journal of Chemical Physics 1999, 111: 11192-11206*.
- [9] Johannsmann D, Piezoelectric sensors. *Springer Berlin Heidelberg 2007*.
- [10] Biolinscientific, [Http://qtools.Software.Informer.Com/](http://qtools.software.informer.com/).
- [11] Eisele NB; Andersson, FI; Frey, S; Richter, RP, Viscoelasticity of thin biomolecular films: A case study on nucleoporin phenylalanine-glycine repeats grafted to a histidine-tag capturing qcm-d sensor. *Biomacromolecules 2012, 13: 2322-2332*.
- [12] Miao Z; Kujawa, P; Lau, Y-TR; Toita, S; Qi, B; Nakanishi, J; Cloutier, I; Tanguay, J-F; Winnik, FM, Tuning the properties and functions of 17 beta-estradiol-polysaccharide conjugates in thin films: Impact of sample history. *Biomacromolecules 2012, 13: 4098-4108*.
- [13] Höök F. KB, 2007, 5: 425., Springer ser chem sens biosens. **2007**, 5: 425.
- [14] Porus M; Maroni, P; Borkovec, M, Response of adsorbed polyelectrolyte monolayers to changes in solution composition. *Langmuir 2012, 28: 17506-17516*.



- [15] Zipper P; Janosi, A; Wrentschur, E, Scanning-x-ray scattering of moldings from semicrystalline polymers. *Journal De Physique Iv* **1993**, 3: 33-36.
- [16] Errington N; Harding, SE; Varum, KM; Illum, L, Hydrodynamic characterization of chitosans varying in degree of acetylation. *International Journal of Biological Macromolecules* **1993**, 15: 113-117.

## CHAPTER THREE

---

### **Synthesis, characterization and biological study of estrogen grafted chitosan phosphorylcholine polymer conjugates**

Baowen Qi<sup>1</sup>, Xingping Qiu<sup>1</sup>, Jun Nakanishi<sup>2</sup>, Françoise M. Winnik<sup>1,2</sup>

<sup>1</sup>Faculté de Pharmacie and Département de Chimie, Université de Montreal, CP 6128 Succursale Centre Ville, Montreal, QC, H3C 3J7, Canada

<sup>2</sup>World Premier International (WPI) Research Center Initiative, International Center for Materials Nanoarchitectonics (MANA), National Institute for Materials Science (NIMS), 1-1 Namiki Tsukuba, Ibaraki 305-0044, Tsukuba, Japan

#### **Summary of transition**

In this chapter, synthesis and characterization of CH-PC-E2 polymer conjugate was performed as a prodrug strategy. The solution and interface properties of CH-PC-E2 polymer conjugate were also further explored. By a self-assembly bottom-up approach, CH-PC-E2 films demonstrated hydrogel natures, and exerted cardiovascular protective effect through stimulating endogenous NO production. Coupled with ER- $\alpha$  binding study by QCM-D and cell culture-based DAF-FM fluorescence imaging study, biological properties of CH-PC-E2 film were elucidated from protein to cell level. However, investigations with regards to the CH-PC-E2 films applications were not extensively conducted. For example, how CH-PC-E2 films regulate proliferation and differentiation of cardiac stem cells, such as endothelial progenitor cell (EPC), could be carried out in future study. Moreover, CH-PC-E2 film-based toxicity test should be addressed in preclinical studies through discussion its risk to induce breast cancer proliferations (genomic action of E2). However, the cardiovascular protective characteristic of CH-PC-E2 hydrogel-liked film might be associated with non-genomic action of surface-tethered E2. As a result, the detailed non-genomic and genomic mechanisms of surface-tethered E2 will be discussed in the next chapter using micropatterned surface prepared by a top-down approach.

### 3.1 Abstract

Female steroid hormone estradiol (E2) activates the production of nitric oxide (NO), a signaling messenger that functions as an important vasodilator, and hence plays vital protective role in the cardiovascular system. However, estrogen replacement therapies in cardiovascular diseases were in dispute recently because: 1) insolubility of E2 in water limits its bioavailability; 2) supplementary of exogenous E2 may increase the risk of breast cancer. An effective strategy to solve these issues is to tether E2 to a hydrophilic polymer surface. In current approach, a new derivative of E2 (17 $\alpha$ -ethinylestradiol-benzoic acid) was covalently tethered onto a chitosan phosphorylcholine (CH-PC) polymer backbone. The 17 $\alpha$ -ethinylestradiol-benzoic acid grafted CH-PC polymer conjugate (CH-PC-E2) was characterized by several techniques, such as <sup>1</sup>H nuclear magnetic resonance spectrometer (<sup>1</sup>H NMR), Fourier transformed infrared-attenuated total refraction (FTIR-ATR) and UV/vis spectra measurements. Moreover, the hydrogel nature of CH-PC-E2 conjugate was confirmed *via* a quartz crystal microbalance with dissipation (QCM-D) study, through discussion of its mechanical properties. To maintain the activities of surface-tethered E2 in the CH-PC backbone, a drop-casting method was used for a thin film formulation as a self-assembly bottom-up approach. The biological integrity of CH-PC-E2 film was further determined *via* an estrogen receptor- $\alpha$  (ER- $\alpha$ ) binding experiment. In the EA.hy926 endothelial cell, CH-PC-E2 thin film significantly stimulated the production of endothelium-derived NO, through an investigation of a diaminofluorescein-FM diacetate (DAF-FM) imaging study. These results indicate that the CH-PC-E2 thin film serves as an endogenous NO activator and implies its potential use in the cardiovascular regenerative medicine.

### 3.2 Author Keywords

Estradiol; Nitric oxide; Self-assembly bottom-up approach; Thin film formulation

### 3.3 Introduction

Estradiol (E2), a female hormone produced by ovary or adrenal glands, plays a vital role in the reproductive cycle and metabolism.<sup>[1-3]</sup> In recent epidemiology studies, cardiovascular disease rates are significantly different between premenopausal and postmenopausal women, suggesting the cardio-protective effects of E2.<sup>[4-6]</sup> In previous studies, it was demonstrated that direct local delivery of E2 can prevent neointimal hyperplasia, ameliorate late stent thrombosis, and reduce collagen accumulation.<sup>[7-9]</sup> To date, both clinical observations and experimental evidences indicated that the cardio-protective effects of E2 is associated its non-genomic action, *via* binding to membrane-bound estrogen receptors (mERs) and activating endothelial nitric oxide syntheses (e-NOS) in cardiovascular system.<sup>[10, 11]</sup> The generated endogenous NO by E2 leads to arterial vasodilatation within the blood vessel and regulates various biochemical signal pathways in the cardiovascular system.<sup>[12, 13]</sup> Moreover, it is also acknowledged that the high level of NO reduces platelet adhesion and prevents the development of atherosclerosis, which is a major cardiovascular complication that causes extremely high mortality rate.<sup>[14-16]</sup> However, some factors may limit the direct applications of E2 in clinical trial. On one hand, *poorly water-solubility* performance of E2 largely affects its bioavailability *in vivo*. On the other hand, long-term use of E2 will trigger the genomic action and hence induce a higher risk of breast cancer occurrence.<sup>[17]</sup> Therefore, it is highly required to develop novel strategies, that maintains the presentation of E2 only approaching to the cell membrane site without triggering the genomic action to stimulate cancer cell proliferation.<sup>[18]</sup> Recently, an estrogen dendrimer conjugate (EDC) was developed by attaching of 17 $\alpha$ -ethinylestradiol (EE2) to a poly(amido) amine (PAMAM) dendrimer.<sup>[19]</sup> In the cardiovascular system, EDC activated NO production *via* interacting with membrane ER- $\alpha$  without inducing breast cancer growth *in vivo*.<sup>[20]</sup> However, some of recent studies also explored that PAMAM dendrimer is associated with high toxicity due to the high density of its surface charges, which may cause safety issues in a long-term frame applications as well.<sup>[21, 22]</sup>

Prodrug strategy, an approach that covalently tethers drugs to a polymer scaffold, is promising for stimulating long-term frame biological responses.<sup>[23, 24]</sup> In present study, the objective is to tether E2 to a polymer backbone surface as a novel prodrug for cardio-therapy. Chitosan is a natural polysaccharide composed of  $\beta$  (1-4) linked N-acetyl-D-glucosamine

residues, serving to inhibit neointimal hyperplasia in cardiovascular system.<sup>[25, 26]</sup> In our previous study, we found that the use of membrane-mimicking moiety phosphorylcholine (PC), to substitute certain amounts of primary amine in the chitosan backbone, demonstrated prominent biocompatibility nature.<sup>[27]</sup> In present study, an E2 derivative, 17 $\alpha$ -ethinylestradiol-benzoic acid (E2-benzoic acid), is prepared for covalently tethering to a CH-PC polymer backbone. A quartz crystal microbalance (QCM-D) experiment is performed to study the mechanical property and rheology of CH-PC-E2 conjugate. A CH-PC-E2 thin film will be formulated by drop-casting method to maintain the exposure of E2 at the topmost layer of the interface. The biological activity of CH-PC-E2 will be confirmed *via* an estrogen receptor binding experiment. Finally, in order to investigate the cardiovascular protective potentials of CH-PC-E2, a diaminofluorescein-FM diacetate fluorescence probe (DAF-FM) will be used to detect endogenous NO production by culturing a highly expressly estrogen receptor endothelial cell line (EA.hy926 cell) onto the CH-PC-E2 formulated thin film.<sup>[28]</sup> The studies above will show that CH-PC-E2 may account, at least in part, for the noted beneficial actions on the cardiovascular systems.

## 3.4 Experimental section

### 3.4.1 Materials

Deionized water (18.2 M $\Omega$ ·cm) was purified by a Millipore Milli-Q water purification system. 17 $\alpha$ -ethinylestradiol (EE2) was purchased from Toronto Research Chemicals Inc. (North York, ON, Canada). 1-ethyl-3-(3-dimethylaminopropyl) carbodiimide (EDC), N-hydroxysuccinimide (NHS), recombinant human estrogen receptor- $\alpha$  (ER- $\alpha$ ), fulvestrant (ICI 182,780) and 4-amino-5-methyl amino-2, 7'-difluorofluorescein diacetate (DAF-FM) diacetate fluorophore were purchased from Sigma-Aldrich. Chitosan (CH) (molecular weight ranges from 50~100K) was purchased from Fisher Scientific Inc. The original degree of deacetylation (DDA) of chitosan is 88%. A further deacetylation reaction led to a higher DDA (~98%, determined by <sup>1</sup>H NMR spectroscopy). Phosphorylcholine-glyceraldehyde (PC-CHO) was prepared by activation of L- $\alpha$ -glycerophosphorylcholine (purchased from Santa Cruz Biotechnology, Inc) as described previously.<sup>[29]</sup> All other reagents and solvents were of a reagent grade and used as received.

### 3.4.2 Preparation of PC-substituted chitosan (CH-PC)

PC-substituted chitosan in a 20% ratio (CH-PC20) was obtained by the procedure as described previously.<sup>[29]</sup> Briefly, deacetylated chitosan powder (0.5 g, 3.1 mmol of monosaccharide unit) was fully dissolved in aqueous acetic acid (20 mL, 2 wt %). Then, a solution of PC-CHO (0.2g, 0.82 mmol) in water was added dropwise to the solution of deacetylated chitosan at 0 °C. The solution was stirred for 30 min and the pH was adjusted to 6.5 by adding 1M aqueous NaOH. Thereafter, the reaction mixture was stirred for 24 h under ambient temperature. After the reaction, the solution was cooled to 0 °C. A solution of sodium cyanoborohydride (0.5 g, 8 mmol) in water (20 mL) was further added under stirring. The reaction mixture was stirred for 20 h again under ambient temperature. The reaction mixture was firstly dialyzed (membrane of MWCO 12,000-14,000 Da) against DI water for 2 days, then against 0.05 M NaOH aqueous solution for 1 day and finally against DI water for another 2 days. The CH-PC20 polymer powder was finally isolated by freeze-drying for the further use (yield 0.4 g).

### 3.4.3 Conjugation 17 $\alpha$ -ethinylestradiol to 4-iodobenzoic acid

A derivative of 17 $\alpha$ -ethinylestradiol (17-EE2) was synthesized by substitution of ethinyl group to phenyl group for the covalently immobilization to the CH-PC polymer. The synthesis protocol is briefly described below:<sup>[30]</sup> 17-EE2 (888 mg, 3.0 mmol) was added as a solid to a mixture of 4-iodobenzoic acid (744 mg, 3.0 mmol), bis(triphenylphosphine)palladium(II) dichloride [Pd(PPh<sub>3</sub>)<sub>2</sub>Cl<sub>2</sub>] (42 mg, 60 nmol) and CuI (22 mg, 120 nmol) in 30 ml diethylamine solution under an inert atmosphere of nitrogen. The mixture was stirred at room temperature for 10 min and then heated to 65°C to reflux for 12 hours. After cooling to room temperature, the mixture was separated into two layers. The light colour top layer was separated and evaporated to yield a dark red oil-like liquid. After that, this oil-like liquid was re-dissolved in water and acidified by a 1M HCl solution to form a slightly yellow solid product. Then, this solid product was filtered and washed with deionized water twice and dried in vacuum to form a brown colour solid. Finally, this brown solid was re-dissolved in sodium hydroxide solution and filtered to remove insoluble materials. The filtrate was further acidified by the 1M HCl solution to form a slight brownish solid. The

slight brownish solid was collected by filtration and dried in vacuum to obtain the final product, E2-benzoic acid (yield: 800mg, 65%). The final product was characterized by a Bruker ARX-400 400 MHz  $^1\text{H}$  nuclear magnetic resonance spectrometer ( $^1\text{H}$  NMR).  $^1\text{H}$  NMR (400 MHz,  $\text{CDCl}_3$ ):  $\delta$  0.79 (s, 3H), 1.12–2.78 (m, 15H), 6.43 (d,  $J = 2.9$  Hz, 1H), 6.50 (dd,  $J = 3.0$  Hz,  $J = 8.5$  Hz, 1H), 6.98 (d,  $J = 8.3$  Hz, 1H), 7.35 (d,  $J = 8.6$  Hz, 2H), 7.84 (d,  $J = 8.6$  Hz, 2H). Fourier transformed infrared-attenuated total reflection (FTIR-ATR) spectra were recorded on a Thermo Scientific Nicolet 6700 FTIR spectrometer with 32-time scanned interferograms at an  $8\text{ cm}^{-1}$  resolution (see Figure SI.3.1).

#### **3.4.4 Preparation and characterization of CH-PC-E2 conjugates**

A solution of E2-benzoic acid (11.65 mg, 0.028mmol) with 1-ethyl-3-(3-dimethylaminopropyl) carbodiimide (9.55mg, 0.06 mmol) and N-hydroxysuccinimide (6.9mg, 0.06 mmol) was added dropwise to the CH-PC (200mg) aqueous solution. After that, the pH of solution was adjusted to 9 by sodium bicarbonate. The reaction lasted for 24 hours and the product was dialyzed against DI water for 48 hours and then freeze-dried. The  $^1\text{H}$  NMR spectra of CH-PC-E2 sample were recorded on a Bruker ARX-400 MHz spectrometer at  $70^\circ\text{C}$ . UV/vis spectra were obtained using a Hewlett-Packard 8452A photodiode array spectrometer. Fourier transformed infrared-attenuated total reflection (FTIR-ATR) spectra of samples were recorded on a Thermo Scientific Nicolet 6700 FTIR spectrometer with 32-time scanned interferograms at an  $8\text{ cm}^{-1}$  resolution (see Figure SI.3.2).

#### **3.4.5 Dynamic light scattering (DLS) measurements**

For the solution of CH-PC or CH-PC-E2 preparation, CH-PC and CH-PC-E2 polymers were dissolved in PBS and then added a few drops of 1M aqueous HCl at a final concentration of  $1.0\text{ g L}^{-1}$ . The polymer solutions were stirred overnight under ambient temperature. The pH of the solutions was adjusted to 6.8 by adding a few drops of 1M aqueous NaOH. The resulting solutions were stirred overnight again at ambient temperature and filtered through  $0.45\text{ }\mu\text{m}$  PVDF filters. DLS experiments were performed in a fix angular at  $90^\circ$  by an ALV/CGS-3 instrument (ALV GmbH, Germany) equipped with a goniometer. The light source was selected by using a 22mW He–Ne laser (operating at a wavelength of  $\lambda_0 = 632.8\text{ nm}$ ), interfaced with an ALV-5000 multiple digital time correlator. The Stokes–Einstein

relationship was used for the calculation of hydrodynamic radius ( $R_h$ ) from the diffusion coefficients.

### 3.4.6 Spectroscopic ellipsometry analysis

The thicknesses of CH-PC or CH-PC-E2 films were determined by M-2000V multi-wavelength ellipsometer (J.A. Woollam Co.) at an incident angle of  $75^\circ$  with a wavelength range of 370–1000 nm. The CH-PC or CH-PC-E2 films were prepared by casting  $1.0 \text{ g L}^{-1}$  CH-PC or CH-PC-E2 polymer solutions onto the piranha cleaned silicon wafers (*WARNING: see above*) and dried overnight. After that, the films were then rinsed with copious deionized water and followed by air-drying. Each sample was carried out three independent measurements at different spots. The resulting spectra data were analyzed with the WVASE32 software. The film thickness was estimated using the relation of Cauchy:

$$n(\lambda) = A_n + \frac{B_n}{\lambda^2} + \frac{C_n}{\lambda^4} \quad (1)$$

where  $\lambda$  is the wavelength and  $n$  is the refractive index, taken as 1.59, as previously reported.<sup>[31]</sup>

### 3.4.7 Quartz crystal microbalance with dissipation (QCM-D) studies

Quartz crystal microbalance with dissipation monitoring (QCM-D) is a surface analytical technique simultaneous measurements of frequency changes ( $\Delta f$ ) and energy dissipation change ( $\Delta D$ ) by applying external mechanical stresses periodically over the quartz crystal based on the piezoelectricity of quartz.<sup>[32, 33]</sup> It measures the changes of adsorbed mass on the interfaces in nanogram scale which is linearly proportional to the frequency changes. In present study, QCM-D experiments were performed with a Q-sense E4 instrument (Biolin). QCM-D signals were recorded for the fundamental frequency as 5 MHz with six overtones (15, 25, ..., 65 MHz). QCM silicon dioxide sensors (Qsx-303, Q-Sense) were used for the CH-PC and CH-PC-E2 functionalization. Before the experiment, the silicon dioxide sensors were cleaned according to the suggestions by suppliers. Briefly, the silicon dioxide sensors were firstly treated by UV-ozone for 10 min. Then the sensors were subsequently immersed in 2% sodium dodecyl sulphate solutions for 30 min and rinsed 5 times with deionized water. Finally, the sensors were dried with nitrogen and treated by UV-ozone for another 10 min.



In order to obtain the information of viscoelastic properties, CH-PC-E2 and CH-PC were functionalized *in situ* of QCM-D instrument for overnight reaction. The protocol is shown as follow. A cleaned silicon dioxide sensor was firstly placed in the QCM-D sample holder. After flushing with PBS buffer to maintain the QCM-D signal baseline stable, a solution of CH-PC or CH-PC-E2 in PBS buffer with a concentration of 1.0 g L<sup>-1</sup> was introduced into the QCM-D sample chamber at a flow rate of 10 μL min<sup>-1</sup> at room temperature for overnight reaction, which mimics the same protocol for the glass substrate functionalization as subsequent cellular study. After that, the QCM-D sample chamber was flushed with the same buffer again to remove unbound polymer. In order to exclude solvent effect, the data recorded after removal of unbound polymers were used for modeling. The QCM-D data were fitted by using the Voigt viscoelastic model<sup>[34, 35]</sup> with five independent overtones using the QTools 3.0 software (Biolin). The viscoelastic values including thickness *d*, storage modulus G', loss modulus G'', critical exponents α' and α'', were obtained using the parameters in detail as described previously.<sup>[36]</sup>

For the confirmation of the biological activity of rehydrated CH-PC-E2 film, we used *ex-situ* drop-casting method for the film deposition for the simulation of subsequent cellular study. The corresponding ER-α binding experiment was performed as following protocol. CH-PC-E2 and CH-PC solutions in PBS with a 1.0 g L<sup>-1</sup> concentration were drop-casted onto the cleaned QCM-D silicon dioxide sensors and dried overnight, respectively. Then, the sensor surfaces were washed with copious DI water and follow by air-drying again. For ER-α binding experiment, after flushing with PBS to establish a baseline, a solution of ER-α in a concentration of 50 nM was replaced through the measuring chamber at a rate of 10 μL min<sup>-1</sup> at room temperature for CH-PC or CH-PC-E2 functionalized substrates, respectively. When the frequency and dissipation reached constant values, excess unbound ER-α was removed subsequently by rinsing the sample chamber with PBS buffer again. The result in the plot was shown as the fifth overtone. For the calculation of the amount of adsorbed ER-α, the Sauerbrey equation:

$$\Gamma = -\frac{c\Delta f}{n} \quad (2)$$

was used as previously suggested,<sup>[37]</sup> where  $\Gamma$  denotes as surface coverage of the adsorbed protein,  $\Delta f$  is linearly related to the mass of the adsorbed protein,  $C$  is a constant related to the physical properties of the quartz crystal ( $C = 0.177 \text{ mg m}^{-2} \text{ Hz}^{-1}$ ) and  $n$  is the overtone number ( $n = 1, 3, 5\dots$ ).

### 3.4.8 Cell culture

The human vascular endothelial cell line EA.hy926 cells were obtained from American type culture collection (ATCC). The cells were maintained in Dulbecco's Modified Eagle's Medium (DMEM) with 10% fetal bovine serum at 37°C in a humidified atmosphere containing 5% CO<sub>2</sub>. The cells were subculture every 3 days using 0.25% trypsin-EDTA. The cell culture medium was replaced with phenol red-free DMEM 24 hour in advance and then the cells were starved another 6 hour before the cell fluorescence imaging experiment. For the fluorescence imaging study, cells were harvested and loaded in HBSS buffer containing 10 μM DAF-FM for 30 min at a density of 5x10<sup>5</sup>/ml. Then the DAF-FM labeled cells were replaced by HBSS buffer containing with or without 10 μM ICI 182,780 for 1 hour incubation. Finally, the cells were seeded into CH-PC-E2 or CH-PC surfaces for 1 hour incubation and performed fluorescence cell imaging study.

CH-PC and CH-PC-E2-coated glass substrates were prepared by drop-casting 1 mg mL<sup>-1</sup> CH-PC or CH-PC-E2 solutions onto the glass-bottom (MatTek) dish for overnight reaction at ambient conditions. Then, the polymer-coated glass substrates were washed with copious DI water and follow by air-drying. Before cell seeding, the polymer-coated glass substrates were sterilized with 75% ethanol, and followed by washing with PBS buffer and conditioning in the cell culture medium.

### 3.4.9 DAF-FM fluorescence imaging study

DAF-FM is a sensitive fluorescent probe for NO detection at a nanomolar scale.<sup>[38]</sup> Initially, DAF-FM shows weak fluorescence signals. However, after acetate hydrolyzing and subsequently reacting with produced NO in cells, DAF-FM transforms to a highly fluorescent benzotriazole derivative. The cell loaded substrates as stated above were placed on the IX81 microscope (Olympus). Fluorescence images were acquired by and controlled by the MetaMorph imaging System (Molecular Devices) using a 10X-fluor objective at excitation

and emission wavelengths of 488 and 535 nm, respectively. Each sample was prepared in triplicate. The fluorescent intensity of cells was analyzed by using the image analysis software Image Pro Plus (Media Cybernetics), and average fluorescent intensity of total cells per image was obtained by analyzing the best fit circular region of interest. Standard deviations are based on calculations for three independent samples.

### 3.4.10 Statistics

All statistical analysis was performed using SPSS 18.0 software. Statistical differences among each group were assessed by a Student's paired t-test. Probability values of  $p < 0.05$  were considered significant and represented as asterisk (\*). All data are presented as mean  $\pm$  standard deviation.

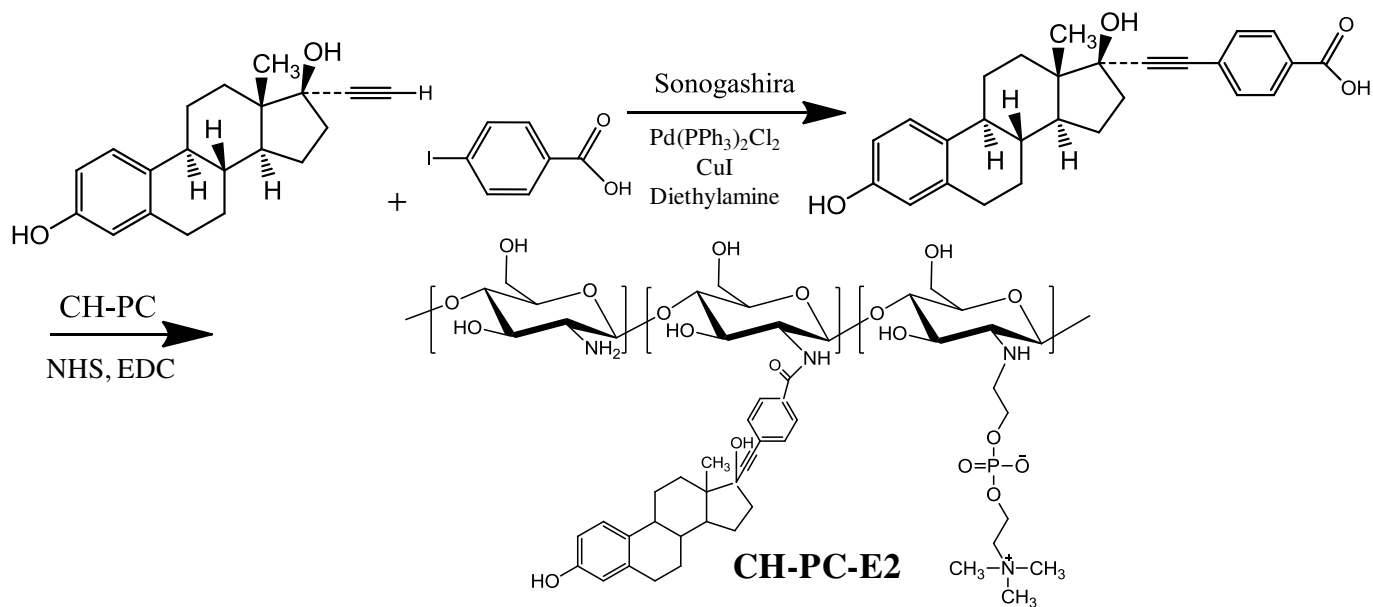


Figure 3.1 Synthetic route of CH-PC-E2 polymer conjugate

## 3.5 Results and discussion

### 3.5.1 Characterization of CH-PC-E2 conjugates

In this study, E2-benzoic acid was covalently tethered to CH-PC *via* an amide linker. The synthesis strategy for the preparation of CH-PC-E2 conjugates involved two steps (Figure 3.1): (1) selective modification of ethinyl group of 17 $\alpha$ -ethinylestradiol with 4-iodobenzoic acid linker, which was further activated to corresponding N-hydroxysuccinimide (NHS) ester; (2) Conjugation of E2-benzoic acid to CH-PC polymer backbone *via* formation of an amide bond. PC-modified chitosan polymer backbone was synthesized *via* conjugation of PC-glyceraldehyde to deacetylated chitosan.<sup>[39]</sup> The content of PC groups was ~20 mol %, calculated from <sup>1</sup>H NMR data.<sup>[29]</sup> As shown in Fig.3.2, the <sup>1</sup>H NMR signal of CH-PC backbone was labeled from C1 to C5, respectively. The successful conjugation of E2-benzoic acid was particularly validated by the appearance of a signal at 1.30 ppm, attributed to the resonance of methyl protons of ethinylestradiol (E18). The <sup>1</sup>H NMR signals at 7.67 ppm, 7.14 and 7.06 ppm assigned to the resonance of aromatic protons of E2 residues (E1, E2 and E4). The aromatic protons of iodobenzoic acid linker were also shown at 8.23 ppm and 7.92 ppm, respectively.

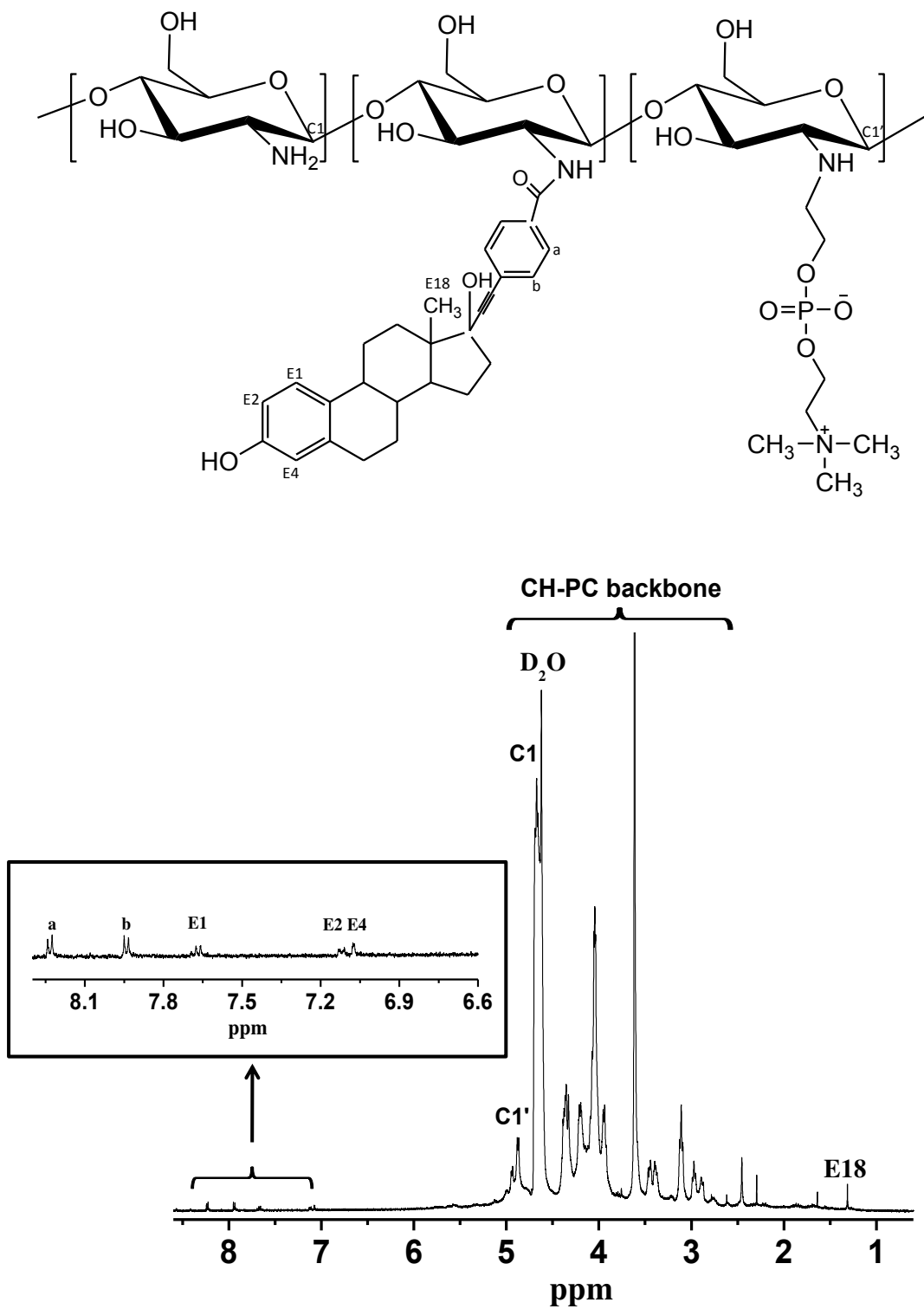


Figure 3.2 <sup>1</sup>H NMR spectrum of CH-PC-E2 conjugate in D<sub>2</sub>O at 70°C.

### 3.5.2 Viscoelastic properties of CH-PC-E2 and CH-PC formulated thin films

When considering the application of biomaterials in the cardiovascular regenerative medicine, viscoelasticity is one of the most important mechanical properties, including the storage modulus  $G'$ , which reflects the elastic property, and the loss modulus  $G''$ , which represents the viscous property.<sup>[40-43]</sup> Complex shear modulus  $G$ , representing to the resistance of materials to deformation, can be represented as  $G = G' + iG''$ , where  $i$  is the imaginary unit.<sup>[33]</sup> QCM-D is a useful surface analytical tool to study the properties of the soft films depositing on the surfaces in real time. The parameters measured by QCM-D, resonance frequency ( $\Delta f$ ) and dissipation ( $\Delta D$ ), reflected the mass of adsorbed molecules and their viscoelastic properties.<sup>[32]</sup>

In present study, the QCM-D resonance frequency and dissipation shifts for CH-PC-E2 and CH-PC were recorded in a time-dependent manner as indicated in the Fig.3.3 (A). For both of the CH-PC (black trace) and CH-PC-E2 (red trace) adsorption, the QCM-D signals reached a plateau of the frequency at ca.  $-20$  Hz and of the dissipation at  $1.7 \times 10^{-6}$  after 2 hours. The results were fitted using Voigt viscoelastic model as shown in Table 3.1. The thickness of CH-PC-E2 film is in a similar range of CH-PC film (CH-PC-E2:  $4.7 \pm 1.7$  nm vs. CH-PC:  $3.9 \pm 0.8$  nm). This films thickness value measured by QCM-D study is also accordance well with the thickness value measured by ellipsometry formed by drop-casting method (CH-PC-E2:  $3.1 \pm 0.2$  nm vs. CH-PC:  $2.6 \pm 0.1$  nm).

$G'$  and  $G''$  are governed by power laws with scaling exponents  $\alpha'$  and  $\alpha''$ , and proportional to the angular frequency of deformation  $\omega$ , as shown follow:  $G'(\omega) = G_0' (\omega / \omega_0)^{\alpha'}$ ,  $G''(\omega) = G_0'' (\omega / \omega_0)^{\alpha''}$ , where  $\omega_0$  is the reference frequency.<sup>[44]</sup> Scaling exponents  $\alpha'$  and  $\alpha''$ , reflect microscopic motions within material.<sup>[45]</sup> As shown in the Figure 3.3(B) and Table 3.1, the estimated loss and storage moduli, and the scaling exponents ( $\alpha'$ ,  $\alpha''$ ) of CH-PC and CH-PC-E2 films demonstrated a typical of hydrogel nature within a range of MPa ( $G' > G''$ ,  $0 < \alpha' < 1$ ,  $0 < \alpha'' < 1$ ). The hydrogel formation is probably due to the crosslinking *via* ionic pairing within PC groups. Considering the identical value of rheological characteristic of CH-PC and CH-PC-E2 hydrogel films, it suggests that the hydrophobic interactions among E2 microdomains are weak and apparently didn't significant affect the mechanical properties of films. Moreover, the elastic modulus of CH-PC and CH-PC-E2 hydrogel films are in the

similar magnitude of cardiac regeneration materials, such as chitosan gelatin hydrogel ( $\sim 0.3\text{MPa}$ )<sup>[46]</sup> or Dacron ( $\sim 0.6\text{MPa}$ )<sup>[47]</sup>.

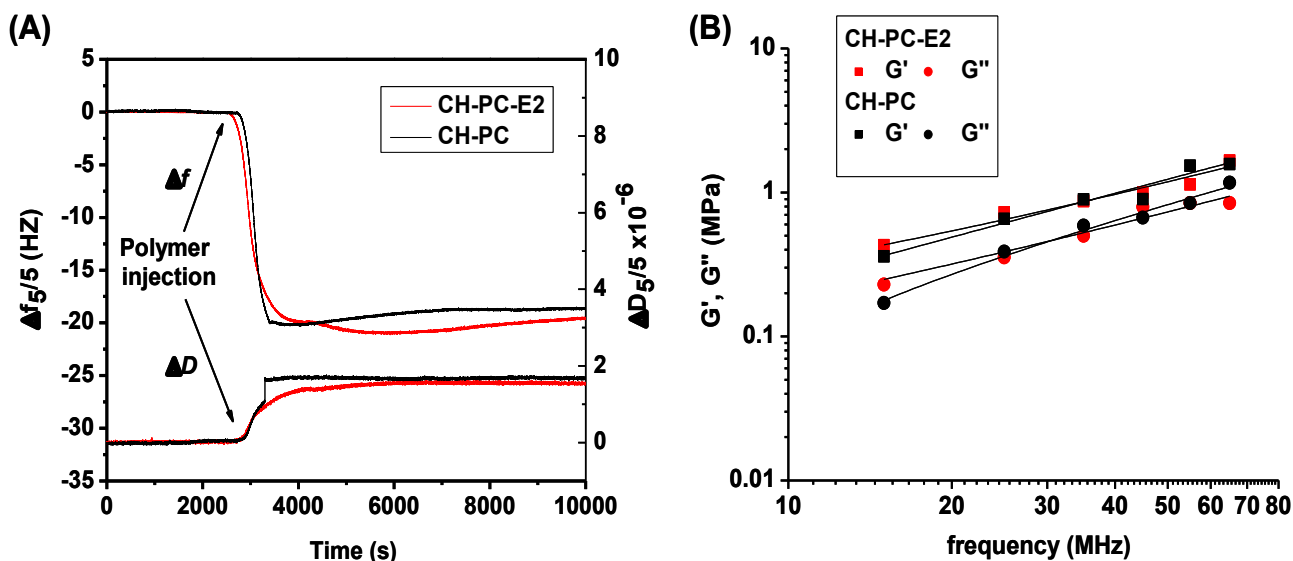


Figure 3.3 QCM-D study of *in situ* formed CH-PC-E2 and CH-PC hydrogel films on the silicon dioxide for overnight reaction at 25°C. (A) The shift of QCM-D frequency ( $\Delta f_5/5$ ) and dissipation ( $\Delta D_5/5$ ) showed the thin film formulations of CH-PC (black trace) and CH-PC-E2 (red trace) onto the silicon dioxide surfaces as a function of time. (B) The storage modulus (squares) and loss modulus (circles) of CH-PC and CH-PC-E2 hydrogel films are shown in a frequency dependent manner.

Table 3.1 Viscoelastic properties of CH-PC and CH-PC-E2 hydrogel films formed *in situ*<sup>a</sup>

Polymer	Thickness (nm)	$G'$ (MPa)	$G''$ (MPa)	$\alpha'$	$\alpha''$
CH-PC	3.9±0.8	0.66	0.62	1.04	0.55
CH-PC-E2	4.7±1.7	0.73	0.57	0.68	0.78

<sup>a</sup>  $G'$  and  $G''$ : hydrated layer storage and loss moduli (represented values at 25 MHz) measured by QCM-D.  $\alpha'$  and  $\alpha''$ : scaling exponents calculated based on the frequency dependence power-law for  $G'$  and  $G''$ , respectively.

### 3.5.3 The binding experiment of ER- $\alpha$ to CH-PC-E2 hydrogel film

QCM-D techniques are flexible to provide additional biologically relevant information, which can mimic the protein interactions with surfaces under real physiological conditions.<sup>[48]</sup> In the previous study, estrogen receptor element (ERE) was immobilized onto a QCM-D sensor surface in order to study its interactions with ERs as well as to understand the relevant biophysical properties, such as the bound ER- $\alpha$  conformation and orientation.<sup>[49, 50]</sup> Herein, QCM-D based ER- $\alpha$  binding experiment is carried out onto the CH-PC-E2/CH-PC thin film-functionalized QCM sensor prepared *ex-situ* using the same strategy as the strategy of subsequent cellular studies.

In the QCM-D related protein adsorption study, the frequency shift is proportional to the mass changes of the CH-PC-E2/CH-PC films induced by protein adsorption while the dissipation shift is relevant of internal energy loss within the adsorbed estrogen receptor protein films with respect to periodic damping.<sup>[51]</sup> In this study, it generally demonstrates the  $\Delta f$  and  $\Delta D$  responses as a function of time for the ER- $\alpha$  binding to the CH-PC-E2-functionalized QCM-D glass crystal sensor (red trace). Control experiments were performed in the CH-PC functionalized control surfaces for the comparison (black trace). In the frequency and dissipation shifts versus time curves as shown in the Fig.3.4 (A), the stable baseline gradually changed upon flowing over 50 nM of ER- $\alpha$  solution onto the CH-PC-E2 functionalized QCM sensor, indicating a constant protein mass accumulation onto the surface. After PBS flushing, the QCM-D frequency and dissipation signal was stabilized at the value of  $-27$  Hz and  $3.3 \times 10^{-6}$ , respectively. However, we can also observe that the flowing through of ER- $\alpha$  solution over CH-PC control surface didn't trigger significant QCM-D frequency and dissipation signal changes. By applying the Sauerbrey model as previously suggested<sup>[52]</sup>, the surface coverage of ER- $\alpha$  for CH-PC-E2 films is  $\sim 6.26 \pm 0.51$  mg m<sup>-2</sup>.

The adsorbed ER- $\alpha$  layer can also be considered as a viscoelastic film, reflecting the conformation and binding energies to the surface.<sup>[53]</sup> Smaller dissipation value per mass unit indicates that the protein layer forms a dehydrated and a well-packed rigid arrangement while larger dissipation value per mass unit demonstrates a lower protein binding strength and a highly extended and hydrated protein arrangement<sup>[54, 55]</sup>. The  $\Delta D$ - $\Delta f$  correlation indicates how dissipation changes upon surface coverage of ER- $\alpha$  independent on time.<sup>[50]</sup> According to



previous studies, the dissipation to frequency ratio (the slope of  $\Delta D$  to  $\Delta f$  curves) reflected the conformational information of adsorbed ER- $\alpha$  layer, which hence can distinguish the specific and non-specific ER adsorption.<sup>[54, 55]</sup> From the Fig.3.4B, the  $\Delta D$  to  $\Delta f$  curves of ER- $\alpha$  binding onto the CH-PC films showed in a linear relationship, suggesting that ER- $\alpha$  didn't undergo significant conformational changes with regard to the accumulation of ER- $\alpha$  coverage. However, the  $\Delta D$  to  $\Delta f$  curves of ER- $\alpha$  binding onto the CH-PC-E2 films display two distinctive features (the transition point is indicated in the Figure 3.4B). At the initial stage ( $\Delta f < 6$  Hz), the slope of ER- $\alpha$  adsorption onto the CH-PC-E2 film showed a similar manner as CH-PC film, indicating that non-specific of ER- $\alpha$  adsorption is dominant. However, the slope of the  $\Delta D$  to  $\Delta f$  plot decreased after sufficient amounts of ER- $\alpha$  adsorption ( $\Delta f > 6$  Hz), suggesting a formation of a more dehydrated and rigid ER- $\alpha$  layer (specific adsorption), which is well accordance with previous study.<sup>[49]</sup> As a result, we can assume that CH-PC-E2 films will be energetically favorable to interact with estrogen receptors around cell membrane considering into future cellular studies.

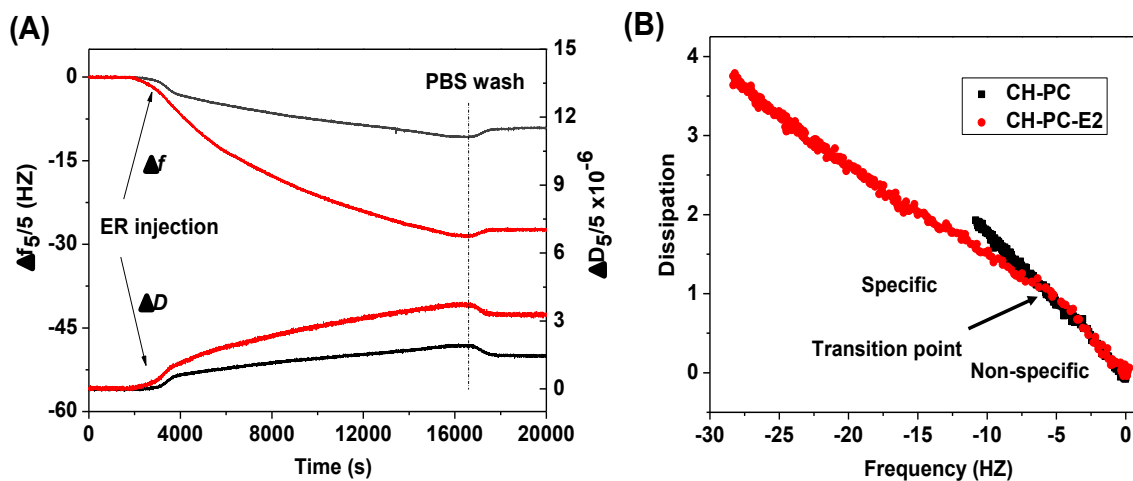


Figure 3.4 ER- $\alpha$  adsorption experiment onto the CH-PC-E2 and CH-PC functionalized silicon dioxide sensor by QCM-D at 25°C. The time of ER- $\alpha$  (concentration: 50 nmol L<sup>-1</sup>) addition and PBS wash are indicated by the arrows. (A) The QCM-D frequency ( $\Delta f_5/5$ ) and dissipation ( $\Delta D_5/5$ ) shift showed the adsorption of ER- $\alpha$  onto the CH-PC film (black trace) and CH-PC-E2 film (red trace) and as a function of time. (B)  $\Delta D$ - $\Delta f$  plots for ER- $\alpha$  adsorption corresponds to the ER- $\alpha$  non-specific adsorption of the CH-PC film (black trace) to the specific adsorption of the CH-PC-E2 film (red trace).

### 3.5.4 CH-PC-E2 hydrogel film promotes intracellular nitric oxide (NO) production

The availability of NO enhanced vascular dynamics of the artery as well as inhibited platelet adhesions and smooth muscle cells proliferation. Currently, NO-based therapies are widely associated with using a nitrous oxide donor, sodium nitroprusside (SNP), in order to deliver therapeutic amounts of NO for the vascular regeneration<sup>[56]</sup>. However, *in vivo* metabolism process of SNP leads to cyanide release and formation of peroxynitrite, which induced high cellular toxicity.<sup>[57]</sup> Locally delivery of E2 can exclusively stimulate endogenous NO production, which might provide a relative more biological friendly strategy for NO-based therapy.<sup>[58]</sup>

In order to determine whether CH-PC-E2 hydrogel films stimulate intracellular NO production, DAF-FM dia a cell permeable reagent, was used. Initially, DAF-FM has no fluorescent until they diffused across the cell membrane. Then, they were hydrolyzed by intracellular esterases and reacted with NO to transform to a fluorescent benzotriazole.<sup>[59]</sup> As shown in the Fig.3.5, microscopic images (A-C) and corresponding fluorescence images (D-F) were obtained from culturing EA.hy926 cells on the CH-PC and CH-PC-E2 films functionalized glass substrates, respectively. DAF-FM fluorescently-labeled NO was observed throughout the region of a cell. The green regions reflect accumulated intercellular distribution of NO resulting from local NO productions. By analyzing the fluorescence intensities, we found that the CH-PC-E2 hydrogel-like film significantly stimulated higher NO release (1.65 times) compared to the CH-PC films. Moreover, the increment was diminished in the cells pre-treated with estrogen receptor inhibitor ICI 182,780. The results confirmed that the NO production by CH-CP-E2 film is specifically due to the E2-ER interactions. Hence, the application of CH-PC-E2 film may extend the applications from novel local E2 delivery platform to the long-term functional coating materials for medical devices, e.g. stent, that serves to inhibit neointimal hyperplasia.

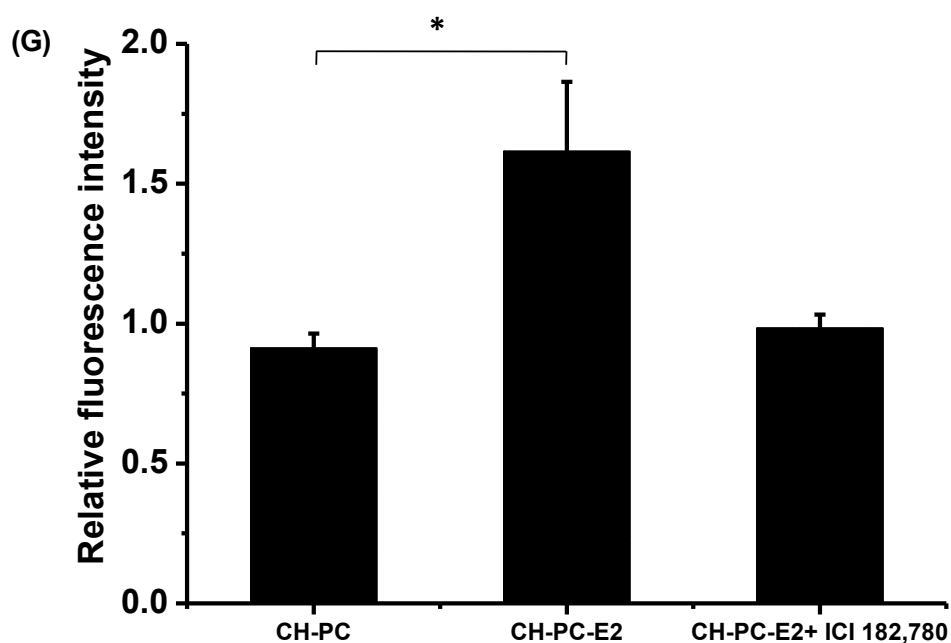
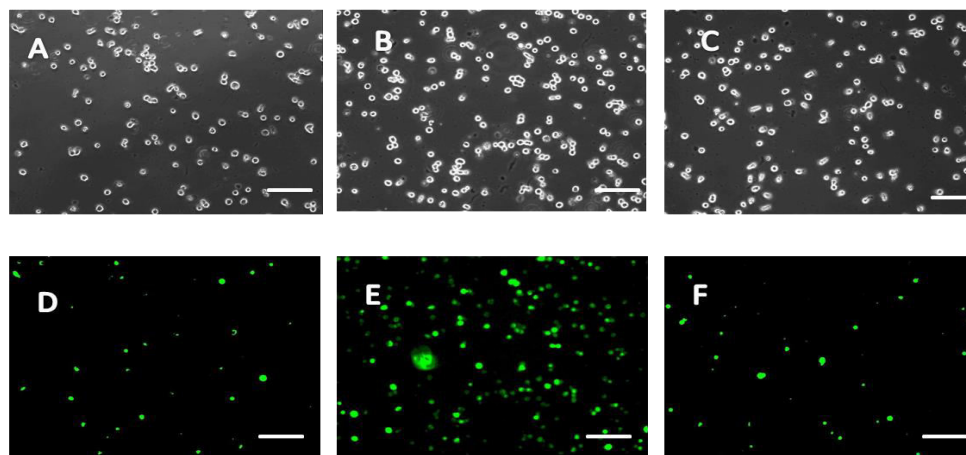


Figure 3.5 DAF-FM fluorescence imaging study of EA.hy926 cells incubated on the CH-PC and CH-PC-E2 films for 1 hour. Nitric oxide production levels were determined by using DAF-FM for the CH-PC functionalized substrates (A&D), CH-PC-E2 functionalized substrates (B&E), and CH-PC-E2 functionalized substrates pretreated with ICI 182,780 (C&F) for 1 hour. The top panels correspond to phase contrast micrographs and the bottom panels correspond to DAF-FM fluorescence images from the identical sites. (Scale bar: 100 $\mu$ m). The quantitative NO production levels were also shown by analyzing the emission peak intensity (G). Data were calculated by three independent samples. Probability values were considered significant which are represented as \* $p < 0.05$ .

### **3.6 Conclusions**

The research described in present study is to graft E2 to the chitosan phosphorylcholine (CH-PC) polymer backbone for the preparation of CH-PC-E2 conjugate as a prodrug strategy. It was successfully demonstrated that the fabrication method significantly influenced mechanical properties, depth-dependent composition, and biological responses of CH-PC-E2 hydrogel like films. The protective effect of CH-PC-E2 hydrogel film in cardiovascular system was conducted *via* investigated with corresponding mechanism of NO stimulation. The further mechanism of CH-PC-E2 hydrogel film as a platform for the cardiovascular regenerative medicine, e.g. to enhance the reendothelialization process or promotes the recovery of the endothelium, will be carried out in future study.

### **3.7 Acknowledgements**

Baowen Qi was supported by the NIMS Internship Program 2011 and 2013, as well as doctoral scholarship from the Natural Sciences and Engineering Research Council of Canada (NSERC) and Chinese Scholarship Council (CSC).

### 3.8 References

- [1] Wells G; Tugwell, P; Shea, B; Guyatt, G; Peterson, J; Zytaruk, N; Robinson, V; Henry, D; O'Connell, D; Cranney, A; Osteoporosis Methodol, G; Osteoporosis Res Advisory, G, Meta-analysis of the efficacy of hormone replacement therapy in treating and preventing osteoporosis in postmenopausal women. *Endocrine Reviews* **2002**, *23*: 529-539.
- [2] Dhandapani KM; Brann, DW, Protective effects of estrogen and selective estrogen receptor modulators in the brain. *Biology of Reproduction* **2002**, *67*: 1379-1385.
- [3] Cao X; Xu, P; Oyola, MG; Xia, Y; Yan, X; Saito, K; Zou, F; Wang, C; Yang, Y; Hinton, A, Jr.; Yan, C; Ding, H; Zhu, L; Yu, L; Yang, B; Feng, Y; Clegg, DJ; Khan, S; DiMarchi, R; Mani, SK; Tong, Q; Xu, Y, Estrogens stimulate serotonin neurons to inhibit binge-like eating in mice. *Journal of Clinical Investigation* **2014**, *124*: 4351-4362.
- [4] Barrettconnor E; Bush, TL, Estrogen and coronary heart-disease in women. *JAMA-J. Am. Med. Assoc.* **1991**, *265*: 1861-1867.
- [5] Guallar E; Manson, JE; Laine, C; Mulrow, C, Postmenopausal hormone therapy: The heart of the matter. *Annals of Internal Medicine* **2013**, *158*: 69-145.
- [6] Knowlton AA; Lee, AR, Estrogen and the cardiovascular system. *Pharmacology & Therapeutics* **2012**, *135*: 54-70.
- [7] Chandrasekar B; Sirois, MG; Geoffroy, P; Lauzier, D; Nattel, S; Tanguay, JF, Local delivery of 17 beta-estradiol improves reendothelialization and decreases inflammation after coronary stenting in a porcine model. *Thrombosis and Haemostasis* **2005**, *94*: 1042-1047.
- [8] Gerald P; Geoffroy, P; Cloutier, I; Sirois, MG; Tanguay, J-F, Local delivery of 17-beta-estradiol modulates collagen content in coronary porcine arteries after ptca and stent implantation. *Journal of Vascular Research* **2008**, *45*: 503-511.
- [9] Chandrasekar B; Nattel, S; Tanguay, JF, Coronary artery endothelial protection after local delivery of 17 beta-estradiol during balloon angioplasty in a porcine model: A potential new pharmacologic approach to improve endothelial function. *Journal of the American College of Cardiology* **2001**, *38*: 1570-1576.
- [10] Kovats S, Estrogen receptors regulate innate immune cells and signaling pathways. *Cellular immunology* **2015**, *294*: 63-9.

- [11] Chambliss KL; Yuhanna, IS; Mineo, C; Liu, PS; German, Z; Sherman, TS; Mendelsohn, ME; Anderson, RGW; Shaul, PW, Estrogen receptor alpha and endothelial nitric oxide synthase are organized into a functional signaling module in caveolae. *Circ.Res.* **2000**, 87: 44-52.
- [12] Hilgers RHP; Das, KC, Role of in vivo vascular redox in resistance arteries. *Hypertension* **2015**, 65: 130-145.
- [13] Kleinert H; Wallerath, T; Euchenhofer, C; Ihrig-Biedert, I; Li, H; Forstermann, U, Estrogens increase transcription of the human endothelial no synthase gene - analysis of the transcription factors involved. *Hypertension* **1998**, 31: 582-588.
- [14] de Mel A; Murad, F; Seifalian, AM, Nitric oxide: A guardian for vascular grafts? *Chemical Reviews* **2011**, 111: 5742-5767.
- [15] Radomski MW; Palmer, RM; Moncada, S, The anti-aggregating properties of vascular endothelium: Interactions between prostacyclin and nitric oxide. *British journal of pharmacology* **1987**, 92: 639-46.
- [16] Ross R, Mechanisms of disease - atherosclerosis - an inflammatory disease. *New England Journal of Medicine* **1999**, 340: 115-126.
- [17] Caldon CE, Estrogen signaling and the DNA damage response in hormone dependent breast cancers. *Frontiers in oncology* **2014**, 4: 106-106.
- [18] Jordan VC, The new biology of estrogen-induced apoptosis applied to treat and prevent breast cancer. *Endocrine-related cancer* **2015**, 22: 1-31.
- [19] Harrington WR; Kim, SH; Funk, CC; Madak-Erdogan, Z; Schiff, R; Katzenellenbogen, JA; Katzenellenbogen, BS, Estrogen dendrimer conjugates that preferentially activate extranuclear, nongenomic versus genomic pathways of estrogen action. *Molecular Endocrinology* **2006**, 20: 491-502.
- [20] Chambliss KL; Wu, Q; Oltmann, S; Konaniah, ES; Umetani, M; Korach, KS; Thomas, GD; Mineo, C; Yuhanna, IS; Kim, SH; Madak-Erdogan, Z; Maggi, A; Dineen, SP; Roland, CL; Hui, DY; Brekken, RA; Katzenellenbogen, JA; Katzenellenbogen, BS; Shaul, PW, Non-nuclear estrogen receptor alpha signaling promotes cardiovascular protection but not uterine or breast cancer growth in mice. *Journal of Clinical Investigation* **2010**, 120: 2319-2330.

- [21] Pryor JB; Harper, BJ; Harper, SL, Comparative toxicological assessment of pamam and thiophosphoryl dendrimers using embryonic zebrafish. *International Journal of Nanomedicine* **2014**, 9: 1947-1956.
- [22] Albertazzi L; Gherardini, L; Brondi, M; Sato, SS; Bifone, A; Pizzorusso, T; Ratto, GM; Bardi, G, In vivo distribution and toxicity of pamam dendrimers in the central nervous system depend on their surface chemistry. *Molecular Pharmaceutics* **2013**, 10: 249-260.
- [23] Liu S; Maheshwari, R; Kiick, KL, Polymer-based therapeutics. *Macromolecules* **2009**, 42: 3-13.
- [24] Nur-E-Kamal A; Ahmed, I; Kamal, J; Babu, AN; Schindler, M; Meiners, S, Covalently attached fgf-2 to three-dimensional polyamide nanofibrillar surfaces demonstrates enhanced biological stability and activity. *Molecular and Cellular Biochemistry* **2008**, 309: 157-166.
- [25] Rinaudo M, Chitin and chitosan: Properties and applications. *Prog. Polym. Sci.* **2006**, 31: 603-632.
- [26] Chen M-C; Mi, F-L; Liao, Z-X; Sung, H-W, Chitosan: Its applications in drug-eluting devices. *Chitosan for Biomaterials I* **2011**, 243: 185-230.
- [27] Tardif K; Cloutier, I; Miao, Z; Lemieux, C; St-Denis, C; Winnik, FM; Tanguay, J-F, A phosphorylcholine-modified chitosan polymer as an endothelial progenitor cell supporting matrix. *Biomaterials* **2011**, 32: 5046-5055.
- [28] Mohan S; Konopinski, R; Yan, B; Centonze, VE; Natarajan, M, High glucose-induced ikk-hsp-90 interaction contributes to endothelial dysfunction. *Am. J. Physiol.-Cell Physiol.* **2009**, 296: 182-192.
- [29] Tiera MJ; Qiu, X-P; Bechaouch, S; Shi, Q; Fernandes, JC; Winnik, FM, Synthesis and characterization of phosphorylcholine-substituted chitosans soluble in physiological ph conditions. *Biomacromolecules* **2006**, 7: 3151-3156.
- [30] Kim SH; Katzenellenbogen, JA, Hormone-pamam dendrimer conjugates: Polymer dynamics and tether structure affect ligand access to receptors. *Angewandte Chemie-International Edition* **2006**, 45: 7243-7248.
- [31] Ligler FS; Lingerfelt, BM; Price, RP; Schoen, PE, Development of uniform chitosan thin-film layers on silicon chips. *Langmuir* **2001**, 17: 5082-5084.

- [32] Dixon MC, Quartz crystal microbalance with dissipation monitoring: Enabling real-time characterization of biological materials and their interactions. *Journal of biomolecular techniques : JBT* **2008**, *19*: 151-158.
- [33] Reviakine I; Johannsmann, D; Richter, RP, Hearing what you cannot see and visualizing what you hear: Interpreting quartz crystal microbalance data from solvated interfaces. *Anal. Chem.* **2011**, *83*: 8838-8848.
- [34] White CC; Schrag, JL, Theoretical predictions for the mechanical response of a model quartz crystal microbalance to two viscoelastic media: A thin sample layer and surrounding bath medium. *Journal of Chemical Physics* **1999**, *111*: 11192-11206.
- [35] Duner G; Thormann, E; Dedinaite, A, Quartz crystal microbalance with dissipation (qcm-d) studies of the viscoelastic response from a continuously growing grafted polyelectrolyte layer. *Journal of Colloid and Interface Science* **2013**, *408*: 229-234.
- [36] Miao Z; Kujawa, P; Lau, Y-TR; Toita, S; Qi, B; Nakanishi, J; Cloutier, I; Tanguay, J-F; Winnik, FM, Tuning the properties and functions of 17 beta-estradiol-polysaccharide conjugates in thin films: Impact of sample history. *Biomacromolecules* **2012**, *13*: 4098-4108.
- [37] Miao ZM; Kujawa, P; Lau, YTR; Toita, S; Qi, BW; Nakanishi, J; Cloutier, I; Tanguay, JF; Winnik, FM, Tuning the properties and functions of 17 beta-estradiol-polysaccharide conjugates in thin films: Impact of sample history. *Biomacromolecules* **2012**, *13*: 4098-4108.
- [38] Namin SM; Nofallah, S; Joshi, MS; Kavallieratos, K; Tsoukias, NM, Kinetic analysis of daf-fm activation by no: Toward calibration of a no-sensitive fluorescent dye. *Nitric Oxide-Biol. Chem.* **2013**, *28*: 39-46.
- [39] Tiera MJ; Qiu, XP; Bechaouch, S; Shi, Q; Fernandes, JC; Winnik, FM, Synthesis and characterization of phosphorylcholine-substituted chitosans soluble in physiological ph conditions. *Biomacromolecules* **2006**, *7*: 3151-3156.
- [40] Voinova MV; Rodahl, M; Jonson, M; Kasemo, B, Viscoelastic acoustic response of layered polymer films at fluid-solid interfaces: Continuum mechanics approach. *Physica Scripta* **1999**, *59*: 391-396.
- [41] Cortes F; Jesus Elejabarrieta, M, Modelling viscoelastic materials whose storage modulus is constant with frequency. *International Journal of Solids and Structures* **2006**, *43*: 7721-7726.



- [42] Meyers MA; Chen, PY; Lin, AYM; Seki, Y, Biological materials: Structure and mechanical properties. *Progress in Materials Science* **2008**, *53*: 1-206.
- [43] Bao G; Suresh, S, Cell and molecular mechanics of biological materials. *Nature Materials* **2003**, *2*: 715-725.
- [44] Eisele NB; Andersson, FI; Frey, S; Richter, RP, Viscoelasticity of thin biomolecular films: A case study on nucleoporin phenylalanine-glycine repeats grafted to a histidine-tag capturing qcm-d sensor. *Biomacromolecules* **2012**, *13*: 2322-2332.
- [45] Schoenwaelder SMS; Bally, F; Heinke, L; Azucena, C; Bulut, OD; Heissler, S; Kirschhoefer, F; Gebauer, TP; Neffe, AT; Lendlein, A; Brenner-Weiss, G; Lahann, J; Welle, A; Overhage, J; Woell, C, Interaction of human plasma proteins with thin gelatin-based hydrogel films: A qcm-d and tof-sims study. *Biomacromolecules* **2014**, *15*: 2398-2406.
- [46] Pok S; Myers, JD; Madihally, SV; Jacot, JG, A multilayered scaffold of a chitosan and gelatin hydrogel supported by a pcl core for cardiac tissue engineering. *Acta Biomaterialia* **2013**, *9*: 5630-5642.
- [47] Tremblay D; Zigras, T; Cartier, R; Leduc, L; Butany, J; Mongrain, R; Leask, RL, A comparison of mechanical properties of materials used in aortic arch reconstruction. *Annals of Thoracic Surgery* **2009**, *88*: 1484-1491.
- [48] Marx KA, Quartz crystal microbalance: A useful tool for studying thin polymer films and complex biomolecular systems at the solution-surface interface. *Biomacromolecules* **2003**, *4*: 1099-1120.
- [49] Su X; Lin, C-Y; O'Shea, SJ; Teh, HF; Peh, WYX; Thomsen, JS, Combinational application of surface plasmon resonance spectroscopy and quartz crystal microbalance for studying nuclear hormone receptor-response element interactions. *Analytical Chemistry* **2006**, *78*: 5552-5558.
- [50] Peh WYX; Reimhult, E; Teh, HF; Thomsen, JS; Su, X, Understanding ligand binding effects on the conformation of estrogen receptor alpha-DNA complexes: A combinational quartz crystal microbalance with dissipation and surface plasmon resonance study. *Biophysical Journal* **2007**, *92*: 4415-4423.
- [51] Hook F; Rodahl, M; Brzezinski, P; Kasemo, B, Energy dissipation kinetics for protein and antibody-antigen adsorption under shear oscillation on a quartz crystal microbalance. *Langmuir* **1998**, *14*: 729-734.

- [52] Hook F; Kasemo, B; Nylander, T; Fant, C; Sott, K; Elwing, H, Variations in coupled water, viscoelastic properties, and film thickness of a mefp-1 protein film during adsorption and cross-linking: A quartz crystal microbalance with dissipation monitoring, ellipsometry, and surface plasmon resonance study. *Analytical Chemistry* **2001**, *73*: 5796-5804.
- [53] Hook F; Ray, A; Norden, B; Kasemo, B, Characterization of pna and DNA immobilization and subsequent hybridization with DNA using acoustic-shear-wave attenuation measurements. *Langmuir* **2001**, *17*: 8305-8312.
- [54] Su XD; Robelek, R; Wu, YJ; Wang, GY; Knoll, W, Detection of point mutation and insertion mutations in DNA using a quartz crystal microbalance and muts, a mismatch binding protein. *Analytical Chemistry* **2004**, *76*: 489-494.
- [55] Zhou C; Friedt, JM; Angelova, A; Choi, KH; Laureyn, W; Frederix, F; Francis, LA; Campitelli, A; Engelborghs, Y; Borghs, G, Human immunoglobulin adsorption investigated by means of quartz crystal microbalance dissipation, atomic force microscopy, surface acoustic wave, and surface plasmon resonance techniques. *Langmuir* **2004**, *20*: 5870-5878.
- [56] Thierry B; Winnik, FM; Merhi, Y; Silver, J; Tabrizian, M, Bioactive coatings of endovascular stents based on polyelectrolyte multilayers. *Biomacromolecules* **2003**, *4*: 1564-1571.
- [57] Wang PG; Xian, M; Tang, XP; Wu, XJ; Wen, Z; Cai, TW; Janczuk, AJ, Nitric oxide donors: Chemical activities and biological applications. *Chemical Reviews* **2002**, *102*: 1091-1134.
- [58] Nichols SP; Storm, WL; Koh, A; Schoenfisch, MH, Local delivery of nitric oxide: Targeted delivery of therapeutics to bone and connective tissues. *Advanced Drug Delivery Reviews* **2012**, *64*: 1177-1188.
- [59] Kojima H; Urano, Y; Kikuchi, K; Higuchi, T; Hirata, Y; Nagano, T, Fluorescent indicators for imaging nitric oxide production. *Angewandte Chemie-International Edition* **1999**, *38*: 3209-3212.

### 3.9 Appendix B. Supporting information

#### Synthesis and characterization of 17 $\alpha$ -ethinylestradiol benzoic acid

In order to covalently conjugate E2 to the surface, a derivative of 17 $\alpha$ -ethinylestradiol (17-EE2) was used by coupling 4-iodobenzoic acid to ethynyl group. The biological activity of E2 has been shown to retain by a similar benzoic modification of 17-EE2 in previous study. The successful selective benzoic group of EE2 was confirmed by analysis of the  $^1\text{H}$  NMR spectrum of the reaction product (Figure SI.3.1), which presents the peak at  $\delta$  7.84 (a) and  $\delta$  7.35 (b) ppm, attributing to the phenol proton of the new linker, while the peak at  $\delta$  6.98, 6.50 and 6.43 ppm, attributing to the proton in the EE2 original phenol ring, respectively (1, 2, and 4 site). A further evidence for the formation of the carboxyl group was obtained from the ATR-FTIR spectrum which displays a band at  $1705\text{ cm}^{-1}$  for C=O stretching and a broad band at  $3382\text{ cm}^{-1}$  for O-H stretching.

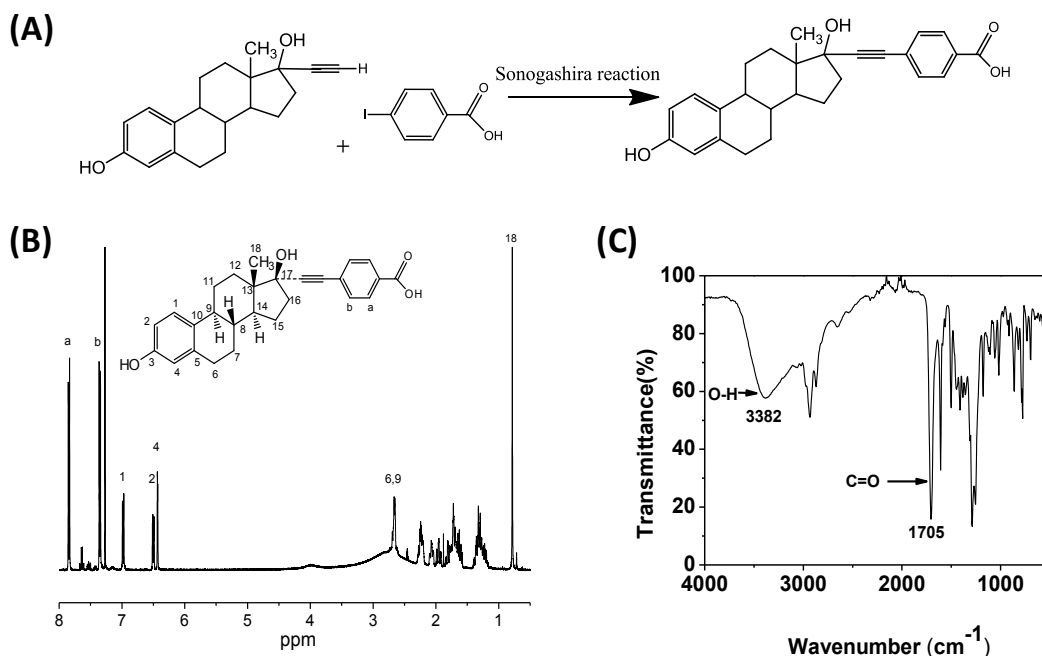


Figure SI.3.1 Synthesis and characterization of 17 $\alpha$ -ethinylestradiol benzoic acid for the surface immobilization. (A) Synthetic route of the 17 $\alpha$ -ethinylestradiol benzoic acid. (B) The  $^1\text{H}$  NMR spectrum of the 17 $\alpha$ -ethinylestradiol benzoic acid in  $\text{CDCl}_3$  at  $25^\circ\text{C}$ . (C) The ATR-FTIR spectrum of the 17 $\alpha$ -ethinylestradiol benzoic acid at  $25^\circ\text{C}$ .

## Characterization of CH-PC-E2 by ATR-FTIR

In order to further confirm the covalent bond formation between E2-benzoic acid and CH-PC polymer backbone, FTIR-ATR spectra of CH-PC and CH-PC-E2 were also shown in the Fig.SI. 3.2. An evidence for the formation of the amide bond between ethinylestradiol and amine group was obtained from the CH-PC-E2 spectrum (red), which displays a band at  $1725\text{ cm}^{-1}$  for C=O stretching. Both samples showed the characteristic bands at  $3300\text{ cm}^{-1}$ , attributed to the stretching vibrations of  $\text{-NH}_2$  and  $\text{-OH}$  groups in the chitosan backbone. Further, the successful conjugation of PC group in the chitosan backbone was confirmed by the presence of the four-band signature explained as following. The band at  $1224$  and  $793\text{ cm}^{-1}$  correspond to the anti-symmetric stretching of  $\text{PO}_2^-$  and  $\text{P (OC)}_2$  moieties, while the band at  $1065\text{ cm}^{-1}$  corresponds to the stretching of  $\text{P-O-C}$  moiety. Moreover, the band at  $1369\text{ cm}^{-1}$  corresponds to the bending of  $\text{N}^+ (\text{CH}_3)_3$  groups.

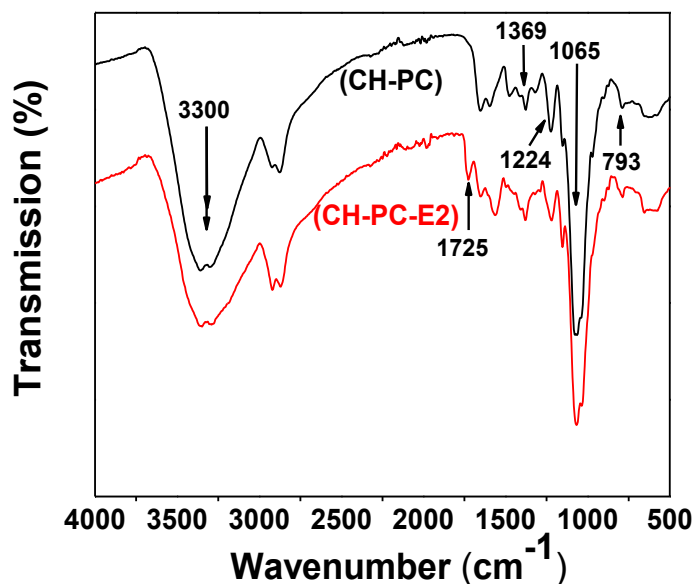


Figure SI.3.2 ATR-FTIR spectra of CH-PC (black) and CH-PC-E2 (red).

## E2 contents in CH-PC-E2 measured by UV/vis

The substituted content of E2 in the CH-PC-E2 polymer conjugates was determined by UV absorbance at 280 nm. As shown in the Fig.SI.3.3,  $17\alpha$ -ethinylestradiol in a concentration of  $5 \times 10^{-4}$  M in acetonitrile showed two signal peaks of absorbance in UV at 203 nm and 282 nm (black trace). However, after grafting onto the CH-PC polymer, the two signal peaks are shifted to 201 and 270 nm in a water/acetonitrile (55:45, v: v) solvent (pH 6.8), respectively (red trace). The content of E2 residues (%) in the CH-PC-E2 polymer conjugates was 4.7 mol% calculated by using Beer–Lambert law from the UV absorbance at 270 nm.<sup>[1]</sup>

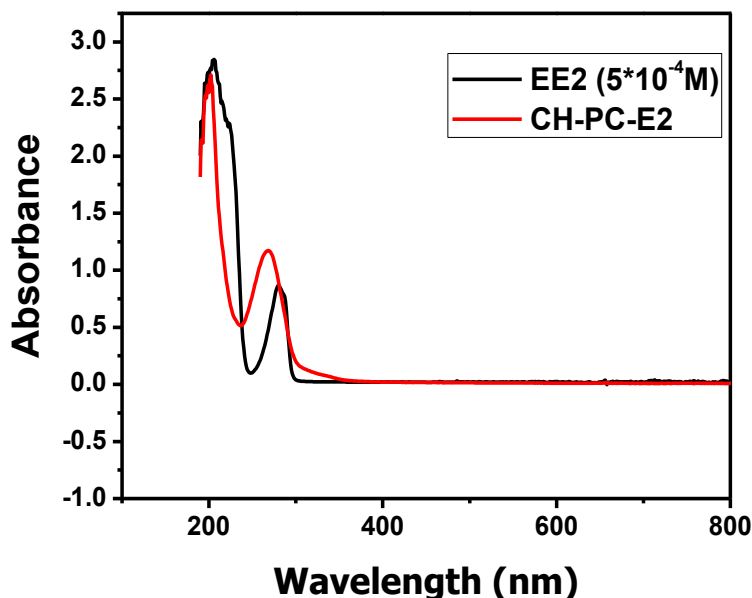


Figure SI.3.3 UV absorbance of CH-PC-E2 polymer conjugates in H<sub>2</sub>O/acetonitrile (55:45) at pH 6.8.

## Dynamic light scattering (DLS) measurement

In aqueous solution phase, CH-PC tends to form self-aggregates due to the occurrence of electrostatic interactions between the amine groups and the PC moiety. In addition, CH-PC-E2 may behave similarly due to two driving forces as synergistic effects: 1) the weaker electrostatic interaction between zwitterionic PC group and positively charged amine groups;

2) the hydrophobic/hydrophilic interactions of hydrophobic E2 residues and hydrophilic CH-PC main chains. In the Fig.SI.3.4, dynamic light scattering (DLS) confirmed that both CH-PC-E2 ( $R_h \sim 63\text{nm}$ ) and CH-PC ( $R_h \sim 89\text{nm}$ ) conjugate in solution form aggregates.

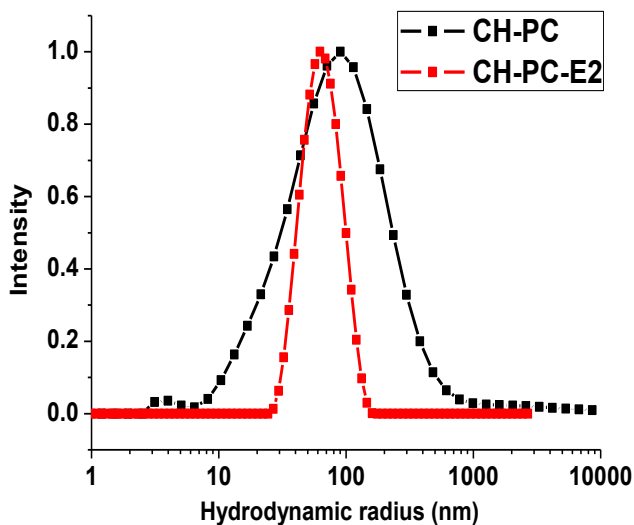


Figure SI.3.4 DLS measurement and size distribution (weight by intensity) of CH-PC (black trace, polydispersity index:  $0.27 \pm 0.1$ ) and CH-PC-E2 (red trace, polydispersity index:  $0.17 \pm 0.1$ ) aggregates in the PBS solution (pH~6.8) at 25°C.

## References

- [1] Holbrook RD; Love, NG; Novak, JT, Sorption of 17-beta-estradiol and 17 alpha-ethinylestradiol by colloidal organic carbon derived from biological wastewater treatment systems. *Environ. Sci. Technol.* **2004**, 38: 3322-3329.

## CHAPTER FOUR

---

### **Estradiol-tethered micropatterned surfaces for the study of estrogenic non-genomic pathways**

Baowen Qi<sup>1</sup>, Yoshihisa Shimizu<sup>2</sup>, Jun Nakanishi<sup>2</sup>, and Françoise M. Winnik<sup>1,2</sup>

<sup>1</sup>Faculté de Pharmacie and Département de Chimie, Université de Montreal, CP 6128 Succursale Centre Ville, Montreal, QC, H3C 3J7, Canada

<sup>2</sup>World Premier International (WPI) Research Center Initiative, International Center for Materials Nanoarchitectonics (MANA), National Institute for Materials Science (NIMS), 1-1 Namiki Tsukuba, Ibaraki 305-0044, Tsukuba, Japan

#### **Summary of transition**

In this chapter, E2 was functionalized to the micropatterned substrates, which are prepared by photolithography using top-down approach. Together with XPS, SPR and QCM-D measurements, it proved that E2 was successfully tethered to a selected gold surface. Through cell ELISA studies, a conclusion that surface-tethered E2 can exclusively act as selective estrogen receptor modulators (SERM) to isolate E2 non-genomic action from cross-talked signaling pathways was further validated. This micropatterning design allows us to understand the fundamental biological mechanisms of surface-tethered E2 in depth. However, the increased ERK phosphorylation level induced by E2-functionalized micropatterned substrate is only 18.7% in the present studies. In future, we expect to see larger responses by using higher gold dot densities of micropatterned substrates for E2 functionalization. Moreover, the other possible estrogen related non-genomic signal pathway, such as PI3K/AKT, should be addressed to validate the role of surface-tethered E2 *in vitro* and *in vivo* by using this biosensor-based technology. The results in this study were also accordance well with the previous chapter of CH-PC-E2 studies by different means of approaches (top-down vs. bottom-up) and biological studies (fundamental mechanisms of surface-tethered E2 vs. cardiovascular protective applications of surface-tethered E2).

## **4.1 Abstract**

In addition to its major role in the regulation of gene expression-mediated processes in the nucleus, estradiol (E2) activates also transient non-genomic pathways through interactions with receptors located on the cell plasma membrane. The mechanism of the latter signaling remains poorly understood due to difficulties in preventing the entry of E2 in the cytoplasm and its subsequent transfer to the nucleus. A solution to this problem is presented in this report of the preparation of micropatterned substrates consisting of arrays of gold dots bearing tethered E2 were distributed on a glass substrate rendered cell-adhesive via covalent linkage of cyclic-RGD (cRGD) of short PEG chains. The E2 immobilization process and its physiological relevant activity were validated with surface plasmon resonance (SPR) and quartz crystal microbalance with dissipation (QCM-D) measurements carried out standard gold surfaces functionalized by an identical procedure and by cell proliferation studies on cRGD-modified glass substrates. MCF-7 cells attached to micropatterned substrates were shown to undergo phosphorylation of the extracellular signal-regulated kinase (ERK), an essential kinase of the E2 non-genomic pathway, without change in cell proliferation. These results demonstrate that the E2-modified micropatterned substrates can serve as non-genomic-selective estrogen modulators, leading the way towards unveiling detailed features of the non-genomic signaling of E2 and related estrogenic molecules.

## **4.2 Authors keywords**

Micropatterning; Estrogen; Non-genomic pathway; ERK; SPR; QCM-D



### 4.3 Introduction

The biological effects of  $17\beta$ -estradiol (E2), the most potent and dominant estrogen, are mediated through estrogen receptors (ERs) acting as ligand-activated transcription factors. The hormonal effects of E2, known as genomic effects of E2,<sup>[1]</sup> which take place over several hours to several days, are initiated through interactions of this steroid with ERs present in the nucleus. E2 is involved also in the regulation of various cellular processes, such as cell proliferation, migration, and differentiation.<sup>[2]</sup> In addition, E2 exerts beneficial effects on the cardiovascular system. For instance, it stimulates the release of nitric oxide, contributes to the repair of injured blood vessels, and lowers the risk of atherosclerosis.<sup>[3]</sup> It is generally recognized that these effects are not initiated in the cell nucleus, but through interactions of E2 with estrogen receptors localized on the cell plasma membrane, known as mERs.<sup>[4-6]</sup> The extra-nuclear or “non-genomic” effects of E2 take place in the course of a few seconds to a few minutes.<sup>[7-12]</sup> There have been indications, though, that in some cases E2-induced extra-nuclear activation persists over much longer periods, up to ~16 hrs.<sup>[13]</sup> This confusing state of affairs is brought about by the inherent difficulties of mechanistic studies involving non-genomic effects of E2.<sup>[14]</sup> For example, E2 has a very low solubility in water, therefore it is usually added to cell culture media as a solution in dimethylsulfoxide. This cosolvent remains in the media throughout the biological testing and may affect the outcome of the studies.<sup>[15]</sup> Also, it is critical to ensure that E2 interacts only with mER and does not enter the cell. One strategy to overcome these difficulties consists in linking E2 to large soluble proteins, such as bovine serum albumin (BSA)<sup>[16]</sup> or peroxidase,<sup>[17]</sup> or to synthetic macromolecules, such as poly(amido)amine dendrimers.<sup>[18-20]</sup> E2 macromolecular conjugates are soluble in cell culture media, hence a cosolvent is no longer required. It is thought also that, in view of their size and physicochemical properties, E2-conjugates do not transit through the cell membranes.<sup>[21]</sup> This may not always be the case. For instance, the estrogen-dendrimer-E2 complex was detected in the cytoplasm of treated cells even though the dendrimer was expected to be too hydrophilic to penetrate lipid bilayers.<sup>[20]</sup> Intriguing evidence about the location of the E2-dendrimer conjugate calls for a re-evaluation of previous results<sup>[22]</sup> and, in the broader perspective, points to the need for better diagnostic tools.

Covalent immobilization of biosignaling molecules to solid substrates is a well-established tool to study biological effects induced by contact of signaling agents with receptors located on the plasma membrane.<sup>[23-30]</sup> In the case of E2, which can act both at the level of the plasma membrane (outside the cell) and within the cytoplasm and the nucleus, immobilization onto a solid substrate via a non-cleavable covalent bond would allow one to monitor non-genomic pathways exclusively and unequivocally. Based on this premise, we set about to design and fabricate solid substrates that can be used to induce cellular responses known to involve specifically the interaction of E2 with mERs. Among various possible approaches, we opted for a micropatterned substrate consisting of arrays of micron-sized islands functionalized with E2 distributed within a cell-adhesive domain. Such bifunctional surfaces can be obtained by chemical modification of glass substrates arrayed with gold dots, using gold- and glass-specific chemical reactions to attach E2 to the gold islands and a cell-adhesion promoter to the glass. Of course, the gold islands need to be small, compared to the size of cells, so that they do not prevent cell adhesion on the patterned substrates. The work described in this report led us to construct micropatterning surfaces useful for the study of E2 non-genomic effect.

The feasibility of the approach was established first on two model substrates, namely glass slides functionalized with cell-adhesion promoters and gold substrates bearing E2 on their surface. Several cellular and physical techniques were used to monitor the chemical modifications performed on the two types of substrates and to test their functionality. A cell adhesion test was employed in the case of the glass substrate. To study the attachment of E2 to gold and to test the ability of tethered E2 to interact with mER, we used surface plasmon resonance (SPR) spectroscopy, which allows one to determine the optical thickness of layers deposited on gold<sup>[31]</sup> and quartz crystal microbalance with dissipation (QCM-D), which senses the total mass deposited on a vibrating quartz crystal and is often used for studying protein adsorption.<sup>[32]</sup> Subsequently, micropatterned substrates were prepared and their ability to activate the phosphorylation of extracellular regulated kinase (ERK), an essential enzyme of the non-genomic pathway,<sup>[33]</sup> was assessed by cell enzyme-linked immunosorbent analysis (ELISA) and cell proliferation assays. These biological assays, together with the physico-chemical evaluations of homogeneously modified substrates, indicate that E2-patterned

substrates are powerful and versatile tools to assay cellular mechanisms initiated via receptors located on the plasma membrane.

## 4.4 Materials and methods

### 4.4.1 Materials

17 $\alpha$ -ethinylestradiol was purchased from Toronto Research Chemicals Inc (North York, ON, Canada). 17 $\alpha$ -ethinylestradiol-benzoic acid (E2-benzoic acid) was prepared as described in a following a known procedure.<sup>[19]</sup> Hereafter, we will call this compound E2 for the simplicity. ER- $\alpha$ , 2-chloro-4, 6-dimethoxy-1,3,5-triazine (CDMT) and N-methylmorpholine (NMM) were purchased from Sigma (MO, USA). Amino-terminated linear RGD (Gly-Arg-Gly-Asp-Ser) and cyclic RGD (Product name: cyclo[Arg-Gly-Asp-D-Phe-Lys(PEG-PEG), M.W. 894.0]) were purchased from the Peptide Institute (Japan) and Peptide International (KY, USA), respectively. The Hoechst 33342 staining kit was purchased from Life Technologies (CA, USA). Amino-PEG2k-thiol and NHS-PEG2k-trimethoxysilane were purchased from NANOCS (NY, USA). PEG2k-triethoxysilane was synthesized based on the literature method.<sup>[34]</sup> Anti-phospho-ERK1/2 antibody was included in the cell-based ERK1/2 (T202/Y204) ELISA kit purchased from Raybiotech (GA, USA). Other chemicals and reagents were of analytical grade and used as received.

### 4.4.2 Cell culture

MCF-7 human breast cancer cells (HTB-22<sup>TM</sup>) were purchased from the American Type Culture Collection (ATCC) and were routinely cultured in Eagle's Minimum Essential Medium (MEM, Sigma Aldrich), supplemented with 10% (v/v) fetal bovine serum (FBS, BioWest, France), 2 mM L-glutamine (Wako, Japan), 1 mM sodium pyruvate (Wako, Japan), 1% non-essential amino acids (Gibco, USA), and 1% penicillin-streptomycin (Wako, Japan), in a humidified atmosphere (5% CO<sub>2</sub> and 95% air) at 37°C. For the cell ELISA studies, the cells were starved based on the protocol described by Hamelers et al.<sup>[35]</sup> In brief, the cells grown to the 50% confluence in the above-mentioned culture medium were conditioned with phenol red-free DMEM/F12 (Life technologies, USA) containing 5% charcoal-stripped FBS (Life technologies, USA) for 24 hrs. Then the cells were starved with the DMEM/F12 supplemented

with 0.2% bovine serum albumin (BSA, Wako), 30 nM sodium selenite (Sigma Aldrich, USA), 10 µg/ml of transferrin (Sigma-Aldrich, USA), and 2 ng/ml of insulin-like growth factor type I (Life Technologies, USA) for 24 hrs. For the cell proliferation assay, cells were conditioned in phenol red-free DMEM containing 10% charcoal-stripped FBS for one week and starved in a serum free medium for 24 hrs.

#### **4.4.3 Glass surface modification and characterization**

Glass coverslips (2.2 x 2.2 cm, 0.13–0.17 mm thick, Matsunami, Japan) were cleaned and activated in a UV-ozone cleaner (UV253, Filgen; O<sub>2</sub>: 6 L min<sup>-1</sup>, 0.1 MPa) for 1 hr. The substrates were transferred into a solution of NHS-PEG2k-silane (0.2 mg/mL) and PEG2k-silane (0.2 mg/mL) in 1:9 v:v toluene: 0.01% acetic acid and kept at 80°C overnight. At the end of the reaction, the PEGylated substrates were washed with toluene 5 times, sonicated for 5 mins in toluene and washed once more with toluene, followed by a similar treatment with methanol, after which the substrates were dried under a flow of nitrogen. For the linear RGD (IRGD) and cyclic RGD (cRGD) functionalization, the PEGylated substrates were covered with a 10 µl aliquot of a solution of IRGD or cRGD in phosphate buffered saline (0.5 mM, PBS) and placed on a teflon plate. The substrates were kept at room temperature overnight in a petri dish sealed with parafilm and wet tissues to prevent water evaporation. The recovered IRGD or cRGD modified substrates were washed with 3 times with PBS and treated for 2 hrs with a 0.5 mM solution of aminoethanol in PBS to quench unreacted NHS groups. Finally, the substrates were washed thrice with water and dried under a flow of nitrogen.

MCF-7 cells were seeded onto the IRGD or cRGD modified glass surfaces at a density of 20,000 cells/ml. After 1 hr cultivation, the cells were stained with Hoechst and cell counting was performed by observation with an Axiovert 200 fluorescence microscope (Zeiss, Germany) equipped with a charge-coupled device camera (Rolera-MGi, Q-imaging, Canada). Data were compared for significance of differences using the student's t-test.

#### **4.4.4 Gold surface modification monitored by XPS, SPR and QCM**

Angle resolved X-ray photoelectron spectroscopy (AR-XPS) measurements were performed on a Theta Probe X-ray photoelectron spectrometer (Thermo Fisher Scientific, Waltham, MA) equipped with a monochromatic Al K X-ray source (1486.6 eV) and a low-

energy flood gun for charge compensation. The beam spot size was 400  $\mu\text{m}$ . XPS survey spectra were collected at 65° takeoff angle, representing the angle of electron path between the analyzer and the sample surface. The narrow scans of C 1s and N 1s spectra were obtained by a pass energy of 40 eV, a step size of 0.1 eV, with a dwell time of 50 ms. All spectra were internally referenced by setting the hydrocarbon (C–C/C–H) component peak at 285.0 eV.

Surface plasmon resonance (SPR) measurements were performed using a computer-controlled SPR Navi-200 model instrument (Bionavis, Finland). SPR gold-coated sensors (Bionavis, Finland) were cleaned with a piranha solution containing 70 % concentrated sulfuric acid and 30 % (v/v) hydrogen peroxide (35 %) (*WARNING: Piranha solution is extremely reactive and must be handled with extreme caution.*). The cleaned sensors were rinsed with deionized water, dried under nitrogen, and immersed in a 0.5 mM amino-PEG2k-thiol ethanol solution gently swirled overnight. Subsequently, the PEG-modified sensor was washed thrice with ethanol, dried with nitrogen and placed in the mixture solution containing EE2-benzoic acid (1.2 mg) and CDMT (0.9 mg), which were dissolved in 1 mL dry dioxane. After 1 hr incubation, NMM (0.6 mg) was added to the solution. Control substrates were prepared by keeping amino-PEG2k-thiol-modified SPR gold sensor immersed in dioxane overnight. All substrates were washed thrice with dioxane and methanol and dried under nitrogen. An E2-modified SPR sensor was placed in the SPR cell compartment. PBS (10 mM, pH~7.4) was passed through the cell until the baseline was stable. Thereafter, solutions of increasing ER- $\alpha$  concentration (1 to 100 nM) in PBS were introduced sequentially in the sample cell with a flow rate of 10  $\mu\text{L min}^{-1}$ . At the end of the treatment, the sample cell was flushed with the PBS buffer to remove excess ER- $\alpha$ . Adsorption of ER- $\alpha$  onto amino-PEG2k coated SPR sensor surface was evaluated under the same conditions. All measurements were performed at room temperature. The SPR instrument records the angle of minimum resonance ( $\Theta_m$ ). The surface coverage ( $I$ ) was calculated using the Fresnel model reported previously using the Winspall software (version 3.02) using the following parameters<sup>[36]</sup>: the real and imaginary parts of the dielectric constant,  $\varepsilon'$  and  $\varepsilon''$ , respectively, for each surface plasmon-supporting metal layer at the wavelength of excitation 780 nm were  $\varepsilon' = 3.1002$ ,  $\varepsilon'' = 0$  for the sapphire prism,  $\varepsilon' = -2.0185$ ,  $\varepsilon'' = 35.755$  for the Cr adhesion layer,  $\varepsilon' = -23.886$ ,  $\varepsilon'' = 1.7435$  for the Au layer,  $\varepsilon' = 1.8824$ ,  $\varepsilon'' = 0$  for the film tested, and  $\varepsilon' = 1.7814$ ,  $\varepsilon'' = 0$  for water.<sup>[37]</sup>

Quartz crystal microbalances with dissipation (QCM-D) studies were carried out with an E4 system (Biolin, Sweden). Gold-coated 5-MHz AT-cut quartz crystals (Quartz Pro, Sweden) were cleaned with a piranha solution (*WARNING: see above.*). The E2 functionalization as well as ER- $\alpha$  adsorption studies were using the same protocol as depicted in SPR part. The QCM-D results are presented as the normalized frequency shift recorded for the fifth overtone (25 MHz).

The QCM-D data were analyzed with the QTools 3.0 software (Biolin, Sweden) based on the Sauerbrey equation that is widely used for modeling thin protein films.<sup>[38]</sup> In this model, the frequency shift ( $\Delta f$ ) is related linearly to the total adsorbed mass, expressed as surface coverage ( $\Gamma$ ), as shown in the following equation (1):

$$\Gamma = -\frac{c\Delta f}{n} \quad (1)$$

where  $C$  is a constant based on the physical properties of the quartz crystal ( $C = 0.177 \text{ mg m}^{-2} \text{ Hz}^{-1}$ ) and  $n$  represents the overtone number ( $n = 1, 3, \dots$ ). The buffer density and viscosity were set at  $1000 \text{ g dm}^{-3}$  and  $1 \text{ mPa s}^{-1}$ , respectively.

#### 4.4.5 Fabrication and modification of micropatterned surfaces

Glass coverslips (3.0 x 3.0 cm, 0.13–0.17 mm thick, Matsunami) were sonicated three times in acetone, rinsed twice with isopropanol, and dried under a flow of nitrogen. They were treated by O<sub>2</sub>-plasma asher (PB600, Yamato Scientific) under a stream of O<sub>2</sub> at 300 W for 3 mins. A hexamethyldisilazane (Tokyo Ohka Kogyo, Japan) adhesion layer was deposited on the cleaned substrates by spin-coating. Subsequently, the photoresist (OFPR-800 LB 54 cp, Tokyo Ohka Kogyo, Japan) was spin-coated on the modified substrate to achieve a thin uniform layer. The substrates were baked at 90 °C for 3 mins. A second photoresist (AZ 5214-E, Clariant, Switzerland) was spin-coated on the substrates followed by a 6 mins bake at 90 °C. The substrates were irradiated through a photomask using the g-and i-lines of the UV light emitted by a mercury lamp (18 mW/cm<sup>2</sup> for 6 secs). After irradiation, the substrates were baked at 120 °C for 30 secs. They were immersed in a NMD-3 developer solution (Tokyo Ohka Kogyo, Japan), gently agitated for 60 secs, rinsed with water, and dried with a flow of nitrogen. The dried substrates were descummed with the plasma asher for 30 secs. A 5-nm titanium layer and a 20 nm-gold layer were vacuum-deposited consecutively on the substrates

using an E-beam evaporator. The coated substrates were immersed in AZ remover 100 (Clariant, Switzerland) for several hrs. They were rinsed with isopropanol and dried with nitrogen. They were cut to size with an automatic dicing saw (DAD3220, Disco, Japan) and kept in a desiccator until use. SEM (scanning electron microscopy) images of the patterned substrates were recorded with a SU8230 field emission SEM (Hitachi, Japan) at an accelerating voltage of 1 kV.

Prior to functionalization, the micropatterned surfaces were washed 5 times with acetone and sonicated in acetone for 5 mins. The same procedure was repeated with 2-propanol and hexane. Finally, the substrates were dried with nitrogen, cleaned with the O<sub>2</sub>-plasma asher for 5 mins and placed in an UV-ozone cleaner for 1 hr to activate the silica areas of the patterned surfaces, which, subsequently, were functionalized with cRGD on the glass areas as described above and, afterwards, E2 was immobilized on the gold islands, as described above.

#### **4.4.6 Detection of ERK phosphorylation by cell ELISA**

The functionalized micropatterned surfaces were placed on a glass bottomed 35-mm dish (MatTek, USA). Starved MCF7 cells were harvested with 5 mM EDTA/PBS for 15 mins at 37 °C and seeded on the micropatterned surfaces at  $3.1 \times 10^5$  cells/cm<sup>2</sup> in a serum-free DMEM/f12 medium. After incubation at 37 °C for 1 hr, cells were fixed overnight at 4 °C with 4% paraformaldehyde in phosphate buffer (Wako, Japan). The surfaces were placed in a 96-wells plate (Thermo, USA) and the cells were permeabilized with 0.5% Triton X-100 in PBS for 15 mins at room temperature. The wells were blocked with 2% BSA/PBS for 1 hr after washing each well with PBS. For the detection of ERK phosphorylation, the cells were reacted with mouse immunoglobulin G (IgG) for phospho-ERK1/2 (T202/Y204) for 2 hrs, followed by washing with PBS for 4 times. Subsequently, the cells were treated with anti-mouse IgG alkaline phosphatase conjugate (Sigma Aldrich, USA) for 1 hr at room temperature and washed in the same way. The amount of phosphorylated ERK was detected by adding p-nitrophenyl phosphate (Sigma Aldrich) in a Tris/HCl buffer (1 M, pH~ 9.8) containing 0.5 mM MgCl<sub>2</sub>, and the optical density (OD) at 405 nm was recorded using a microplate reader (BioRad, model 680, USA). Data were compared for significance of differences using the student's t-test (P < 0.05).

#### 4.4.7 MCF-7 cell proliferation assay

Functionalized micropatterned surfaces were placed in a 96-well plate and conditioned cells were seeded on them at a concentration of 5,000 cells/well. The cells were incubated for 2 days at 37 °C, 5% CO<sub>2</sub>. Cell proliferation was evaluated using a CellTiter 96 AQueous Non-Radioactive Cell Proliferation Assay (Promega, USA) according to the protocol supplied by the manufacturer. The optical density at 490 nm was measured with the plate reader. Data were compared for significance of differences using the student's t-test.

### 4.5 Results and discussions

#### 4.5.1 Design of micropatterned substrates

Figure 4.1 depicts the interactions at play between a cell and the patterned substrate (A: side view and B: top view). Integrins on the plasma membrane of the cell (blue rectangles), responsible for cell adhesion, interact with cRGD (blue ovals), a glass-linked peptide with Arg-Gly-Asp sequences known to promote cell adhesion, while mERs (red rectangles) on the plasma membrane interacts with E2 (light blue triangles) bound to the gold islands (yellow rectangles in A or yellow discs in B). A scanning electron micrograph (SEM) of the micropatterned substrate prior to chemical modification is presented in Figure 4.1C. It consists of gold dots, with a diameter of 2 μm, arrayed on glass with a 12-μm pitch. Micropatterns with different gold dot arrangements were available (see Figure SI.4.1). The chemical functionality of the substrates was introduced in two steps. First, the glass sections were modified by a sequence of reactions (Figure 4.1D) involving, treatment of the glass with a 1:1 w:w mixture of PEGylated-triethoxysilane and NHS-PEG2k-trimethoxysilane, followed by introduction of cRGD by reaction with NHS-activated carboxylic acid groups tethered to the glass. Subsequently, the gold disks were modified by treatment with amino-PEG2k-thiol, followed by coupling of 17α-ethinylestradiol benzoic acid (E2) to the tethered amines (Figure 4.1E). Special care was taken to minimize possible cross-reactions between the reagents used to treat the glass and gold regions. For example, excess NHS groups in the glass regions were quenched by addition of excess aminoethanol. In addition, E2 was incubated with the coupling agents, CDMT and NMM, prior to addition to the amino-PEG2k-thiol-functionalized



patterned substrates. All other aspects of the functionalized were identical to the treatments validated on either glass or gold substrates and described in detail in the following sections.

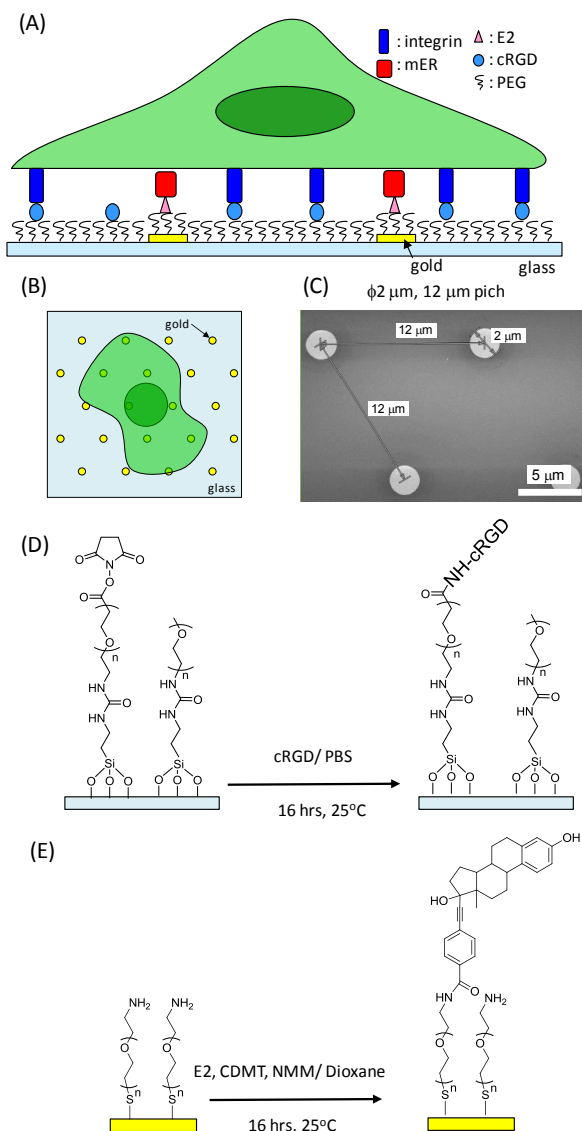


Figure 4.1 (A and B) Schematic representations of the micropatterned substrate employed. cRGD (for the interaction with integrin) and E2 (for the interaction with mER) are co-immobilized onto a PEGylated micropatterned surface to ensure cell adhesion and E2 presentation to the cell membrane. (C) SEM image of the micropatterned surface consisting of gold circular regions (diameter: 2  $\mu\text{m}$ ) arrayed with a 12- $\mu\text{m}$  pitch (scale bar: 5  $\mu\text{m}$ ); and chemical sequences performed on glass surfaces (D) and on gold surfaces (E).

## 4.5.2 Immobilization of cRGD onto glass substrates

Model glass substrates (coverslips) coated with a mixture of PEG (2 kDa) and NHS-terminated PEG (2 kDa) chains were treated with either IRGD or cRGD, two peptides known to promote cell adhesion. A third glass substrate, coated with PEG alone, served as control. The substrates were incubated with MCF-7 cells (20,000 cells/mL) for 1 hr and observed by phase contrast microscopy, revealed that both IRGD and cRGD promote cell adhesion, cRGD being more effective than IRGD. Micrographs of control, IRGD-coated, and cRGD substrates after a 1 hr-incubation with MCF-7 cells are shown in Figure 4.2 (A-C) together with a quantitative analysis of the number of cells attached on each substrate Figure 4.2D. This experiment indicates that cRGD, significantly enhances the number of adhered cells ( $P < 0.05$ ) whereas IRGD only marginally enhances cell adhesion, compared to the control substrate. As reported earlier, the conformation of cRGD is more amenable to interaction with integrins, compared to IRGD.<sup>[39]</sup> In view of this result, the experiments described below were carried out exclusively with cRGD-modified glass surfaces.

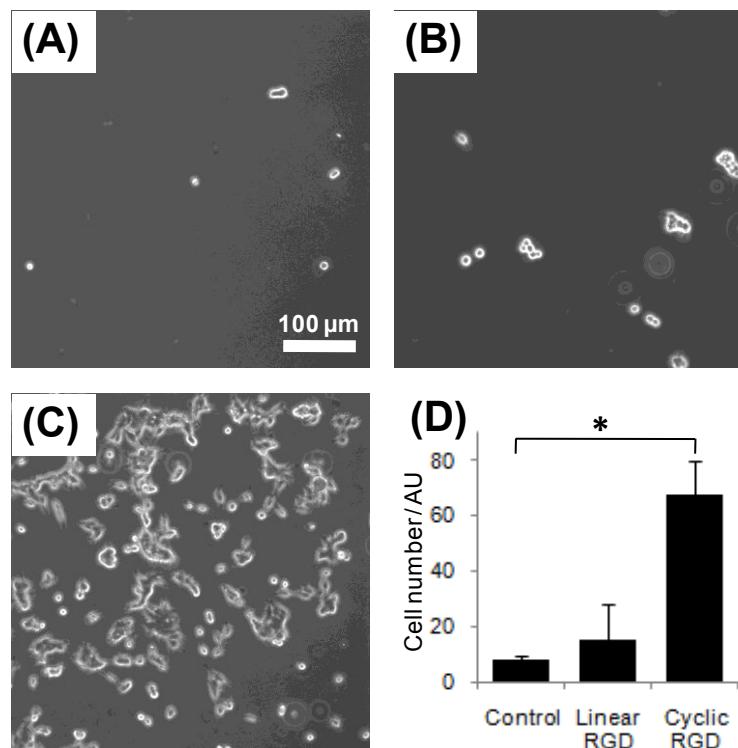


Figure 4.2 Cyclic RGD (cRGD) functionalized glass substrate enhanced MCF-7 cell adhesion. (A) Optical images of MCF-7 cell onto the PEGylated glass substrate after 1 hour incubation at 37 °C, 5% CO<sub>2</sub>. (B) Optical images of MCF-7 cell onto the linear RGD functionalized glass substrate after 1 hour incubation at 37 °C, 5% CO<sub>2</sub>. (C) Optical images of MCF-7 cell onto the cRGD functionalized glass substrate after 1 hour incubation at 37 °C, 5% CO<sub>2</sub>. (D) Quantification analysis of cell numbers. All the data are expressed as mean ±S.E. of triplicate determinations. P<0.05 is considered as the significantly statistical difference.

#### 4.5.3 XPS characterization of E2-PEG2k modified gold surfaces.

Having established a robust protocol for the fabrication of glass-supported cell-adhesive surfaces, we turned our attention to the immobilization of E2 on gold-coated substrates, following the protocol depicted in Figure 4.1E. An amino-functionalized PEG thin film was deposited on a gold substrate using amino-PEG2k-thiol. E2 was linked to the substrate via an amide linkage of the 17 $\alpha$ -ethinylestradiol-benzoic acid to the amine groups of amino-PEG2k-thiol. The success of the chemical modification was evaluated by XPS analysis of the substrates after each chemical modification. XPS survey scans of bare gold, amino-

PEG2k-coated gold and E2-modified PEG-coated gold are presented in Figure SI.4.2. The XPS scan of amino-PEG2k-thiol coated gold presents a signal at 285 eV, attributed to the 1s carbon atoms of the PEG chain.<sup>[40]</sup> This signal is enhanced after modification of the surface with E2, as evidenced by increases in the C/Au ratio from 5.53 to 6.84 as well as the C/O ratio, from 3.93 to 4.39. Considering the fact that the theoretical C/O for the PEG chain is  $\sim 2.02$  and C/O for E2 is  $\sim 8.33$ , the increase in the C/O ratio represents successful conjugation of E2 to the PEG.

#### **4.5.4 SPR evaluation of the interaction of ER- $\alpha$ with E2-modified gold substrates**

ER- $\alpha$  solutions ranging in concentration from 1 to 100 nM were passed sequentially over E2-coated substrates placed in the flow cell of an SPR system. An example of the SPR real-time mass adsorption at each ER- $\alpha$  concentration is shown in Figure 4.3A. The SPR signal yields information on the association of ER- $\alpha$  to the E2-modified surface. The injection of each ER- $\alpha$  solution triggered a significant increase of the SPR minimum resonance angle,  $\Theta_m$ . After rinsing the SPR cell with buffer, the  $\Theta_m$  value was at  $\sim 0.0556^\circ$ . The black trace in Figure 4.3A corresponds to the injection of ER- $\alpha$  solutions of increasing concentration in the SPR flow cell fitted with an amino-PEGylated surface devoid of E2. In this case, the  $\Theta_m$  value after the final rinse was nearly identical to the initial  $\Theta_m$ . The ER- $\alpha$  surface coverage values on the E2-modified surface and on the control surface, calculated from the corresponding  $\Theta_m$  values, are plotted as a function of the ER- $\alpha$  solution concentration in Figure 4.3B (red and black triangles). Also shown in Figure 4.3B are the values recorded after the final rinse (red and black circles). The final ER- $\alpha$  surface coverage of the E2-modified surface ( $\sim 120 \pm 1.6$  ng/cm<sup>2</sup>) of the same order as data reported previously for the binding of ER- $\alpha$  to E2 immobilized to chitosan phosphorylcholine films<sup>[41]</sup> and on carboxymethylated dextran gels.<sup>[42]</sup>

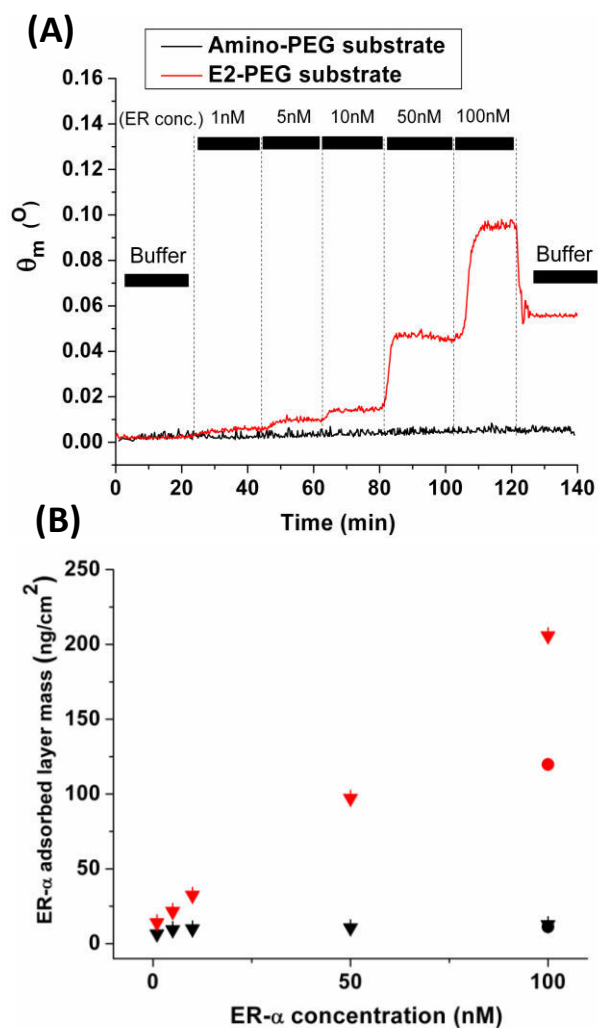


Figure 4.3 (A) SPR traces corresponding to the addition of ER- $\alpha$  solutions onto the E2-modified PEGylated gold substrate (red) and a control PEGylated gold substrate (black); temperature: 25°C. (B) ER- $\alpha$  coverage (ng/cm<sup>2</sup>) as a function of ER- $\alpha$  concentration of the solution injected on the E2-modified PEGylated gold substrate (red symbols) and on the control PEGylated gold substrate (black symbols); the circles are the surface coverage values after rinsing the substrates with buffer.

### 4.5.5 QCM-D studies of the adsorption of ER- $\alpha$ on gold substrates modified with E2-PEG2k

The QCM-D experiments described next were performed with gold-coated quartz crystals modified *ex-situ* with E2-PEG or with amino-PEG (control) according to the sequence presented in Figure 4.1E. The substrates were placed in the QCM-D cell and conditioned in PBS buffer. Examples of real-time ER- $\alpha$  adsorption scans are shown in Figure 4.4A, where the red traces correspond to experiments carried out with E2-modified substrates and the black traces are scans of control measurements done with amino-PEG films. Sequential addition of solutions of increasing ER- $\alpha$  concentration (1 nM to 100 nM) was performed similarly to the SPR experiment. Finally, buffer was passed over the films to remove loosely bound protein. The ER- $\alpha$  binding kinetics monitored by QCM-D are reflected by changes versus time in frequency ( $\Delta f_5$ , 5<sup>th</sup> overtone) (Figure 4.4A, top) and in dissipation ( $\Delta D_5$ ) (Figure 4.4A, bottom). Changes in the frequency report on the mass of the protein adsorbed to the surface of the vibrating crystal including the water hydrodynamically coupled to the protein. In the case of thin rigid films, the mass uptake is related to the frequency shift by the Sauerbrey equation (see experimental section). This equation was employed here as it was shown to be applicable to thin protein films.<sup>[38]</sup> The added mass values of the E2-modified and amino-PEG-modified as a function of the injected ER- $\alpha$  solution concentration are plotted in Figure 4.4B. For both films, the bound mass increases as a function of the ER- $\alpha$  solution concentration. The values recorded after the buffer rinse were  $\sim 161.4$  ng/cm<sup>2</sup> and  $\sim 20.3$  ng/cm<sup>2</sup>, respectively, for E2-PEG films and amino-PEG films. By comparing the QCM-D derived mass to the SPR data, it is possible to determine the water content of the protein layer. The w% (26%) of water is small which may indicate that the protein forms a rigid layer on the surface.<sup>[43]</sup>

The dissipation factor (D) reveals the viscous losses induced by the deposited mass and carries information on the viscoelasticity of the adsorbed layer, reflecting the conformation and binding strength of the adsorbed protein layer.<sup>[44, 45]</sup> Plots of  $\Delta D$  as a function of  $\Delta f$  shown in Figure 4.4C, reflect the dissipation changes depending on surface mass<sup>[45]</sup> and provide information on the conformational changes of ER- $\alpha$  during the adsorption process.<sup>[46]</sup> The  $\Delta D$ - $\Delta f$  correlation shows distinctive viscoelastic features on both the E2 modified surface and the control surface. For the control surface, it would suggest that non-specific ER- $\alpha$  adsorption

generate higher internal molecule friction, leading to the energy loss in oscillation. However, the slope of the  $\Delta D$ - $\Delta f$  plot is smaller in the case of the E2-functionalized surface, suggesting the formation of a dehydrated and tightly-bound protein layer.<sup>[31]</sup>

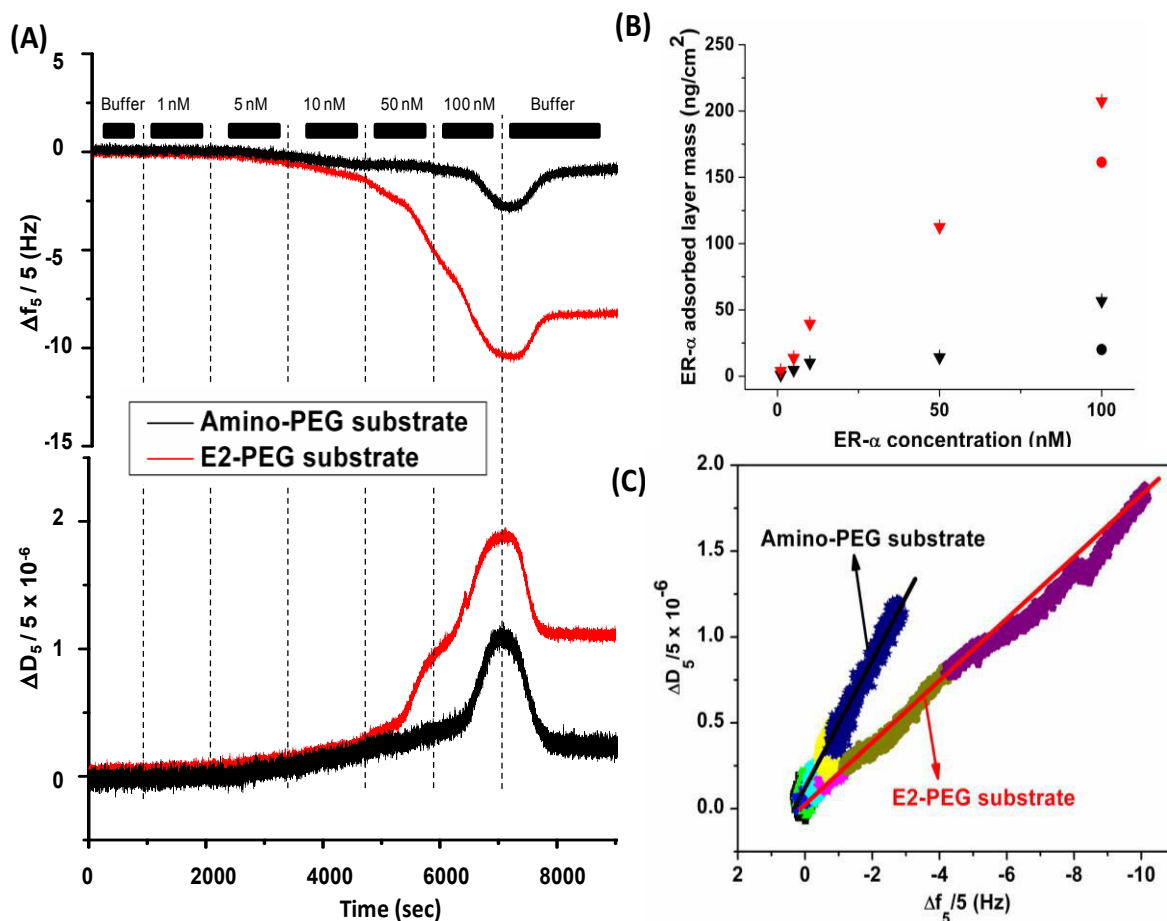


Figure 4.4 (A) Frequency ( $\Delta f$ ) and dissipation ( $\Delta D$ ) shifts as a function of the concentration of the ER- $\alpha$  solution injected in the QCM-D cell compartment fitted an E2-modified substrate (red trace) and the control substrate (black trace); (B) ER- $\alpha$  coverage (ng/cm<sup>2</sup>) as a function of ER- $\alpha$  concentration of the solution injected on the E2-modified PEGylated gold substrate (red symbols) and on the control PEGylated gold substrate (black symbols); the circles are the surface coverage values after rinsing the substrates with buffer; (C)  $\Delta D$ - $\Delta f$  plots for the ER- $\alpha$  adsorption onto the E2-modified surface (red trace) and the control surface (black trace). Different concentrations are also indicated by different colors for amino-PEG substrate and E2-PEG substrate.

#### 4.5.6 Biological activity of E2-modified micropatterned substrates

Having established robust protocols to modify glass surfaces, to render them cell-adhesive, and to tether E2 to gold substrates while preserving the interaction of ER- $\alpha$  with E2, we functionalized micropatterned substrates as described in experimental section and depicted in Figure 4.1. We confirmed that micropatterned surfaces with gold islands bearing amino-PEG2k-thiol and those with E2-bound islands exhibit the same cell adhesiveness as surfaces without E2, as observed by comparing Figures 4.5A and 4.5B. The MCF-7 cells exhibited similar adhesion to both patterned substrates, indicating that the activity of the cRGD ligands was not affected significantly by the sequential functionalization of the gold islands. It should be noted that the separation distance ( $\sim 10 \mu\text{m}$ ) between the gold islands is smaller than the size of single MCF-7 cells, as seen in the enlarged micrograph shown in Figure 4.5C, where gold dots are visible in areas devoid of cells. Under these conditions, most cells attached to a micropatterned surface should be able to interact with the surface-immobilized E2 ligands. Cells were harvested with EDTA, rather than trypsin, in order to ensure that membrane proteins remain intact (undigested), favoring rapid cell adhesion. Therefore it should be possible to monitor cellular responses within the first hour following cell contact with the substrate.

Next, we analyzed by cell ELISA of the ERK phosphorylation activation level upon cellular adhesion to the substrates. As observed in Figure 4.5D, the ERK phosphorylation level was significantly higher in cells grown on E2-functionalized substrates, compared to cells on control ( $\text{NH}_2$ ) substrates:  $0.563 \pm 0.056$  vs.  $0.475 \pm 0.036$ , or 18.7%,  $P < 0.05$ . The difference in ERK phosphorylation levels is small, but it is of reasonable value knowing that even “soluble E2” at a concentration of  $10^{-6}$  M, which is significantly higher than physiological concentrations, evoked only 27% increment, under the experimental conditions employed here (Figure SI.4.3). Moreover, similar ratios of ERK phosphorylation in E2-conjugates versus to free E2 (10% vs. 20%) were reported previously in a study of the response of clonal rat prolactinoma cell lines to E2-peroxidase conjugates.<sup>[47]</sup>

We also investigated whether surface-immobilized E2 stimulates the proliferation of MCF-7 cells. As seen in Figure 4.5E, the growth of MCF-7 cells on E2-functionalized substrates was approximately the same as in the case of control substrates. This observation is



important, as it suggests strongly that the genomic signaling pathway is not stimulated by surface-immobilized E2. Taken together, these initial results indicate that E2-functionalized micropatterned substrates described here may be extremely useful tools for systematic studies of the estrogen non-genomic pathway and its selective activation.

Recently, an estrogen-dendrimer conjugate (EDC) was reported to modulate selectively non-genomic estrogen response. However, the observation that EDC was localized in the cytoplasm raises questions on the actual nature of its interaction with ER- $\alpha$  and transportation mechanisms.<sup>[20]</sup> Our demonstration that estrogen immobilized micropatterned surfaces are able to evoke estrogenic non-genomic pathways implies that the E2-conjugates initiate the estrogenic activity via the plasma membrane ER and precludes the possibility of membrane ER transportation to a cytoplasmic site for downstream signaling. Thus, this feature of E2-immobilized micropatterned substrates is critical as it isolates plasma membrane associated non-genomic effect efficiently. The micropatterned surfaces can be modified readily with molecules other than E2 for use in selective hormonal drug screening, a subject of intensive current research.<sup>[48]</sup>

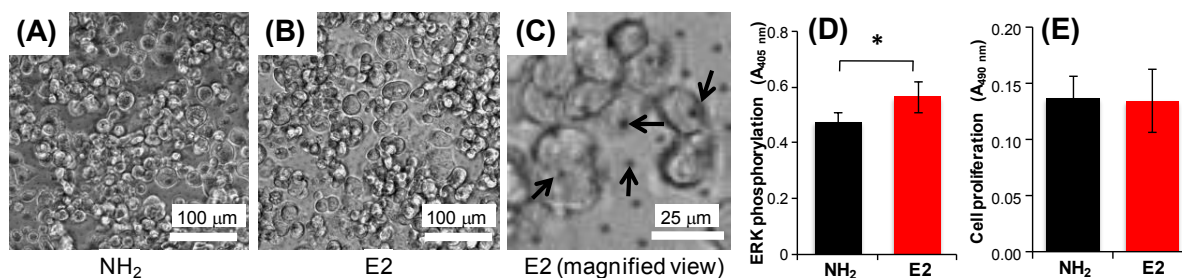


Figure 4.5 Cellular response to E2-functionalized micropatterned substrates. Optical micrographs of starved MCF-7 cells seeded on micropatterned substrates which glass areas functionalized with cRGD and gold dots modified with NH<sub>2</sub> (A) or E2 (B) incubated for 1 hr at 37 °C, 5% CO<sub>2</sub>; scale bars: 100 μm; the micrograph (C) is a magnified view of (B); scale bar: 25 μm; the arrows point to gold dots. (D) ERK phosphorylation of MCF-7 cells on each substrate; bars: mean ± S.E. of triplicate determinations. (E) MCF-7 cell proliferation on amino- or E2-immobilized micropatterned substrates after a 2-day incubation.

## 4.6 Conclusions

The objective of this study was to prepare E2-immobilized micropatterned surfaces and to demonstrate their use in studies of the non-genomic effects of E2 and, eventually, other steroids. Studies by SPR and QCM-D confirmed the successful immobilization of estrogen on the selected substrates and the abilities of tethered E2 to interact with ER- $\alpha$ . Furthermore, using a cell ELISA study, it was possible to detect the stimulation of a key component of the estrogenic non-genomic signal pathway, namely ERK phosphorylation, in MCF-7 cells placed in contact with E2-modified micropatterned substrates. Future studies will focus on the use of estrogen patterned surfaces to trigger faster signal transduction pathways associated to the non-genomic effect and to understand the crosstalk within these pathways. A detailed pathway profiling in response to biomedical applications of estrogen non-genomic effects, such as reproduction or neuroprotection, will be the next challenge, to be addressed using the tool described in this report.

## 4.7 Acknowledgements

The authors thank to A.Ohi, T. Ohki, H. Yoshikawa and H. Iga (NIMS) for preparation of micropatterned surfaces, Dr. X.-P. Qiu (Univ. Montreal) for the assistance of synthesis of E2, Dr. P. Kujawa (NIMS) for helpful discussions on SPR data analysis and Dr. Y.-T. R. Lau for the XPS analysis. BQ was supported by the NIMS Internship Program 2011 and 2013, and doctoral scholarship from Chinese Scholarship Council (CSC). F.M. Winnik acknowledges financial support of the Natural Sciences and Engineering Research Council of Canada (NSERC).

## 4.8 References

- [1] Grober OMV; Mutarelli, M; Giurato, G; Ravo, M; Cicatiello, L; De Filippo, MR; Ferraro, L; Nassa, G; Papa, MF; Paris, O; Tarallo, R; Luo, S; Schroth, GP; Benes, V; Weisz, A, Global analysis of estrogen receptor beta binding to breast cancer cell genome reveals an extensive interplay with estrogen receptor alpha for target gene regulation. *Bmc Genomics* **2011**, *12*:36-52.
- [2] Gruber CJ; Tschugguel, W; Schneeberger, C; Huber, JC, Mechanisms of disease - production and actions of estrogens. *N. Engl. J. Med.* **2002**, *346*: 340-352.
- [3] Mendelsohn ME, Protective effects of estrogen on the cardiovascular system. *Am. J. Cardiol.* **2002**, *89*: 12-17.
- [4] Thomas P; Pang, Y; Filardo, EJ; Dong, J, Identity of an estrogen membrane receptor coupled to a g protein in human breast cancer cells. *Endocrinology* **2005**, *146*: 624-632.
- [5] Pedram A; Razandi, M; Lewis, M; Hammes, S; Levin, ER, Membrane-localized estrogen receptor alpha is required for normal organ development and function. *Developmental Cell* **2014**, *29*: 482-490.
- [6] Prossnitz ER; Barton, M, Estrogen biology: New insights into gper function and clinical opportunities. *Molecular and Cellular Endocrinology* **2014**, *389*: 71-83.
- [7] Improta-Brears T; Whorton, AR; Codazzi, F; York, JD; Meyer, T; McDonnell, DP, Estrogen-induced activation of mitogen-activated protein kinase requires mobilization of intracellular calcium. *Proceedings of the National Academy of Sciences of the United States of America* **1999**, *96*: 4686-4691.
- [8] Reddy K; Keshamouni, V, Mechanism of 17-b-estradiol-induced erk1/2 activation in breast cancer cells: A role for her2 and pkc-delta. *Eur. J. Cancer* **2002**, *38*: S59-S60.
- [9] Hammes SR; Levin, ER, Extranuclear steroid receptors: Nature and actions. *Endocr. Rev.* **2007**, *28*: 726-741.
- [10] Farach-Carson MC; Davis, PJ, Steroid hormone interactions with target cells: Cross talk between membrane and nuclear pathways. *J. Pharmacol. Exp. Ther.* **2003**, *307*: 839-845.
- [11] Losel R; Wehling, M, Nongenomic actions of steroid hormones. *Nat. Rev. Mol. Cell Biol.* **2003**, *4*: 46-56.

- [12] Levin ER, Integration of the extranuclear and nuclear actions of estrogen. *Mol. Endocrinol.* **2005**, *19*: 1951-1959.
- [13] Wang GS; Huang, YG; Li, H; Bi, SJ; Zhao, JL, Erk/canp rapid signaling mediates 17 beta-estradiol-induced proliferation of human breast cancer cell line mcf-7 cells. *Int. J. Clin. Exp. Med.* **2014**, *7*: 156-162.
- [14] Losel RM; Falkenstein, E; Feuring, M; Schultz, A; Tillmann, HC; Rossol-Haseroth, K; Wehling, M, Nongenomic steroid action: Controversies, questions, and answers. *Physiological Reviews* **2003**, *83*: 965-1016.
- [15] Brower SL; Roberts, JR; Antonini, JM; Miller, MR, Difficulty demonstrating estradiol-mediated erk1/2 phosphorylation in mcf-7 cells. *J. Steroid Biochem. Mol. Biol.* **2005**, *96*: 375-385.
- [16] Aguilar R; Bellido, C; Garrido-Gracia, JC; Alonso, R; Sanchez-Criado, JE, Estradiol and its membrane-impermeable conjugate estradiol-bsa inhibit tamoxifen-stimulated prolactin secretion in incubated rat pituitaries. *Reproduction* **2006**, *131*: 763-769.
- [17] Bhattacharjee M; Ali, E, Binding of estradiol-peroxidase conjugate to estrogen receptor. *J. Steroid Biochem. Mol. Biol.* **1990**, *37*: 693-696.
- [18] Chambliss KL; Wu, QA; Oltmann, S; Konaniah, ES; Umetani, M; Korach, KS; Thomas, GD; Mineo, C; Yuhanna, IS; Kim, SH; Madak-Erdogan, Z; Maggi, A; Dineen, SP; Roland, CL; Hui, DY; Brekken, RA; Katzenellenbogen, JA; Katzenellenbogen, BS; Shaul, PW, Non-nuclear estrogen receptor alpha signaling promotes cardiovascular protection but not uterine or breast cancer growth in mice. *Journal of Clinical Investigation* **2010**, *120*: 2319-2330.
- [19] Kim SH; Katzenellenbogen, JA, Hormone-pamam dendrimer conjugates: Polymer dynamics and tether structure affect ligand access to receptors. *Angew. Chem.-Int. Edit.* **2006**, *45*: 7243-7248.
- [20] Harrington WR; Kim, SH; Funk, CC; Madak-Erdogan, Z; Schiff, R; Katzenellenbogen, JA; Katzenellenbogen, BS, Estrogen dendrimer conjugates that preferentially activate extranuclear, nongenomic versus genomic pathways of estrogen action. *Molecular Endocrinology* **2006**, *20*: 491-502.
- [21] Shearer KE; Rickert, EL; Peterson, AC; Weatherman, RV, Dissecting rapid estrogen signaling with conjugates. *Steroids* **2012**, *77*: 968-973.

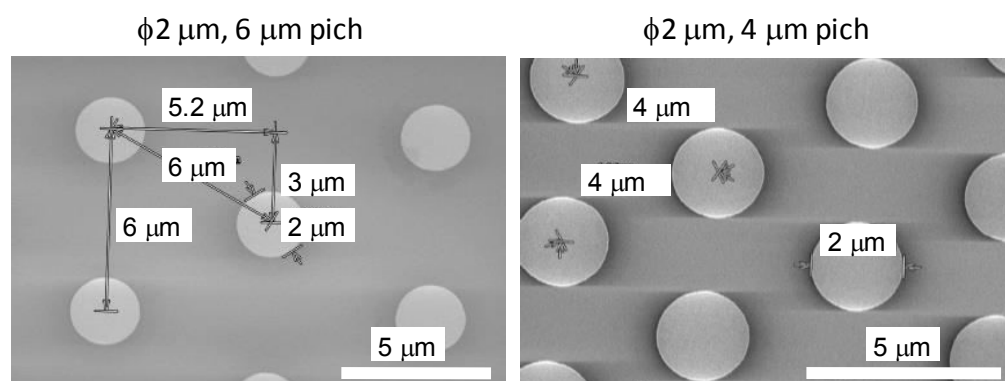
- [22] Mendelsohn ME; Karas, RH, Rapid progress for non-nuclear estrogen receptor signaling. *Journal of Clinical Investigation* **2010**, *120*: 2277-2279.
- [23] Liu SQ; Ito, Y; Imanishi, Y, Cell growth on immobilized cell growth factor. 9. Covalent immobilization of insulin, transferrin, and collagen to enhance growth of bovine endothelial cells. *J. Biomed. Mater. Res.* **1993**, *27*: 909-915.
- [24] McCormick AM; Wijekoon, A; Leipzig, ND, Specific immobilization of biotinylated fusion proteins ngf and sema3a utilizing a photo-cross-linkable diazirine compound for controlling neurite extension. *Bioconjugate Chem.* **2013**, *24*: 1515-1526.
- [25] Klenkler BJ; Griffith, M; Becerril, C; West-Mays, JA; Sheardown, H, Egf-grafted pdms surfaces in artificial cornea applications. *Biomaterials* **2005**, *26*: 7286-7296.
- [26] Liberelle B; Boucher, C; Chen, JK; Jolicoeur, M; Durocher, Y; De Crescenzo, G, Impact of epidermal growth factor tethering strategy on cellular response. *Bioconjugate Chemistry* **2010**, *21*: 2257-2266.
- [27] Ito Y; Hasuda, H; Terai, H; Kitajima, T, Culture of human umbilical vein endothelial cells on immobilized vascular endothelial growth factor. *J. Biomed. Mater. Res. Part A* **2005**, *74A*: 659-665.
- [28] Chiu LLY; Radisic, M, Scaffolds with covalently immobilized vegf and angiopoietin-1 for vascularization of engineered tissues. *Biomaterials* **2010**, *31*: 226-241.
- [29] Ito Y, Covalently immobilized biosignal molecule materials for tissue engineering. *Soft Matter* **2008**, *4*: 46-56.
- [30] Masters KS, Covalent growth factor immobilization strategies for tissue repair and regeneration. *Macromolecular Bioscience* **2011**, *11*: 1149-1163.
- [31] Su X; Lin, C-Y; O'Shea, SJ; Teh, HF; Peh, WYX; Thomsen, JS, Combinational application of surface plasmon resonance spectroscopy and quartz crystal microbalance for studying nuclear hormone receptor-response element interactions. *Analytical Chemistry* **2006**, *78*: 5552-5558.
- [32] Dixon MC, Quartz crystal microbalance with dissipation monitoring: Enabling real-time characterization of biological materials and their interactions. *J. Biomol. Tech.* **2008**, *19*: 151-158.

- [33] Migliaccio A; DiDomenico, M; Castoria, G; deFalco, A; Bontempo, P; Nola, E; Auricchio, F, Tyrosine kinase/p21(ras)/map-kinase pathway activation by estradiol-receptor complex in mcf-7 cells. *Embo J.* **1996**, *15*: 1292-1300.
- [34] Bluemmel J; Perschmann, N; Aydin, D; Drinjakovic, J; Surrey, T; Lopez-Garcia, M; Kessler, H; Spatz, JP, Protein repellent properties of covalently attached peg coatings on nanostructured sio2-based interfaces. *Biomaterials* **2007**, *28*: 4739-4747.
- [35] Hamelers IH; van Schaik, RFMA; Sussenbach, JS; Steenbergh, PH, 17 beta-estradiol responsiveness of mcf-7 laboratory strains is dependent on an autocrine signal activating the igf type i receptor. *Cancer Cell International* **2003**, *3*:78-95.
- [36] Kujawa P; Moraille, P; Sanchez, J; Badia, A; Winnik, FM, Effect of molecular weight on the exponential growth and morphology of hyaluronan/chitosan multilayers: A surface plasmon resonance spectroscopy and atomic force microscopy investigation. *Journal of the American Chemical Society* **2005**, *127*: 9224-9234.
- [37] Qi B; Kujawa, P; Toita, S; Beaune, G; Winnik, FM, Phosphorylcholine-modified chitosan films as effective promoters of cell aggregation: Correlation between the films properties and cellular response. *Macromolecular Bioscience* **2015**, *15*: 490-500.
- [38] Hook F; Kasemo, B; Nylander, T; Fant, C; Sott, K; Elwing, H, Variations in coupled water, viscoelastic properties, and film thickness of a mefp-1 protein film during adsorption and cross-linking: A quartz crystal microbalance with dissipation monitoring, ellipsometry, and surface plasmon resonance study. *Analytical Chemistry* **2001**, *73*: 5796-5804.
- [39] Lord R; Parsons, M; Kirby, I; Beavil, A; Hunt, J; Sutton, B; Santis, G, Analysis of the interaction between rgd-expressing adenovirus type 5 fiber knob domains and alpha v beta 3 integrin reveals distinct binding profiles and intracellular trafficking. *J. Gen. Virol.* **2006**, *87*: 2497-2505.
- [40] Sharma S; Johnson, RW; Desai, TA, Xps and afm analysis of antifouling peg interfaces for microfabricated silicon biosensors. *Biosens. Bioelectron.* **2004**, *20*: 227-239.
- [41] Miao Z; Kujawa, P; Lau, Y-TR; Toita, S; Qi, B; Nakanishi, J; Cloutier, I; Tanguay, J-F; Winnik, FM, Tuning the properties and functions of 17 beta-estradiol-polysaccharide conjugates in thin films: Impact of sample history. *Biomacromolecules* **2012**, *13*: 4098-4108.
- [42] Usami M; Mitsunaga, K; Ohno, Y, Estrogen receptor binding assay of chemicals with a surface plasmon resonance biosensor. *J. Steroid Biochem. Mol. Biol.* **2002**, *81*: 47-55.

- [43] Peh WYX; Reimhult, E; Teh, HF; Thomsen, JS; Su, X, Understanding ligand binding effects on the conformation of estrogen receptor alpha-DNA complexes: A combinational quartz crystal microbalance with dissipation and surface plasmon resonance study. *Biophysical Journal* **2007**, *92*: 4415-4423.
- [44] Su XD; Robelek, R; Wu, YJ; Wang, GY; Knoll, W, Detection of point mutation and insertion mutations in DNA using a quartz crystal microbalance and muts, a mismatch binding protein. *Analytical Chemistry* **2004**, *76*: 489-494.
- [45] Zhou C; Friedt, JM; Angelova, A; Choi, KH; Laureyn, W; Frederix, F; Francis, LA; Campitelli, A; Engelborghs, Y; Borghs, G, Human immunoglobulin adsorption investigated by means of quartz crystal microbalance dissipation, atomic force microscopy, surface acoustic wave, and surface plasmon resonance techniques. *Langmuir* **2004**, *20*: 5870-5878.
- [46] Hook F; Ray, A; Norden, B; Kasemo, B, Characterization of pna and DNA immobilization and subsequent hybridization with DNA using acoustic-shear-wave attenuation measurements. *Langmuir* **2001**, *17*: 8305-8312.
- [47] Bulayeva NN; Gametchu, B; Watson, CS, Quantitative measurement of estrogen-induced erk 1 and 2 activation via multiple membrane-initiated signaling pathways. *Steroids* **2004**, *69*: 181-192.
- [48] Hong JA; Neel, DV; Wassaf, D; Caballero, F; Koehler, AN, Recent discoveries and applications involving small-molecule microarrays. *Current Opinion in Chemical Biology* **2014**, *18*: 21-28.

## 4.9 Appendix C. Supporting information

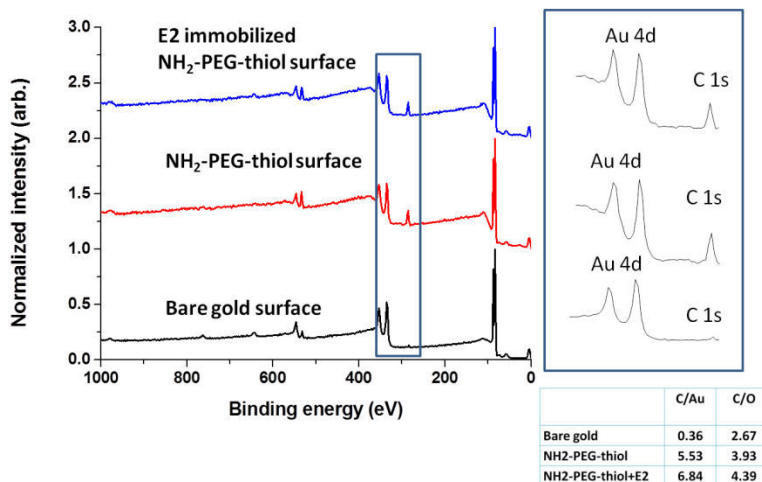
### Preparation of micropatterned substrates with different gold dots densities



**Figure SI.4.1** SEM images of micropatterned surfaces in different densities. Left: diameter in 2-μm gold circular regions were arrayed in 6-μm pitches; Right: diameter in 2-μm gold circular regions were arrayed in 4-μm pitches.



## XPS analysis of E2-immobilized gold surface

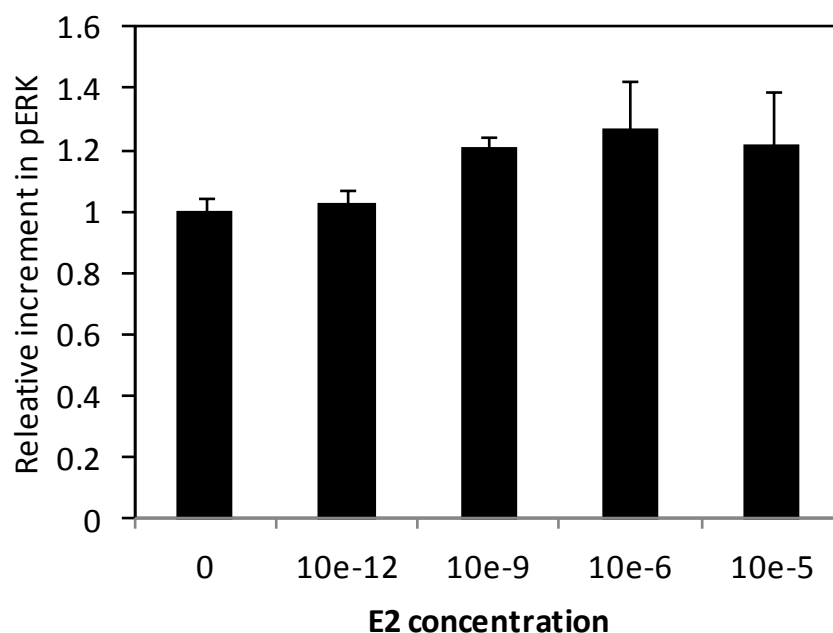


**Figure SI.4.2** XPS analysis of E2-immobilized gold surface (bare gold: black trace; NH<sub>2</sub>-PEG-thiol surface: red trace; E2 immobilized NH<sub>2</sub>-PEG-thiol surface: blue trace). E2 immobilization onto amino-PEG-thiol modified gold surface is validated by comparing the ratio of C/Au and C/O as depicted in the results section. After the E2 immobilization, both of the ratio of C/Au increased from 5.53 to 6.84 and the ratio of C/O increased from 3.93 to 4.39, suggesting the success of E2 immobilization on the topmost layer of the surface.

## Cell ELISA study of ERK phosphorylation by soluble E2

To look at the ability of free E2 in activation of non-genomic pathways, cell ELISA experiments were performed in a similar fashion to those described in the text. We focused on the very early stage of ERK activation (5 min), as MCF-7 cells are known to exhibit a transient response to soluble E2 due to the following rapid desensitization processes.<sup>[1, 2]</sup> Cells were seeded in a plastic 96-well plate at  $5 \times 10^4$  cells/well and serum-starved for 4 hrs. Just before E2 administration, DMSO stock solutions of E2 were diluted in the serum free medium and then added to each well. The final E2 concentrations were 0,  $10^{-12}$ ,  $10^{-9}$ ,  $10^{-6}$  and  $10^{-5}$  M, keeping the DMSO solution constant (0.1%). After incubating for 10 min, the cells were fixed with 4% paraformaldehyde and the cells were processed to the same procedure as described in the experimental section of the main text. The cellular responses were normalized for that

without E2. They exhibit concentration-dependent increase in ERK phosphorylation with saturation around  $10^{-6}$  M E2. It should be noted that physiological E2 concentration is around  $10^{-9}$  M based on literature.<sup>[3]</sup>



**Figure SI.4.3** ERK phosphorylation by soluble E2. Starved MCF-7 cells were seeded in plastic a 96-well plate. The cells were stimulated in the corresponding concentrations of E2 dissolved in DMSO and incubated for 5 min before fixation. ERK phosphorylation was quantified with cell-based ELISA. The values were normalized with that without E2 (E2 concentration, 0). Bars mean $\pm$ S.E. of triplicate determinations.

## References

- [1] Harrington WR; Kim, SH; Funk, CC; Madak-Erdogan, Z; Schiff, R; Katzenellenbogen, JA; Katzenellenbogen, BS, Estrogen dendrimer conjugates that preferentially activate extranuclear, nongenomic versus genomic pathways of estrogen action. *Molecular Endocrinology* **2006**, *20*: 491-502.
- [2] Reddy K; Keshamouni, V, Mechanism of 17- $\beta$ -estradiol-induced erk1/2 activation in breast cancer cells: A role for her2 and pkc-delta. *Eur. J. Cancer* **2002**, *38*: 59-60.
- [3] Nishimura I; Ui-Tei, K; Saigo, K; Ishii, H; Sakuma, Y; Kato, M, 17 beta-estradiol at physiological concentrations augments ca<sup>2+</sup>-activated k<sup>+</sup> currents via estrogen receptor beta in the gonadotropin-releasing hormone neuronal cell line gt1-7. *Endocrinology* **2008**, *149*: 774-782.

## **CHAPTER FIVE**

---

### **GENERAL DISCUSSION**

In cardiovascular medicine, E2 binds to membrane ERs, induces acute non-genomic effect and thereafter possesses endothelium-dependent protective effects.<sup>[1]</sup> However, E2-mediated non-genomic events happen in a very transient time scale and hence are difficult to detect experimentally.<sup>[2]</sup> In attempting to maintain the activation of membrane ERs in a long-term frame, some efforts have been made *via* using E2-conjugates, such as E2-BSA or E2-dendrimer, those can retain staying in the extra-nucleus localization.<sup>[3]</sup> But they are arguably recognized as stable systems due to the discrepancies of their *in vitro* localization and *in vivo* distributions.<sup>[4]</sup> Moreover, E2-conjugates can easily form aggregates because of the hydrophobic nature of E2, which also leads to difficulties in inducing biological responses. To solve these issues, surface-tethered E2 was prepared by both bottom-up and top-down approaches in this project. By bottom-up approach, E2 was tethered onto a phosphorylcholine grafted chitosan (CH-PC) polymer backbone and formulated to self-assembled functional film. The physical chemistry properties and *in vitro* cellular responses of CH-PC-E2 and CH-PC polymer films were separately investigated. Based on these studies, such E2 tethered CH-PC polymeric platform would be beneficial for protection of the cardiovascular system. In order to further elucidate the biological mechanisms of surface-tethered E2, E2 was functionalized onto micropatterned substrate based biosensor, which were prepared with a photolithography by top-down approach. The relevant cell signaling study and cell proliferation study showed that E2-functionalized micropatterned biosensors can efficiently isolate non-genomic signaling pathways from genomic signaling pathways without inducing cell internalization. This E2-biosensor-based technology controlled exposure concentration and time of surface-tethered E2 to cells in a well-defined manner and enabled us to investigate the fundamental steroid biology in depth.

## **5.1 Physical and biological properties of CH-PC polymer thin films**

As an appropriate polymer backbone for E2 surface tetheration, chitosan substituted with various degrees of phosphorylcholine (15, 25, 40 mol% to per glucosamine unit) was selected in view of its excellent mechanical property, cationic nature for the cell adhesion, and non-fouling characters. Before E2 tetheration, an independent study related to the physical and

biological properties of CH-PC polymer solution and thin films was firstly systematically performed, from a polymer perspective. In solution phase, CH-PC polymers contain polymer chains interconnected by hydrogen bonds and ionic interactions, so they form aggregates. By increasing the incorporated amount of PC groups (from 15 to 40 mol %), CH-PC polymers in solution self-assembled into more compacted aggregates due to inter- or intra-particle ion pairing. After depositing CH-PC solutions onto solid supporting substrate, they formed films with similar mechanical properties.

In order to confirm the non-fouling character of CH-PC film, the interactions between non-specific proteins/cells and CH-PC films incorporated with different PC levels were investigated. Generally, fibrinogen adsorption on CH-PC films formulated *in situ* significantly decreased upon increasing the PC incorporated level from 15% to 40%. This result was in accordance well with the subsequent ER- $\alpha$  binding study that only very small portion of ER- $\alpha$  non-specific adsorption occurs in the CH-PC films. However, we need to find a moderate level of PC incorporation in the CH backbone in terms of balancing its solubility in physiological conditions and non-fouling characters. In a previous study, Tardif et al., suggested that PC-substituted chitosans was capable of supporting the survival and amplification of EPCs and was readily soluble under physiological conditions if the level of PC incorporation equals to ~20 %.<sup>[5]</sup> As a result, a CH-PC20 polymer conjugate will be used to the subsequent E2 tetheration studies. Besides, it is also expected that other zwitterionic groups, such as sulfobetaine or carboxylbetaine, could be linked to chitosan backbone with the similar chemical reactions as phosphorylcholine. The physiochemical properties among those chitosan-zwitterionic conjugates could be further studied and discussed in the comparison of CH-PC conjugates.

Meng et al. reported that a CH-PC synthesized by an heterogeneous process formed substrates adhesive towards HUVECs even though the PC content of the polymer was high (~0.60 wt. % phosphorus).<sup>[6]</sup> The CH-PC samples described in my project were obtained under homogeneous conditions that favor random distribution of the PC groups along the CH chain. They are expected to present a more homogeneous PC distribution on the film/water interface, compared to the films studied by Meng et al. In addition, HUVECs formed three dimensional spheroids on drop-casted CH-PC films when the PC incorporated level exceeds 25% due to

their non-adhesive properties. The size of the cellular spheroids increased dependent on PC incorporated levels and culturing time. Compared to the traditional grafts containing a two-dimensional cell monolayer, three-dimensional HUVEC spheroid culture in CH-PC coated substrates possibly results in a higher cell survival rate and enhanced angiogenesis post-grafting, which mimics the *in vivo* physiological conditions more realistically.<sup>[7, 8]</sup> To sum up, our study demonstrates that CH-PC films form a promising platform for 3D-cellular grafts to promote vascular healing in future in-vivo applications.

In the future, more *in vitro* and *in vivo* biological studies could be performed on the CH-PC coated substrates to investigate their possible roles in tissue engineering. For example, “Live/Dead” long-term endothelial cell viability and proliferation tests could be carried out by Alamar blue/Trypan blue staining assay to determine the cell survival rate cultured in the CH-PC coated substrates.<sup>[9]</sup>

## **5.2 Synthesis, characterization and biological studies of CH-PC-E2 self-assembled films in the cardiovascular regenerative medicine**

In this project, an activated E2 ligand (E2-benzoic acid) was covalently tethered to the CH-PC backbone *via* an amide linker as a prodrug strategy. The substitution degree of E2 per glucosamine unit is ~5%, while the PC content was ~20% as introduced in the previous section. It was shown that the mechanical properties and cellular responses of CH-PC-E2 samples are greatly associated with various formulation methods. CH-PC-E2 formed hydrogel-like thin films by self-assembly bottom-up approach and significantly stimulated NO production in endothelial cells by a diaminofluorescein-FM diacetate (DAF-FM) imaging study, indicating its protective effect in cardiovascular system.

Polymer conjugates based prodrug strategy were attracted interest due to its unique therapeutic efficacy, e.g. enhanced bioavailability and cell specificity, in cardiovascular medicine.<sup>[10-12]</sup> In a previous study, an E2 derivative, estradiol-3-benzoate (EB), was attached to copolymer to poly( $\alpha,\beta$ -(N-2-hydroxyethyl-DL-aspartamide))-poly( $\alpha,\beta$ -(N-2-aminoethyl-DL-aspartamide)) copolymer (PAHA) PAHA as a prodrug in order to enhance its solubility and stability.<sup>[13]</sup> But unfortunately, the clinical efficacy of PAHA-EB was not addressed yet.<sup>[14]</sup>

Previously, E2-dendrimer conjugates showed *in vivo* beneficial vascular protection effects without inducing proliferation of breast cancer cells, which is associated with its non-genomic behavior.<sup>[15]</sup> In this study, the E2-dendrimer conjugates significantly increase around ~2 times vs. free E2 (conc.  $10^{-8}$  M) ~1.7 times of the expression of endothelial nitric oxide synthase (eNOS) level, which is critical in the regulation of the NO. Moreover, EDC didn't lead MCF-7 breast cancer cell proliferation *in vivo* while free E2 induced ~3 times significant higher growth of tumor weight. In our present CH-PC-E2 films, NO production was significantly increased (~1.65 times higher NO production) compared to CH-PC control film, which is accordance well with EDC studies. However, due to the thin film formulation of our CH-PC-E2 sample, it is impossible to directly determine its potential risk of MCF-7 breast cancer cells proliferations. The reason is because that MCF-7 cells form spheroid structures on CH-PC substrates (explained in the previous chapter), leading the cell counting experiment difficult to be performed. As a result, a selected surface tethered E2-based cancer cell proliferation study could be developed to evaluate its risk in clinical therapy. More importantly, the E2 distribution onto the CH-PC polymer backbone was random. As a result, it is highly required that develop a biosensor to control the concentration and time of surface-tethered E2 presentation to cells in order to elucidate more details about biological mechanisms. We will further to discriminate non-genomic and genomic action of surface-tethered E2 in the subsequent E2-functionalized micropatterned biosensor study by controlling MCF-7 cell attachment and E2 densities in a well defined manner. Finally, single cell based non-genomic effect studies could be performed by using E2-functionalized micropatterned substrates that confine the cells to restricted spaces.<sup>[16]</sup>

In the future, *in vitro* and *in vivo* studies could be performed to determine whether CH-PC-E2 hydrogel stimulates endothelial cell growth and promotes blood vessel formation. In this sense, CH-PC-E2 hydrogels would possibly induce the regeneration of vasculature/endothelium and engage in angiogenesis/neovasculogenesis processes, which hence decrease the progression of cardiovascular disease, such as atherosclerosis.



### **5.3 E2-tethered micropatterned substrates selectively activate non-genomic signal pathways**

In this section, the activated E2 ligand (E2-benzoic acid, the same as the one used for CH-PC-E2 preparation) and a cell-adhesive ligand (cyclic RGD) were covalently co-immobilized onto a micropatterned substrate to construct a biosensor for E2 non-genomic effect study. Recently, the report on the cytoplasmic localization of estrogen-dendrimer conjugate (EDC) raised questions on its interaction and transportation mechanisms.<sup>[17]</sup> Our results on the ability of the E2-tethered micropatterned surface to evoke estrogenic non-genomic pathways clearly demonstrates that the reaction of E2-conjugates does initiate at the cell membrane ER and meanwhile precluding the necessity of membrane ER transportation (even after surface immobilized E2/ER binding) to the cytoplasm site for the downstream signaling.

In the current study, the ERK phosphorylation level was more significantly increased (18.7%) on the E2-functionalized micropatterned substrates than the control surfaces after 1 hour of incubation. These data are promising since free E2 alone induced ERK activity usually occurs within 15 minutes.<sup>[18]</sup> In our case, the increment can be maintained up for to 1 hour which indicates that our E2-functionalized micropatterned substrate can stimulate non-genomic effects constantly. However, the difference in ERK phosphorylation levels is not so big, but it is reasonable considering the fact that even soluble E2 (at  $10^{-6}$  M, sufficiently higher than physiological concentrations) can evoke only 27% increment in our experimental conditions. Moreover, similar smaller ERK phosphorylation in E2-conjugates compared to free E2 (10% vs. 20%) has been reported previously in the study of the response of clonal rat prolactinoma cell lines to E2-peroxidase.<sup>[19]</sup> In the upcoming work, the ERK activation at various points in time should be determined to obtain a time-dependent curve. In the present study, we found that MCF-7 cells didn't adhere well on the E2-functionalized micropatterned substrates in a longer time incubation (>1 hour). So how to optimize cell culture conditions, e.g. to control cRGD densities or geometries of gold regions, will be the next challenge.

Further, a spatial and temporal dynamic control of E2 exposure to cells in E2-functionalized micropatterned substrates could be implemented to enhance the sensitivity of

our biosensor. For spatial control, different densities of gold circular regions in a 2- $\mu\text{m}$  diameter were prepared with the pitches of 4- $\mu\text{m}$ , 6- $\mu\text{m}$ , and 12- $\mu\text{m}$ , respectively. The densities of golden circular regions with a 12- $\mu\text{m}$  pitch were used for the current cellular study. In the future, other densities of golden circular regions should be investigated and compared by optimizing cell culture conditions. In addition, cells can contact E2 in a gradient concentration and the relationship of cellular responses to E2 concentration can be achieved. In order to temporal control, one idea is to co-immobilize photo-cleavable PEG ( $M_w = 12$  kDa)<sup>[20]</sup> with E2 together onto the gold surface. Photocleavable PEG is capable of preventing the exposure of adjacent ligands to the cell surface.<sup>[21]</sup> Hence the time of E2 exposure to cells can be precisely regulated by controlling the time of photo-irradiation.

Furthermore, it is widely accepted that the exact cellular location of ER is still enigmatic.<sup>[22]</sup> Another studies reported that E2-induced ERK/MAPK activation was mediated through a G protein-coupled receptor, GPR30.<sup>[23]</sup> Recent studies have also implicated that GPR30, a G protein-coupled seven transmembrane receptor target, functions as a plausible candidate for mediating membrane initiated steroid signaling in breast cancer.<sup>[24]</sup> But the assumption that GPR30 mediated E2 non-genomic pathway continues to be disputed.<sup>[25]</sup> Therefore, GPR30 signaling was not analyzed by surface E2-tethered micropatterned substrates in present study. However, some additional experiments could be performed to examine whether the activation of ERK is induced due to the direct interaction between E2 and ER or due to the other possible factors' contributions.

## 5.4 References

- [1] Simoncini T; Mannella, P; Fornari, L; Caruso, A; Varone, G; Genazzani, AR, Genomic and non-genomic effects of estrogens on endothelial cells. *Steroids* **2004**, *69*: 537-542.
- [2] Simoncini T; Genazzani, AR, Non-genomic actions of sex steroid hormones. *Eur. J. Endocrinol.* **2003**, *148*: 281-292.
- [3] Yang L-c; Zhang, Q-G; Zhou, C-f; Yang, F; Zhang, Y-d; Wang, R-m; Brann, DW, Extranuclear estrogen receptors mediate the neuroprotective effects of estrogen in the rat hippocampus. *Plos One* **2010**, *5*: 72-84.

- [4] Chambliss KL; Wu, Q; Oltmann, S; Konaniah, ES; Umetani, M; Korach, KS; Thomas, GD; Mineo, C; Yuhanna, IS; Kim, SH; Madak-Erdogan, Z; Maggi, A; Dineen, SP; Roland, CL; Hui, DY; Brekken, RA; Katzenellenbogen, JA; Katzenellenbogen, BS; Shaul, PW, Non-nuclear estrogen receptor alpha signaling promotes cardiovascular protection but not uterine or breast cancer growth in mice. *J. Clin. Invest.* **2010**, *120*: 2319-2330.
- [5] Tardif K; Cloutier, I; Miao, Z; Lemieux, C; St-Denis, C; Winnik, FM; Tanguay, J-F, A phosphorylcholine-modified chitosan polymer as an endothelial progenitor cell supporting matrix. *Biomaterials* **2011**, *32*: 5046-5055.
- [6] Meng S; Liu, Z; Zhong, W; Wang, Q; Du, Q, Phosphorylcholine modified chitosan: Appetent and safe material for cells. *Carbohydrate Polymers* **2007**, *70*: 82-88.
- [7] Alajati A; Laib, AM; Weber, H; Boos, AM; Bartol, A; Ikenberg, K; Korff, T; Zentgraf, H; Obodozie, C; Graeser, R; Christian, S; Finkenzeller, G; Stark, GB; Heroult, M; Augustin, HG, Spheroid-based engineering of a human vasculature in mice. *Nature Methods* **2008**, *5*: 439-445.
- [8] Bhang SH; Lee, S; Lee, T-J; La, W-G; Yang, H-S; Cho, S-W; Kim, B-S, Three-dimensional cell grafting enhances the angiogenic efficacy of human umbilical vein endothelial cells. *Tissue Engineering Part A* **2012**, *18*: 310-319.
- [9] McGuigan AP; Bruzewicz, DA; Glavan, A; Butte, M; Whitesides, GM, Cell encapsulation in sub-mm sized gel modules using replica molding. *Plos One* **2008**, *3*: 678-698.
- [10] Zou MJ; Okamoto, H; Cheng, G; Hao, XH; Sun, J; Cui, FD; Danjo, K, Synthesis and properties of polysaccharide prodrugs of 5-aminosalicylic acid as potential colon-specific delivery systems. *European Journal of Pharmaceutics and Biopharmaceutics* **2005**, *59*: 155-160.
- [11] Lee E; Lee, J; Lee, I-H; Yu, M; Kim, H; Chae, SY; Jon, S, Conjugated chitosan as a novel platform for oral delivery of paclitaxel. *Journal of Medicinal Chemistry* **2008**, *51*: 6442-6449.
- [12] Vinsova J; Vavrikova, E, Recent advances in drugs and prodrugs design of chitosan. *Current Pharmaceutical Design* **2008**, *14*: 1311-1326.

- [13] Zovko M; Zorc, B; Novak, P; Tepes, P; Cetina-Cizmek, B; Horvat, M, Macromolecular prodrugs xi. Synthesis and characterization of polymer-estradiol conjugate. *International Journal of Pharmaceutics* **2004**, 285: 35-41.
- [14] Sandros MG; Sarraf, CB; Tabrizian, M, Prodrugs in cardiovascular therapy. *Molecules* **2008**, 13: 1156-1178.
- [15] Chambliss KL; Wu, QA; Oltmann, S; Konaniah, ES; Umetani, M; Korach, KS; Thomas, GD; Mineo, C; Yuhanna, IS; Kim, SH; Madak-Erdogan, Z; Maggi, A; Dineen, SP; Roland, CL; Hui, DY; Brekken, RA; Katzenellenbogen, JA; Katzenellenbogen, BS; Shaul, PW, Non-nuclear estrogen receptor alpha signaling promotes cardiovascular protection but not uterine or breast cancer growth in mice. *Journal of Clinical Investigation* **2010**, 120: 2319-2330.
- [16] Machado JD; Alonso, C; Morales, A; Borges, RD, A novel nongenomic action of estrogens the regulation of exocytotic kinetics. In *Chromaffin cell: Trnsmmitter biosynthesis, storage, release, actions, and informatics*, Oconnor, D. T.; Eiden, L. E., Eds. 2002; Vol. 971, pp 284-286.
- [17] Mendelsohn ME; Karas, RH, Rapid progress for non-nuclear estrogen receptor signaling. *Journal of Clinical Investigation* **2010**, 120: 2277-2279.
- [18] Migliaccio A; DiDomenico, M; Castoria, G; deFalco, A; Bontempo, P; Nola, E; Auricchio, F, Tyrosine kinase/p21(ras)/map-kinase pathway activation by estradiol-receptor complex in mcf-7 cells. *Embo Journal* **1996**, 15: 1292-1300.
- [19] Bulayeva NN; Gametchu, B; Watson, CS, Quantitative measurement of estrogen-induced erk 1 and 2 activation via multiple membrane-initiated signaling pathways. *Steroids* **2004**, 69: 181-192.
- [20] Kaneko S; Nakayama, H; Yoshino, Y; Fushimi, D; Yamaguchi, K; Horiike, Y; Nakanishi, J, Photocontrol of cell adhesion on amino-bearing surfaces by reversible conjugation of poly(ethylene glycol) via a photocleavable linker. *Physical Chemistry Chemical Physics* **2011**, 13: 4051-4059.
- [21] Shimizu Y; Boehm, H; Yamaguchi, K; Spatz, JP; Nakanishi, J, A photoactivatable nanopatterned substrate for analyzing collective cell migration with precisely tuned cell-extracellular matrix ligand interactions. *Plos One* **2014**, 9: 12-24.

- [22] Nadal A; Diaz, M; Valverde, MA, The estrogen trinity: Membrane, cytosolic, and nuclear effects. *News in Physiological Sciences* **2001**, *16*: 251-255.
- [23] Filardo EJ; Quinn, JA; Bland, KI; Frackelton, AR, Estrogen-induced activation of erk-1 and erk-2 requires the g protein-coupled receptor homolog, gpr30, and occurs via trans-activation of the epidermal growth factor receptor through release of hb-egf. *Molecular Endocrinology* **2000**, *14*: 1649-1660.
- [24] Thomas P; Pang, Y; Filardo, EJ; Dong, J, Identity of an estrogen membrane receptor coupled to a g protein in human breast cancer cells. *Endocrinology* **2005**, *146*: 624-632.
- [25] Razandi M; Pedram, A; Merchenthaler, I; Greene, GL; Levin, ER, Plasma membrane estrogen receptors exist and functions as dimers. *Molecular Endocrinology* **2004**, *18*: 2854-2865.

## **CHAPTER SIX**

---

### **CONCLUSIONS AND FUTURE WORKS**

## 6.1 Conclusions

The objective of research described in this thesis aims to develop surface-tethered E2 based biomaterials and biosensors for cardiovascular regenerative medicine through the investigation of E2 non-genomic actions. To begin with, E2 was grafted onto the chitosan phosphorylcholine (CH-PC) polymer. The characterization and cellular studies of the CH-PC functional films were performed. It was demonstrated that the fabrication method significantly influences mechanical properties, depth-dependent composition, and biological responses of the films. A selected method was developed by grafting E2 to the CH-PC backbone for the preparation of self-assembled interfaces *via* a bottom-up approach. The rehydrated CH-PC-E2 film could maintain E2 exposure to the topmost layer of the interfaces due to its hydrophobic nature. Throughout QCM-D measurements, hydrated CH-PC-E2 films possess similar visco-elastic properties as hydrogels. By investigating its effect in the process of NO production, the CH-PC-E2 hydrogel films could be considered as new coating materials for the cardiovascular contacting devices. In another aspect, E2 was covalently immobilized onto the PEG-functionalized micropatterned substrate, which is fabricated by aligning gold circular regions onto the glass substrate *via* a photolithography. A selected non-genomic ERK signal pathway was successfully activated in the E2-functionalized micropatterned substrates coupled by cell ELISA technique. Moreover, E2-functionalized micropatterned substrate didn't induce breast cancer (MCF-7) cell proliferation, suggesting that it had no influence to genomic effect. Compared to previous E2 conjugated dendrimer study, E2-functionalized micropatterned substrate can provide new insights to specifically interact with plasma mERs and meanwhile to preclude the possibility of mERs transportation to the cytoplasm site. Moreover, it also provides indirect evidence to confirm the presence of estrogen receptors in the plasma membrane site.

## 6.2 Future perspectives

Dysfunction, damage and ageing of endothelium are key factors in the development of cardiovascular disease. Recently, endothelial progenitor cells (EPCs) based strategies have been emerged as a potential way for the repair and regeneration of damaged vessel.<sup>[1, 2]</sup> To achieve this goal, various substrates for supporting the proliferation and differentiation of

EPCs to mature ECs, considered as extracellular matrix (ECM), are widely studied.<sup>[3, 4]</sup> Previous results suggested that CH-PC was capable of supporting the survival and amplification of EPCs.<sup>[5]</sup> Moreover, administration of E2 at physiological concentration also influenced several physiological functions of EPCs, including regulation of cell cycle, apoptosis, proliferation and differentiation.<sup>[6]</sup> In addition, E2 can also greatly enhance EPCs proliferation rate *in vitro* involved in the mitogenic effect of E2 as a consequence of the activations of MAPK signaling pathway.<sup>[7, 8]</sup> The mechanism of E2 influence on EPCs proliferation is through triggering the reendothelialization process, which promotes the regeneration and recovery of the endothelium.<sup>[9]</sup> Thus a synergistic effect of E2 and CH-PC in the CH-PC-E2 polymeric scaffold for supporting EPCs proliferation could be investigated in future study. Relevant mechanisms will also be explored and interpreted. Therefore, the collected knowledge may promote the applications of CH-PC-E2 hydrogel biomaterial as a platform for stem cell delivery in the vascular healing process.

On the other hand, more *in vitro* or *in vivo* studies of E2-functionalized micropatterned substrate could also be carried out. Multiple non-genomic signaling pathways, such as PI3K/AKT, can be justified by the E2-functionalized micropatterned substrate *in vitro* and enrich our knowledge of steroid biology. In addition, E2-functionalized micropatterned substrates are not only limited to cardiovascular medicine, but also expandable to solve the controversial issues in the other tissues or organs corresponding with genomic or non-genomic mechanisms. For example, administration of E2-dendrimer is an important therapeutic strategy in the treatment of osteoporosis mainly due to its non-genomic actions in osteobiology.<sup>[10]</sup> However, E2 non-genomic actions failed to decrease osteoporosis *in vivo* transgenic model studies.<sup>[11]</sup> In neurobiology, the non-genomic actions of E2-dendrimer or E2-BSA conjugates demonstrated protective effects and cognitive recovery against global cerebral ischemia in the hippocampal region although how this occurs still needs to be confirmed. Therefore, further investigations are required to clarify the precise roles of the non-genomic actions of E2 by using micropatterned substrates in bone or neural systems. Finally, one of the possible *in vivo* studies for E2-functionalized micropatterned substrate may focus on how to develop it as an implantable device in the cardiovascular system. By taking advantage of its unique non-genomic nature, E2-functionalized micropatterned substrate will possibly perform as a



biosensor in the diagnosis, prevention and treatment of hormone related diseases. In sum, our E2-functionalized micropatterned will facilitate the study of more detailed profiles of fundamental steroid biology and advance the progress of clinical medicine.

### 6.3 References

- [1] George J; Afek, A; Abashidze, A; Shmilovich, H; Deutsch, V; Kopolovich, J; Miller, H; Keren, G, Transfer of endothelial progenitor and bone marrow cells influences atherosclerotic plaque size and composition in apolipoprotein e knockout mice. *Arterioscler. Thromb. Vasc. Biol.* **2005**, *25*: 2636-2641.
- [2] Shintani S; Murohara, T; Ikeda, H; Ueno, T; Sasaki, K; Duan, JL; Imaizumi, T, Augmentation of postnatal neovascularization with autologous bone marrow transplantation. *Circulation* **2001**, *103*: 897-903.
- [43] Colombo E; Calcaterra, F; Cappelletti, M; Mavilio, D; Della Bella, S, Comparison of fibronectin and collagen in supporting the isolation and expansion of endothelial progenitor cells from human adult peripheral blood. *Plos One* **2013**, *8*: 532-551.
- [4] Kusuma S; Zhao, S; Gerecht, S, The extracellular matrix is a novel attribute of endothelial progenitors and of hypoxic mature endothelial cells. *Faseb Journal* **2012**, *26*: 4925-4936.
- [45] Tardif K; Cloutier, I; Miao, Z; Lemieux, C; St-Denis, C; Winnik, FM; Tanguay, J-F, A phosphorylcholine-modified chitosan polymer as an endothelial progenitor cell supporting matrix. *Biomaterials* **2011**, *32*: 5046-5055.
- [6] Lemieux C; Cloutier, I; Tanguay, J-F, Estrogen-induced gene expression in bone marrow c-kit plus stem cells and stromal cells: Identification of specific biological processes involved in the functional organization of the stem cell niche. *Stem Cells and Development* **2008**, *17*: 1153-1163.
- [7] Geraldes P; Sirois, MG; Bernatchez, PN; Tanguay, JF, Estrogen regulation of endothelial and smooth muscle cell migration and proliferation - role of p38 and p42/44 mitogen-activated protein kinase. *Arteriosclerosis Thrombosis and Vascular Biology* **2002**, *22*: 1585-1590.
- [8] Imanishi T; Hano, T; Nishio, I, Estrogen reduces endothelial progenitor cell senescence through augmentation of telomerase activity. *J. Hypertens.* **2005**, *23*: 1699-1706.

- [9] Masuda H; Kalka, C; Takahashi, T; Yoshida, M; Wada, M; Kobori, M; Itoh, R; Iwaguro, H; Eguchi, M; Iwami, Y; Tanaka, R; Nakagawa, Y; Sugimoto, A; Ninomiya, S; Hayashi, S; Kato, S; Asahara, T, Estrogen-mediated endothelial progenitor cell biology and kinetics for physiological postnatal vasculogenesis. *Circulation Research* **2007**, *101*: 598-606.
- [10] Martin-Millan M; Almeida, M; Ambrogini, E; Han, L; Zhao, H; Weinstein, RS; Jilka, RL; O'Brien, CA; Manolagas, SC, The estrogen receptor-alpha in osteoclasts mediates the protective effects of estrogens on cancellous but not cortical bone. *Molecular Endocrinology* **2010**, *24*: 323-334.
- [11] Chokalingam K; Roforth, MM; Nicks, KM; McGregor, U; Fraser, D; Khosla, S; Monroe, DG, Examination of er alpha signaling pathways in bone of mutant mouse models reveals the importance of ere-dependent signaling. *Endocrinology* **2012**, *153*: 5325-5333.